Thermomechanical Characterization of Rapid Thermal Denaturation in Load-Bearing Collagenous Cardiac Tissues Under Isometric Constraints

by

Alireza Jahangir

Submitted in partial fulfilment of the requirements
for the degree of Interdisciplinary Ph.D.
at
Dalhousie University
Halifax, Nova Scotia
October, 2004

Your file Votre référence
ISBN: 0-494-00955-1
Our file Notre référence
ISBN: 0-494-00955-1

DALHOUSIE UNIVERSITY

To comply with the Canadian Privacy Act the National Library of Canada has requested that the following pages be removed from this copy of the thesis:

Preliminary Pages

Examiners Signature Page (pii)

Dalhousie Library Copyright Agreement (piii)

Appendices

Copyright Releases (if applicable)

TABLE OF CONTENTS

LIST OF TABLES

CHAPTER 2

CHAPTER 3

CHAPTER 4

CHAPTER 5

APPENDIX 1

LIST OF FIGURES

CHAPTER 1

CHAPTER 2

CHAPTER 3

CHAPTER 4

CHAPTER 5

APPENDIX 1

APPENDIX 2

ABSTRACT

For the first time a novel thermomechanical approach has been used to study the dynamics of the rapid thermal denaturation of two different collagenous tissues (bovine pericardium and mitral chordae tendineae) and the various factors influencing this important event. Specifically, a custom-made, computer-controlled, dynamic hydrothermal isometric tension (DHIT) system allowed for the rapid change of tissue temperature, from 25°C to 90°C in less than 1 s, while the samples are held under isometric constraint. The data for all the experiments were well-fitted using the Levenberg-Marquardt nonlinear least-squares method and a 3-exponential function each having unique time constant τ_i and corresponding coefficients (C_i). The data for all tissues revealed that rapid thermal denaturation of the collagenous tissues was a dynamic, 3-step process, and that the first step, as characterized by (τ_1) was both the fastest, and the most significant (as indicated by C_1) during the entire denaturation process. The reversibility experiments indicated that the rapid step-change in temperature in both collagenous tissues, under isometric and isothermal conditions led to the observation that the first heating cycle resulted in the transformation of ordered, native collagenous tissues into less ordered and rubber elastic materials. The molecular events occurring during the first heating cycle represented the only irreversible transitions; the thermoelastic contraction and relaxation of the rubbery, denatured collagen during the subsequent thermal and cooling cycles occurred in a repeatable manner. The effects of increased loads and various concentrations of NaCl on the dynamics of rapid thermal denaturation indicated that both factors delayed the dynamics of thermal denaturation and, more importantly that the denaturation remained a dynamic 3-staged event. Finally, the DHIT system was used to comparatively investigate the structure-function relations in various load-bearing components of bovine heart including: mitral and tricuspid chordae tendineae, aortic and mitral valves, and pericardium. It was shown that tissues sustaining higher mechanical loads were less thermally stable, perhaps due to a higher level of immature crosslinks than those under lower stress. This new thermomechanical approach demonstrated that rapid thermal denaturation of different collagenous tissues, under isometric constraints and isothermal heating conditions, is a dynamic, largely irreversible, 3-step mechanism.

LIST OF ABBREVIATIONS and SYMBOLS USED

A/D	Analog/Digital
ANOVA	Analysis of Variance
AV	Aortic Valve
BHV	Bioprosthetic Heart Valve
CCD	Charge-Coupled Device
CT	Chordae Tendineae
D/A	Digital/Analog
DHIT	Dynamic Hydrothermal Isometric Tension
DSC	Differential Scanning Calorimetry
DTT	Denaturation Temperature Tester
EDC	1-ethyl-3-(3-dimethyaminopropyl)carbodiimide
FACIT	Fibril Associated Collagen with Interrupted Triple Helices
FTIR	Fourier Transform IR spectroscopy
GAG	Glycosaminoglycan
GH	Glenohumeral
Gly	Glycine
GTA	Glutaraldehyde
HACS	Heat Assisted Capsular Shift
HIT	Hydrothermal Isometric Tension
Hyp	Hydroxyproline
MCT	Mitral Chorda Tendinea
MTS	Mechanical Testing System
MV	Mitral Valve
NHS	N-Hydroxysuccinimide
PBS	Phosphate Buffer Solution
PC	Pericardium
PG	Proteoglycan
Pro	Proline
SALS	Small Angle Light Scattering

SE	Standard Error
SEM	Standard Error of the Mean
TCT	Tricuspid Chordae Tendineae
TEM	Transmission Electron Microscopy
UTS	Ultimate Tensile Strength (MPa)
ξ	Extension used in Chen's studies
κ	Diffusivity used in heat transfer analysis
β	Material Parameter
τ_i	Time Constant to describe the normalized load-time data
ΔC_p	Heat Capacity Change
ΔH	Enthalpy Change
ΔS	Entropy Change
A	Material Parameter
C_i	Coefficient used to characterize the contribution of τ_i
D	Denatured Protein
E_a	Activation Energy
F	Force (N)
F_{max}	Averaged Maximum Force
g	Gravitational Acceleration(9.81 m/s^2)
k	Rate constant
m	Material Parameter
m_{max}	Averaged Maximum Load (kg)
N	Native Protein
P	Load (kPa)
R	Universal Gas Constant (8.314 J/mol K or 1.987 cal/mol K)
r^2	Regression Coefficient
t	Specific Time Point during the Heat Transfer
T	Temperature (°C or °K)
$t_{1/2}$	Half-life of load decay during HIT test
T_d	Denaturation Temperature (°C) from DTT test
T_i	Inner Surface Temperature used for heat transfer calculations

T_m	Melting Temperature (°C) of Collagen
T_o	Outer Surface Temperature used for heat transfer calculations
T_s	Shrinkage Temperature (°C) of Collagen
U	Partially Unfolded Protein

ACKNOWLEDGMENTS

My first, and most earnest, acknowledgment must go to my advisor Professor J. Michael Lee. During the past five exciting years, Dr. Lee has been an incomparable teacher, mentor, and most important of all, a great friend. By his allowing me to think freely, and providing me with the most timely advice, I have evolved into a more competent, and knowledgeable human being and at the same time a skilled scientist. You will be remembered as one of the greatest influences in my life. Thank you for all your support, encouragement and kindness.

I also wish to extend my many thanks to my advisory committee: Drs: Wells, White and Gratzer, for their invaluable advices, timely criticism, and of course editorial revisions. I also extend my gratitude to Drs. Sacks and Watters. This journey would not have been completed if it were not for the intellectual discussion between myself and the following friends and colleagues: Dr. Steven Waldman, Dr. Mark Glazebrook, Ian Aldous and Sean Margueratt. I also wish to acknowledge the encouragement and the support of many of the Biomedical Engineering (BME) faculty and staff including: Drs. K. Deluzio, Dr. M. Filiaggi, Dr. Kathy Russell, Mrs. Denise Lynds-Brown and Mrs. Sandy Mansfield. I am also thankful to many of the current and former Tissue Mechanics Group and BME students. On a more personal note, I wish to extend my appreciation to the following friends who made my stay in Halifax, by far the best time of my life: Dr. Ian MacDougall, Carl Petrone, Janie Astephan, Anna Dion, and Chris Rose. I would also like to extend my most heartfelt gratitude to Miss. Michelle MacAskill whom I have met just prior to writing my thesis. Thank you for the patience, support and the comfort you have provided me during the past eight months.

Finally, I would like to dedicate this doctorate dissertation to the three most important individuals in my life, without whom none of my dreams would have been realised: My loving parents (Jaleh and Bijan) and my amazing brother (Arash). All my life and especially during my doctorate training, I have been inspired by their love, support, perseverance, warmth and most importantly their optimistic views on life. *Merci, az hameye khod ghozashtegeeha va poshtbaniha daemi.*

1 Literature Review

1.1 Introduction

Collagen-based biomaterials are being employed in numerous medical applications such as: cardiac prostheses [1-3], nerve regeneration [4], tissue augmentation [5, 6], burn and wound dressings [7-9], drug delivery systems [10, 11], ocular surfaces [12], and urinary track surgery [13]. Bioprosthetic heart valves (BHVs), in particular, were introduced in the early 1970s as an attempt to avoid some disadvantages of mechanical valves, especially the need for anticoagulants [14]. Unfortunately, BHVs have experienced a separate problem, that of limited durability. The most commonly implanted BHVs have been those constructed from xenografts (i.e. porcine aortic valves and bovine pericardium). To provide increased resistance to enzymatic degradation, and reduced immunogenicity, xenograft devices undergo physical or chemical processing prior to implantation. Treatment with glutaraldehyde has become the industrial standard. After such treatment, the xenograft tissues are left non-viable, since they contain no cells and must rely on the integrity of native structural proteins (collagen and elastin) throughout the lifetime of the implant.

Generally, collagen fibril bundles can fail either by tearing, where collagen fibrils break as their tensile strength is exceeded, or by creeping, which occurs when fibrils slide past each other resulting in tissue disaggregation [15]. Cyclic bending of collagen fibres as well as tissue buckling have been implicated in limiting the longevity of the BHVs. Recently, in vitro accelerated fatigue studies (5-500 million cycles) with glutaraldehyde-fixed porcine aortic valve bioprostheses has been shown to produce progressive damage to the molecular structure of type I collagen [as well as loss of glycosamineglycans (GAGs)] as assessed by Fourier transform IR spectroscopy (FTIR) [16]. Such structural damage was suggested to be the result of collagen denaturation, as shown by the progressive loss of helicity of the bioprosthetic cuspal collagen. Moreover, damage to the structural integrity of collagen may expose calcium-binding sites in the molecule, thereby acting as possible initiation sites for the calcification of the BHV, another potential cause of failure [17].

Clinically, due to the advances over the past two decades in lasers, microwave, radio-frequency, and similar technologies, the application of thermal therapies to treat various

pathological conditions and injuries has become quite widespread [18, 19]. Some examples include: welding [20] , thermokeratoplasty [21], skin resurfacing [22, 23] and treatment of joint instability [24, 25].

Arthroscopic thermotherapies, in particular, are used to treat instabilities of knee, ankle and shoulder joints as well as eliminating discogenic pain in the spine. For instance, the glenohumeral (GH) joint is a dense fibrous connective tissue composed principally of type I collagen fibre. The application of heat to treat patients with shoulder instability results in shrinkage of the redundant glenohumeral (GH) joint capsule [26]. It is believed that such ultrastructural changes in the collagen molecule occur by uncoiling (i.e. denaturation) of the collagen triple-helix as a result of a temperature rise in the tissue [26, 27]. Although, post-operative and short-term follow-up results have indicated that such therapy is indeed promising, questions about long-term success remain unanswered [28]. Improved range of motion of the repaired shoulder, accelerated patient healing, as well as lower recurrence rates are the major advantages of this therapy. The disadvantages are the time-dependent decrease of tissue stiffness and strength and the trend for tissue recovery back to its untreated length. This kind of response is observed in thermomechanical investigation conducted on animal tissue models [29-31]. Time-dependent changes in mechanical properties and behaviour are thought to be the major reason for recurrence and failure of the therapy in the long run.

1.2 Objectives

Although our understanding of thermal damage to the collagenous tissues has improved recently [30, 32-35], there are still many unanswered questions with regards to the dynamics of denaturation, its possible renaturation and the effects of various factors influencing this process. This doctoral thesis, therefore, describes research directed towards characterising and understanding the *rapid* thermal denaturation of two collagenous tissue models: bovine pericardium and mitral chordae tendineae under isometric and isothermal conditions. Studying the thermal denaturation of collagen under dynamic conditions may reveal the presence of different processes with characteristic time constants, relevant to both: (i) fatigue damage and (ii) time-dependent responses to temperature change. Therefore, understanding

the thermal denaturation under such unique conditions will help to improve the predictability various clinical procedures as well as development of novel biomaterials and tissues-engineered products.

1.3 The Collagen: Structure and Stability

Collagen, which derives it name from two Greek words: *kolla* and *genan* meaning glue and to produce respectively, is a major fibrous protein, an essential component of the various connective tissues found in all multicellular animals, and exists in a variety of different forms [36-38]. Collagen's pivotal function is to maintain and to provide structural integrity in various connective tissues [39].

So far, close to 20 genetically distinct types of collagen have been identified and their classification is based on their basic polymeric structures or related structural features. The four main classes of collagen include: (i) fibrous collagens (types I, II, III, V, and XI) (ii) network collagens (types IV, VIII, and X) (iii) filamentous collagen (type VI) (iv) and fibril associated collagen with interrupted triple helices (FACIT) collagens (Types IX, XII, XIV, XVI, and XIX)[40]. Of the many types of collagen, the fibrillar types (especially type I) are of particular concern herein.

Collagen molecules are comprised of three α-helix polypeptide chains, wound around each other as a helix. Each of the α-chains is made up of some 1300-1700 amino acids residues, and is on the order of 285 nm long and 1.4 nm in diameter. Additionally, most collagens exhibit a characteristic 67 nm periodicity that results from long assemblies of quarter-staggered molecules (4-5 in a cross-section) with a characteristic banding pattern when formed into microfibrils [40, 41]. The basic unit of the collagen polypeptide chain is composed of repeats of the amino acid sequence Gly-X-Y, where Gly represents glycine and X and Y are often proline (Pro) or 4-hydroxyproline (Hyp) residues respectively [42-44]. The presence of glycine (the amino acid with only hydrogen for a side chain) as every first amino acid in the triplet is essential since any larger amino acid will not fit in the central core of the triple helix where the three chains come together [41]. Such strategic positioning of glycine in the interior of the triple helix enables it to form hydrogen bonds between its own amino

terminal and the carboxyl end of an amino acid residue located in the X position of an adjacent helix [45]. Due to the bulky nature of the pyrrolidine ring in both imino acid residues (i.e. Pro & Hyp), they are found on the outside of the collagen triple helix [38, 41]. Both Pro and Hyp have pivotal roles in stabilisation of the triple helix. More importantly, such stability is dependent on the particular isomeric configuration of both Pro and Hyp. While 4-trans-Hyp in the Y position is especially stabilizing [46], the 4-cis-Hyp [47], 3-Hyp or Hyp in the X position are somewhat destabilising [48, 49]. Several suggestions were introduced to explain the stabilising effect of the imino acids. For instance, one effect of imino acid residues is to restrict the conformations available to the polypeptide chain. This can be regarded as an entropic effect. On the other hand, collagen also has a particularly high enthalpy of unfolding (~16-18 kJ/mole tripeptide units), which increases with imino acid content [50]; hence there must be another reason to explain the stabilizing effect of imino acids. In fact, hydrogen bonding (both intra- and interhelical), is considered by many to be the most important single factor in collagen stabilization [41, 51, 52]. As mentioned, hydrogen bonding exists between the hydrogen side group of glycine and the carbonyl oxygen of the X-residue of an adjacent chain [53, 54]. If the X- and Y- residues are not imino acids, then further hydrogen bonds between chains can be formed involving one or two water molecules [55, 56]. This highlights the crucial role of the water molecule in organizing the collagen triple helix. The particular effectiveness of trans 4-Hyp in stabilizing the triple helix has led to suggestions that it may promote the formation of an extended water structure involved in hydrogen bonding with the collagen helix [50, 57]. Privalov [50] suggested that this may be related to the ring structure of the Hyp which can serve as a coordination centre of an extensive network of water molecules. Others pointed instead to the electron withdrawing (i.e. inductive) effects of the hydroxyl group of the Hyp residue as the source of stability [58, 59]. In fact, Holmgren et al. [42, 60] showed that when Hyp hydroxyl groups were substituted by highly electronegative fluorine atoms, the melting temperature of the trimeric species formed by the synthetic collagen-like peptide $(Gly\text{-}Hyp\text{-}Pro)_{10}$ increased.

In addition to the important role of non-covalent hydrogen bonds in stabilising collagen microfibrils, these molecules are further stabilised post-translationally and throughout life, by more heat-stable, covalent, intra- and intermolecular crosslinks [36]. Formation of

intramolecular crosslinks occurs soon after lysine (Lys) and hydroxylysine's (OH-Lys) ε-amino groups have been converted to semi-aldehydes in a reaction catalyzed by lysyl oxidase [61]. The aldehydes then undergo an aldol condensation within a single molecule at the non-helical telopeptides (i.e. non-triplet containing sequence) region to form intramolecular crosslinks [61]. Intermolecular crosslinks, on the other hand, which are considered physiologically more relevant, are derived either from the reaction between two semi-aldehyde (aldol condensation) from adjacent collagen fibrils or the reaction between one semi-aldehyde in one fibril and an unmodified Lys or OH-Lys from the helical portion of an adjacent fibril. [62]. This latter reaction is of the Schiff base type [61, 63]. Nimni et al. [61] have suggested that further stabilization involving reduction or addition to the double bond seems to be a necessary step to render these crosslinks hydrolytically stable under heat or acid.

1.4 The Exogenous Crosslinking of Collagen

1.4.1 Mechanism and Properties of Glutaraldehyde-Crosslinked Tissue

As mentioned earlier, collagenous bioprosthetic tissues (e.g. bovine pericardial tissues and porcine aortic valves) are generally required to undergo some chemical or physical crosslinking procedure to improve their mechanical and immunogenic properties [64]. The industry standard glutaraldehyde treatment is nominally intended to: (i) reduce immunogenicity of the material, (ii) increase resistance to degradation by host and bacterial enzymes as well as (iii) sterilize the material. However, none of these objectives is incompletely achieved [65].

Glutaraldehyde is a five–carbon, water soluble, bi-functional molecule with an aldehyde group at each end of the structure that reacts primarily with the ε-amino groups of Lys and/or OH-Lys of collagen to form covalent intermolecular or interfibrillar crosslinks [66]. In aqueous solution, glutaraldehyde is present as a complex mixture of free aldehyde, mono and dihydrates (acetal and hemiacetal), monomeric and polymeric cyclic hemiacetal, and α,β-unsaturated compounds [67, 68].

Despite the complex structure of glutaraldehyde in aqueous solution, the general mechanism by which crosslinking occurs involves the initial formation of a Schiff base intermediate [67]. A Schiff base is created by nucleophilic attack on the slightly positive carbonyl carbon of glutaraldehyde by the nitrogen of Lys or OH-Lys. Glutaraldehyde can also self-polymerize through an aldol-type condensation reaction that may be partially catalyzed by the presence of amines. Hence, an α,β-unsaturated conjugate Schiff base is formed. Subsequent reactions with Lys or OH-Lys result in stable crosslinks as suggested by Cheung and co-workers [69, 70].

Mechanically, glutaraldehyde crosslinking alters the properties of the fresh tissue by reducing the structural rearrangement of the collagen network in response to stress and decreasing the collagen crimp wavelength, causing planar shrinkage of the tissue [71, 72]. It is believed the reason for this latter phenomenon is the collagen fibres being locked into one geometrical configuration depending on the mechanical constraint applied during fixation [71, 72]. As mentioned earlier, such altered configuration could change the flexural behaviour of the tissue leading to its buckling and fatigue damage to collagen fibres [73]. For instance, Talman et al. [14] have shown that glutaraldehyde-fixed porcine aortic valve cusp tissue is 100 times stiffer in shear than the natural cusp tissue leading to much greater cyclic internal stresses during the cusp bending [74-78] Alternatively, delamination could result, leading to increased infiltration of blood components and calcification at sites of cellular debris. While neither of these latter mechanisms has been fully understood, research establishing linkages between glutaraldehyde treatment and degeneration has accelerated the search for alternative tissue stabilization techniques. These include: carbodiimide [79, 80], acyl azide [81-84], hexamethylene-diisocyanate [85], diamines [86], and polyepoxidic resin [87-91] treatments.

1.4.2 Mechanism and Properties of Carbodiimide (EDC)-Crosslinked Tissue

Due to dissatisfaction over the performance of glutaraldehyde in the pre-treatment of bioprostheses, a particular alternative crosslinking agent, 1-ethyl-3-(3-dimethylaminopropyl)-carbodiimide (EDC), has been well studied. EDC can be categorized under a class of

reagents, known as zero-length crosslinkers, that modify the side-groups on a protein to make them reactive with other side-groups, and allow crosslinks to be formed; however, zero-length crosslinkers, do not themselves remain in the linkage [92]. In particular, EDC crosslinking in collagen is performed by the activation of the carboxylic acid groups on a polypeptide chain followed by reaction with free amino groups on another polypeptide chain [80]. In contrast to glutaraldehyde, which remains in the linkage when crosslinks are formed, EDC is not incorporated into the tissue during treatment and produces only peptide bonds.

In a multi-step process, EDC initially activates the carboxylic acid groups of aspartic or glutamic acid residues on the collagen fibre to form an activated O-urea group [80, 93, 94]. Since this group has short half-life, it will either (i) react with an amino group of Lys or OH-Lys residue to from a crosslink, or (ii) hydrolyze reforming the carboxyl group and a soluble product [80, 93]. In the presence of PBS, Hanks' and Tris buffers, this latter hydrolysis is exacerbated [95, 96]. For the procedure to be successful, the active form of a protein would have to be more stable than the O-acylisourea derivative. Such a condition is fulfilled by the so-called "active esters", in particular the N-hydroxysuccinimidyl esters. The resulting product is an activated ester, a the molecule quite resistant to hydrolysis [97].

A study from our research group has compared the thermal stability and the enzymatic resistance of both EDC/NHS- and glutaraldehyde-treated bovine pericardium. Although comparable results for the denaturation temperature (> 85°C) of crosslinked tissues were obtained, the enzymatic studies have revealed that the EDC-treated samples were significantly more resistant to solubilization by collagenase and trypsin than were those crosslinked with glutaraldehyde [93]. It was hypothesized that the explanation for these events may lie in the fact that EDC penetrates the tissue sample better than does glutaraldehyde (due to latter's tendency to form polymers) and it may also form more crosslinks due to the availability of more potential reactive sites.

1.5 Structure-Function of Collagenous Tissue Models

1.5.1 Pericardium

Pericardium is a soft connective tissue that surrounds the heart. Its main physiological functions are to: (i) limit the dilation of the heart, especially over the right ventricle during diastole and (ii) secure the heart in the thoracic cavity [98].
The arrays of structural elements that comprise the pericardial matrix create a truly composite material. Of the protein family, collagen types I and III (less than 10%) represent the major subclasses within the pericardium [99]. A small amount of elastin is also found embedded within a highly hydrated matrix in which water accounts for 87% of the matrix weight [90, 100]. Elastin is the extracellular matrix protein that imparts elastic recoil to tissues. Its crosslinked nature and extreme hydrophobicity make it one of the most stable proteins in the body [101, 102]. A contributing factor to elastin's longevity is its relative resistance to proteolysis by all but a limited number of proteinases (i.e. elastases) that are capable of degrading the mature, insoluble protein under physiological conditions [103]. In addition to collagen and elastin, some proteoglycans (i.e. dermatan-sulfate in particular) have also been identified in the pericardium as having some structural and immunologic functions similar to those found in tendons [104, 105].

The structure of the pericardium (or pericardial sac) has been studied by several groups [106-108]. Histologically, pericardium consists of three distinct layers: (i) The mesothelium is a smooth serosal layer that is designed to maintain mechanical stability while permitting changes in surface configuration. The presence of various cytoskeletal filaments in this layer provide general structural support; Actin filaments (located within mesothelial cells) in particular, participate in cellular shape changes [109]. (ii) The fibrosa contains diversely oriented, wavy bundles of fibrocollagenous tissues, nerves, blood vessels, and lymphatics. The presence of variously oriented layers of small elastic fibres and crimped collagen in this layer are believed to contribute to the stretching capabilities of the tissue. The particular patterns of fibre orientation appear to be dictated by mechanical factors, particularly external traction forces such as respiratory movements and internal pressures from changes in the

heart and the pericardial fluid [109]. (iii) The rough epicardial connective tissue contains loosely arranged collagen and elastic fibres.

Mechanically, the pericardium may be considered to be a fibre-reinforced composite material composed of collagen and elastin fibres. The mechanical properties of such materials are of paramount importance since, as in bioprosthetic heart valves, the material would have to endure dynamic loads and experience complex loading regimes, including bending. In fact, there is a general consensus that mechanical stress is a major factor responsible for valve deterioration [110]. The mechanical properties of the tissue are dependent on both the individual components as well as interactions between these components. While the largely inextensible collagen fibres serve to reinforce the tissue, the mechanical properties of the tissue include an array of features that are dependent on the complex interactions between components. Pericardium's multi-layered, multidirectional, interwoven collagen/elastin morphology is designed to transmit the biaxial forces that the tissue experiences during normal physiological function [72, 111]. Such a characteristic morphology results in at least some collagen bundles being aligned in the bioprosthetic valve leaflet's radial direction, promoting increased bending stresses and limiting the amount of shear between the fibre layers during the leaflet's flexure [112]. It is known that collagen fibres would provide a maximum tensile strength along the direction they are oriented, with the majority of fibrils arranged in the direction of stress [113]. For example, it was discovered that in tendons, where collagen fibrils are densely packed in parallel arrangements, they are capable of enduring high tensile forces (100-300 MPa). Meanwhile, in skin, where collagen fibres are arranged in many directions, a lower relative tensile strength is observed (100 MPa) [114]. Fibre diameter has also been suggested as an important determinant of mechanical properties [62]. Large diameter fibrils are thought to better sustain tensile loads as a result of increased lateral crosslinks, while creep inhibition is attributed to small diameter fibres owing to an enhanced surface area. Parry et al. [62] have hypothesized that the increased fibre surface area over which shear stress can be transmitted to the ground substance matrix or other fibres decreases the potential for creep.

Furthermore, Lee et al. [65] have discovered that significant viscoelastic energy loss observed under large deformations was believed to be a result of the shearing of the proteoglycan

matrix as the fibres were stretched. Naimark et al. [100] found that such behaviour is not observed during small deformation where the tissue displays predominantly elastic properties. Altogether, pericardial tissue possesses anisotropic mechanical properties, non-linear stress-strain responses to applied load, and viscoelastic characteristics including stress relaxation, creep and hysteresis [65, 71, 72, 115].

1.5.2 Chordae Tendineae

Chordae tendineae are fibrous strings that connect on one end to the edges of the atrioventicular valves (i.e. tricuspid on the right side and the mitral on the left side) of the heart and on the other end to the papillary muscles, small muscles within the heart that serve to anchor the valves. Chordae are very dynamic structures. With each beat of the heart, chordae stretch and relax repeatedly (~ 2×10^9 during normal life span) and hence the specific configuration of the collagen fibres must satisfy very demanding mechanical requirements to withstand these forces and ensure the proper functioning of the valves. In fact, any conditions affecting the chordae will interfere with the proper functioning of the valves, leading to such conditions as leaflet prolapse or regurgitation [116, 117].

Several microscopic studies have revealed that the structure of the chordae consist mainly of straight collagen bundles that run approximately parallel to the long axis of the chordae [118-123]. A diagrammatic representation of the structure of the chordae is provided in Figure 1.1. A single layer of endothelium (endocardium) provides coverage around the entire circumference of the chordae. Immediately underneath this layer, in the spongiosa, there are irregularly arranged fibroblasts, elastic fibres, proteoglycans and of course the collagen layers [124, 125]. Recent immunolocalization studies have indicated that collagen type I and III and as well as fibronectin can be found in the spongiosa [126]. The layer underneath the spongiosa is known as fibrosa, which consists mainly of denser collagenous bundles arranged parallel to the long axis of the chordae and with the characteristic banding patterns typical of collagen. Elastic fibres and proteoglycans were also observed in the fibrosa [124]. Proteoglycans (PGs) were also observed in the spongiosa and between the spongiosa and fibrosa, where they may have a protective function in cushioning or minimizing the friction between the two layers [124].

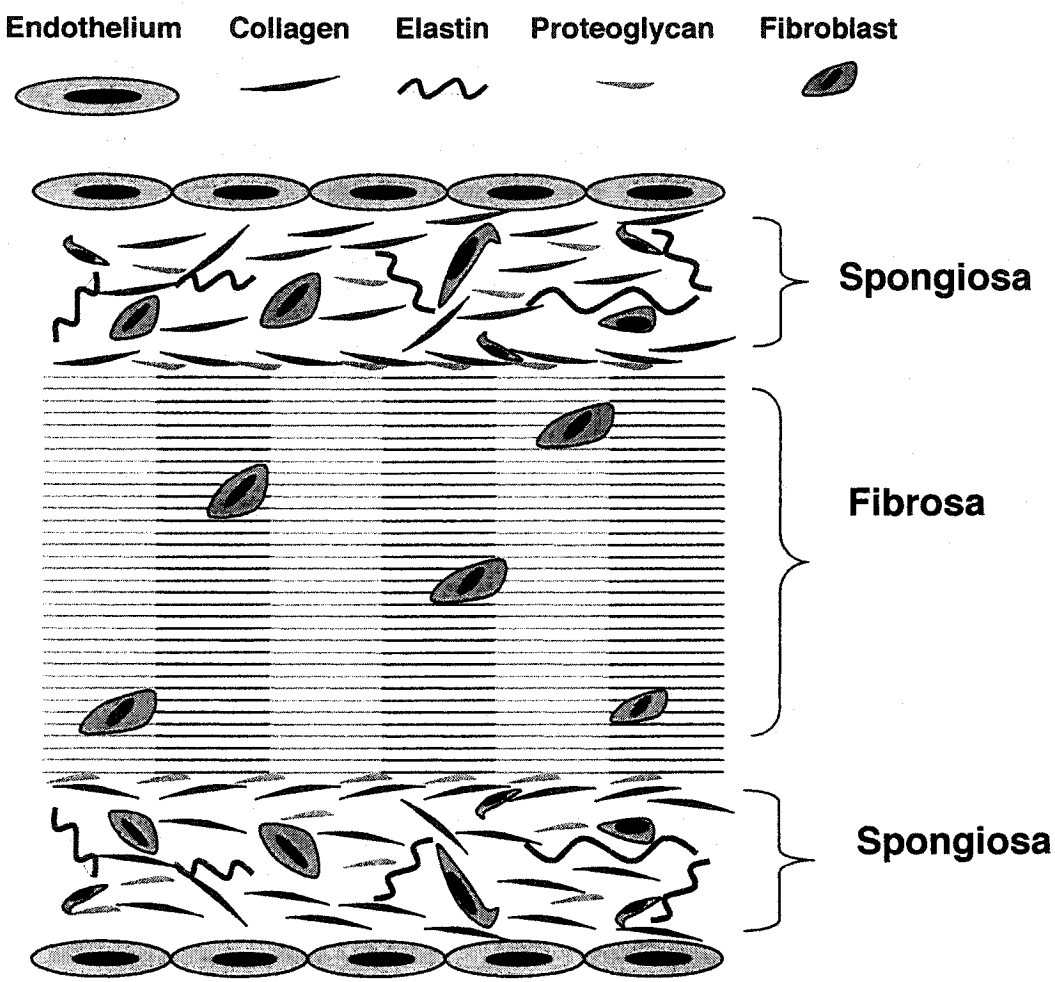

Figure 1.1. A diagrammatic cross-sectional representation of chordae tendineae. The long axis of the chorda runs left-to-right on the diagram.

Using scanning electron microscopy, Sato et al. [121] observed that while the network of collagen fibres on the surface and in the inter-surface layers exhibit a cylindrical arrangement around the longitudinal axis, those fibres in the inner core have a more "coil-like" structure. More detailed analysis of the human left chordae from various age groups, revealed the wavy pattern of collagen fibres both within and outside of the inner core [120]. Such specific architectural features of the collagen fibrils are believed to be essential to proper functioning of the chordae and may be a strong determinant of their extensibility. Furthermore, it was observed that while the wave patterns were much more organized and regular (i.e. 11 μm periodicity) in the chordae of the young subjects, aging led to a gradual change and elongation of these undulations, eventually becoming more "randomised showing an irregular broad stripped pattern" [120, 127]. Millington et al. [120] further suggested that: "the wavy arrangement of collagen surrounded by elastic fibres is very well adapted for the cyclic stresses to which the chordae are continuously subjected. It also provides a mechanism for a smooth transfer of forces to the valve leaflets efficiently protecting the structural components of the valve, which have to withstand rapidly applied forces at the systole. The undulating internal structure of the collagenous core reflects a very efficient design which has to maintain its integrity, strength and elasticity throughout the entire life of the organ" [120].

Classification and Mechanical Properties of Various Chordae Tendineae: Investigators have used different criteria to classify the chordae tendineae [128-133]. The one selected for use in this thesis is based on the points of attachment of the chordae to the valve leaflet. For instance, while the first order (or marginal) chordae insert into the free edge of the valve leaflet, the second order (or basal) chordae insert farther back, toward the annulus [116, 134]. There are also the third order chordae that extend from the papillary muscles to the ventricular wall.

The number and distribution of chordae, in both porcine and human subjects, reveals that there is an approximate a 2:1 ratio of marginal to basal insertions into the leaflets [116]. Mechanically, uniaxial stress-strain tests on both types of chordae have revealed that the marginal chordae are significantly stiffer and less extensible than the basal chordae [116,

135]. Thereby, Kunzelman et al. [116] concluded that " both the ratio of insertions and the mechanical property data suggest that the systolic pressure load on the mitral valves leaflets is supported primarily by the marginal chordae, due to their greater number and stiffness".

Berkovitz et al. [136] have studied the structural differences between the chordae supporting the mitral valve in the left side of the human heart and those supporting the tricuspid valves in the right side of the heart. Interestingly, they discovered that values for collagen fibril diameter on the left side in sheep were significantly greater than those on the right. They presumed that such differences may be related to a greater tension generated in the left side of the heart, in accordance with the maxim that in most biological tissues form follows function [136]. Moreover, they were able to demonstrate that collagen fibrils diameter in the base of the chordae was significantly higher than at the apex; possibly because of the greater force being generated in the base of the chordae versus the apex (sic.). Lim and Boughner [137] have conducted a similar type of analysis with human chordae from the left and right side of the heart and discovered that average diameter of collagen fibrils was significantly higher in left side of the heart relative to its right side. Interestingly, a more detailed analysis of the cross-sectional area of the chordae (of comparable size) revealed that the actual area occupied by the collagen fibrils in the left-side chordae was also larger than that in the right side. It was suggested that: "this difference in microstructure may be attributed to the fact that the mitral (left) chordae, being in higher pressure chamber, are subjected to greater mechanical forces. That the mitral chordae are effectively covered by collagen fibrils will enable them to withstand greater stresses than similar size tricuspid chordae" [137]. Their uniaxial stress-strain analysis revealed that tricuspid chordae was not only less extensible but also stiffer than the mitral chordae [137]. Such mechanical differences were related to the subtle structural differences that may exist between the tricuspid and mitral chordae due to chamber pressure differences.

1.6 Collagen Thermal Denaturation

1.6.1 The Basic Phenomenon

Collagen denaturation is a complex process. Despite several years of investigation, its exact molecular mechanisms are not fully understood [21, 34, 50, 91, 138-145]. Generally, thermal denaturation of the fibrous collagen is accompanied by a collapse of the helical structure of collagen in which the three chains are separated under isotonic conditions. This collapse is physically manifested as shrinkage in the direction of the longitudinal axis of the fibre [146]. Since the early 1900s, leather chemists were fully aware that the thermal and chemical treatment of various collagenous tissues would cause their shrinkage [147]. The contraction of the heat-treated collagen is attributed to the rubber-elastic properties that denaturation confers on the non-native collagen polymeric network [140]. It is known that, during the heating, collagen transforms from a near-crystalline form (right-handed superhelix) to a more amorphous gel (i.e. gelatin) with concomitant loss of birefringence and a peculiar staining behaviour with dyes (e.g. hematoxylin-eosin) [148]. Early works of Flory and Garret [149] suggested that such an unravelling phenomenon resembled a first-order phase transition involving the conversion of the crystalline triple helical collagen structure into an amorphous random coil. In other words, such a transition was very similar to the manifestation of the melting of the crystalline regions in a synthetic polymer. Further studies also led to the conclusion that the transition is an entropy-driven, multi-step phenomena [50, 140, 150, 151], and that it varies between mammalian species as well as between ages within a species [152-154].

The first step in collagen denaturation is believed to occur with the rupture of hydrogen bonds within the triple helical chains. Experimentally, the loss of these intra-chain hydrogen bonds results in a rapid rise in tension (when the fibres are held isometrically). Further heating induces partial relaxation through rupture of intermolecular heat-labile covalent crosslinks; indeed, the tension begins to decrease as temperature rises beyond 70°C over several minutes [138, 140, 155]. In reality, denaturation begins well before visible collagen shrinkage and probably before apparent microscopic architectural changes on routine

microscopy (including birefringence loss) [156]. It follows that a critical mass of fibrils must be denatured before bulk isotonic shrinkage is observed. Allain et al. [155] have confirmed that it is the number of participating molecules within the bulk-denatured extracellular matrix that results in the amount of tension and shrinkage.

1.6.2 Theories of Thermal Denaturation

As mentioned in the previous section, early work by Flory et al. [149] revealed that the thermal denaturation of the collagen resembled a melting process whereby the crystalline triple helical collagen is converted to an amorphous random coil. Indeed, the term melting is often found in the literature, suggesting the influence of the early work by Flory and his workers. During the recent years, however, Miles et al. [150, 157] have put forward a new kinetic model of thermal denaturation (also known as thermal activation model) in which the thermostability of a collagen molecule varies along its length, being weakest in an area known as the "thermally labile domain". According to this theory, an irreversible rate process governs the thermal denaturation of collagen where the denaturation is proceeding under a temperature-dependent rate constant. Consequently, it is reasonable to assume that the effect of heating on the collagen molecule can either be reversible or irreversible depending on such factors as the severity of thermal energy, the rate of its delivery and length of heating [150, 158-160]. For instance, moderate heating has been shown to result in a local unfolding within the protein that is reversed upon a return to normal temperature [150]. Such unfolding may be due to the rupturing of a small number of consecutive hydrogen bonds. Furthermore, upon severe heating, collagen may undergo a time dependent, irreversible transformation of the triple helix into a more random (coiled) structure [150]. It was suggested that such a dramatic transformation and the ensuing irreversibility was mainly related to the breakage of longer sequence of hydrogen bonds as well as heat-induced rupturing of reducible covalent crosslinks [140, 161].

These studies have led to the identification of the major thermally labile domain from which unfolding (denaturation) of the triple helix may be initiated [150, 162]. According to the thermal activation model, the collagen molecule differs in its thermal stability along its chain length [162]. It follows that the process of denaturation initiates primarily within the so-

called thermally labile regions where partial uncoupling of the individual α-chains occur [162]. In collagen type I, the thermally labile region is believed to be 65-residues in length (from 877-941), and devoid of Hyp (which readily forms hydrogen bonds that stabilize the molecule) [150, 162]. The partial uncoupling of the α-chains results in a domino-like effect where the entire structure becomes unstable and the triple helix unzips along its length [157, 162-164]. Interestingly, the presence of the Hyp is believed to reduce the length of the thermal labile domain resulting in a larger activation enthalpy (as shown by DSC) and hence serves to stabilise the collagen triple helix [165]. Interestingly, the considerable homology of the primary amino acid sequence in other fibrillar collagens (i.e. type II and III), suggests the presence of similar intermolecular interaction in the thermally labile regions of these collagen subtypes [162].

1.6.3 The Influence of Mechanical Load on Thermal Stability of Collagen

Generally collagen within a tissue is much more thermally stable than it is in solution. It is believed that collagen molecules and fibrils in various soft tissues are stabilised by molecular interactions that include covalent crosslinks (enzymatic, glycation), disulphide bonds (in type III) and interactions with proteoglycans (type II) [166]. Miles et al. [162] suggested that " the increased thermal stability of the intact fibre compared to the molecule in solution is brought about mainly by a reduction in the entropy of activation, but the precise mechanisms have not been worked out. We speculate that this is caused by a loss of configurational entropy induced by spatial confinement of the molecules within lattice of the fibre". The details of this mechanism will be discussed later.

The influence of imposed mechanical load on thermal denaturation of collagen has also been studied by a number of other investigators [149, 167-169]. Isometric mechanical loads, in general, were shown to reduce the shrinkage of a given collagenous tissue, thereby minimizing "the heat-induced damage" to the collagen structure [168, 170]. It is suggested that the application of mechanical constraints to the collagen molecule during thermal gyration may enhance the order of the α-helix, thereby decreasing the configurational entropy without interfering with heat labile bonds [19]. Furthermore, in the presence of such

constraints, collagen structure may tend to remain more organized, promoting the reformation of the triple helix during the renaturation phase [169].

1.7 Measurement of Collagen Thermal Stability

Thermal contraction has long been used as a measure of heat-induced damage to collagenous tissues [171-173]. The extent of tissue shrinkage may reveal some details about the overall condition of the crosslinks in the collagen network as well as their stability [174]. Other parameters have also been used to monitor the thermal stability of fibrillar collagen, including variations in enthalpy [151], and loss of birefringence [175]. When collagen is solubilised, changes in viscosity have also been correlated with the degree of denaturation [176, 177].

Historically, the studies of collagen denaturation fall under two categories depending on particular heating protocols used: (i) temperature jump and (ii) controlled heating rate. The application of these methodologies illustrates that while some investigators considered the thermal denaturation of collagen as an endothermic process occurring under very slow rate conditions [141], others emphasized its kinetic nature [30, 32, 171, 178]. In the temperature-jump protocol, as the name suggests, the tissue samples have been heated rather quickly (~ 1-3 seconds) to a specific temperature and maintained during the entire test period [19]. This protocol allows the evaluation of the kinetic parameters using the results of several tests conducted with different temperature jumps and, in the case of endpoint measurements, with different heating durations at each temperature [18, 29, 30, 32-34, 145, 160, 168, 179]. As such, the time and temperature are left explicitly as independent variables, thus easing the recognition of their individual characters. Nevertheless, one disadvantage of such tests may be that many tests and specimens are required to reveal fully the material response.

On the other hand, the slow and endothermic view of the thermal denaturation [140] has led to the extensive application of controlled heating rate experiments, wherein the increase in temperature occurs over time at a constant rate (1-10°C /min), and various parameters (i.e. enthalpy or force) are monitored throughout heating. Kinetic or thermodynamic parameters

are then calculated based on an assumed reaction model: e.g. first-order kinetics or equilibrium thermodynamics. Such protocols are particularly prevalent in differential scanning calorimetry and hydrothermal isometric tension tests.

1.8 The Significance of the Arrhenius Equation

Various theories of reaction kinetics can be applied to explain the thermal denaturation of collagen. As mentioned earlier, denaturation of collagen has traditionally been described as a first-order, two state chemical reaction in which the protein must overcome an energy barrier known as the "activation energy (E_a)" to go from a native state to a denatured state at some particular rate [180]. In the case of denaturation of collagen the reaction rates are related to temperature via the Arrhenius relation or absolute reaction rate theory [181]. Arrhenius suggested that the rate k at which many chemical reactions proceed depends on temperature according to the Equation 1.1:

$$k(T) = A\exp\left[\frac{-E_a}{RT}\right] \qquad \textbf{Equation 1.1}$$

where A is a temperature-independent material parameter, E_a is the activation energy, R is the universal gas constant (8.314 J/mol K or 1.987 cal/mol K) and T is the absolute temperature. If the natural logarithm of the maximum rate of reaction ($\ln k$) is plotted versus the inverse temperature ($1/T$), there will be straight line whose slope is E_a/R. From the Equation 1.1, it can be inferred that a reaction proceeds faster with larger values for T and A, or with smaller values of E_a. The significance of the Arrhenius relation remains in the fact that it can be used rather effectively to describe many temperature-dependent phenomena, including the thermal denaturation of various collagenous tissues [18, 150, 152, 180] or heating-induced cell death [182, 183].

1.9 Thermal Tests Conducted Under Controlled Heating Rate

For many years the basic idea that "collagen denaturation is an endothermic reaction which occurs at very slow rate under equilibrium conditions" [140] led to widespread use of constant heating rate protocols where the heating rate is typically around 1-10°C /min over temperatures from 15-100°C [19]. The following section reviews two important thermal tests [i.e. differential scanning calorimetry (DSC) and hydrothermal isometric tension (HIT) tests] where the controlled heating rate is particularly prevalent.

1.9.1 Differential Scanning Calorimetry (DSC)

In polymer chemistry, DSC has been one of the most common techniques used to investigate the thermal behaviour of a polymer as it undergoes a physical and chemical transformation. Equally important is the application of this technique to determine the energies of a protein folding/unfolding transformation and the thermodynamic mechanisms underlying those relations [184]. Briefly, DSC measures the heat flow necessary for heating of the sample at a constant temperature rate (°C/min) [185]. Generally, DSC can be used to calculate such thermodynamic information as enthalpy change (ΔH), entropy change (ΔS), and heat capacity change (ΔC_p) [184, 186]. The area under the curve is directly proportional to the enthalpy change, while its height is a measure of heat capacity [50]. More importantly, denaturation temperature (T_d) can be detected from either the onset or the peak of the specific heat versus the temperature plot.

During thermal transitions of proteins, there is a change in the absorption of heat, giving rise to an endothermic peak over its shrinkage temperature range [185, 187]. It was observed that the presence of crosslinks will increase both the denaturation (or shrinkage) temperature and ΔH [188]. Furthermore, it was shown that, in a highly crosslinked tissue, the peak width will decrease due to a better organization and stabilisation of the helices [188]. These interesting findings originate from a study conducted by Miles et al. [151] in which the thermal stability of rat-tail tendon in water and in 0.5 M acetic acid was compared. Treating the native collagenous tissue in acetic acid causes the tissue to swell and hence simulates the behaviour

of the collagen in dilute suspension. Their results indicated that in water the activation energy (which was almost identical to activation enthalpy) was 518 kJ/mol, the activation entropy for collagen thermal transition was 1.485 kJ/mol K and the denaturation temperature was 60°C; while in acetic acid the corresponding parameters were 1306 kJ/mol, 4.142 kJ/mol K and 37°C! These values indicated that the intact fibres in the water were more thermally stable than those in the acetic solution. According to the absolute rate theory (Equation 1.1), the stabilization of collagen in the intact fibril (relative to that in suspension) must be due to either an increase in the activation energy or a decrease in the activation entropy. Miles' results have clearly indicated that the mechanism of the thermal stability must involve a reduction in activation entropy and not an increase in activation energy [151]. This was attributed to a reduced level of intermolecular interaction that tends to stabilize collagen. It was further elaborated that: " In intact fibrils, the disorder introduced by the process of activation would be less because of the limitations on the number of molecular conformations that would be allowed by contacts with neighbouring collagen molecules".

1.9.2 Hydrothermal Isometric Tension (HIT) Tests

Heating various collagenous tissues, while held at fixed length (i.e. isometric constraint) will lead to the development of a hydrothermal isometric tension [142, 149, 189, 190]. Development of such tensions has been attributed to the process of thermal denaturation [191]. In general, an HIT test measures a change in the uniaxial force needed to maintain a tissue at a fixed length during constant heating rate (1-10°C /min) up to some sustained maximum value (e.g. 90°C [152, 153, 192]); the force increases when the tissue attempts to shrink against the fixed constraint. Briefly, as the tissues are immersed in an aqueous bath and are initially placed under an isometric constraint, the load begins to decrease (i.e. stress relaxation). The relaxation continues as the temperature is increased linearly with time (i.e. 1-10°C/min), until thermal gyration leads to the rupture of the hydrogen bonds as well as some heat-labile crosslinks within the collagen triple helix, denaturing the tissue samples and rendering them more random, globular, gelatinous and rubber-like [141, 193]. Under these conditions denaturation/shrinkage will be marked as a sharp increase in the force exerted by the tissue strip [142, 155, 192, 194]. The corresponding inflection point in the load/temperature curve is termed the denaturation temperature, T_d [192]. As the temperature

of the aqueous environment is increased above T_d, the force also continues to increase until reaching a maximum value. By around 90°C, only thermally stable, mature crosslinks remain intact to support the tension within the denatured collagen matrix [142, 155, 190]. At this point the thermally denatured collagen exhibits rubber elastic properties [193]. After reaching 90°C, the temperature is held constant (isothermal condition), and the force required to maintain the sample at fixed length begins to decrease nearly exponentially (again, stress relaxation). This relaxation has been attributed to hydrolysis of peptide bonds along the polymeric backbone of denatured collagen α-chains with slippage of chain fragments [141, 142].

The relaxation data have been analyzed using a simple Maxwell model for the decay force,

$$f(t) = f(0)\exp(-kt) \qquad \textbf{Equation 1.2}$$

where, k is the Boltzmann constant, and $t = 0$ is the beginning of the relaxation and the viscoelastic rate constant was assumed to follow an Arrhenius behaviour, as shown in Equation 1.1. Defining half-life $t_{1/2}$ of the relaxation by:

$$f(t_{1/2}) = 0.5 f(0) \qquad \textbf{Equation 1.3}$$

allows the determination of the following [141, 195]:

$$k = \ln(2)/t_{1/2} \qquad \textbf{Equation 1.4}$$

Moreover, assuming a constant temperature (e.g. 100°C) the activation energy for the stress relaxation was calculated via:

$$\ln(t_{1/2}) = \ln\left(\frac{\ln(2)}{A}\right) + \frac{E_a}{RT} \qquad \textbf{Equation 1.4}$$

That is, E_a can be calculated from the slope by plotting ln ($t_{1/2}$) versus $1/T$ [141, 195]. Using rat skin from animals of various ages (9-28 months), Le Lous found that $t_{1/2}$ increases with

age, and that this parameter depends strongly on the initial density of irreducible crosslinks. In other words, thermally stable crosslinks within the denatured network provide structural reinforcement and delay slippage, thus increasing $t_{1/2}$. This approach was also used by Naimark et al. [152] and Wells et al. [153] to study crosslinking as a function of development in bovine pericardium and ovine thoracic aorta respectively.

The most fundamental function of collagen is to provide mechanical support for the tissues and to withstand tensile stress [196]. However, as suggested in the previous section, under special circumstances (i.e. following the thermal denaturation), collagen exhibits rubber elastic behaviour [141, 193]. What is the origin of this elasticity? Generally, there are two main ways by which elastic behaviour occurs: energetic processes (i.e. internal energy) that dominate in such stiff materials as metals and concrete, and entropic processes that dominate in elastomers [197, 198]. Consistent with its microstructure, soft tissue elasticity is believed to be primarily entropic [172, 199-201]. In other words, the elasticity is governed more by changes in the conformation of the long chain molecules than by changes in inter-atomic bonds.

It is emphasized that the conformational changes from the crystalline state to the extended state (i.e. random coil), result in the contraction of the collagenous tissues [172, 202, 203]. It appears then that thermal denaturation indeed alters the configurational entropy of the tissues, hence it is not surprising that there are marked changes in mechanical properties such as extensibility, stiffness and strength [158, 204, 205]. Using strips of porcine cornea (type I collagen), Spörl et al. [205] conducted a series of uniaxial stress-strain tests at various temperatures (i.e. 35-120°C) in paraffin oil. Their results indicated that from 60–100°C there was a marked, progressive loss of stiffness and strength. Krag et al. [204] performed uniaxial tests on thin rings of human lens capsule (collagen type IV) before and after exposure to 61°C and indicated that "the capsule became slightly more extensible with increasing temperature, and that there was an increased ultimate strain, a reduced ultimate stiffness and a slightly reduced ultimate stress". Based on preceding studies, it is therefore concluded that thermal damage to the various collagenous structures will change their material properties and may make them become more rubbery.

1.9.3 Shrinkage Temperature Tests

As early as 1949, Lennox et al. [202] reported shrinkage data for sheep skin and rat tail tendon. Uniaxial tissue samples were heated at a constant rate (10°C/min) while subjected to a constant load (between 0-10 g) under different values of pH. The temperature at which the tissue began to shrink was defined as shrinkage temperature (T_s). It was shown that while hydration of the tissue samples decreased the T_s, isotonic loads increased it. The shrinkage tests can be conducted with or without any isotonic loads. Nonetheless, under both conditions the shrinkage is manifested as a sigmoidal shrinkage versus the time [166, 204, 206].

1.9.4 Shortcomings of Controlled Heating Rate Protocol

Although DSC, HIT and shrinkage tests have provided invaluable information about the thermal stability of the collagen molecule, there are limitations associated with each of these techniques. For instance, it has already been established that mechanical loads play significant roles in determining the outcome of thermal denaturation [167-169, 193, 207]. Moreover, collagen within soft tissues is in close contact with many other elements including: extracellular membranes, cells, proteins, water and ions [208]. It has been suggested, for example, that non-collagenous components (i.e. proteoglycans and structural glycoproteins) that exist in the ground substance in close vicinity of the collagen fibrils [209] may indirectly contribute to the thermal stability of the collagen by means of mechanical restraint [142, 166]. Hence, in light of these findings and the importance of mechanical loads in stabilizing the collagen molecule, it is surprising that DSC tests are performed in the absence of applied traction, indicating that these tests cannot be used to explain the combined thermal and mechanical behaviour exhibited by the native collagen molecule [19].

The issue of imposed mechanical loads is to some extent addressed in HIT protocols, in that these tests are typically run under isometric, uniaxial conditions. During the thermal transition of collagen, the deformation pattern is quite complicated and occurs both in the isometric direction along the axis of interest as well as in a lateral direction [19, 153, 155]. However, the analysis of data from HIT tests does not consider the time-dependent changes

in the lateral direction in tissues, even though anisotropy is important (i.e. pericardium and skin). Moreover, due to the multidirectional nature of some collagenous tissues, the fibres may not run in absolute axial and normal directions. Depending on the nature of the tissue sample used, the isometric constraint may not restrict the slippage of these fibres and may result in "directionality dependent chain cleavage and load transfer" [152]. More importantly, the major shortfall of both DSC and HIT is that they are both scan-rate dependent techniques and that the unfolding, and hence the measured T_d and/or T_m can vary quite dramatically depending on the heating rate [159]. This means that thermal denaturation is indeed a rate process [171, 172], and as such it could occur at a range of temperatures.

There is still much debate over whether the process of thermal denaturation is an irreversible process that can be described by first order reaction kinetics or a simple Arrhenius temperature dependence [150, 178, 210]. Leikina et al. [159] stated that "The description of denaturation of this large protein in terms of first-order reaction kinetics with single energy barrier may not be appropriate. Collagen denaturation/renaturation may also be extremely slow because complete unfolding/refolding of the helix may occur in many steps and via different pathways" [211, 212].

1.10 Temperature-jump Tests

As mentioned previously, an advantage of the temperature-jump protocol is that time and temperature are left explicitly as independent variables, thus easing recognition of their individual roles [19]. As a result, Humphrey and co-workers [19, 30, 34, 145, 160, 168] have used temperature-jump tests (both free- and isotonic shrinkage) to understand and to quantify the role of various parameters (i.e. mechanical stress, temperatures, and duration of heating) during the thermal denaturation of a given collagenous tissue. Their findings are likely the first attempt to establish a unique relationship that couples thermal and mechanical factors together in a model of a tissue is thermomechanical response.

Studies of the kinetic nature of the thermal denaturation of collagen dates back to almost sixty years ago, when Weir et al. [171] performed a series of uniaxial isotonic tests on

kangaroo tail tendon. The tissue samples (10-cm long and 1-mm diameter) were subjected to a range of temperature (58-60°C) by immersing in water and the tissues responses were examined with respect to the effect of different temperature levels, isotonic loading during heating, pH, NaCl and tissue crosslinking with formaldehyde. A cathetometer was used to measure the length of the specimen. In particular, his results indicated that while shrinkage was accelerated by increased hydration, the presence of crosslinking decelerated the process [171]. Furthermore, it was stated that "it has been found that a two degree rise in temperature results in reduction of the time required for shrinkage by a factor of 0.5" [171]. The latter finding suggests a time-temperature dependency of thermal denaturation. The shrinkage was also correlated with first-order chemical kinetics, with specific rates related to temperature via the Arrhenius relation or absolute reaction rate theory.

Chen et al. [30, 160] have confirmed these findings by conducting a series of uniaxial isothermal shrinkage tests with and without loads, wherein chordae tendineae (10 mm in length and 7.0 mm in diameter) were subjected to well-defined temperature (65, 70, 75, 80, 85 and 90°C) and load ranges (0, 100, 300, 500, and 650 kPa). Heat transfer calculations revealed that their centre line of the tissue samples reached the target temperature in approximately 1.7 seconds. It was noted that, when plotting extension (ξ) versus time (t) irrespective of loading and temperature, the behaviour of the tissues was sigmoidal (Figure 1.2). In other words, there was initially a "slow, small-shrinkage regime, then a rapid shrinkage (or transition) regime, and finally a long term, slowing shrinkage regime". Furthermore, the two intersection points, which clearly delineated the transitions from one "regime" to the next, were defined as the characteristic time constants (e.g. τ_1 and τ_2). The τ_2 was defined as the characteristic shrinkage time, which varied with load (P) and temperature (T) during isotonic, isothermal measurements of shrinkage of chordae tendineae. As Chen et al. [30, 160] indicated, a comparison of these time constants revealed that: an increase "in the temperature level always hastened the denaturation process, whereas increase in the mechanical loading during the heating delayed it". Furthermore, an Arrhenius type relation was obtained when the inverse log of τ_2 ($\ln \tau_2$) was plotted against the $1/T$ (in K); this meant that the effect of applied load and temperature level are both equally important on the kinetics of thermal denaturation and exhibit an exponential relation as shown below (Equation 1.5):

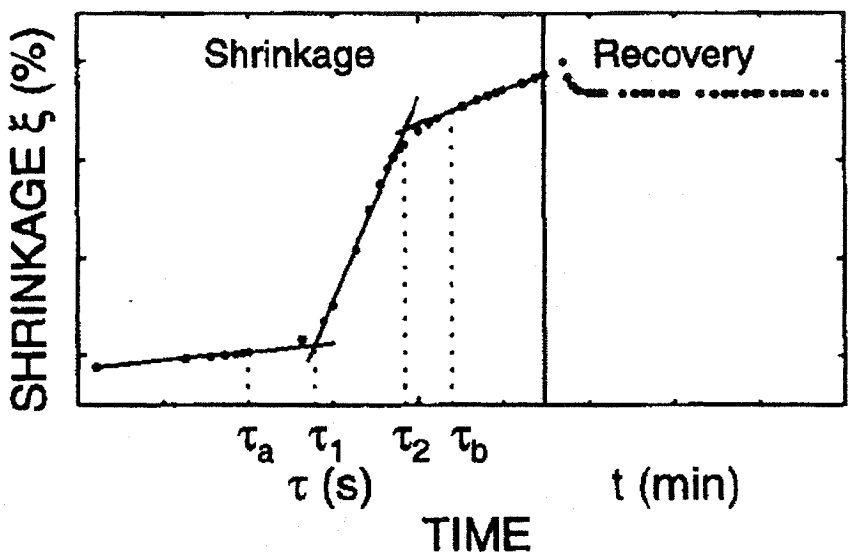

Figure 1.2 Axial shrinkage of bovine chordae tendineae under isotonic, isothermal loading. Adapted from [30, 32].

$$\tau_2(T,P) = e^{(\alpha+\beta P)} e^{m/T} = A e^{\beta P} e^{m/T} \qquad \textbf{Equation 1.5}$$

The A, β, and m are material parameters. In fact, Chen has "cautiously" concluded that since the characteristic time can be associated with the maximum rate constant, then one may wish to relate the βP term with the activation entropy and the m with the activation energy. When the regression lines of the ln τ_2 vs. $1/T$, were plotted, it was realised that the slopes (m or activation energy) of these lines hardly changed while their intercepts (activation entropy) varied with applied loads. In other words, mechanical stress applied to the tissue did not affect the activation energy of denaturation but merely delayed the onset of denaturation by decreasing the entropy difference between the ordered and amorphous states. Hence, by increasing the order of the collagen, the applied load decreased the entropy and did not affect the heat-labile bonds or (in turn) the activation energy. It was also noted that tissues with increasing degrees of "thermal damage" as indicated by the shrinkage, were progressively more extensible, compliant and had higher hysteresis [29].

More importantly, Chen's [29, 30] data suggested a time-temperature-load equivalency, which meant that a specific level of denaturation can be achieved via a multitude of combinations of temperature level, applied mechanical stress, and duration of heating provided that scaled time is the same. This is obtained by dividing the actual heating time (τ) by a temperature- and load-dependent characteristic time (τ_2) (e.g. normalizing with respect to τ_2). This collapsed the shrinkage data from all different thermomechanical tests (i.e. T and P) to a single master curve. This has important practical implications in that one may pick from multiple protocols that would achieve the outcome via different paths. Similar studies have long been conducted in polymer mechanics, where "shift factors" are often used to scale time so that viscoelastic properties at different temperatures may be superimposed to a master curve based on some arbitrary temperature [213]. Finally, Chen's analysis revealed that when tissues were cooled down to 37°C there was a "time-dependent" partial recovery in the axial length in both free shrinkage and shrinkage in the presence of isotonic loads. Also, for the first time it was shown that this recovery depends on the mechanical loads imposed during heating; the higher the load during heating, the smaller the recovery.

In their recent studies, Humphrey and co-workers [33, 34, 145] have further broadened the spectrum of their thermomechanical analyses of collagenous tissues, by constraining the tissue model (i.e. epicardium) under biaxial isotonic loads. This choice of loading originated from the fact that the soft tissues in vivo are indeed under multiaxial stress. Although both chordae tendineae and epicardium consist of type I collagen, collagen fibres in the chordae are mainly uniaxially oriented [116, 136], while in the epicardium the fibres are multiaxial, with various degree of physical entanglements, crosslinking and a wide variations in crimp [34].

The isothermal, biaxial, isotonic shrinkage tests revealed that (consistent with the uniaxial studies), epicardial shrinkage generally increased sigmoidally with heating time, and a characteristic time τ_2 revealed increases in the rate of shrinkage with higher temperature and decreases with larger biaxial loads [145]. However, although the τ_2 time exhibited an Arrhenius type response, time-temperature-load equivalency was not obtained when normalizing the time. It was suggested this might be due to two reasons: "1) time-temperature-load equivalency does not hold in biaxial setting or for particular tissues, or 2) time-temperature-load equivalency exists, but since we chose an inappropriate metric of multi-axial shrinkage, the data represent integrated effects of multiple equivalencies with different ones dominating in different cases, or the equivalency has been masked by other factors" [145]. Furthermore, the actual physical entanglement between the collagen fibres in the epicardium may alter the amount of shrinkage when compared to that seen in the chordae tendineae where such physical barriers are few [145]. Nevertheless, both isothermal uni- and biaxial isotonic tests have revealed a tremendous deal about the dynamics of collagen denaturation under temperature jump conditions.

1.11 Hypotheses

1. **The Characterization of Dynamic Mechanism(s) of Collagen Transformation**

Thermal transitions in fresh or crosslinked pericardium (PC) and chordae tendineae (CT) are multi-mechanistic in nature. The architectural differences between the PC and CT will result in unique thermal transition dynamics. Crosslinking of PC and CT by glutaraldehyde or carbodiimide (EDC) will reduce the rates of the thermal transitions.

2. **Reversibility Mechanism(s) of Collagen Transformation**

Exposure of bovine PC and CT to repeated and rapid hot-cold cycle transitions, will result in an irreversible dynamic transformation. The dynamics of thermal denaturation are dependent on tissue architecture. Exogenous tissue crosslinking will slow the dynamics of denaturation—even with repeated heating/cooling cycles.

3. **The Influence of Increased Mechanical Loads on the Dynamics of Collagen Transformation**

Increasing the mechanical loads (i.e. lowering the chain's entropy) limits the α-chains mobility in fresh and crosslinked CT, resulting in a delay of the rapid thermal denaturation.

4. **The Influence of External *Milieu* on the Dynamics of Collagen Transformation**

Due to the importance of the electrostatic interactions in stabilising collagen fibrils, the dynamics of thermal denaturation of the CT and hydrothermal stability will be reduced due to the presence of neutral salt ions, which will interfere with these interactions.

5. The Thermomechanical Stability of the Various Load-Bearing Components of the Heart

The structure—and hence the thermal stability—of collagen from various valve components in the heart will vary with the mechanical loads to which they are subjected during physiological function. The mechanical strength of equivalent-sized chordae tendineae from the left and right sides of the heart will reflect the degree of crosslinking as determined in thermomechanical testing.

2 Kinetic Characterization of Multi-Staged Thermal Denaturation of Tissue-Derived Collagen Under Isometric Constraint and Rapid Temperature Changes

2.1 Introduction

Thermotherapies have increasingly been used to treat patients with various pathological conditions. For instance, in orthopaedic surgery, mechanically deformed, lax collagenous tissues surrounding the shoulder joint (the shoulder capsule and the underlying ligaments) are thermally shrunk by means of laser or radiofrequency heating arthroscopic thermotherapy in the form of the Heat Assisted Capsular Shift (HACS) procedure [24]. In ophthalmology shrinkage of corneal collagen is performed by minimally invasive laser method such as thermokeratoplasty, to correct the corneal curvature [205, 214]. Despite promising clinical outcomes, very little is known about the underlying molecular mechanism(s) leading to such events.

Similarly, failure analyses of explanted bioprosthetic heart valves have shown evidence of progressive collagen deterioration. In vitro accelerated fatigue studies with glutaraldehyde fixed porcine aortic valve bioprostheses have shown evidence of damage to the collagen type I as indicated by changes in the carbonyl peaks of the amide I band [16]. The changes in the amide bond were interpreted as indications of collagen uncoiling (i.e. "denaturation"); Nevertheless, similar to the previous cases, the exact molecular mechanism(s) of such an event remain unclear [16].

The collagens, a family of structural proteins of the extracellular matrix, represent about one third of the total protein content of vertebrate animals [215]. At the most basic level, a collagen molecule consists of three α-chains of polypeptides arranged in a tri-helical configuration ending in nonhelical (i.e. telopeptides region) carboxyl and amino terminal, one at each end [216-218]. This secondary structure is generally maintained in an extended conformation [219, 220], and must be stabilized by both intra-molecular (within) and inter-molecular (between) interactions, since the thermodynamic preferred state (at least at the tropocollagen level) is that of a contracted, random coil conformation [172, 203, 219]. Some of the molecular forces stabilizing this extended conformation include hydrogen bonds, water-bridged crosslinks, and covalent crosslinks [172, 203, 218]. The highly ordered or "crystalline" arrangement of the molecule forms the structural basis for the relative

inextensibility and its densely organized morphology [203]. On a macro-scale, the helix-coil transition of collagen during thermal denaturation is accompanied by tissue shrinkage in the direction of primary collagen fibre orientation, resulting in changes in mechanical properties of the tissues [30, 142, 168, 221]. This phenomenon results from the sufficient absorption of thermal energy leading to the cooperative rupturing of intra-molecular hydrogen bonds [172]. Upon continued heating, the stronger covalent bonds (e.g. peptide) will eventually rupture leading to an irreversible structural transition [138, 222]. Treatment of various biological tissues with various exogenous crosslinking agents [e.g. glutaraldehyde and carbodiimide (EDC)], results in a significant enhancement of the tissue's thermal stability, as indicated by increased denaturation temperature (T_d) [94, 192].

Numerous in vitro experimental studies have been conducted to quantify and to interpret the heat-induced shrinkage of collagenous tissues [21, 30, 142, 152, 153]. Generally, these tests are classified according to a specific rate of heat delivery to the tissues, i.e.: the quasi-static (controlled heating rate) and the dynamic (temperature jump) [140, 150, 151, 155, 195]. Wright et al. [19] has suggested that "an advantage of the temperature-jump experiments is that time and temperature are left explicitly as independent variables, thus easing recognition of their individual roles". Recently Chen et al. [30, 32, 160] have published a series of studies where the heat-induced changes in the mechanics of a collagenous tissue (i.e. chordae tendineae, CT) have been studied. The kinetic nature of collagen thermal denaturation as studied by the tissue shrinkage (both under isotonic and free conditions), was demonstrated through the applicability of time-temperature-load equivalence over wide rages of temperatures.

Despite many probing investigations to date, the dynamics of collagen denaturation under isometric, isothermal, and rapid temperature changes remain unclear. In this study, using a novel temperature-jump technique, the multi-mechanistic dynamics of thermal denaturation of two collagenous tissues [bovine chordae tendineae (CT), and pericardium (PC)], under various crosslinking conditions is investigated and examined.

2.2 Materials and Methods

2.2.1 Tissue Preparation

Bovine hearts (from mature cattle) were obtained immediately after the slaughter from a local abattoir (O.H. Armstrong, Kingston, NS) and were transported to the laboratory on ice. In this study two tissue types from the bovine heart (PC and CT) were selected mainly due to their unique architectural features and differences. The left ventral surfaces of the pericardia were cleaned from any adherent fat by gently stripping off the attachments with a scalpel. Subsequently, the base-to-apex direction was marked using one suture placed at the aortic root and the other at the apex of the heart. A large rectangular section of the ventral PC (~10 cm square) was excised with sutures included and kept in a beaker containing Hanks' solution. The experimental rectangular samples measuring 0.5 mm x 2.0 mm were excised in the loading direction (base-to-apex) using a double scalpel blade.

The chordae tendineae were obtained from the same fresh bovine hearts. For this experiment all mitral chordae tendineae samples were marginal and were obtained from the left ventricular chamber of the heart. The sample length ranged from 15 to 30 mm, and the mean unloaded diameter (n = 12) was 0.89 ± 0.04 (mm) as individually measured by a digital caliper (Mitutoyo Corp.).

Both the chordae and the pericardium, were rinsed three times for 5 minutes in Hanks' solution (pH 7.4, 310 mOs), and then kept within Hanks' at 4°C until subsequent treatment with two exogenous crosslinking agents.

2.2.2 Crosslinking Procedure

Tissue samples were assigned to one of the three treatment groups: (1) Fresh, (2) glutaraldehyde (GTA) and (3) 1-ethyl-3-(3-dimethylaminopropyl) carbodiimide-hydrochloride (EDC). The glutaraldehyde-treated samples were incubated in a 0.5% by volume of glutaraldehyde at pH 7.0 in 0.1 M phosphate buffer for 24 h at room temperature

under gentle and continuous stirring condition. Upon termination of the crosslinking procedure, the tissues were washed first in Hanks' (3 x 10 min), followed by a wash in 0.1 M glycine. The glycine washing procedure was performed to inactivate any unreacted or partially reacted glutaraldehyde [223]. The EDC-treated samples were incubated in a 1.15% (w/w) with a 2:1 molar ratio of EDC to N-hydroxysuccinimide (NHS) in distilled water for 3 hr at room temperature also under gentle and continuous stirring. The EDC solution's pH was then adjusted to 5.5 by addition of 1 M HCl or 1 M NaOH during treatment. Upon termination of the crosslinking procedure, the tissues were washed in 0.1 M Na_2HPO_4 (3 x 10 min) to ensure the hydrolysis of any remaining NHS-activated carboxylic acid groups [80, 93]. The final wash consisted of a 30 minute rinse with Hanks' solution (3 x 10 min).

Following the crosslinking procedures, the crosslinked as well as the fresh samples were kept in separate beakers of Hanks' solution at 4°C. The maximum time period between tissue harvest and initiation of crosslinking treatments was approximately 24 hours.

Visual examination of both PC and CT after the fixation revealed that both tissues changed appearances. The fixation with the glutaraldehyde turned the tissues pale brown, whereas EDC-treated samples were slightly whiter than the fresh tissues. Furthermore, it was noted during the fixation that the glutaraldehyde-treated PC shrank in the plane of the tissue more than did the EDC-treated ones. The shrinkage of tissue suggested a contraction of the collagen network, which may be associated with intrahelical, interhelical, or intermolecular crosslinks introduced into the collagen fibres. Finally, unlike the EDC-treated chordae tendineae, the glutaraldehyde-treated CT appeared more or less leather-like.

2.2.3 Dynamic Hydrothermal Isometric Tension (DHIT) Testing

System Description: The two-container, quick-change temperature system developed for these experiments, allowed for the simultaneous exposure of up to six samples to near-step changes in temperature (transition time < 1 s). The DHIT consists of a stationary and a mobile module (as shown in Figure 2.1):

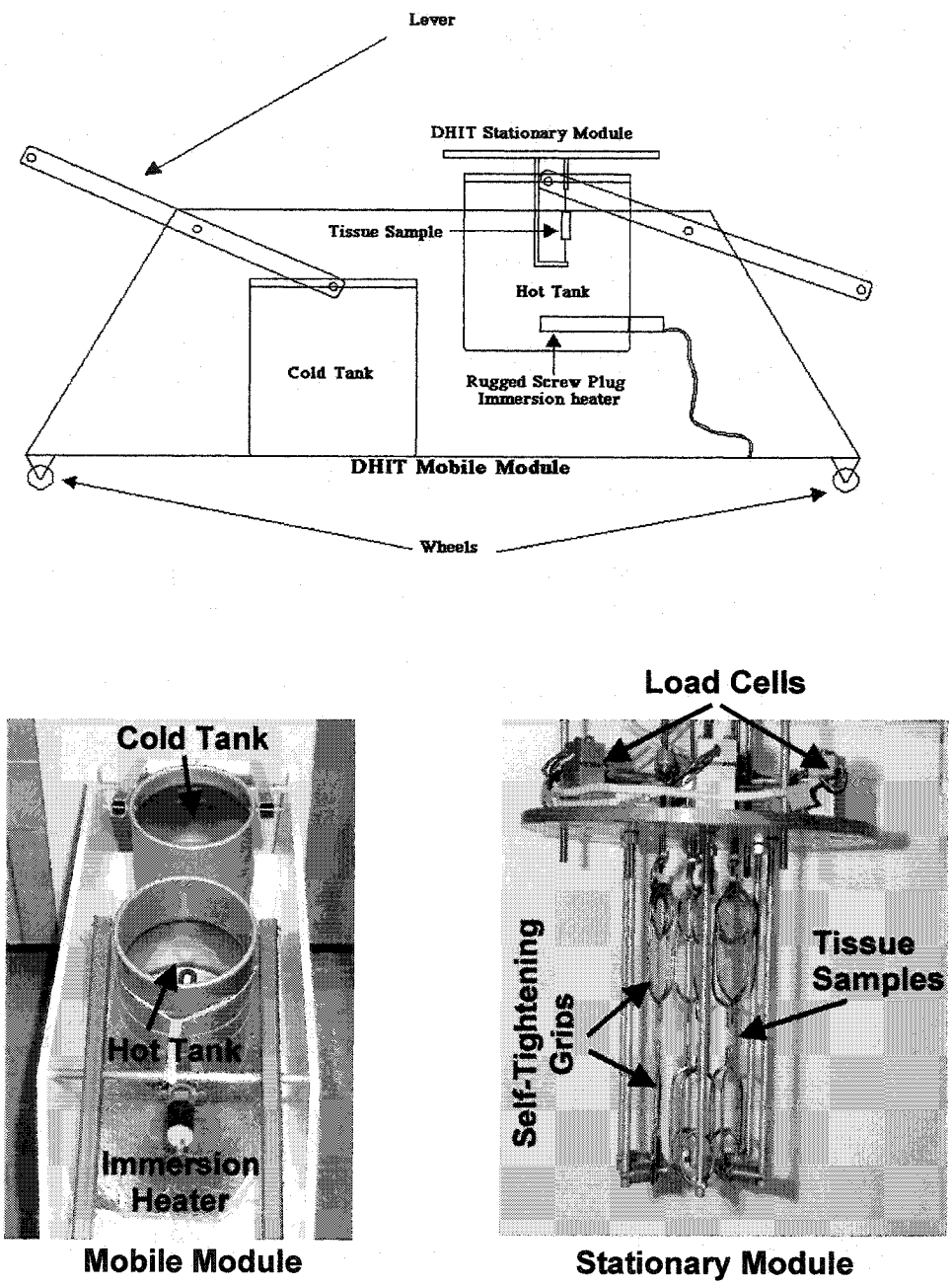

Figure 2.1 Schematic diagram and the pictures of the of Dynamic Hydrothermal Isometric Tension (DHIT) System (mobile and stationary modules).

The Stationary Module: Tissue samples were held vertically under isometric constraint between two parallel plate grips (gauge length 10 mm), while the changes in load using strain-gauged cantilever load cells were monitored. This module was essentially the same one used in our previously published thermomechanical investigations (i.e. DTT and HIT) and the full operational details were reported [192]. Similar to these studies, the mounted tissue samples were extended to yield an initial load of 50 g for PC and 30 g for CT. This extension was maintained isometrically thereafter. The variations in loads were monitored using the previously described strain-gauged cantilever load cells and associated strain gauge amplifier/conditioners [192]. The thermal monitoring was conducted using a centrally located thermistor probe interfaced with a conditioning amplifier. The analog outputs of both the strain gauge conditioners and the thermistor amplifier were acquired by a 12-bit A/D, D/A board (Model NB-MIO-16L, National Instruments, Austin, TX) in a Macintosh Centris 650 computer. Maintenance of the temperature during the isothermal period was achieved by connecting the analog output of the board to a custom-built transistor relay device which was connected in turn to a variable autotransformer (Staco Energy Products Co). To maintain the temperature at 90°C, the transformer was set at 70 % of maximum output voltage (140 V); i.e. 50 % power output. The load-temperature-time data were collected and heater control was accomplished over the isothermal period using software custom-written by Mr. Christopher Pereira under LabVIEW 3.0 software (National Instruments).

The Mobile Module: This module was designed to allow the rapid and reliable exchange of thermal energy in various tissue samples in the fastest time possible. The mobile unit resembled a carriage containing a hot and a cold stainless steel tank, with the ability to move from one side to another by virtue of four castors guided by an aluminium track. Relative to the other dynamic hydrothermal techniques [18, 29], where the temperature change in tissues occurred within 2-3 s, the DHIT unique design allowed for even faster time of transition time (< 1 s) from 25 to 90°C. To facilitate the rapid tissue transfer, a movable lever was built into each of the tanks. As such, the transferring of tissue samples (held isometrically on the stationary module) from the hot to cold tank was accomplished by lifting the tank by the lever until the water was entirely covering the tissues. At that point a hook was used to stabilise the tank in a suspended position for the entire isothermal period. Upon the end of

this period (~ 1500 seconds), the hook was disengaged, the tank was lowered and the tissues samples were subsequently removed from the stationary module. The hot tank was heated by a copper-coated rugged screw plug immersion heater (Omega Engineering Inc.), welded in the tank, and the isotherm was maintained throughout the entire length of the experiment using a transformer set at 70 % of maximum output voltage.

2.2.4 Heat Transfer Analysis

To better appreciate the thermally-induced changes taking place in both the CT and the PC, the time length for the centreline of the ideal tissue geometry (cylinder, slab) to reach 70°C was estimated. The 70°C target was arbitrarily selected since this temperature is slightly higher than the denaturation temperature for both fresh pericardium (67.7 ± 0.3°C) [192] and chordae (69.0 ± 0.4°C). The heat transfer analysis was conducted based on the principles presented by Carslaw and Jaeger [224]. They have developed heat transfer solutions for various geometric shapes (i.e. infinite slab, infinite cylinder, and sphere) and plotted the ratio of inner surface temperature (T_i) to the outer surface (T_o) temperature (T_i/T_o) of the form for normalized time-distance from the surface region to the centreline. Some assumptions were invoked. First, heat transfer was purely by conduction; convection of the fluid at the surface was ignored and the exterior was treated as a massive, uniform temperature sink. Second, both tissue samples were treated as highly hydrated structures. The thermal diffusivity (κ) for a water-saturated tissue [1.50 x 10^{-3} (cm^2/s)], was calculated by Choi et al. [225]. The mean half-thicknesses and radii for the pericardium and chordae samples was taken to be 0.22 ± 0.07 mm (n = 10) and 0.52 ± 0.02 mm (n = 63) mm respectively. Finally, since the thicknesses/radii of the samples were less than 1/10 of their lengths, it was assumed that negligible heat flow occurred longitudinally. Thus, due to the geometric symmetry of the samples, the analysis reduces to single-dimensional heat flow and has been completely solved by Carslaw and Jaeger. The desired numerical values of T_i/T_o were identified on plots supplied by the authors (0.175). Theoretically, the following parameter was obtained:

$$\frac{T_i}{T_o} = \frac{\kappa t}{\alpha^2} \qquad \textbf{Equation 2.3}$$

where, κ is the thermal diffusivity of the tissue, t is the specific time point during the heat transfer, and α is the half-thickness or radius of the sample. The specific time point (t) can then be calculated by a simple rearrangement of Equation 2.3:

$$t = \frac{\frac{T_i}{T_o}\alpha^2}{\kappa} \qquad \textbf{Equation 2.4}$$

The analysis revealed that the centreline of both pericardium and chordae would likely reach the target temperature (70°C) in 0.1 and 0.4 s respectively. The time value for CT, is in agreement with that estimated by Chen et al. who have used a somewhat different analytical heat transfer analysis to reach similar conclusions [160].

2.2.5 Data Analysis

Prior to curve-fitting, the following alterations were made to the original load-time data set: (i) the original data (thin dark line in Figure 2.2) were corrected initially to set t = 0, at first load rise, and subsequently baseline-subtracting the load prior to the temperature step. In Figure 2.2, the initial portion of data is characterized by a constant load as indicated by a horizontal line lasting for ~140 s. (ii) Following this subtraction, the data were then normalized with respect to the maximum/minimum asymptotic load and finally inverted (Figure 2.3).

The corrected raw data (thick grey line), as represented by the Figure 2.2, were used to calculate the averaged maximum stress achieved by each tissue under their corresponding treatments during the 90°C isotherm. The maximum stress was computed based on average maximum load taken from the "last" 1000 seconds of the base-line corrected load-time data during the isothermal incubation. Following the calculation of averaged maximum loads the corresponding maximum force (N) was then calculated using the Equation 2.3:

$$\overline{F}_{\max} = \overline{m}_{\max} g \qquad \textbf{Equation 2.3}$$

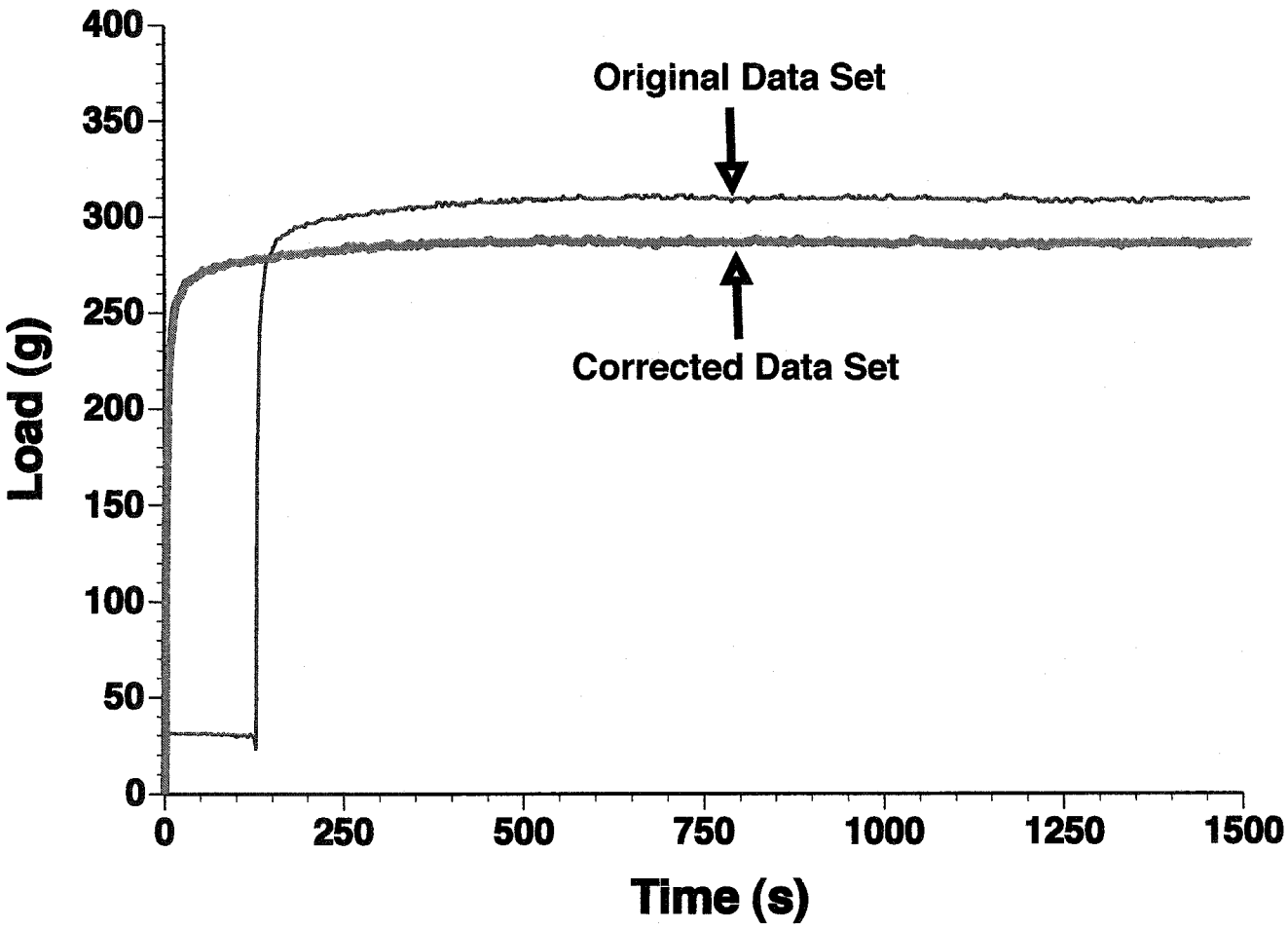

Figure 2.2 Typical load-time graph of the raw and the corrected data for the rapid thermal contraction of the different collagenous tissues under isometric and isothermal conditions.

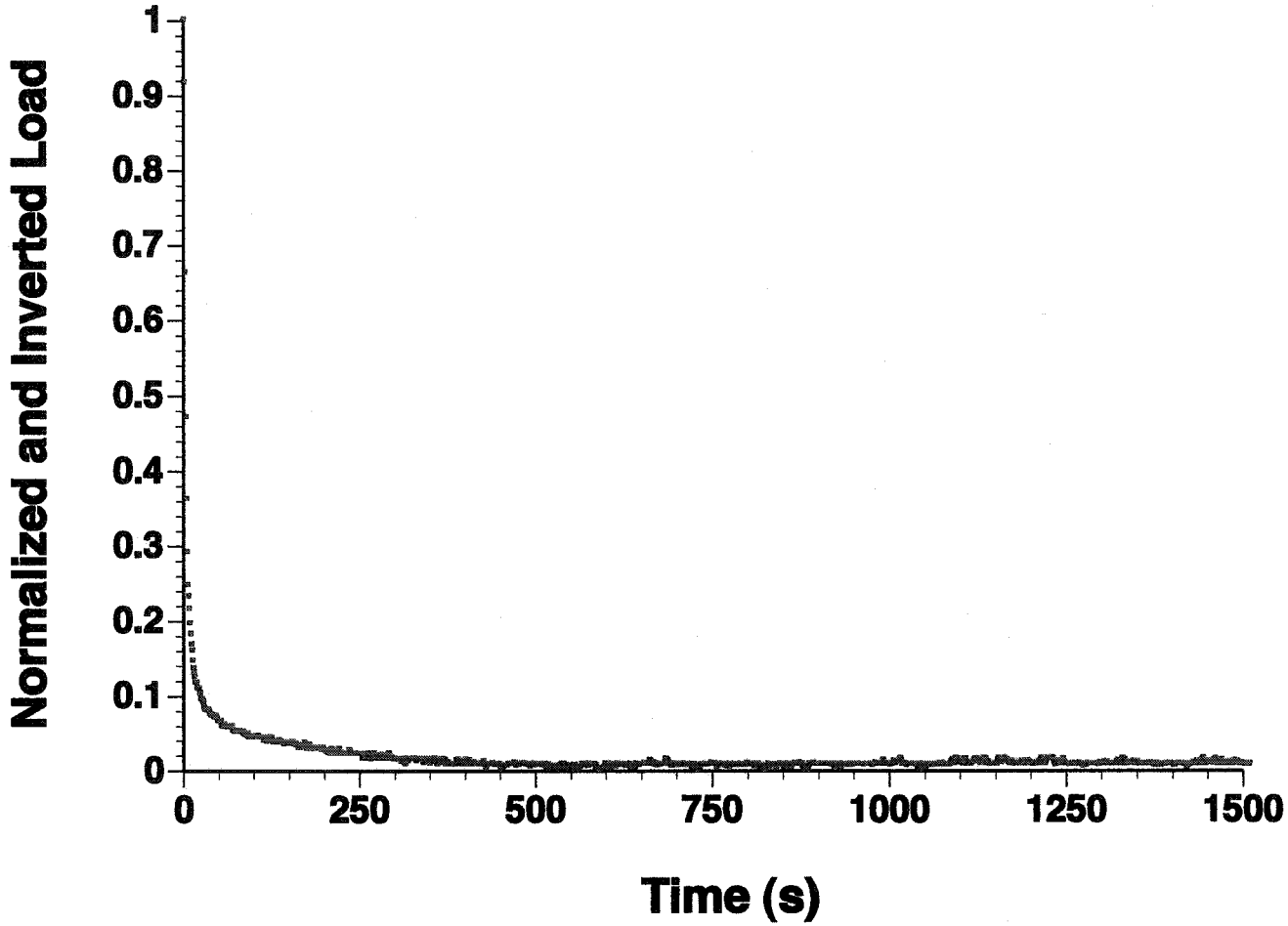

Figure 2.3 Representative normalized and inverted load-time graph during the rapid thermal contraction of collagenous tissue under isometric and isothermal conditions.

where, the $\overline{F}_{max}$ is the maximum average force (N), $\overline{m}_{max}$ is the average maximum load (kg) and g is the gravitational acceleration (9.81 m/s^2). Finally, the average maximum stress developed in each tissue sample was calculated according to:

$$\overline{\sigma}_{max} = \frac{\overline{F}_{max}}{\overline{A}} \qquad \textbf{Equation 2.4}$$

where the $\overline{\sigma}_{max}$ is the average stress (kPa), and the $\overline{A}$ is the average cross-sectional area: [width x thickness] of the PC (2.15 x 10^{-6} m^2) and [π x radius^2] CT (8.70 x 10^{-7} m^2).

The Levant-Marquardt nonlinear least squares method (DeltaGraph 5.0) was applied to the inverted/normalized data (as represented by the Figure 2.5) to identify three characteristic time constants (τ_i) and corresponding coefficients (C_i). A general three exponential model is shown in the Equation 2.5, relating the F(t) and to various time constants and the coefficients:

$$F(t) = F_{max}\left[1-\left(C_1 e^{-t/\tau_1} + C_2 e^{-t/\tau_2} + C_3 e^{-t/\tau_3}\right)\right] \qquad \textbf{Equation 2.5}$$

Here, the F_{max} is the maximum force achieved and $C_1 + C_2 + C_3 = 1$. However, the final equation that was used to fit the normalized exponential decay data, was obtained by rearrangements that were made to Equation 2.5:

$$\frac{F(t)}{F_{max}} = \left[1-\left(C_1 e^{-t/\tau_1} + C_2 e^{-t/\tau_2} + C_3 e^{-t/\tau_3}\right)\right] \qquad \textbf{Equation 2.6}$$

then,

$$\frac{F(t)}{F_{max}} - 1 = -\left(C_1 e^{-t/\tau_1} + C_2 e^{-t/\tau_2} + C_3 e^{-t/\tau_3}\right) \qquad \textbf{Equation 2.7}$$

and finally,

$$1 - \frac{F(t)}{F_{max}} = C_1 e^{-t/\tau_1} + C_2 e^{-t/\tau_2} + C_3 e^{-t/\tau_3} \qquad \textbf{Equation 2.8}$$

While single- and double-exponential models were unsuccessful, a triple-exponential model provided an excellent fit to the data from PC and CT for all tissue treatments. A representative load decay graph fitted with a three exponential model is shown in Figure 2.6. The robustness and uniqueness of the three-exponential fits was established using wide variations in the seeds supplied to the nonlinear least-squares routine. A sample calculation is provided in Appendix 1.

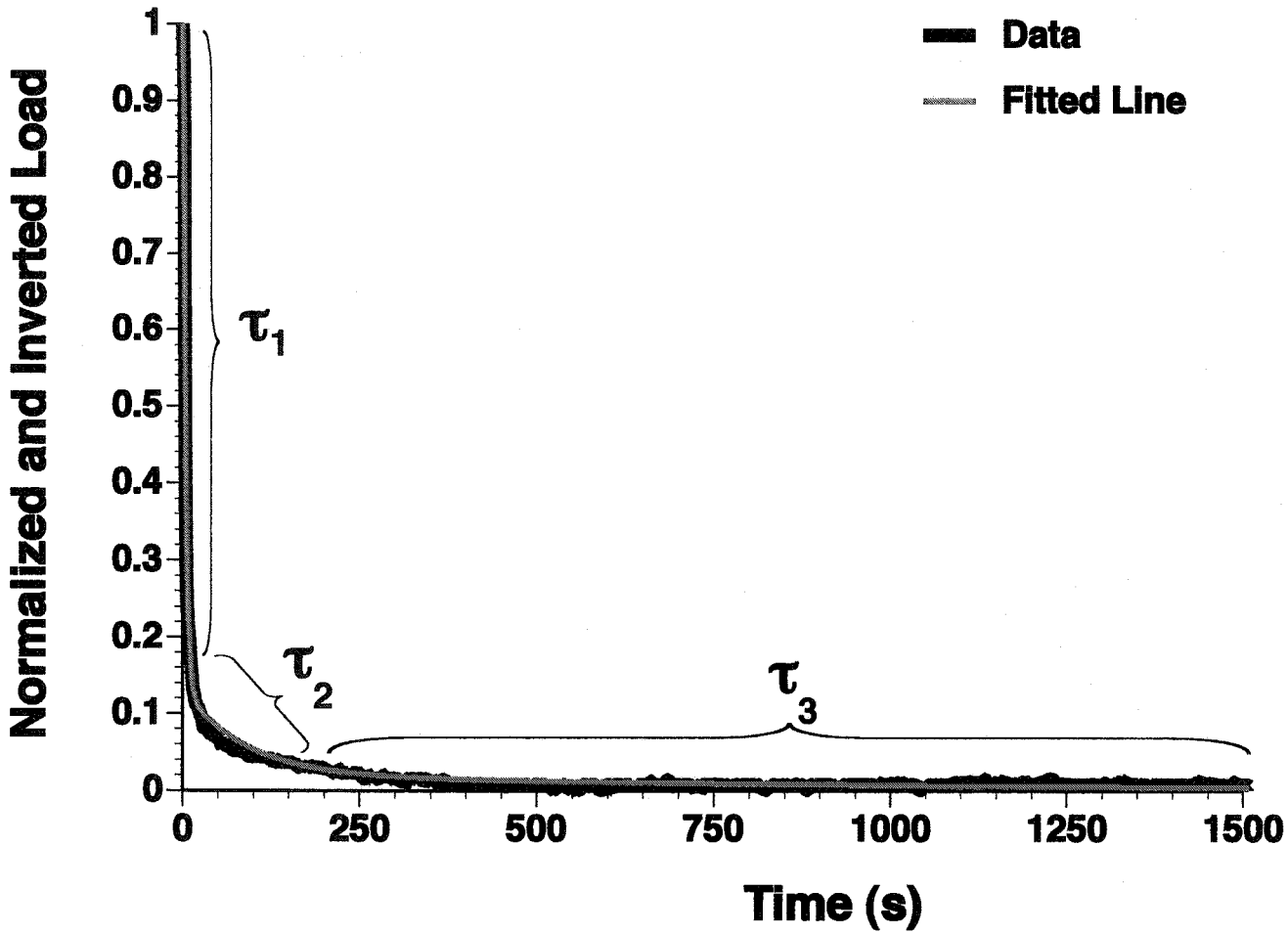

Figure 2.4 Representative graph of the normalized and inverted data set fitted with the Levant-Marquardt nonlinear least squares method, using a three exponential model to identify three characteristic time constants (τ_i) and their corresponding coefficients (C_i not shown in this graph).

2.2.6 Determination of the Denaturation Temperature (T_d)

The Denaturation Temperature Test (DTT) was used to measure the denaturation temperature *(T_d)* of the fresh chordae tendineae as well as their crosslinked counterparts. The full operational description the DTT system is discussed elsewhere [192]. The main distinguishing feature between the DTT and the DHIT is the rate of heating. In DTT, the samples are heated from the room temperature to the 95°C slowly at 1-2°C /min. Briefly the tissues samples were loaded to different levels depending on the specific tissue [PC: 50 g and CT: 30 g], and held at constant extension. As the temperature increased, the computer monitored the temperature of the bath as well the loads on the six tissues samples, and recorded these measurements at 1°C increments. The thermal denaturation of the collagenous tissue appeared as a sudden and a sharp increase in load, and this point was chosen as the denaturation temperature of the various samples [192].

2.2.7 Statistical Analysis

The time constants, coefficients as well as the maximum stress data were statistically analysed using analysis of variance (ANOVA) tests. The 2-way ANOVA were initially conducted with variables of tissue type and treatment, and the *p*-values were noted. Subsequently, more detailed individual one-way ANOVAs, with variables of tissue types (PC, CT), and different crosslinking treatments (fresh, glutaraldehyde, EDC) were conducted for each experiment. Finally, Fisher's least significant difference post-hoc tests were used to extract the individual differences (StatView 5.0.1. SAS). All data are presented as the mean ± one standard error of the mean (SEM). The minimal level of statistical significance was set at p-value < 0.05.

2.3 Results

2.3.1 Denaturation Temperature Test (DTT) Data

Figure 2.5 shows a representative diagram of the force-temperature data for fresh crosslinked chorda tendinea and its crosslinked counterpart (i.e. glutaraldehyde and EDC). The initial sections of all three curves highlights the viscoelastic nature of these tissues as indicated by an observable stress relaxation during the slow heating. Furthermore, the measurement of the denaturation temperature of the three groups (only in CT) specifies the stabilizing influence of the various crosslinkers. Crosslinking by the exogenous agents increased the denaturation temperatures significantly (p-value <0.0001) for chordae from 69.0 ± 1.0°C to 86.0 ± 0.3°C in the case of glutaraldehyde and 83.0 ± 1.0°C for EDC (Table 2.1). The denaturation temperatures for the PC were obtained from the earlier DTT investigation from our group [93]. The statistical differences between the two tissue types were established using a student t-test. It is important to note that despite structural and architectural differences, as well as the different collagen fibre arrangements in PC and CT, the T_d's were quite similar in all fresh, glutaraldehyde, and EDC-treated tissues. Finally, using an one-way ANOVA, on chordae tendineae, with crosslinking treatment as the variable of interest, suggested statistical differences among all three groups (Table 2.1).

2.3.2 Maximum Stress Rise Analysis

The maximum stress rise analyses were mainly conducted to demonstrate the differences between PC and the CT during the rapid thermal contraction, and to possibly suggest that such differences may arise from each tissue's unique architectural/structural features (e.g. collagen fibre orientation, contents and etc.) (Figure 2.6). The maximum stress rises were calculated from the "corrected load-time" curves as shown in Figure 2.2.

As shown in Figure 2.6, the one-way analysis of variance with variable of tissues type (shown by capital letters) indicated that the maximum stress rises between the pericardium and the chordal samples in each treatment group indeed changes dramatically and that this may

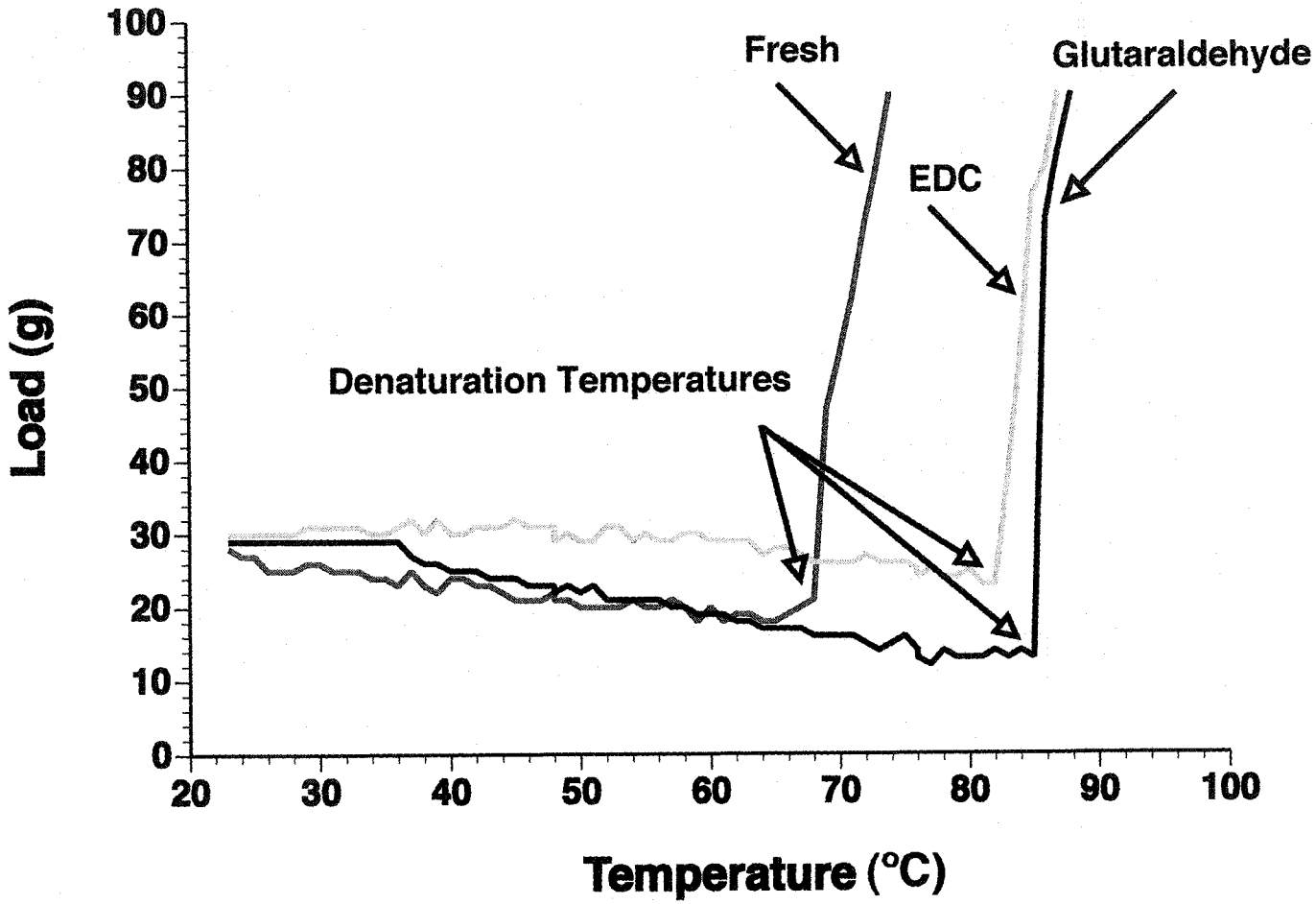

Figure 2.5 Sample force-temperature curves for fresh, glutaraldehyde-, EDC-treated bovine chordae tendineae during the DTT experiment at an initial load of 30 g under slow heating conditions. The denaturation temperature is taken as the temperature of the last point before a steady rise in force.

Treatment	Fresh	Glutaraldehyde	EDC
Chordae Tendineae	$69.0 \pm 1.0^{a,A}$ (n = 7)	$86.0 \pm 0.3^{b,A}$ (n = 5)	$83.0 \pm 1.0^{c,A}$ (n = 5)
Pericardium*	$69.7 \pm 1.2^{a,A}$ (n = 6)	$86.0 \pm 0.3^{b,A}$ (n = 6)	$85.3 \pm 0.8^{b,A}$ (n = 6)

* The DTT measurements for pericardium was previously conducted by Prof. J. M. Lee [93]

Table 2.1. Mean denaturation temperature (T_d) of the chordae tendineae and pericardium obtained via DTT tests. Values are mean ± SE, p-value < 0.05 was created by a single-factor analysis of variance with then crosslinking treatment (shown by small letter) as the variable of interest. A post-hoc Fisher's test was the conducted. To establish the statistical differences between the two tissues types, a student t-test was conducted. These differences are highlighted by capital letters. Values labelled with the same letter are not significantly different.

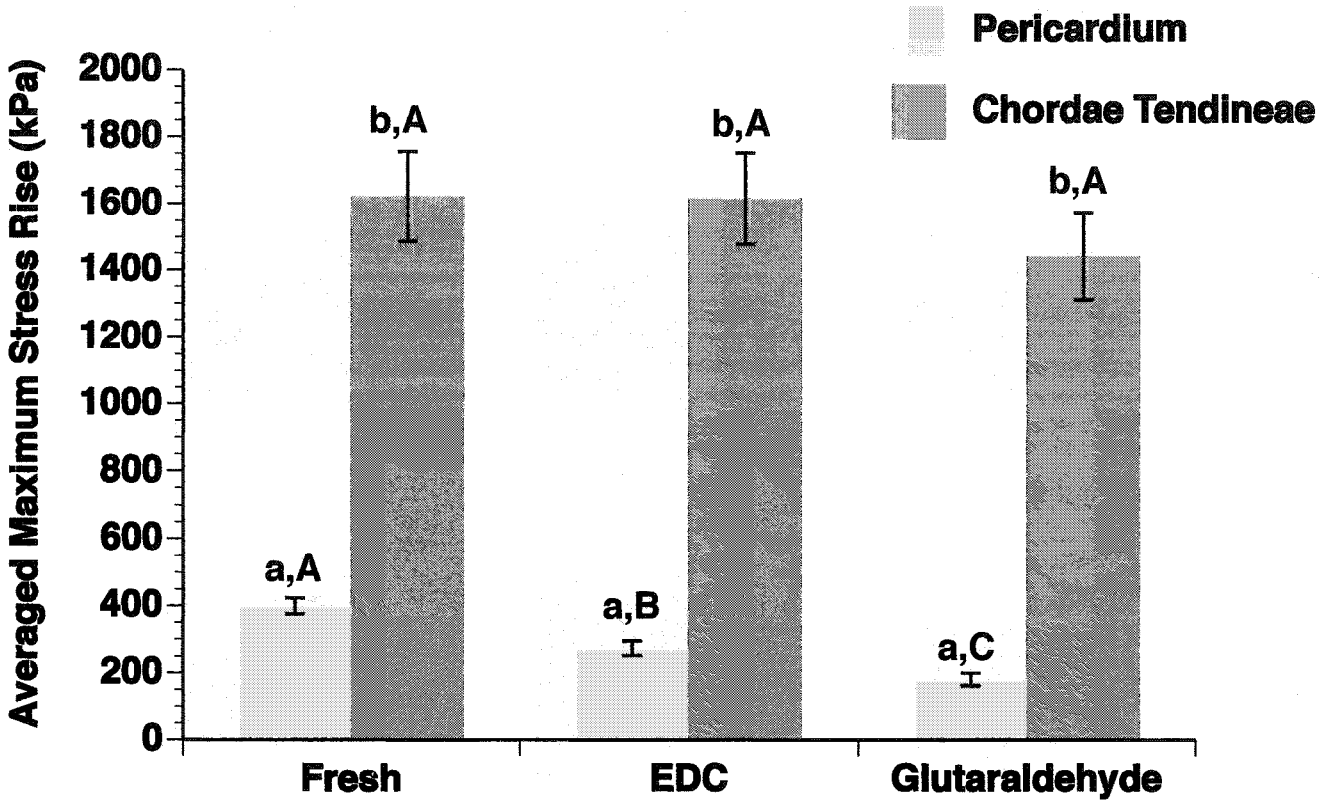

Figure 2.6 The graph of averaged maximum stress rise (kPa) developed by fresh and crosslinked pericardia and chordae tendineae. The number of samples (n) for the pericardium are as follow: fresh = 20, EDC = 14, and glutaraldehyde = 15. Similarly, the n for the chordae tendineae are follows: fresh = 24, EDC = 27, and glutaraldehyde = 23. Mean ± SE, the *p*-value: < 0.05 was created by two different, one-way analyses of variance with variables tissue types and crosslinking treatments. While the small letters corresponded to the differences in tissue type, the capital letters are differences related to the crosslinking treatments. All analyses were followed by a post-hoc Fisher's test. Values labelled with the same letter are not significantly different.

indeed be related to the architectural differences that may exist between these two tissue types. For instance, the data for the untreated samples indicate that the averaged maximum stress rise exerted by the CT (1621± 130.0 kPa) was approximately four times greater than in the PC (400 ± 2.0 kPa). Interestingly, this trend remains the same even after crosslinking with either glutaraldehyde or EDC. Another one-way ANOVA, this time, with the crosslinking treatments (shown by capital letters) as the variable of interest, indicated that while there were statistical differences in maximum stress rise among various groups in the PC, no such differences were detected in the chordal samples.

2.3.3 Characterization of the Rapid Thermal Denaturation of PC and CT Using the Triple Exponential Model

The Levenberg-Marquardt nonlinear least-square fitting method was applied to the normalized and inverted data (Figure 2.3) to analyse the multi-staged mechanisms of the rapid thermal denaturation. A triple exponential model was subsequently used to fit these data, and to characterize them based on the three time constants (Equation 2.6, Figure 2.4 and Table 2.2) as well as their corresponding coefficients (Table 2.3). This procedure was applied to all the tissue types as well as their crosslinked counterparts.

2.3.4 The Multi-Staged Nature of the Thermal Denaturation in Fresh PC and CT

Table 2.2 represents the complete time constant data for the initial (τ_1), intermediate (τ_2) and final intervals (τ_3) for both tissues and various treatments. Table 2.3 represents the data for the relative contributions (C_i) of the corresponding time constants, shown in Table 2.2. The single-factor ANOVA with tissue type as the variable interest revealed that the τ_1 value belonging to fresh PC (0.6 ± 0.1 s) is significantly smaller than that of CT (2.0 ± 0.2 s). This implied that the initial unwinding event occurred more rapidly in fresh PC than in fresh CT. A similar observation was made with the EDC group as well, but not glutaraldehyde treated samples. To analyse the role of exogenous crosslinking in altering the dynamics of rapid thermal denaturation, another one-way ANOVA was conducted, this time with crosslinking treatments as the variable interest. These analyses revealed that, for instance in

	Fresh		Glutaraldehyde		EDC	
	Pericardium	**Chordae Tendineae**	**Pericardium**	**Chordae Tendineae**	**Pericardium**	**Chordae Tendineae**
τ_1	$0.60 \pm 0.1^{A,a}$	$2.0 \pm 0.2^{A,b}$	$4.0 \pm 0.4^{B,a}$	$2.5 \pm 0.2^{A,b}$	$0.8 \pm 0.2^{A,a}$	$2.0 \pm 0.1^{A,b}$
	(n = 19)	(n = 14)	(n = 7)	(n = 15)	(n = 10)	(n = 16)
τ_2	$4.0 \pm 0.3^{A,a}$	$73.0 \pm 17^{A,b}$	$39.0 \pm 8.0^{B,a}$	$43.0 \pm 8.0^{B,a}$	$10.0 \pm 2.0^{C,a}$	$38.0 \pm 6.0^{B,b}$
	(n = 19)	(n = 14)	(n = 7)	(n = 15)	(n = 10)	(n = 16)
τ_3	$615 \pm 66^{A,a}$	$803 \pm 213^{A,a}$	$700 \pm 76^{A,a}$	$560 \pm 32^{B,a}$	$700 \pm 40^{A,a}$	$525 \pm 30^{B,b}$
	(n = 19)	(n = 14)	(n = 7)	(n = 15)	(n = 10)	(n = 16)

Table 2.2 Multi-staged nature of rapid thermal denaturation as shown by three time constants in fresh, glutaraldehyde and EDC-treated pericardium and chordae tendineae. The averaged values of time constants (τ_i) are calculated as the mean ± SE, *p*-value < 0.05, created by single factor analysis of variance (ANOVA) with two variables. The first one-way ANOVA was conducted within a given τ_i value in both tissues (e.g. Fresh τ_2 in pericardium and chordae tendineae), and second one-way ANOVA was conducted for each time constants with respect to crosslinking treatments (e.g. pericardium's τ_1 in fresh, glutaraldehyde and EDC). While the former differences are shown with small letters the latter differences are shown by capital letters. All analyses were followed by a post-hoc Fisher's test. Values labelled with the same letter are not significantly different.

	Fresh		Glutaraldehyde		EDC	
	Pericardium	**Chordae Tendineae**	**Pericardium**	**Chordae Tendineae**	**Pericardium**	**Chordae Tendineae**
C_1	$50 \pm 5.0^{A,a}$	$70 \pm 3.0^{A,b}$	$56 \pm 8.0^{A,a}$	$71 \pm 2.0^{A,b}$	$40 \pm 5.0^{A,a}$	$70 \pm 2.0^{A,b}$
	(n = 19)	(n = 14)	(n = 7)	(n = 15)	(n = 10)	(n = 16)
C_2	$40 \pm 4.0^{A,a}$	$16 \pm 2.0^{A,b}$	$28 \pm 6.0^{A,a}$	$19 \pm 1.5^{A,a}$	$34 \pm 5.0^{A,a}$	$20 \pm 2.0^{B,b}$
	(n = 19)	(n = 14)	(n = 7)	(n = 15)	(n = 10)	(n = 16)
C_3	$10 \pm 1.3^{A,a}$	$14 \pm 2.5^{A,a}$	$16 \pm 4.0^{A,a}$	$10 \pm 1.5^{A,a}$	$26 \pm 2.5^{B,a}$	$10 \pm 2.0^{A,b}$
	(n = 19)	(n = 14)	(n = 7)	(n = 15)	(n = 10)	(n = 16)

Table 2.3 Corresponding percent coefficients of fresh pericardium and chordae tendineae as well as glutaraldehyde- and EDC-treated tissue samples. These values indicate the contribution of each time constant (as shown in Table 2.2) to the entire rapid thermal denaturation process. The averaged values of coefficients are calculated as the mean ± SE, p-value < 0.05, created by single factor analysis of variance (ANOVA) with two variables. The first one-way ANOVA was conducted within a given C_i value in both tissues, and second one-way ANOVA was conducted for each coefficient with respect to crosslinking treatments. The differences among the three crosslinking treatments are shown with capital letters, while the differences between the time constants in two tissues, are shown in small letters. All analyses were followed by a post-hoc Fisher's test. Values labelled with the same letter are not significantly different.

PC while the τ_1 value of the fresh samples are significantly different from GTA, crosslinking with EDC did not have the same effect. However, if the same comparison were to be conducted in CT, no differences are observed among any groups. This may, once again, highlight the structural differences between two tissues. Finally, the significant differences among the τ_1, τ_2 and τ_3, indicate the multi-(three-)staged nature of the rapid thermal denaturation, in both tissues types and irrespective of their crosslinking treatments.

Similar types of analyses were conducted on the corresponding coefficients. These results are shown in Table 2.3. For instance, the C_1 suggests not only that τ_1 represents the fastest time constants, but also that it dominates, contributing 70% of the thermal denaturation process in the fresh CT and 50% of the fresh PC. This observation is quite noteworthy, since it may suggest that τ_1 represents the most significant time period, during which the most significant molecular changes occur to both PC and CT. As shown in Table 2.2 and 2.3, as the values for the other two time constants (τ_2 and τ_3) become larger, their corresponding coefficients (C_2 and C_3), and hence their contributions to the entire thermal denaturation process becomes smaller.

Given our experimental protocol, the current data suggest that the rapid thermal denaturation of these collagenous tissues is, at least mathematically, a three-staged event, characterized by three time constants and three coefficients.

2.3.5 *The Influence of Tissue Architecture on Altering the Dynamics of Rapid Thermal Denaturation in Fresh PC and CT*

Figure 2.6 has already shown that architectural and structural differences in the PC and CT may have contributed to the differences in averaged maximum stresses imposed during the thermal denaturation. To establish whether or not there are architectural factors influencing the dynamics of the rapid thermal denaturation, various time constants in the untreated PC and CT were compared and statistically analyzed by two-way analysis of variance. As shown in Figure 2.7, the τ_1 for PC (0.6 ± 0.1 s) and the CT (2.0 ± 0.2 s) were significantly (p-value < 0.0001) different from one another. Although the similar trend was also observed for the τ_2 in both PC and CT, no statistical differences were observed for the τ_3 values

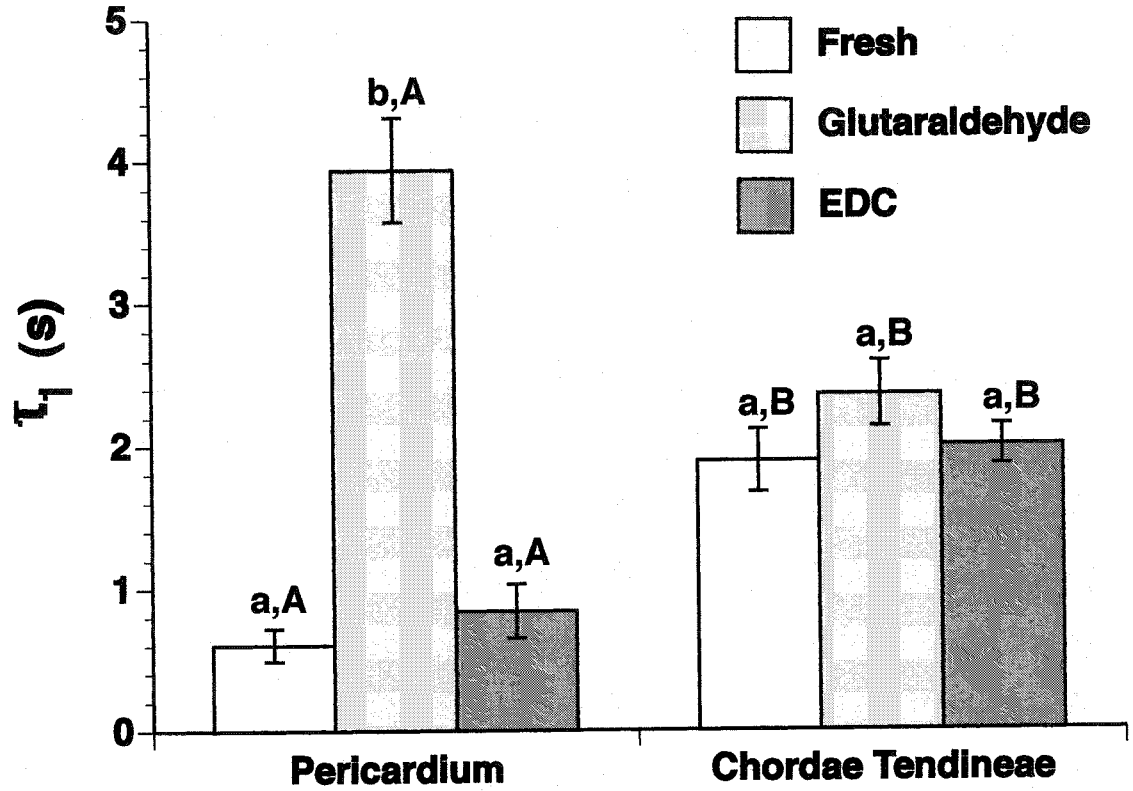

Figure 2.7 The graph of initial time constant (τ_1) for fresh, glutaraldehyde- and EDC-treated pericardium and chordae tendinea exhibit the influence of crosslinking on modifying the dynamics of the rapid thermal denaturation. The number of samples (n) f chordae tendineae are as follow: Fresh = 14, EDC = 16, and glutaraldehyde = 15. The n for the pericardium are as follow: Fresh EDC = 10, and glutaraldehyde = 7. Mean ± SE, the *p*-value: < 0.05 created by two, single-factor analyses of variance with varia tissue types and crosslinking treatments. While the small letters corresponded to the differences in crosslinking within each tissu type, the capital letters are differences with respect to the tissue types. All analyses were followed by a post-hoc Fisher's test. V labelled with the same letter are not significantly different.

(Table 2.2). Furthermore, a comparison of the coefficients also highlights these architectural differences (Table 2.3): whereas the C_1 value for the fresh PC accounts for 50 ± 5% of the thermal denaturation, the contribution is increased by a factor of 1.5 to 70 ± 3 % for the CT. As mentioned earlier, the coefficients highlighted the contribution of each time constants (τ_i) during the denaturation process. Interestingly, an analysis of the C_2 indicates that the trends have reversed during the second time period in that, unlike the τ_1, the τ_2 values make more significant contributions in PC (40 ± 4 %) rather than CT (16 ± 2 %). To further emphasize the latter point, the ratio of τ_2 /τ_1 in each tissue was calculated suggesting that while the τ_2 for the PC is only 6 times longer than the τ_1, this ratio is 36 times longer for the CT.

2.3.6 *The Influence of Exogenous Crosslinking on Altering the Dynamics of Rapid Thermal Denaturation in Fresh PC and CT*

To assess the influence of two crosslinking agents (EDC and glutaraldehyde) in modifying the multi-staged dynamics of the thermal denaturation, Figure 2.7 shows a diagram of the initial time constants (τ_1) for the untreated as well as crosslinked PC and CT. The τ_1 was selected based on its significant contribution to the entire denaturation process. Following a one-way ANOVA with crosslinking treatment as the variable of interest, our results indicated that the effect of exogenous crosslinking appears to be minimal in altering the dynamics of the denaturation, at least in the CT. This conclusion was reached based on the observation that all CT samples irrespective of their crosslinking treatments have shown similar τ_1 value (Figure 2.7). However, in the PC samples, the glutaraldehyde appears to drastically change the dynamics of the denaturation when compared to either fresh samples or the EDC treated ones (p-value < 0.0001) (Figure 2.6); however, no statistical differences were observed between Fresh and the EDC treated samples. Interestingly, the same trends are observed in the τ_2 values for both CT and PC.

2.4 Discussion

The main objective of the current study was to apply a multi-exponential model to characterize the changes that occurred during the rapid thermal denaturation of two collagenous tissues, namely bovine chordae tendineae and the pericardial sac. Our results indicated that such heat-induced denaturation under rapid thermal transitions is indeed a three-staged phenomenon and the dynamics of the thermal denaturation can be affected by such factors as tissue architecture and the exogenous crosslinking. Although many studies have been conducted on the thermal denaturation of collagen under controlled temperature rate (e.g. HIT and DSC), the exact characteristics and mechanisms of the thermal denaturation under temperature-jump conditions had yet to be determined.

To allow for such rapid temperature transitions, a mobile unit has been built in our laboratory and was added to the original Denaturation Temperature Tester (DTT) and Hydrothermal Isometric Tension (HIT) system [192]. Other rapid thermal studies have been conducted, using the uniaxial shrinkage as a metric to study the thermal denaturation of collagen and their transition time values ranged between 2-3 seconds [18, 160, 171]. Some of the most interesting analyses have been done by Chen et al. [30, 32] who have used an explicit scaling of time to quantify heat-induced shrinkage of chordae tendineae. Upon heating the tissue sample, irrespective of loading and temperature, tissue underwent shrinkage and the plot of displacement versus time, revealed a sigmoidal graph (Figure 1.2). The two intersection points which delineated the transitions from one regime to the next, were defined as the characteristic time constants (similar to our designation, τ was used to specify the various time constants. For sake of clarity and distinction, those τ used in Chen's studies will have a "c" subscript; i.e. τ_c). One of the time constants (τ_{2c}) was defined as the characteristic shrinkage time, which varied with load and temperature, during isotonic, isothermal measurements of tissue shrinkage. Furthermore, plotting the inverse log of τ_{2c} against 1/T revealed an Arrhenius type relation, further suggesting that both applied load and temperature level are equally important on altering the dynamics of thermal denaturation, exhibiting an exponential relation [160]. Furthermore, their data revealed a time-temperature equivalence for the heat-induced denaturation. The concept of time-

temperature superposition has long been used in polymer mechanics [213]. Similar to a polymeric material, the implication of time-load-temperature superposition to a collagenous tissue, is that viscoelastic properties at one temperature can be related to those at another temperature by a shift along the time axis [226]. Methodologically, Chen's experimental system was designed to perform uniaxial tests on small specimens at multiple temperatures, similar to our system. However, where as a system of buckets and levers were used in our DHIT design to transfer the tissue samples more efficiently, Chen has used a water reservoir (400 ml) where, to change the temperature required a drainage of the water and replacement with a warmer temperature solution–an inherently slower approach. Also, since the experiments were conducted under isotonic and free shrinkage conditions, the changes in strain in tissue were monitored by a CCD camera. More importantly, Chen's shrinkage studies of bovine chordae were conducted over a wide range of temperature ($65 < T < 90°C$) and loads ($0 \leq P \leq 650$ kPa). In the current study, the load used on the CT was equivalent to 470 kPa (30 g), at 90°C isotherm. Other methods such as linear birefringence have also been used to characterize the collagen denaturation on a millisecond timescale, using a pulsed Ho:YAG laser as the heat source [180]. The birefringence decay curves were fitted with a single exponential model and the heat transfer rates were estimated. It is important to note that appropriate analytical systems must be used to allow for the measurement of such rapid thermal transitions. Despite such observations the exact mechanism(s) and characterization of these events has yet to be determined.

2.4.1 Rapid Thermal Denaturation of the PC and CT is a Three-Staged Event

A triple exponential decay function (Equation 2.6) was used to fit the normalized load-time data. Such exponential models are often used in polymer chemistry to understand and characterize the viscoelastic behaviour of synthetic polymers [213]. These functions have also been used to describe the viscoelastic properties of different tissues, including: bovine femur [227], aortic valve leaflets [228, 229], and ligaments [230]. The viscoelasticity of many collagenous tissues originates from the ability of collagen fibres to rearrange and change their geometry within the viscous matrix [229]. The viscoelastic response of soft tissues is likely affected by their two most abundant components: water and collagen [231-233]. In general two types of viscoelastic response can be defined: linear and non-linear. The linear

viscoelasticity is defined as a time-dependent material behaviour where the stress response of that material depends on both strain applied and the strain rate at which it was applied. These parameters (i.e. stress, strain and their times dependencies) are described by a "constitutive equation" or a "rheological equation of state" [234]. However, in many instances and for many polymers, the theory of linear elasticity does not hold. For instance, semi-crystalline polymers do not obey the Boltzmann superposition principle even at low strains and it is found that exact loading route influences the final state of stress and strain [234]. In these instances, the mechanical properties are evaluated for the range of conditions (e.g. stress, strain, time and temperature) and a new equation is developed to explain the materials' properties. In fact, collagen type I which exists in many different kinds of soft tissues (i.e. rat tail tendon, pericardium and chordae tendineae), has been extensively investigated, and were found to exhibit a nonlinear viscoelastic behaviour [100, 235-242].

Each of the individual exponential functions (Equation 2.6) used to characterize the heat-induced changes is expected to represent a distinct or class of molecular event. The first function, as represented by the time constant τ_1, signals the rapid onset of the helix-coil transition, taking place in both collagenous tissues. In fact, τ_1 values for fresh pericardium (0.6 ± 0.1 s) and chordae tendineae (2.0 ± 0.2 s) may indicate a rapid phenomenon leading to rupturing of the non-covalent hydrogen bonds (Table 2.2). It is important to mention that these time constants measurements were conducted under current experimental setup with their associated limitations. In other words, using a different heat source as well as more accurate techniques to measure the collagen's molecular transition, it may be possible to detect an even faster structural response. In fact, when using the laser as the heat source (i.e. pulsed Ho:YAG laser), more rapid (milliseconds) structural responses were indeed measured from the structural changes occurring in the rat tail tendon [180]. Sankaran et al. [180] used linear birefringence, an optical property that results from a material's structure and composition, to study dynamic changes in tissues structure. Their findings were remarkable in that for the first time it was reported that tissue birefringence decayed rapidly (< 2 ms), and more importantly, it was found that Arrhenius-type kinetic model was not adequate to describe such rapid thermal transition.

Exactly what happens during this brief time period is the matter of speculation. Nevertheless, the experimental evidence obtained from rate-controlled studies indicated that this initial phase of thermal uncoiling may involve the rupturing of the hydrogen-bonded water bridges between the three polypeptide chains of the tropocollagen and rearrangement of the triple helix into a random configuration of α-chains [54, 149, 243]. Hydrogen-bonded water is believed to play a crucial role in the stabilization of the collagen triple helix [244] . In addition, other non-covalent bonds (e.g. hydrophobic, van der Waals, and interactions between the oppositely charged residues on side chains) may also be involved during this initial phase of thermal denaturation. Experimental evidence, using bovine tendon collagen have indicated that these non-covalent bonds (hydrogen and electrostatic bonds) begin to rupture just below 71°C, and that the covalent bonds (mostly aldimine in nature, formed between one molecule of hydroxyleucine and one molecule of hydroxyallysine) are cleaved above this temperature [245]. A similar observation was reported in human tendon [246]. Our DTT analyses are also in support of these observations, and indicated that both bovine PC and CT have a denaturation temperature around 69°C (Table 2.1).

Mechanistically, Miles et al. [150] have further hypothesized that this primary event occurs via the breaking of long sequence of hydrogen bonds (e.g., between residues 877 and 936) that stabilize the triple helix and may be more susceptible to thermal denaturation. According to the "thermal activation model", the thermal stability of collagen varies along its length and the process of denaturation starts within the so-called thermally labile regions where the partial uncoupling of the individual α-chains occurs. Energetically, these sites represent the lowest energy interactions where the denaturation may be initiated [247]. A combination of DSC and HIT studies has shed some light into the exact nature of the crosslinkages involved during the early stages of denaturation [140, 190, 209]. Most of these studies have looked into the influence of age-related changes as well as the reducible and the nonreducible crosslinks. In fact, Flandin et al. [209] have concluded that one of the first peaks that appeared in the DSC endotherm was associated with destruction of heat-labile aldimine crosslinks, which account in part for collagen stabilization. They have also concluded that these heat-labile crosslinks decrease linearly as the animal ages and are replaced by heat-stable non-reducible crosslinks [248].

The role of water in stabilization of collagen fibrils cannot be underestimated. Water plays a crucial role in governing the macroscopic properties of soft collagenous tissues [249]. Mechanically, for instance, articular cartilage and intervertebral disc materials become generally more deformable as water content is increased [250, 251]. On the other hand, dehydration in air causes tendons and ligaments to become stronger and stiffer than their moist counterparts [250, 252]. Furthermore, the viscoelastic properties (i.e. creep and stress relaxation) of a soft tissue is also influenced by its water content. Thornton et al. [253] suggested that water influences creep and stress relaxation by allowing greater interfibrillar movement with increasing water content. The importance of water molecules during the thermal transition is highlighted by the suggestion that while the thermal denaturation of collagen may be caused by the release of water molecules from the collagen, its partial renaturation may result from reformation of water bridges within the amorphous protein [169, 254]. It may therefore be suggested that water potentially plays a significant role during the early phase of the rapid thermal denaturation under isometric constraints.

To ensure the validity of the time constants and their relevance in the rapid structural transition of collagen, heat transfer calculations were conducted to assess the time within which the centre line of the tissue samples reaches 70°C. The heat transfer analyses revealed that the centreline of the tissue reached 70°C on the order of 0.1 and 0.4 seconds for PC and CT, respectively. By subtracting the first time constant (τ_1) of each untreated tissue from the corresponding heat transfer time, one may estimate the time period just prior to the thermal contraction event. This time period was estimated to be around 0.5 s for PC and 1.5 for CT. In fact, this may highlight the time period when a series of heat-labile bonds are progressively being ruptured.

Following this initial uncoiling event as represented by τ_1, the second phase may begin where the temperature has surpassed the 70°C mark, and the load curve is beginning to reach its load plateau (Figure 2.4). This transition may represent the collapse of more heat-stable crosslinks [140, 161, 255]. The time constants during this period as represented by the τ_2 suggest that the process is proceeding at a slower rate than with the first time constant, i.e. 4.0 ± 0.3 s and 73 ± 17 s, for the PC and the CT respectively (Table 2.2 and Figure 2.7). Once again such significant differences in these time values may suggest the architectural

differences that exist between the PC and CT samples. Jackson et al. [245] indeed indicated that the rupturing of even more heat-stable crosslinkages (i.e. aldimine bonds), which require more energy to cleave, occurs at temperatures above 80°C [245, 256].

Finally, the third time constant (τ_3) represents the longest time period during the dynamic thermal denaturation process in both the PC and the CT (Table 2.2). The third coefficient (C_3) (Table 2.3) associated with τ_3 indicates a very minute contribution (less than 20%) to the entire denaturation process. It has been established that the amount of thermal damage to the native collagen structure occurs in a time-dependent manner [50]. As a result, the third time constant may represent the time period when collagenous tissues sustain most of the thermal damage during the denaturation process. It is also speculated that by the end of this time period, the highly crystalline and well-ordered structure of native collagen is reduced to an amorphous gel, behaving more like a rubber-elastic material [149, 193].

Hence, the thermal denaturation of the two collagenous tissues under rapid temperature transition is indeed a multi-, three-staged phenomenon, each representing more than one molecular mechanism leading to helix-coil transitions. It is important to clarify the interpretation of these events. Although it seems that the denaturation events occur in three distinct and sequential phase in reality such transitional events may occur in a continuum. On a molecular level, this essentially implies that while the early structural changes occur as a result of alterations to the thermally weak and noncovalent bonds, eventually such changes will influence the stability of the more heat-stable crosslinks, and given the time and sustained energy level, the initiation of these two events may lead to complete unravelling of the collagen's triple helical structure. Interestingly, our characterization seems to support Miles' theory of thermal of activation [150], whereby once the α-chains in the thermally labile unit were uncoiled and uncoupled, the whole molecule becomes unstable, rapidly "unzips" and collapses to a random coil.

2.4.2 Effect of Tissue Architecture on the Dynamics of Thermal Denaturation

Our results clearly indicate, that clear distinctions exist between the thermal behaviours of the pericardium and the chordae tendineae. A closer structural examination of two tissues

may provide some explanations for the differences observed in the dynamics of the thermal denaturation. As mentioned in Chapter 1, the pericardium resembles structurally a fibre-reinforced composite material where the collagen and the elastin fibres are embedded in a highly hydrated gel (87%) known as ground substance [100]. More importantly, the orientation of the fibres within these layers suggest that they are quite loosely arranged and approximately 60° apart with variation depending on the anatomical locations [100, 108, 258, 259]. This pattern of fibre orientations is believed to play a crucial role in distributing the stress imposed on the pericardial tissue. Further analysis of bovine pericardial tissue [100] has also revealed that the collagen accounts for 75% of the dry tissue weight.

The chordae tendineae consist of two major components: an outer elastin sheath with scattered collagen and an inner core of collagen with traces of elastin [120, 127, 260]. Scanning electron microscopy analysis has shown that collagen fibres in the inner core have a "coil-like structure" and run parallel to the long axis of the chordae [120, 121, 123]. Furthermore, collagen type I constitutes the main structural components of CT, accounting for 95% of its dry weight [30, 261]; These structural features make CT a better tissue model than PC to study the thermomechanical properties of collagenous tissues.

One way of studying the current differences between the PC and CT would be to consider the collagen density and architectural arrangement of the collagen. In fact, Rasmussen et al. [262, 263], using dermis as their experimental samples, have indicated that both the collagen density and orientation play a role in determining the amount of thermal shrinkage, and that the dermis with higher density of collagens contracts more than loosely packed dermis. Such a trend has also been shown in our study. To further highlight the architectural differences between the PC and CT, the maximum stresses were calculated (Figure 2.6). These results indicate that the fresh CT samples with higher collagen density and more isotropic architecture produced 4 times more stress (1621 ± 134 kPa) than the fresh PC samples (400 ± 24 kPa), where the collagen density was less and the fibres were oriented more loosely. Nevertheless, it is thought that the uniaxial, isometric nature of our testing induces a preferential orientation of the collagen parallel to the stretching direction, imposing an artificial stability on the collagenous tissues in that direction, and decreasing their configuration entropy, thereby affecting their thermal stability. Such influence is believed to

be more prominent in CT than PC, since the collagen density is greater and the fibres are overwhelmingly oriented in a more uniaxial fashion. As presented in Table 2.2, the τ_1 values for PC and CT are 0.6 ± 0.1 and 2.0 ± 0.2 (p-value < 0.001). This means that the denaturation events occurring during the initial phase were much slower in CT *vs.* PC. The role of entropy and its influence in thermally stabilising the collagen molecule has been the subject of many studies. For instance, Na [264] and Tiktopulo [144] have discovered that that collagen molecules embedded in an organized lattice are more thermally stable than the same molecules in dilute solution. In other words, confinement of the collagen molecule within the fibre lattice reduces the configurational entropy of the molecule thereby stabilizing the collagen molecule [178]. It is therefore believed that, indeed, the arrangements of collagen fibres as well as its particular architecture in various collagenous tissues contribute to its increased or decreased thermal stability.

2.4.3 Effect of Exogenous Crosslinking on Altering the Dynamics of Thermal Denaturation

Two exogenous crosslinking agents, glutaraldehyde and EDC, were used in these experiments. Glutaraldehyde is a five-carbon, bi-functional molecule with an aldehyde group at each end of the structure that react primarily with the amine groups of Lys and/or OH-Lys of collagen to form covalent intermolecular or inter-fibrillar crosslinks [69, 70, 265]. On the other hand, 1-ethyl-3-(3-dimethylaminopropyl)-carbodiimide (EDC) is known as a zero-length crosslinker; it modifies the side groups on proteins to make them reactive with other side-groups, allowing the crosslink to be formed. In contrast to glutaraldehyde, which remains in the linkage, EDC is not incorporated into the tissue during treatment [92]. Previous studies from our research group have concluded that the EDC-treated tissue samples were significantly more resistant to solubilisation by collagenase, trypsin and CNBr than those crosslinked with glutaraldehyde [93]. It was hypothesized that EDC may in fact, penetrate the tissues more readily than glutaraldehyde, hence forming more stable crosslinks without polymerization.

The DTT results indicated that crosslinking of both PC and CT, generally increased their thermal stabilities (as shown by the T_d values) relative to the fresh tissue samples. Although,

the pericardial DTT results were obtained from another study conducted by Prof. J.M. Lee, a student t-test allowed for a comparison between the PC and CT model tissues. The comparison suggested that there was no statistical difference between either of the tissue types in a given treatment group.

Generally, the presence of the crosslinks (both endogenous and exogenous) impedes the intramolecular Brownian motions of the chain hence making the collagen more thermally (and mechanically) stable [172]. By supplying the energy in the form of heat, the kinetic energy of the polypeptide chains will eventually increase and such thermal gyration leads to the disruption of noncovalent and eventually covalent bonds [193, 266].

As was seen in fresh tissue, the three-phase thermal denaturation still existed despite the application of either of the crosslinking agents. A general trend seems to indicate that the dynamics of denaturation was slowed due to constraints imposed by various crosslinking agents. A closer examination of these trends however, indicates that significant differences in the effect of crosslinking agents in the two tissues were observed: i.e. crosslinking influenced the dynamics of the denaturation more in the PC than in the CT. Figure 2.7 and Table 2.2, represent the differences in denaturation dynamics in both tissues and the influence of crosslinking agents. Figure 2.7 shows the τ_1 values for glutaraldehyde and EDC crosslinking in PC and CT. Although no statistical differences were observed between fresh and crosslinked (EDC and glutaraldehyde) CT, more differences were observed in the PC. The τ_1 value for glutaraldehyde-treated PC samples is almost four times longer than for either fresh or EDC-treated samples. This may suggest a more effective crosslinking established by the glutaraldehyde than by the EDC.

Interestingly, other factors may account for the difference in crosslinking patterns between glutaraldehyde and EDC. For instance, in the case of EDC-treated materials, hydration level of a given tissue may contribute to higher or lower extent of crosslinking [64]. In other words, a higher hydration level of a given tissue may permit a greater accessibility of the chemical agent to the Lys, Hyl, Glu and Asp residues for their activation of modification, hence creating more crosslinkages. Furthermore, the presence of other basement membrane components (i.e. proteoglycans) than collagen in a tissue such as PC, may also increase the

number of free carboxylic groups susceptible to crosslinking by EDC [267]. Interestingly, Lee et al. [93] have also observed that despite the differences in crosslinking mechanism, EDC and glutaraldehyde-treated PC tend to behave in a similar fashion mechanically, enzymatically and of course thermally. The exact explanations for such events remain to be elucidated.

2.5 Conclusion

Using the new DHIT tests, we have developed a mathematical description of the rapid thermal denaturation of pericardium and chordae tendineae. The interpretation of this model is that the dynamics of denaturation of these collagenous tissues can be described in three phases and that each phase may represent a continual molecular change, starting with the rupture of the low energy hydrogen (noncovalent) bonds and ending with the rupture of the more heat stable bonds. We have shown that native collagen fibre orientation and arrangement may contribute to the helix-coil transition dynamics occurring under the rapid temperature change. And finally, while crosslinking alters the dynamics of the denaturation, the effect remains tissue-dependent.

3 Kinetic Characterization of the Reversibility of Thermal Denaturation of Tissue-derived Collagen Under Isometric Constraint and Rapid Temperature Change

3.1 Introduction

Over the past ten years the application of thermotherapy to treat pathological conditions in various collagenous tissues has increased. Some examples include: tissue welding [20], thermokeratoplasty [21, 268], skin resurfacing [22, 23] and treatment of joint instabilities (i.e. shoulder, knee, ankle, and hip) [24, 25]. In particular, glenohumeral instability is a common orthopedic problem, particularly in the young, active population. Shrinkage of the shoulder capsule by using thermal energy (i.e. laser or radiofrequency heating) [24, 25, 27] is considered a common arthroscopic method to treat patients with capsular injury or pathologic laxity. It is known that heating collagenous tissue results in heat-induced denaturation of the underlying collagen network of the soft tissue, leading to its eventual shrinkage [155, 269, 270]. Despite early clinical success, it appears that the major problem accounting for failure of the arthroscopic approach is excessive or recurrent laxity of the articular capsule [271]. Understanding the basic mechanism(s) of heat-induced denaturation of collagenous tissues leading to their micro-structural transformations as well as their possible underlying renaturation (i.e. reversibility) events can help to minimize the unpredictability of these clinical outcomes, and to improve their reliability.

Heat-induced denaturation of collagen has been defined as a slow and an irreversible rate-process described by first-order reaction kinetics and a simple Arrhenius temperature dependence [150, 154, 178, 272], wherein the native helical structure is transformed into a more random, coiled structure [50, 154, 272]. Leikina et al. [159] have recently conducted a series of experiments to revisit the concept of denaturation/renaturation. Using ultra-slow scanning calorimetry as well as isothermal circular dichroism, and purified collagen solutions from rat tail tendon and human lung sources, their results indicated that the thermal denaturation of collagen type I is indeed a fully reversible phenomenon, and further suggested that the use of a simple first-order reaction kinetics with a single energy barrier may not be an appropriate method to characterize the denaturation of a large and complex protein such as collagen [159].

Typically, collagen fibres are characterized by their stiffness [138]. There are, however, several other proteins (i.e. elastin, resilin, abductin and titin) [197, 273, 274] in nature that are classified as rubbery proteins, due to their high resiliency and their ability to stretch [275]. It is believed that the elastic behavior of rubbery proteins primarily originate from changes in conformational entropy, rather than the internal energy [276]. Only after heat-induced denaturation of collagen, does this otherwise stiff protein, behave as a rubber elastic material [19, 30, 141, 172]. Such significant change in collagen's material properties, may originate from a series of molecular transformations whereby a highly crystalline protein passes through various intermediate stages before it appears as an amorphous protein [171]. Lumry et al. [257] proposed a three-state model for the thermal denaturation of a globular proteins, with an intermediate state that could either refold to the native state or transform irreversibly to the denatured state. Thus, different steps of denaturation are possible and at each one the possibility of a partial or complete "renaturation" may be questioned. Earlier, Verzar et al. [277] have conducted a series of experiments where collagenous tissue (i.e. rat tail tendon fibres) held under isometric conditions, exhibited rubber-like elasticity. In other words, fibres shrank when heated (60°C) and relaxed when cooled (20°C). Interestingly, Verzar did not considered these observations as evidence of "renaturation", but rather an *interruption* of complete denaturation at a certain point. Kühn et al. [278], using an acid soluble collagen, have also shown that the thermal denaturation of collagen can be partially reversible. The conformational changes occurring during renaturation were monitored by measuring light scattering, viscosity and optical rotation. Despite these observations, the existence and the exact mechanism of thermal renaturation remain unclear.

Therefore, the research presented here is aimed to characterize the reversibility of rapidly heat denaturated bovine pericardium (PC) and chordae tendineae (CT), under isometric constraints. In this study, and similar to Chapter 2, a triple exponential model is used to analyze the heat-induced microstructural transformations of the tissues samples using the custom-made DHIT system which delivers very rapid step-heating in less than a second.

3.2 Methods and Materials

3.2.1 Tissue Harvest and Sample Preparation

Bovine hearts (from mature cattle) were obtained immediately after slaughter from a local abattoir (O.H. Armstrong, Kingston, NS) and were transported to the laboratory on ice. In this study, two tissue types from the bovine heart: (i) pericardium (PC) and (ii) chordae tendineae (CT) were selected due to their architectural differences. The left ventral surfaces of the pericardia were cleaned from any adherent fat by gently stripping off the attachments with a scalpel. Subsequently, the base-to-apex direction was marked using one suture placed at the aortic root and the other at the apex of the heart. A large rectangular section of the ventral PC (~10 cm square) was excised with sutures included and kept in Hanks' solution. The experimental rectangular samples measuring 0.5 mm x 2.0 mm were excised in the loading direction (base-to-apex) using a double scalpel blade. The chordae tendineae were obtained from the same fresh bovine hearts. For this experiment all mitral chordae tendineae samples were marginal and were obtained from the left ventricular chamber of the heart. The sample length ranged from 15 to 30 mm, and the mean unloaded diameter (n = 12) was 0.89 ± 0.04 (mm).

Both the chordae and the pericardium, were rinsed three times for 5 minutes in Hanks' solution (pH 7.4, 310 mOs), and then kept within Hanks' at 4°C until subsequent treatment with two exogenous crosslinking agents.

3.2.2 Crosslinking Procedure

Tissue samples were assigned to one of the three treatment groups: (1) fresh, (2) glutaraldehyde (GTA) and (3) 1-ethyl-3-(3-dimethylaminopropyl) carbodiimide hydrochloride (EDC). The exact details of crosslinking procedure were described in Chapter 2.

3.2.3 Dynamic Hydrothermal Isometric Tension (DHIT) Testing

The two-container, quick-change temperature system allowed for the simultaneous exposure of up to six samples to near-step changes in temperature (transition time < 1 second) under computer control. A full description as well as the operational details of the DHIT has been provided in Chapter 2. Briefly, the mounted samples were initially immersed in a 4 L stainless steel vessel (cold tank) of 25°C double-distilled water for 30 minutes and extended to yield an initial load of 50 g for PC and 30 g for CT. The DHIT system was designed for its ability to achieve rapid changes in the temperature of the specimen in a short period of time, as well as the ability to control the isothermal temperature (± 1°C). Using this system, the sample assembly was rapidly transferred into a second 90°C stainless steel vessel (hot tank), by moving the carriage via four castors guided by an aluminium track, and maintaining the isothermal temperature (i.e. 90°C) for 1500 s (heat cycle). Upon the end of this first incubation period in the hot tank, the tissue samples were rapidly transferred into the cold tank (at 25°C) and remained there for the next 1500 s of the cold cycle, still under isometric constraint. To further facilitate the tissue transfer a movable lever was built into each of the tanks. As shown in Figure 3.1, each experiment consisted of three heating cycles and two cooling cycles for a total duration of 7500 s.

3.2.4 Data Analysis:

To analyze each thermal cycle separately, the data sets were cut at specific thermal transition points (i.e. 1500, 3000, 4500, and 6000 s). Each transition point was defined as a sudden rise in the load-time graphs, which occurred due to the transfer of tissues from hot to cold or vice versa. The reversibility of the tissues samples was examined using two criteria: (i) the maximum asymptotic loads reached during the isothermal period and (ii) the use of a triple exponential model to characterize the normalized load decay. A detailed description of the analytical methodology used to curve-fit the load decay data is explained elsewhere (Chapter 2). Briefly, the analyzable data were obtained by manipulating the original load-time data set. The data for both hot and cold cycles were first baseline corrected and then normalized with

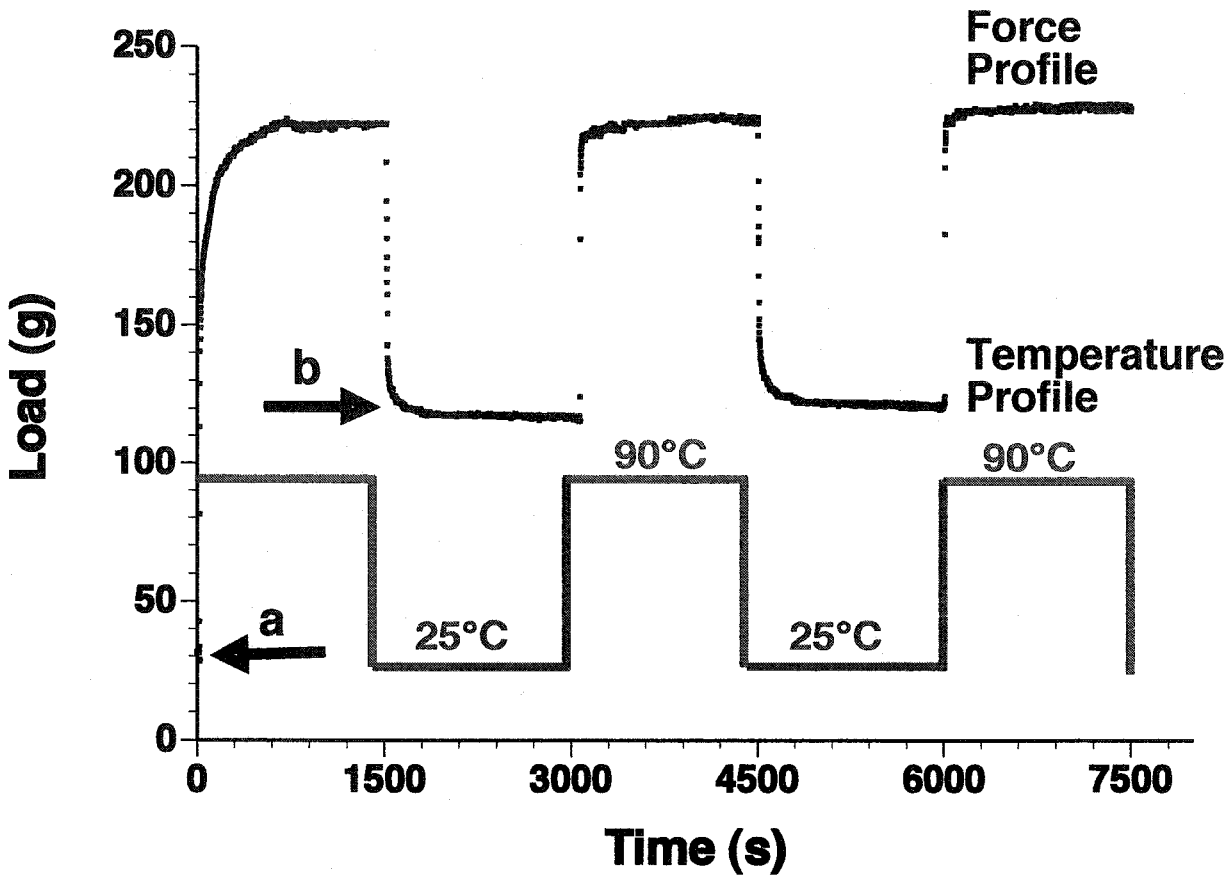

Figure 3.1 A typical raw load-time graph of a fresh bovine chordae tendineae undergoing repeated hot and cold cycles. While the graph on the top represents the raw force profile, the one at the bottom represents the corresponding thermal profile. The peaks in the force graph are evidence of tissue contraction at 90 °C isotherm for 1500 (s) and the troughs represents the tissue relaxation during the cooling cycle at 25°C isotherm. Note that the initial pre-denaturation load (as marked by **a**) does not return to its original value (i.e. 30 g), and assumes a new base value (**b**) (i.e.120 g) during the subsequent heating/cooling cycles.

respect to the maximum/minimum asymptotic load reached during each heating/cooling cycle. To maintain consistency, the normalized data for the cold cycles were inverted for analysis.

The Levant-Marquardt nonlinear least squares method (DeltaGraph 5.0) was applied to all normalized data of both cooling and heating cycles, to identify the three characteristic time constants (τ_i) and corresponding coefficients (C_i). Equation 3.1 represents the typical three exponential model used to characterize the rapid structural changes induced during the hot and the cold cycles in all tissues. This equation related the force ratio to three exponential functions:

$$1 - \frac{F(t)}{F_{max}} = C_1 e^{-t/\tau_1} + C_2 e^{-t/\tau_2} + C_3 e^{-t/\tau_3} \qquad \textbf{Equation 3.1}$$

where $C_1 + C_2 + C_3 = 1$. While single- and double-exponential models were unsuccessful, a triple-exponential model provided an excellent fit to the data from PC and CT for all tissue treatments during both hot and cold treatments. The robustness and uniqueness of the three-exponential fits for both cooling and heating cycles were established using wide variations in the seeds supplied to the nonlinear least-squares routine. An example of this procedure is provided in Appendix 1. It is important to emphasize that despite differences between the heating and cooling cycles, the 3-exponential Levant-Marquardt nonlinear least squares method proved to provide the best fit in all cases. Finally the acceptability of the triple exponential fit for both cooling and heating cycles were verified using regression coefficients (r^2).

3.2.5 Statistical Analysis

The time constants and coefficient data as well as the maximum load data were examined using either a single-factor or two-way analysis of variance (ANOVA) with variables of tissue type (PC, CT), different treatments (fresh, glutaraldehyde, EDC), and thermal cycles (heating and cooling). A Fisher's least significant difference post-hoc test was then used for multiple comparisons, to highlight individual differences (StatView 5.0.1. SAS). All data are presented

as the mean ± one standard error of the mean (SEM). The minimal level of statistical significance was set at p-value < 0.05.

3.3 Results

A series of experiments was conducted to test the following hypothesis: rapid heat-induced denaturation of two collagenous tissues (CT and PC), both fresh and crosslinked with EDC and glutaraldehyde, is a reversible phenomenon as characterized by a triple exponential model.

Figure 3.1 represents a typical raw load-time graph (top curve), and the corresponding thermal protocol (bottom curve) to which each tissue was exposed during the reversibility studies. The three peaks on the load graph are attributed to tissue contraction (under isometric constraint) during the thermal isotherms at 90°C and, similarly the two troughs are indications of tissue relaxation that occurred during the cold cycle (at 25°C). These load pattern transitions occurred in all tissues irrespective of their crosslinking treatments.

To analyze the dynamics of thermal transition and its possible repeatability as a result of exposure to the rapid hot-cold cycles, two main approaches were taken: (i) comparison of asymptotic loads in various thermal/cooling cycles and (ii) comparison of the denaturation dynamics in each thermal/cooling cycle, using the time constants (τ_i).

Briefly, the initial isometric loads (as set prior to the first heating cycle) were compared to the subsequent minimum asymptotic loads reached *after* the second and the third heating cycles. Whereas the initial isometric load was taken as a fixed value (CT: 30 g, PC: 50 g), the loads for the cooling cycles 1 and 2 were calculated as an average of 500 data points during the cooling isotherms. The main load criterion for the repeatability was based on similarity and ideally the absence of any statistical differences between the two thermal cycles. The repeatability based on the dynamics of denaturation on other hand, relied on the mathematical parameters obtained from the 3-exponential model used to fit the normalized load-time data, and comparing the characteristic time constants (τ_i) and their corresponding coefficients (C_i) for each tissue sample under the segmental heating/cooling regimens.

3.3.1 Reversibility Based on Isothermal Load

A closer look at the top diagram in Figure 3.1 reveals that the heat-induced rapid thermal transition of the PC and CT was only partially reversible upon re-immersion into the colder temperature. The asymptotic loads during cooling cycles 1 and 2 never returned to the values set prior to heat cycle 1. Therefore, solely based on this simple observation, it appears that following the first heating cycle, both collagenous tissues (PC and CT) have undergone significant and irreversible microstructural changes due to thermal denaturation process, perhaps altering the native collagen structure into a more rubber elastic material.

To further investigate these preliminary observations and more detailed analyses of the loads were conducted. A single-factor analysis of variance was conducted to establish if there were significant statistical differences between each of the thermal cycles in each tissue. Figures 3.2-3.4 represent the initial/relaxed asymptotic loads in fresh, EDC and glutaraldehyde treated PC and CT respectively.

Figure 3.2 is the initial/relaxed bar plots for the fresh PC and CT. This diagram showed that, in both CT and PC, the averaged cooling cycle asymptotic loads did not return to the initial load values (i.e. PC: 30, and CT: 50 g). In fact, the pre-denaturation loads were significantly lower from the asymptotic loads in cooling cycle 1 and 2 (p-value < 0.0001). More importantly, the asymptotic load values were not significantly different in either the PC or the CT, during the cooling cycles 1 and 2. Hence, subsequent to this first irreversible heating cycle, both collagenous tissues reversibly contract and relax upon heating and cooling respectively. Such behaviour is attributed to the rubber elasticity of the tissues samples following the thermal denaturation event: undergoing thermoelastic contraction with heating and relaxation with cooling.

Similar analyses were conducted on both EDC and glutaraldehyde-treated PC and CT. Generally, the crosslinking of both tissues with either of the exogenous agents significantly altered the features of the denaturation, as indicated by lower asymptotic loads during the cooling cycle 1 and 2 (Figures 3.3, and 3.4). Statistical analysis revealed that, in general, exogenous treatments of PC and CT with either EDC or glutaraldehyde, led to an overall

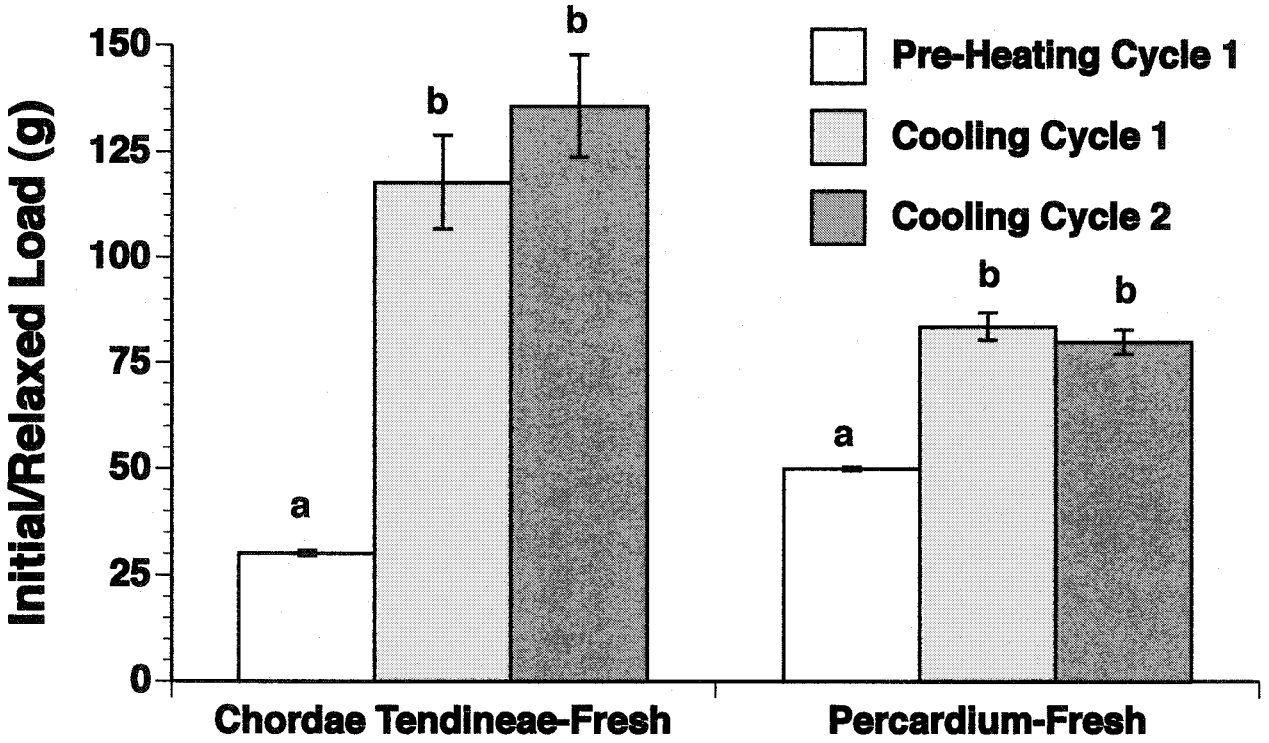

Figure 3.2 Comparative bar graphs of the averaged initial/relaxed loads of fresh bovine chordae tendineae and pericardium prior to the rapid thermal denaturation (white column), and subsequently after cooling cycles 1 and 2 (light grey and dark grey bars respectively). Note that the loads never return to the pre-denaturation value, but that there is load reversibility between cooling cycles 1 and 2. The number of samples (n) for chordae tendineae and pericardium are 26 and 15 respectively. Values shown are mean ± SE, the p-value < 0.05, was created by single-factor analysis of variance with variable of cycle numbers, followed by Fisher's test. Within each tissue group, values labelled with the same letters are not significantly different.

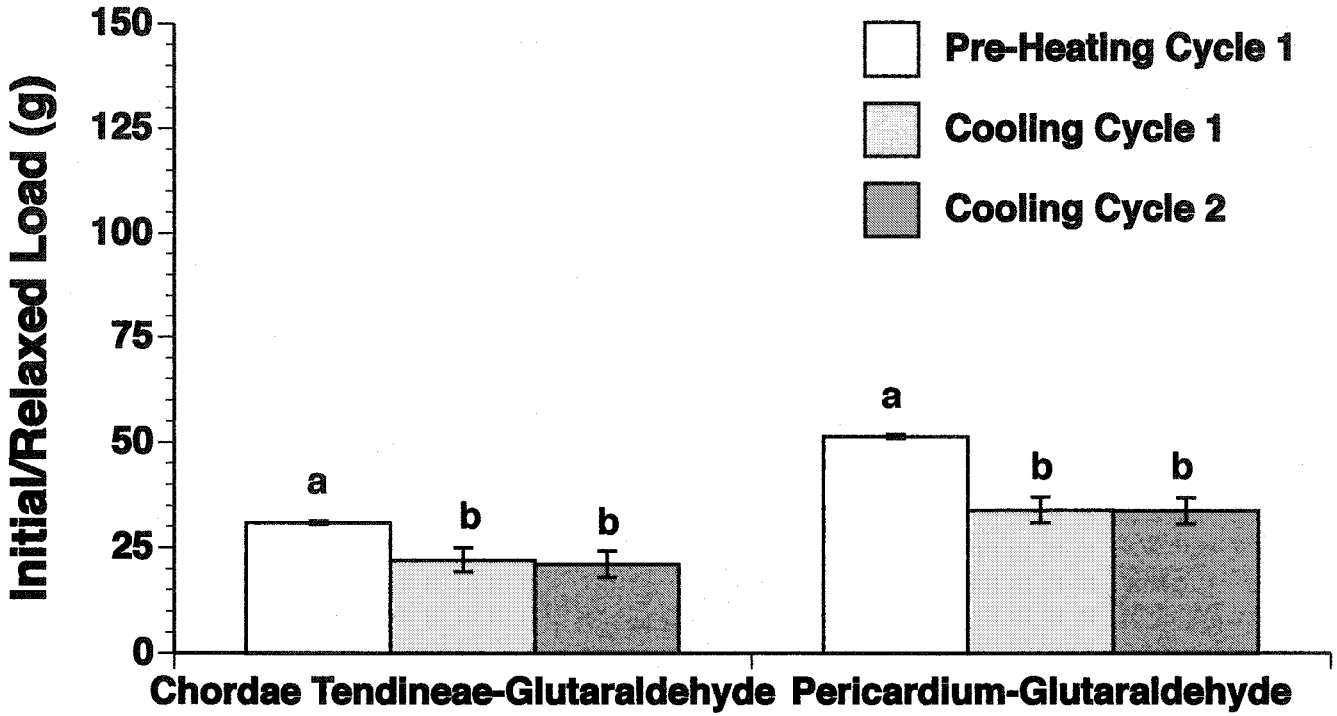

Figure 3.3 Comparative bar graphs of the averaged initial/relaxed loads of glutaraldehyde-treated bovine chordae tendineae and pericardium prior to the rapid thermal denaturation (white column), and subsequently after cooling cycles 1 and 2 (light grey and dark grey bars respectively). Note that the loads never return to the pre-denaturation value, but that there is load reversibility between cooling cycles 1 and 2. The number of samples (n) for chordae tendineae and pericardium are 20 and 17 respectively. Values shown are mean ± SE, the p-value < 0.05, was created by single-factor analysis of variance with variable of cycle numbers, followed by Fisher's test. Within each tissue, values labelled with the same letters are not significantly different.

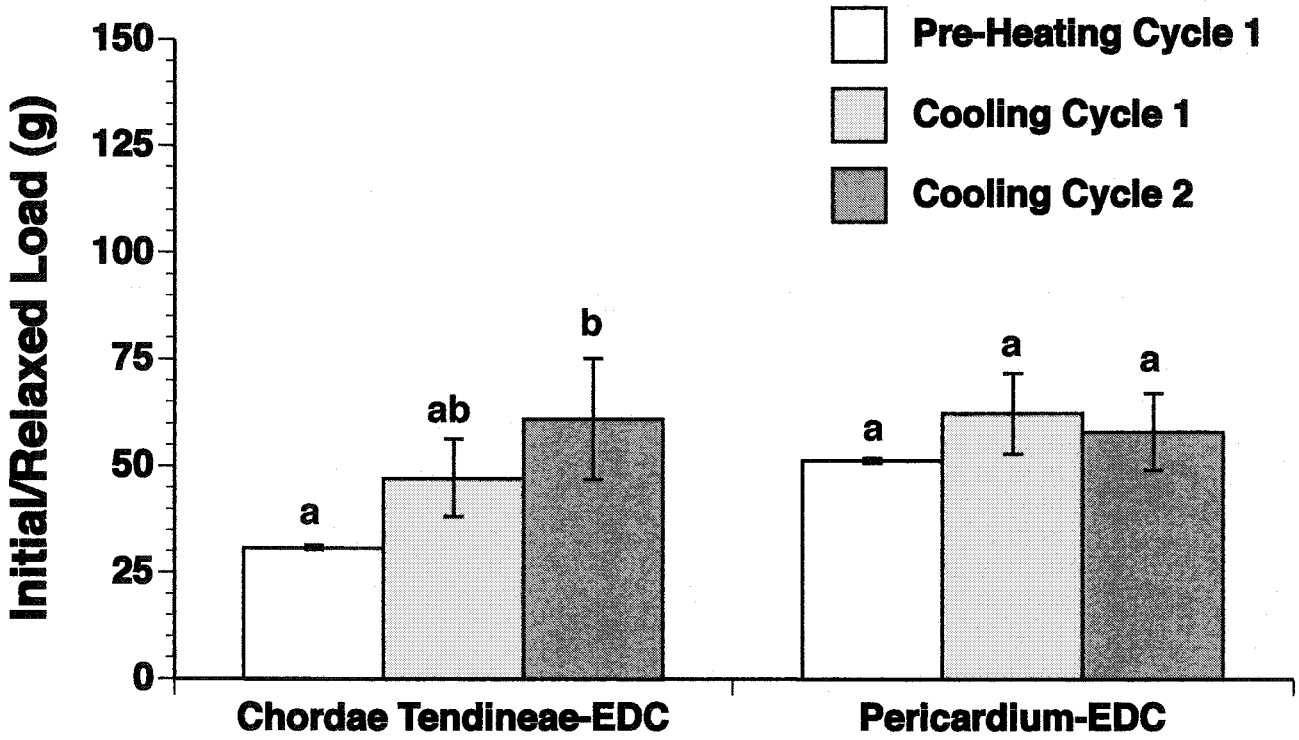

Figure 3.4 Comparative bar graphs of the averaged initial/relaxed loads of EDC-treated bovine chordae tendineae and pericardium prior to the rapid thermal denaturation (white column), and subsequently after cooling cycles 1 and 2 (light grey and dark grey bars respectively). Note that unlike glutaraldehyde-treated tissue there is reversibility in EDC-treated PC in all three bars. The number of samples (n) for chordae tendineae and pericardium are 16 and 13 respectively. Values shown here are mean ± SE, the p-value < 0.05, was created by single-factor analysis of variance with variable of cycle numbers, followed by Fisher's test. Within each tissue group, values labelled with the same letters are not significantly different.

decrease of asymptotic loads relative to the fresh tissue samples (p-value < 0.0001) in both cooling cycles. More detailed analyses indicated that the extent of the load differences appear to be dependent on tissue types and crosslinking treatments. The lack of any statistical differences in asymptotic loads during the cooling cycles 1 and 2 in each crosslinked tissue may indicate that the crosslinking influence persists after a single or even after consecutive heating cycles in both PC and CT. These analyses were also conducted using a single-factor (i.e. thermal cycles) analysis of variance. Interestingly, the only exception was the EDC-treated PC where the absence of any statistical differences among any of the groups, may suggest complete load repeatability in all heating cycles.

Another important of aspect of this study was to compare the differences in asymptotic loads between two tissues, in a given thermal cycle. However, since the DHIT protocol required a different set of starting loads for each tissue (i.e. PC: 30, and CT: 50 g), the variation in loads were expressed in terms of changes in the relaxed asymptotic loads in each thermal/cooling cycles. For each tissue type and treatment, three parameters based on asymptotic load differences were defined. This included differences between (i) initial load and first cooling cycle relaxed asymptotic load, (ii) initial load and second cooling cycle relaxed asymptotic load and (iii) first and second cooling cycles relaxed asymptotic loads. While the comparison between the initial and cooling cycles 1 and 2 are shown in Figures 3.5-3.7, the differences between the first and second cooling cycles are shown in Figure 3.8. The statistical differences were established using a one-way analysis of variance method, with thermal cycles (Figures 3.5-3.8) and tissue types (Figure 3.8) as the variables of interest.

Generally, Figures 3.5-3.7 indicated that the differences between the initial loads and the subsequent asymptotic loads obtained in either cooling cycle 1(white column) or 2 (light grey column), were large and more importantly not statistically different from one another. These large differences in load simply suggest there is no repeatability between the load values set prior to the first thermal denaturation event and those obtained during the cooling cycles 1 and 2. Furthermore, a comparison of these load changes in CT versus PC suggested that such effects are more pronounced (p-value < 0.0001) in the latter than the former tissue. This may be contributed to the architectural differences between the two tissues. Interestingly, a comparison of the relaxed load changes in the crosslinked tissues versus the

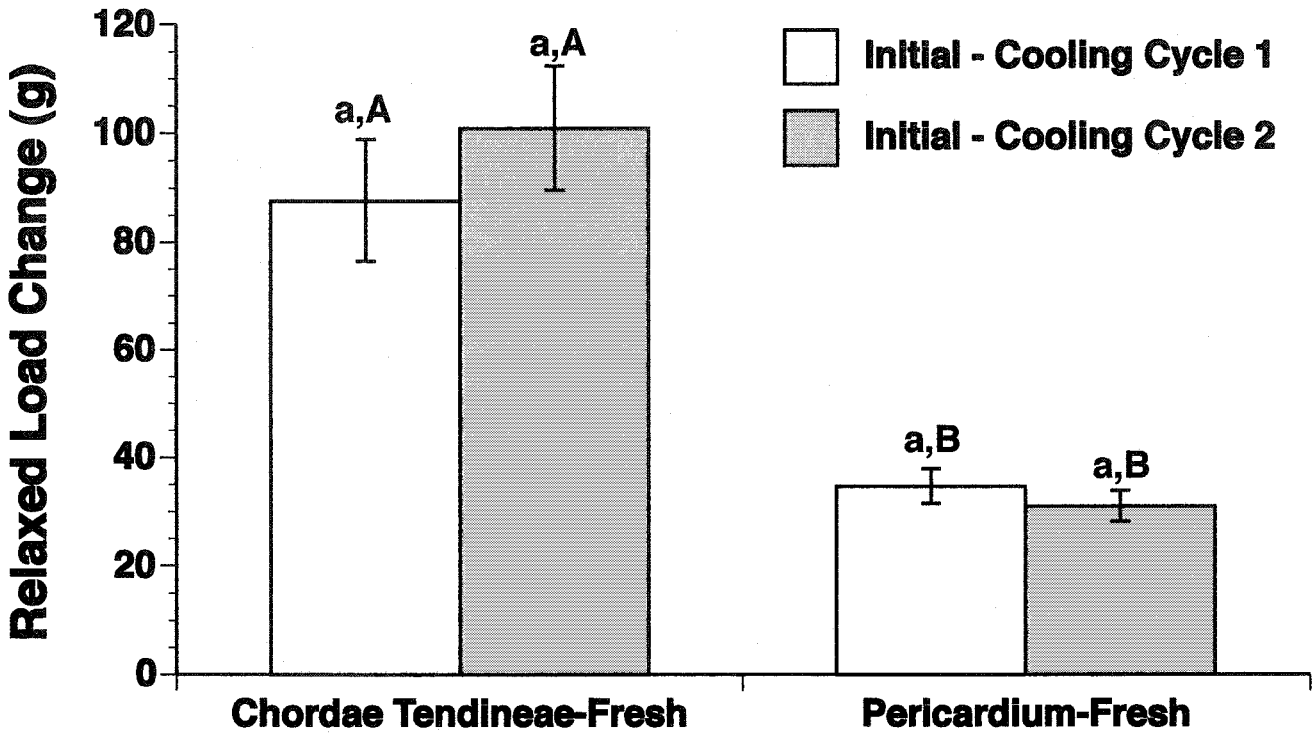

Figure 3.5 Comparative bar graphs of relaxed load changes (asymptotic load – initial pre-denaturation load) to assess the reversibility of rapid thermal denaturation, in terms of differences in the asymptotic loads of initial and cooling cycles 1 and 2, in fresh chordae tendineae and pericardium. The number of samples (n) for each treatment are as follow: chordae tendineae = 14, pericardium = 26. Values shown here are mean ± SE, the *p*-value < 0.05, was created by two, single-factor analysis of variance with variables of tissue types and cycle numbers, followed by Fisher's test. While the capital letters correspond to the differences in tissue types, the small letters correspond to those with respect to cycle numbers. Values labelled with the same letters are not significantly different.

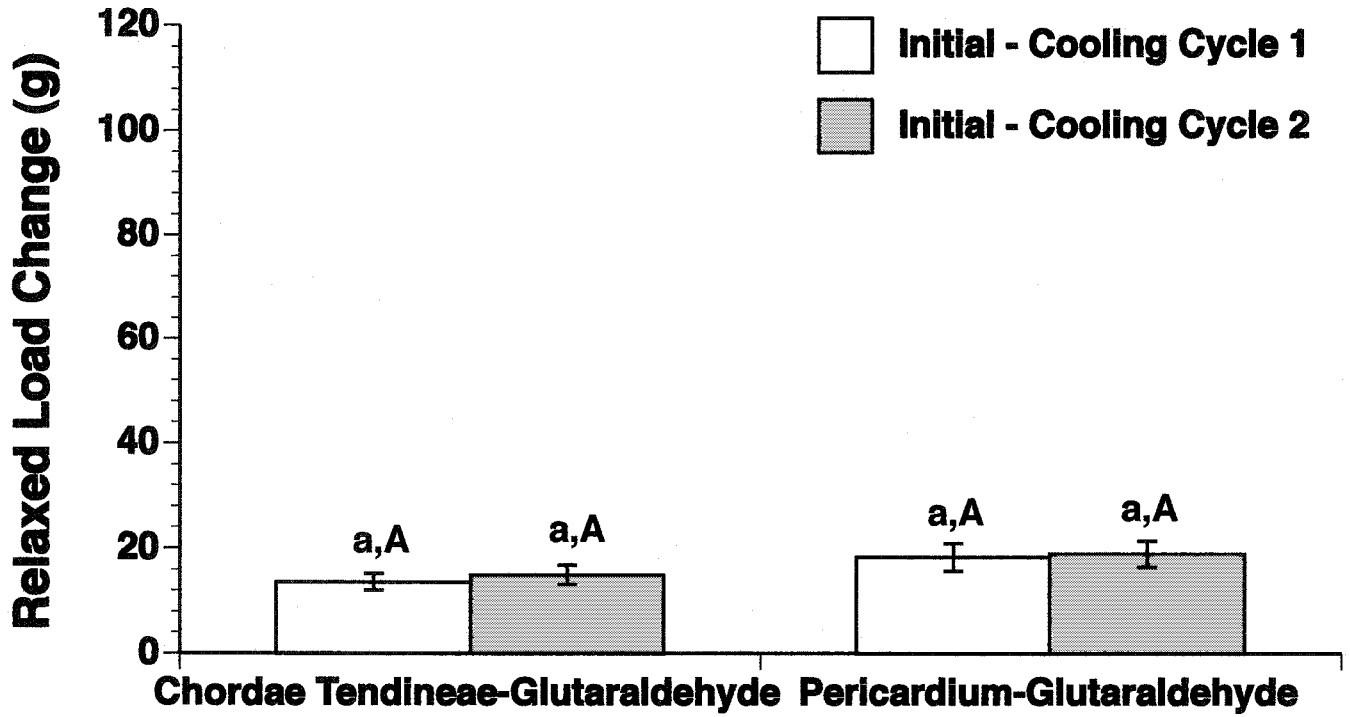

Figure 3.6 Comparative bar graphs of relaxed load changes (asymptotic load – initial pre-denaturation load) to assess the reversibility of rapid thermal denaturation, in terms of differences in the asymptotic loads of initial and cooling cycles 1 and 2, in glutaraldehyde-treated chordae tendineae and pericardium. The number of samples (n) for each treatment are as follow: chordae tendineae = 20, pericardium = 17. Values shown here are mean ± SE, the p-value < 0.05, was created by two, single-factor analysis of variance with variables of tissue types and cycle numbers, followed by Fisher's test. While the capital letters correspond to the differences in tissue types, the small letters correspond to those with respect to cycle numbers. Values labelled with the same letters are not significantly different.

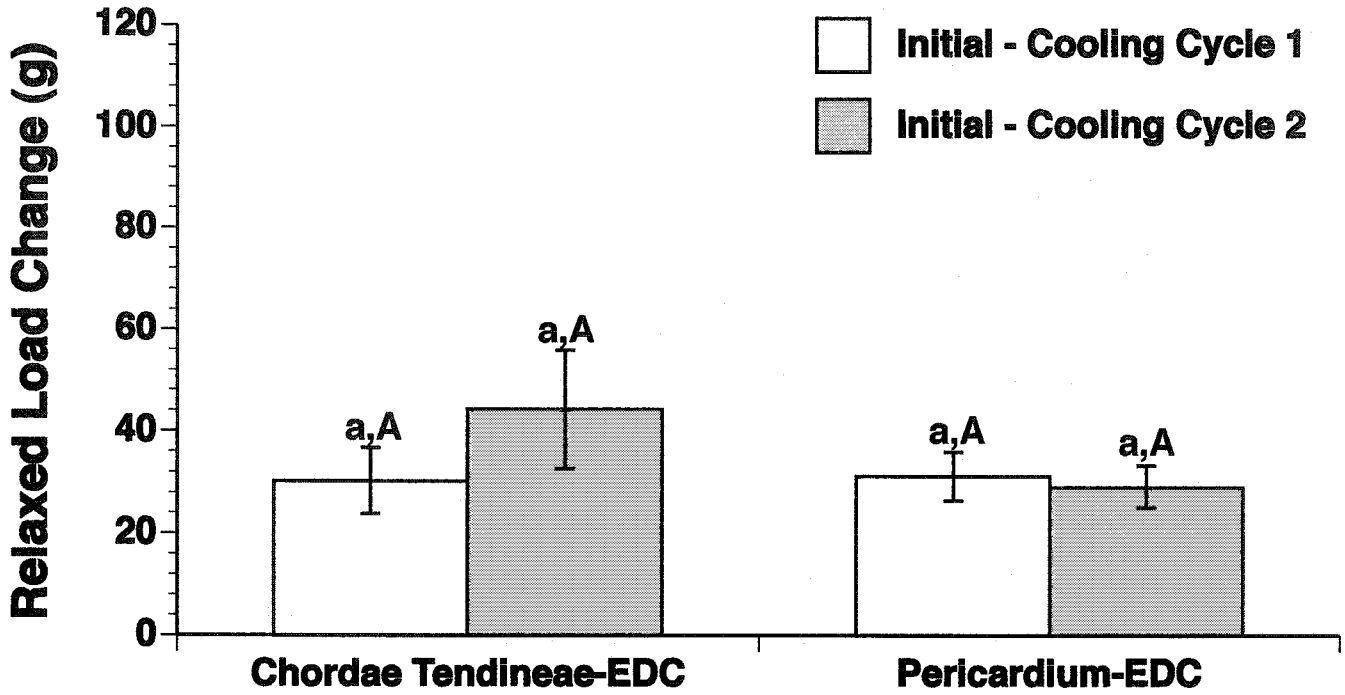

Figure 3.7 Comparative bar graphs of relaxed load changes (asymptotic load – initial pre-denaturation load) to assess the reversibility of rapid thermal denaturation, in terms of differences in the asymptotic loads of initial and cooling cycles 1 and 2, in EDC-treated chordae tendineae and pericardium. The number of samples (n) for each treatment are as follow: chordae tendineae = 16, pericardium = 13. Values shown here are mean ± SE, the p-value < 0.05, was created by two, single-factor analysis of variance with variables of tissue types and cycle numbers, followed by Fisher's test. While the capital letters correspond to the differences in tissue types, the small letters correspond to those with respect to cycle numbers. Values labelled with the same letters are not significantly different.

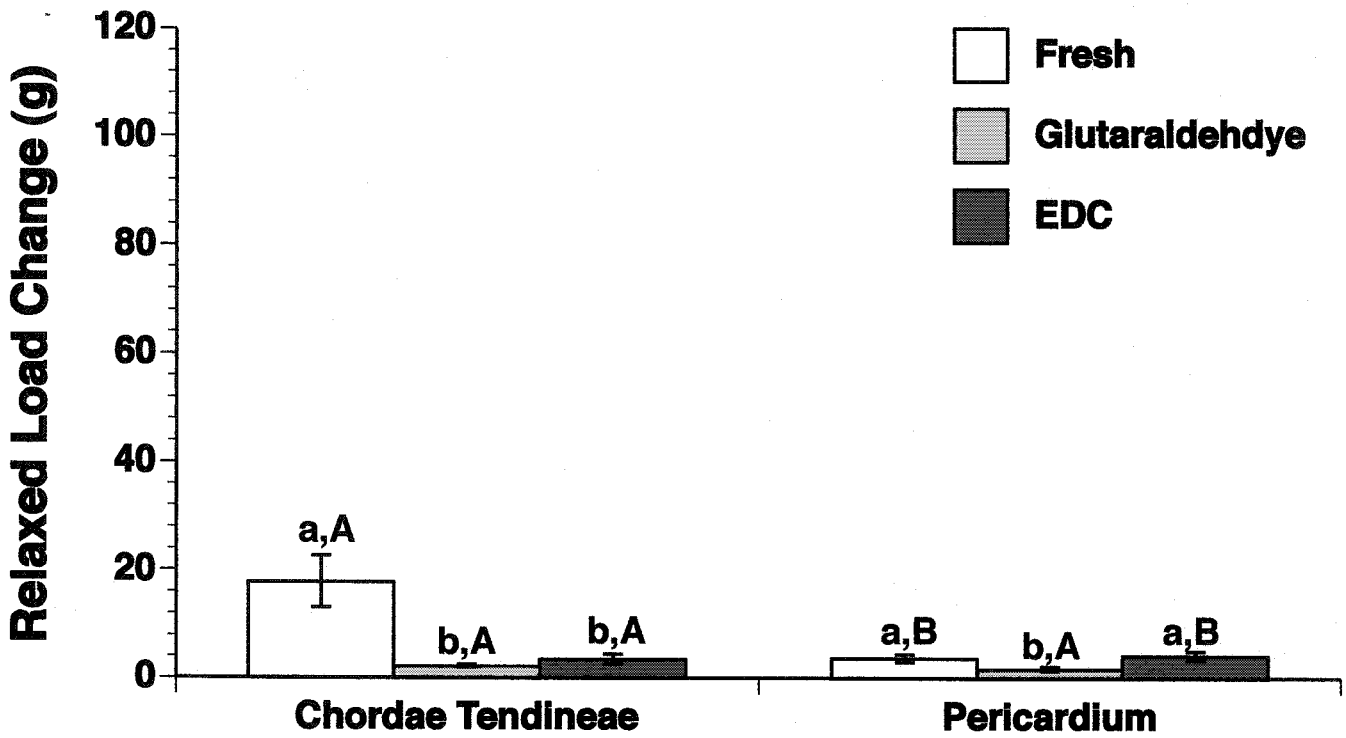

Figure 3.8 Comparative bar graphs of relaxed load changes (between cooling cycles 1 and 2) to assess the reversibility of the two cooling cycles, in terms of differences in the asymptotic loads in fresh, EDC- and glutaraldehyde-treated chordae tendineae and pericardium. The number of samples (n) for each treatment are as follow: chordae tendineae: fresh = 26, EDC = 15, glutaraldehyde = 20; pericardium: fresh = 14, EDC = 17, glutaraldehyde = 13. The p-value < 0.05, was created by two, single-factor analysis of variance with variables of tissue types and crosslinking treatments, followed by Fisher's test. While the capital letters correspond to the differences in tissue types, the small letters correspond to those with respect to crosslinking treatments. Values labelled with the same letters are not significantly different.

fresh one revealed that crosslinking has significantly (p-value < 0.0001) decreased the extent of load changes. The analysis of relaxed load changes between the cooling cycles 1 and 2 revealed that reversibility indeed existed during these cycles following heat cycle 1(Figure 3.8). As mentioned before, an indication of a reversible event would be when the differences between the two cooling cycles are either ideally zero or quite small. Figure 3.8 indicates that such criterion is upheld for almost all tissues groups (as shown by load differences less than 5 g), irrespective of their crosslinking treatments. The only exception is in the fresh chordae tendineae, which exhibits a significantly (p-value < 0.001) larger load change (between cooling cycles 1 and 2) relative to all other groups. This might suggest that unlike other tissue types and treatments, the entire process of rapid thermal denaturation in fresh chordae, when assessed by the relaxed load change parameter, is a non-repeatable event. Despite such exception, it appears that rapid thermal transition of the collagenous tissues, when assessed by relaxed load change, remain mainly a partially reversible process. In other words, while the events occurring during the two cooling cycles were reversible (as indicated by the small differences in asymptotic loads) the relatively larger differences between pre-denaturation loads and subsequent two cooling cycles corresponded to the denaturation events.

3.3.2 Repeatability Based on the Variables in the Three Exponential Model

As explained earlier, upon the completion of each the DHIT experiments, individual heating and cooling cycles were dissected at particular time points, corrected, normalized and then fitted with the a three exponential model to characterize the load decay (Equation 3.1). Before discussing the various time constants and the corresponding coefficients to explore the repeatability of the thermal denaturation, it is instructive to pay closer attention to another general trend observed during each of the thermal cycles. Figure 3.9 shows a representative graph of three heating cycles as a function of normalized load and time. The inserted graph is from the same data but at a much shorter time scale (i.e. 80 seconds) to highlight the differences among the various heating cycles. Interestingly, this graph confirms the conclusions of the previous section, in that, the shape of the contraction curve during the first heating cycle is quite different than those obtained in heating cycles 2 and 3. This

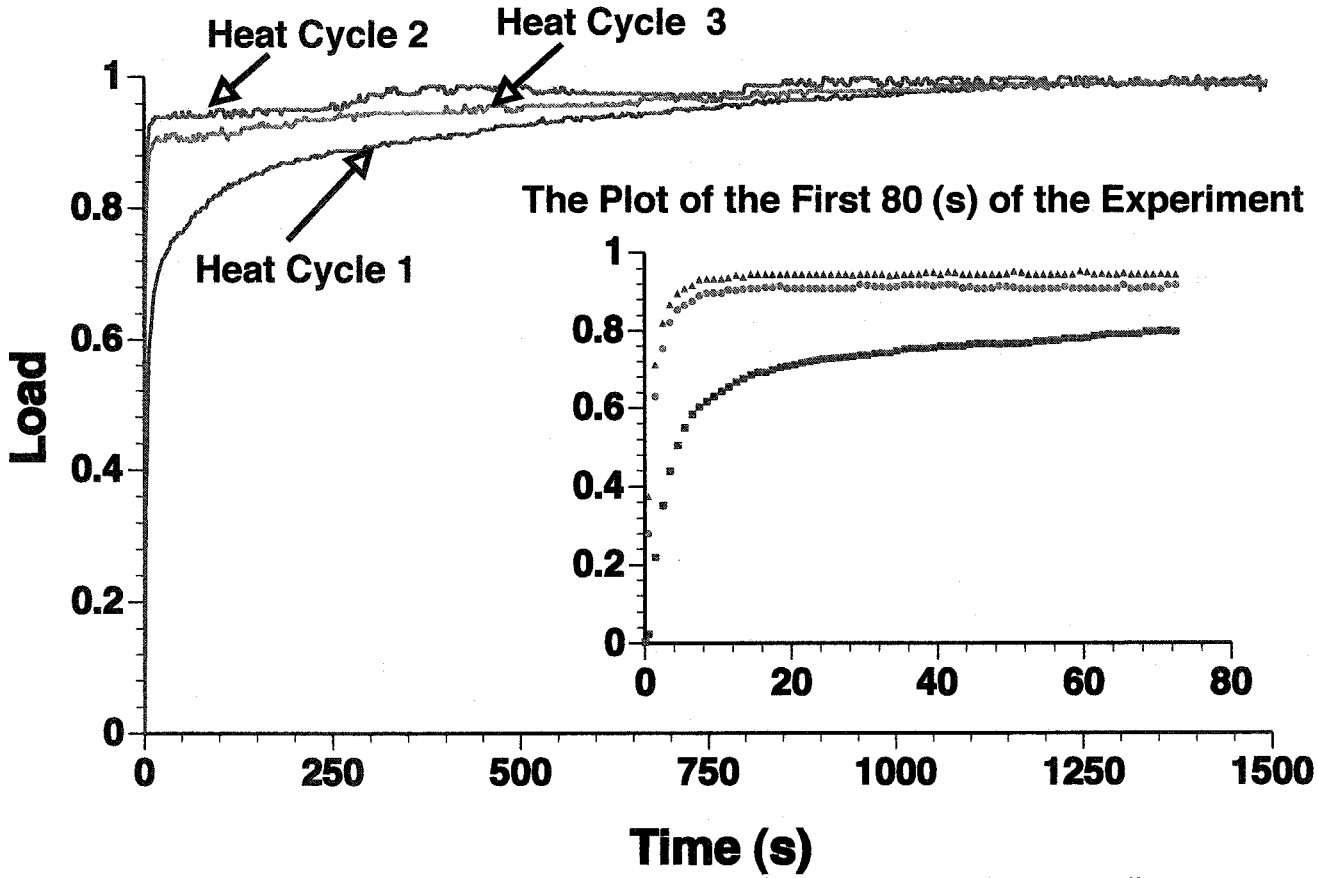

Figure 3.9 Typical normalized load-time graphs for fresh bovine chordae tendineae during the three heating cycles. The embedded graph represents the same data during the first 80 seconds of the experiment. This plot highlights the differences between the initial heating cycle and the heat cycles 2 and 3 and indicates that while the initial event of the thermal denaturation was irreversible, there was relative reversibility between heat cycles 2 and 3.

may indicate that while there is repeatability between the heating cycle 2 and 3, what happens during the first heating cycle remain unique and irreversible. It may be that the tissue contraction during the heating cycle 1 proceeds via a completely different pathway (i.e. mechanism) than that during the heating cycles 2 and 3. Furthermore, Figure 3.10 shows a representative graph of the two cooling cycles showing that the two plots are superimposed on each other, suggesting a clear repeatability between the cooling cycles. It is quite important to emphasize the point that despite the apparent differences in shapes of the load-time curves during heating and cooling cycles, the 3-exponential model still provided the best fit for the data (as assessed by the regression coefficient r^2).

Finally, to examine the dynamics of the reversibility during the various heating and cooling cycles, the characteristic time constants (τ_i) and their coefficients (C_i) were used to characterize the load decay during each of the cycles. Our previous study has clearly established the significance of the first time constant (τ_1) and its overwhelming contribution (as shown by the C_1 value) to the thermal denaturation process. A complete set of data of the time constants and the corresponding coefficients in the three heat cycles as well as the two cooling cycles for all treatments of the chordae tendineae and the pericardium are presented in Tables 3.1-3.4. These data support the findings of Chapter 1, that irrespective of the thermal cycles, the process of rapid thermal transition remains a three-staged event and that the first time constants contributes ~60 % to the rapid thermal transition, in all tissues, irrespective of their crosslinking treatments. The τ_i and C_i of each tissue were compared using a single-factor analysis of variance with variable of heating cycles.

Figure 3.11 shows a comparative diagram of the τ_1 values for the three heating cycles in fresh PC and CT. Two one-way analyses of variance with variables tissue types and thermal cycles were used to analyse these results. Interestingly, there were no statistical differences among the τ_1 values of the three heating cycles in the fresh PC. This would mean that it would take the same initial time period (~ 1.4 s) for the fresh PC to respond to a rapid thermal transition, irrespective whether they were exposed to repeated thermal cycles or not. On the contrary, under repeated heating, the τ_1 values for the fresh CT were significantly different in all three heating cycles. Interestingly, as can be seen in heat cycle 1, the τ_1 value is

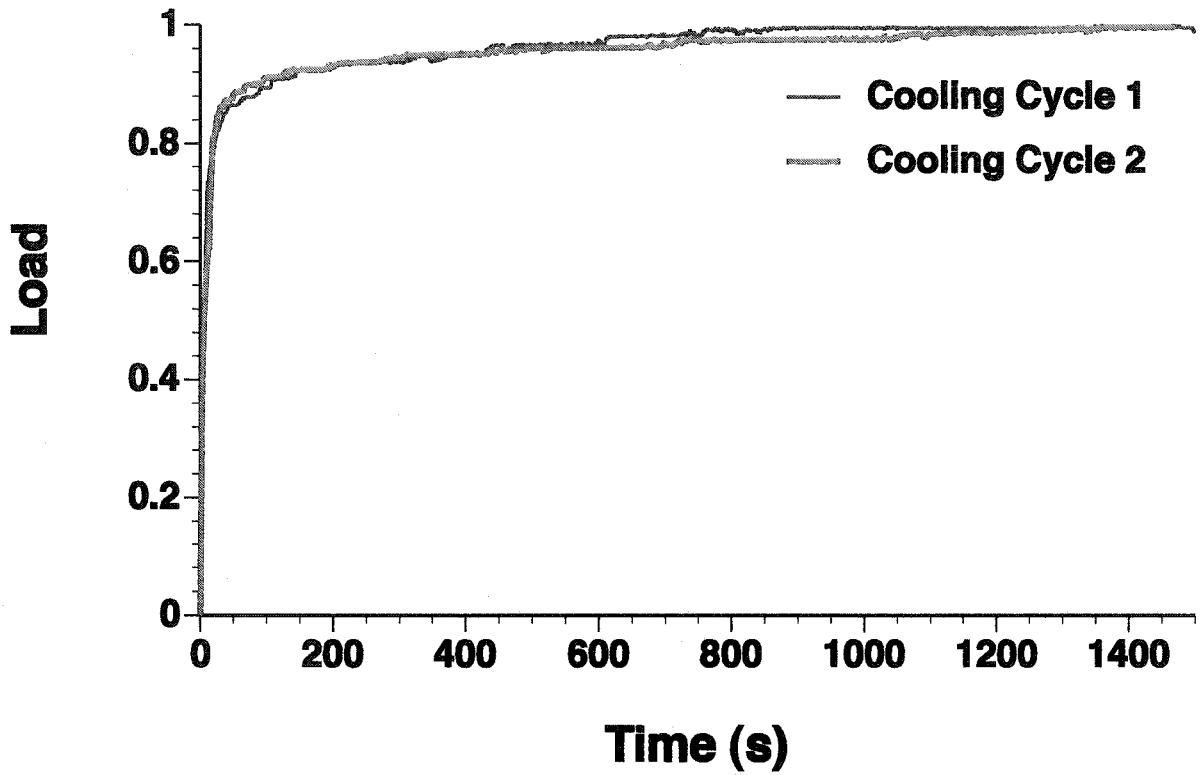

Figure 3.10 Typical normalized load-time graph of the fresh bovine chordae tendineae during the two cooling cycles. Note that the two graphs are clearly superimposed on top of each other, further suggesting a relative reversibility between these two cycles. (More detailed description of these data is shown in Tables 3.3 and 3.4 for PC and CT respectively).

	Fresh (n = 15)			Glutaraldehyde (n = 8)			EDC (n = 8)		
	Time Constants (s)								
	Heat Cycle 1	Heat Cycle 2	Heat Cycle 3	Heat Cycle 1	Heat Cycle 2	Heat Cycle 3	Heat Cycle 1	Heat Cycle 2	Heat Cycle 3
τ_1	2.5 ± 0.3[a]	0.6 ± 0.04[b]	1.4 ± 0.3[c]	13 ± 2.0[a]	0.9 ± 0.1[b]	0.5 ± 0.1[b]	4.5 ± 0.7[a]	1.3 ± 0.2[b]	3.8 ± 1.2[a]
τ_2	57 ± 5.0[a]	60 ± 20[a]	79 ± 27[a]	106 ± 23[a]	313 ± 61[a]	112 ± 63[a]	125 ± 30[a]	88 ± 42[a]	145 ± 68[a]
τ_3	410 ± 20[a]	850 ± 194[a]	905 ± 170[a]	925 ± 180[a]	850 ± 185[a]	930 ± 166[a]	680 ± 180[a]	700 ± 60[a]	726 ± 90[a]
	Coefficients (%)								
C_1	57 ± 2.4[a]	69 ± 5.0[b]	60 ± 4.4[a]	57 ± 5.0[a]	66 ± 5.2[a]	62 ± 4.0[a]	63 ± 2.0[a]	73 ± 6.0[a]	55 ± 9.0[a]
C_2	20 ± 1.3[a]	15 ± 3.0[a]	20 ± 4.0[a]	29 ± 4.0[a]	21 ± 6.7[b]	22 ± 2.0[b]	17 ± 5.0[a]	15 ± 4.0[a]	25 ± 7.0[a]
C_3	23 ± 1.6[a]	16 ± 2.8[a]	20 ± 3.5[a]	14 ± 3.4[a]	13 ± 5.2[a]	16 ± 3.0[a]	20 ± 5.0[a]	12 ± 3.0[a]	20 ± 4.0[a]

Table 3.1. Overall representation of the time constants and the corresponding coefficients for the fresh and crosslinked chordae tendineae, during the three heat cycles. Mean ± SE was created by a single-factor analysis of variance with cycle numbers as the variable of interest, followed by the Fisher's test (p-value < 0.05). Within each τ_i and C_i, values labelled with the same letters are not significantly different.

	Fresh (n = 6)			Glutaraldehyde (n = 9)			EDC (n = 5)		
	Time Constants (s)								
	Heat Cycle 1	**Heat Cycle 2**	**Heat Cycle 3**	**Heat Cycle 1**	**Heat Cycle 2**	**Heat Cycle 3**	**Heat Cycle 1**	**Heat Cycle 2**	**Heat Cycle 3**
τ_1	1.2 ± 0.1[a]	1.3 ± 0.5[a]	1.6 ± 0.4[a]	7.4 ± 0.4[a]	2.0 ± 0.6[b]	2.6 ± 0.9[b]	7.6 ± 2.5[a]	3.4 ± 0.7[a]	2.2 ± 0.4[b]
τ_2	260 ± 100[a]	43 ± 20[b]	201 ± 68[a]	110 ± 20[a]	101 ± 55[a]	245 ± 60[a]	250 ± 40[a]	270 ± 90[a]	135 ± 41[a]
τ_3	1430 ± 590[a]	3112 ± 1206[a]	1735 ± 630[a]	785 ± 77[a]	801 ± 122[a]	771 ± 110[a]	2720 ± 1400[a]	1309 ± 234[a]	840 ± 206[a]
	Coefficients (%)								
C_1	86 ± 2.5[a]	63 ± 3.1[b]	86 ± 2.5[a]	63 ± 1.7[a]	61 ± 5.7[a]	48 ± 4.0[b]	70 ± 9.0[a]	53 ± 7.7[a]	58 ± 8.0[a]
C_2	11 ± 1.0[a]	29 ± 2.0[a]	9.0 ± 1.0[a]	13 ± 1.6[a]	14 ± 3.7[a]	25 ± 6.8[a]	24 ± 7.0[a]	24 ± 11[a]	21 ± 4.0[a]
C_3	3.0 ± 2.0[a]	10 ± 2.0[a]	5.0 ± 3.0[a]	24 ± 3.0[a]	25 ± 4.5[a]	23 ± 8.0[a]	6.0 ± 0.4[a]	23 ± 8.0[a]	21 ± 7.0[a]

Table 3.2. Overall representation of the time constants and the corresponding coefficients for the fresh and crosslinked pericardium, during the three heat cycles. Mean ± SE was created by a single-factor analysis of variance with cycle numbers as the variable of interest, followed by the Fisher's test (p-value < 0.05). Within each τ_i and C_i, values labelled with the same letters are not significantly different.

	Fresh (n = 6)		Glutaraldehyde (n = 9)		EDC (n = 5)	
			Time Constants (s)			
	Cooling Cycle 1	Cooling Cycle 2	Cooling Cycle 1	Cooling Cycle 2	Cooling Cycle 1	Cooling Cycle 2
τ_1	4.8 ± 0.8[a]	5.6 ± 0.3 [a]	4.0 ± 0.8[a]	6.4 ± 0.5[b]	5.6 ± 0.9 [a]	5.5 ± 0.6[a]
τ_2	54 ± 8.4[a]	58 ± 7.0 [a]	46 ± 10 [a]	53 ± 9.0 [a]	46 ± 20 [a]	90 ± 20 [a]
τ_3	860 ± 220[a]	810 ± 90[a]	625 ± 40[a]	785 ± 153[a]	970 ± 149[a]	1080 ± 200[a]
			Coefficients (%)			
C_1	62 ± 4.0 [a]	61 ± 2.9 [a]	60 ± 6.8 [a]	66 ± 5.0 [a]	50 ± 12 [a]	55 ± 8.3 [a]
C_2	20 ± 3.0 [a]	20 ± 2.2 [a]	20 ± 3.0 [a]	20 ± 3.0 [a]	28 ± 10 [a]	22 ± 5.5 [a]
C_3	18 ± 2.0 [a]	19 ± 1.7 [a]	20 ± 4.5 [a]	14 ± 2.3 [a]	22 ± 6.0 [a]	23 ± 5.0 [a]

Table 3.3 Overall representation of the time constants and the corresponding coefficients for the fresh and crosslinked pericardium, during the two cooling cycles. Mean ± SE was created by a single-factor analysis of variance with cycle numbers as the variable of interest, followed by the Fisher's test (p-value < 0.05). Within each τ_i and C_i, values labelled with the same letters are not significantly different.

	Fresh (n = 15)		Glutaraldehyde (n = 8)		EDC (n = 8)	
			Time Constants (s)			
	Cooling Cycle 1	Cooling Cycle 2	Cooling Cycle 1	Cooling Cycle 2	Cooling Cycle 1	Cooling Cycle 2
τ_1	6.0 ± 0.1[a]	6.0 ± 0.1[a]	5.1 ± 4.1 [a]	4.7 ± 0.3 [a]	4.8 ± 0.7 [a]	4.8 ± 1.0 [a]
τ_2	57 ± 7.0 [a]	77 ± 9.1[a]	187 ± 80 [a]	82 ± 23 [a]	46 ± 15 [a]	31 ± 10 [a]
τ_3	810 ± 164[a]	1210 ± 195[a]	1560 ± 770[a]	1120 ± 270[a]	670 ± 60[a]	630 ± 42[a]
			Coefficients (%)			
C_1	72 ± 3.5 [a]	75 ± 1.0 [a]	87 ± 3.0 [a]	87 ± 2.0 [a]	70 ± 8.0 [a]	43 ± 10 [a]
C_2	16 ± 3.0 [a]	12 ± 1.0 [a]	7.0 ± 2.0[a]	5.0 ± 1.0[a]	20 ± 6.0 [a]	44 ± 11[a]
C_3	12 ± 1.0 [a]	13 ± 1.0 [a]	6.0 ± 1.5 [a]	8.0 ± 1.0[a]	12 ± 2.0 [a]	13 ± 3.0 [a]

Table 3.4 Overall representation of the time constants and the corresponding coefficients for the fresh and crosslinked chordae tendineae, during the two cooling cycles. Mean ± SE was created by a single-factor analysis of variance with cycle numbers as the variable of interest, followed by the Fisher's test (p-value < 0.05). Within each τ_i and C_i values labelled with the same letters are not significantly different.

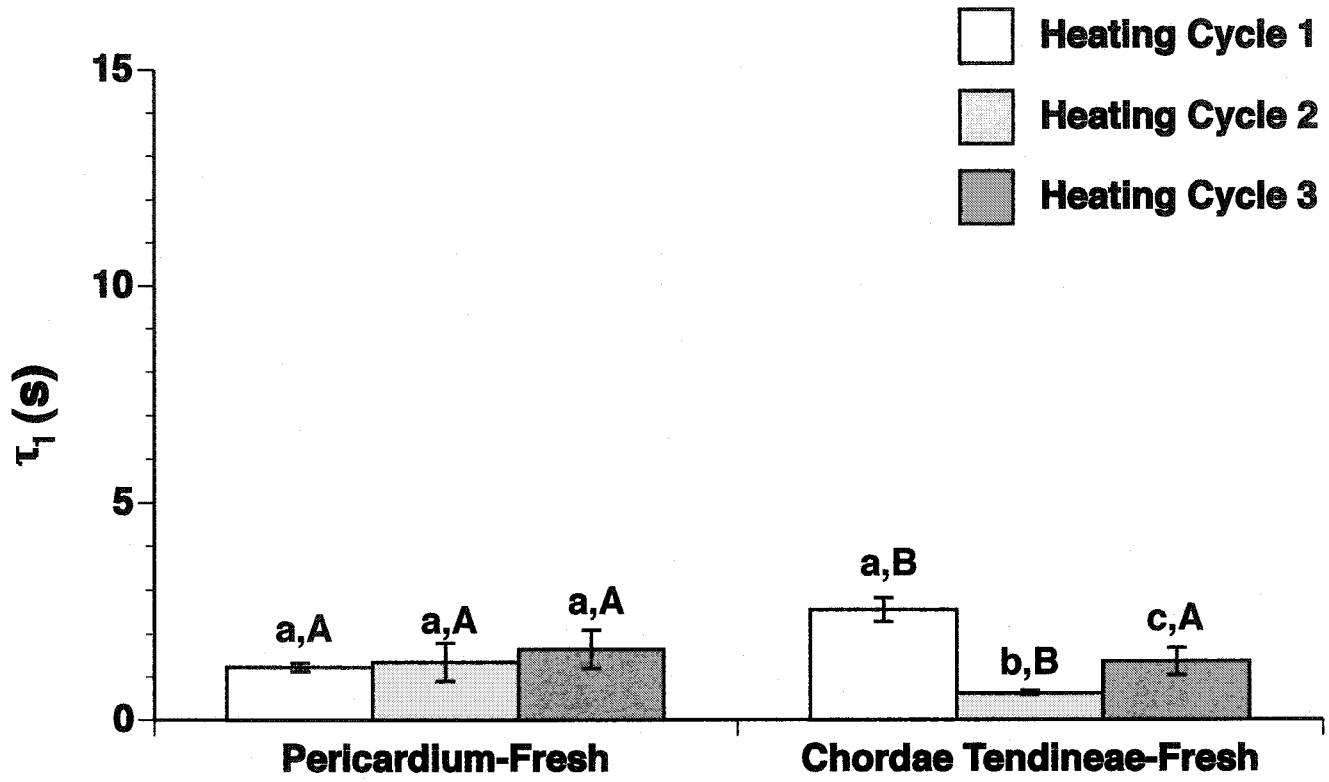

Figure 3.11 Comparative bar graphs of the first time constants (τ_1) during the three heat cycles in fresh pericardium and chordae tendineae. The number of samples (n) for the tissues are as follow: pericardium = 6 and chordae tendineae = 15. Mean ± SE, the *p*-value < 0.05, was created by two, single-factor analysis of variance with variables of tissue types and cycle numbers, followed by Fisher's test. While the capital letters correspond the differences with respect to the tissue types, the small letters correspond to those with respect to heat cycles. Values labelled with the same letters are not significantly different.

2.5 ± 0.30 s and it diminishes to 0.6 ± 0.04 s and 1.4 ± 0.40 s in the subsequent heating cycles 2 and 3 respectively. The *p*-value for heat cycle 1-2 was at < 0.0001, heat cycle 1 and 3 at 0.0002 and heat cycle 2 and 3 at 0.018. Once again, the differences in the dynamics of thermal denaturation in various heating cycles in both PC and CT may suggest that the architectural differences may play a pivotal role in determining reversibility between the various thermal cycles. In this case, the data indicated while the PC samples exhibited full repeatability (per τ_1) in all heating cycles as well as cooling cycles, the CT samples showed only partial repeatability. Furthermore, the lack of statistical differences among the τ_1 values for the two cooling cycles indicated that full reversibility existed in either of the tissues following the first heating cycle (Figure 3.12). Similar behaviour in the cooling cycles were observed for both the exogenously crosslinked tissues (Tables 3.3, and 3.4).

Figures 3.13 and 3.14 show the influence of the two exogenous crosslinking agents in altering the dynamics of reversibility in both pericardium and chordae tendineae as measured by the values of τ_1. Two, one-way analyses of variance were used to determine the statistical differences among the various tissue treatments and heating cycles. As shown in Figure 3.13, crosslinking of the PC with either of the exogenous agents has dramatically altered (i.e. increased) the dynamics of the thermal denaturation in the first heating cycles as measured by the τ_1 values. This means that the initial response of the EDC- or glutaraldehyde-fixed tissues has been slowed down by a factor of 7 relative to untreated tissues. The same general effect of crosslinking is also observed for the CT (Figure 3.13), except that in the case of glutaraldehyde the response is rather drastic and quite different from EDC during the first heating cycle. What happens in the second heating cycle is quite interesting. As shown in Figure 3.13, during the second heating cycle, the τ_1 of all the treatments seems to become quite similar to that the fresh tissue, irrespective of their crosslinking. Hence, the thermal stabilising effect of the crosslinked agents seemed to be diminished following the thermal denaturation event occurring during the first heating cycle. This is supported by the statistical analyses, as shown on Figures 3.13 and 3.14, as well as Tables 3.1 and 3.2, suggesting that although there are significant differences in the dynamics (τ_1) of denaturation during the first heating cycle relative to second and third heating cycles, no such dynamic differences are observed between second and third heating cycles. Hence, these results are reaffirming the earlier findings that, while the thermal transition during the first heating cycle

was irreproducible, those occurring during the second and third heating cycles were indeed repeatable. Finally, as shown in Tables 3.1-3.4, the first coefficients C_1, irrespective of tissue types and treatments still predominate the thermal denaturation process, followed by C_2 and C_3.

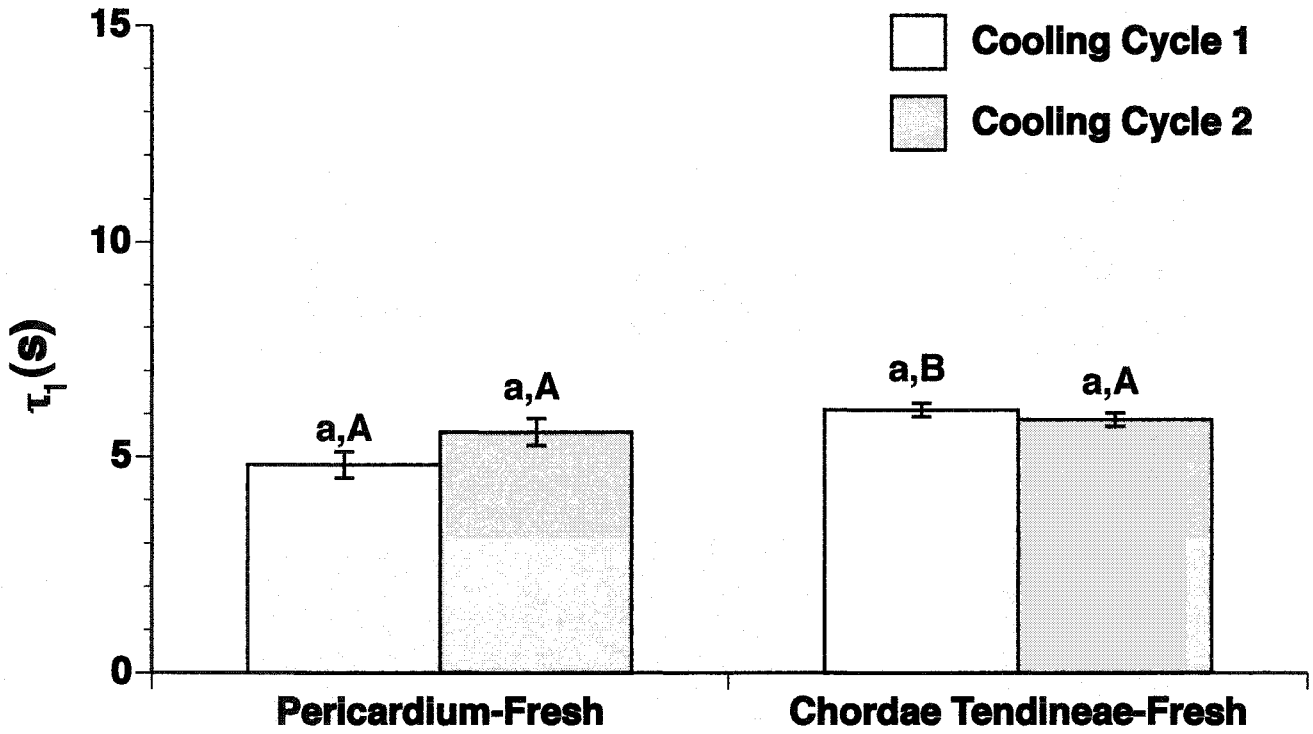

Figure 3.12 Comparative bar graphs of the first time constants (τ_1) during the two cooling cycles in fresh pericardium and chordae tendineae. The number of samples (n) for the tissues are as follow: pericardium = 6 and chordae tendineae = 15. Mean ± SE, the *p*-value < 0.05, was created by two, single-factor analysis of variance with variables of tissue types and heat cycles, followed by Fisher's test. While the capital letters correspond the differences with respect to the tissue types, the small letters correspond to those with respect to heat cycles. Values labelled with the same letters are not significantly different.

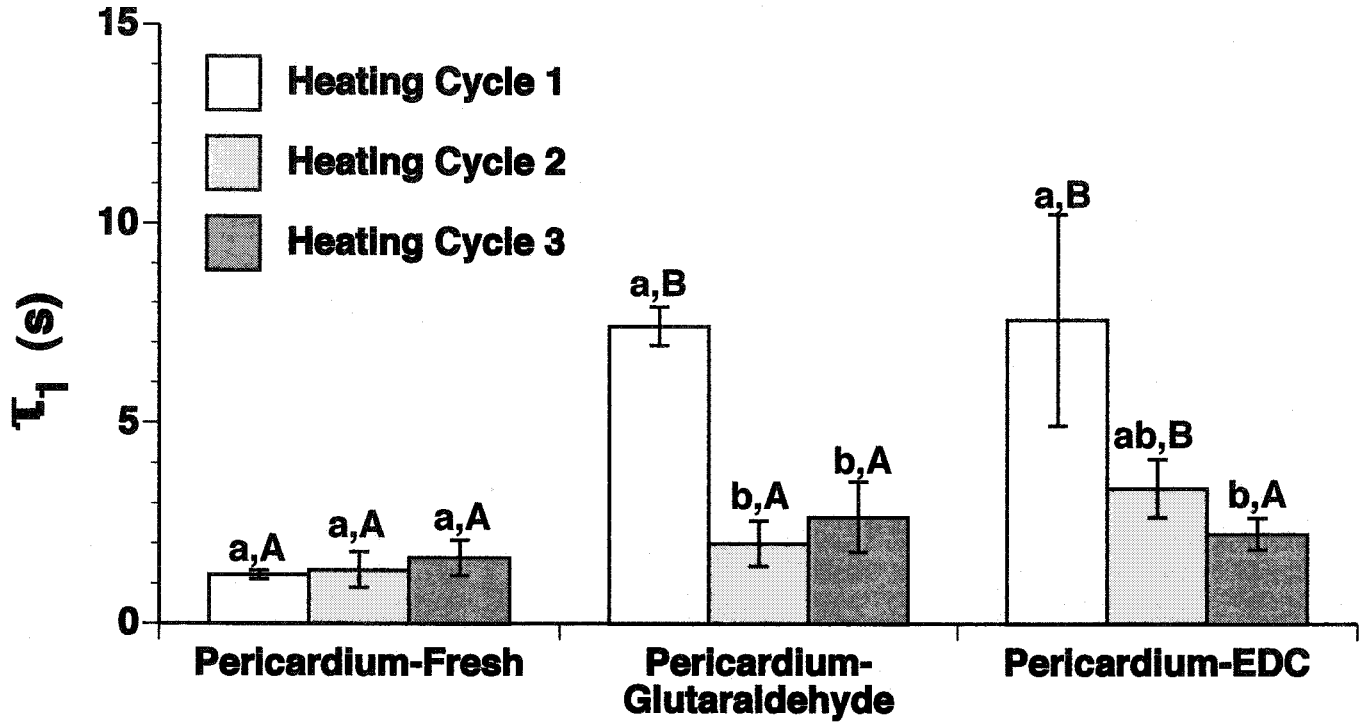

Figure 3.13 Comparative bar plots of the first time constants (τ_1) for the three heating cycles in fresh and crosslinked bovine pericardium. The number of samples (n) for each treatment are as follow: fresh = 6, glutaraldehyde = 9 and EDC = 5. Mean ± SE, the *p*-value < 0.05, was created by two, single-factor analysis of variance with variables of crosslinking treatments and heat cycles, followed by Fisher's test. While the capital letters correspond the differences with respect to the crosslinking treatments, the small letters correspond to those with respect to heat cycles. Values labelled with the same letters are not significantly different.

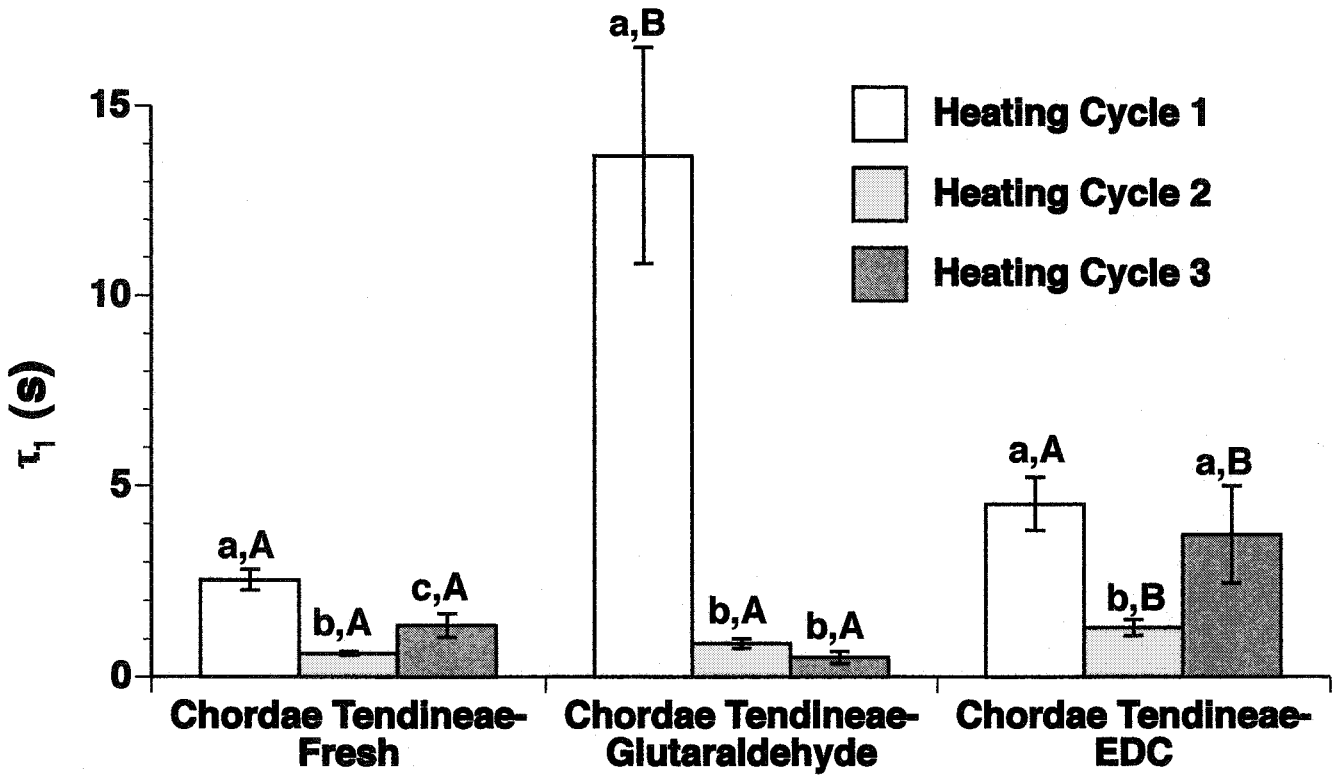

Figure 3.14 Comparative bar plots of the first time constants (τ_1) for the three heating cycles in fresh and crosslinked bovine chordae tendineae. The number of samples (n) for each treatment are as follow: fresh = 15, glutaraldehyde = 8 and EDC = 8. Mean ± SE, the *p*-value < 0.05, was created by two, single-factor analysis of variance with variables of tissue treatments and heat cycles, followed by Fisher's test. While the capital letters correspond the differences with respect to the tissue treatments, the small letters correspond to those with respect to heat cycles. Values labelled with the same letters are not significantly different.

3.4 Discussion

The objective of the current study was to use dynamic HIT (DHIT) tests to examine the reversibility of two collagenous tissues after repeated cycles of heat-induced denaturation, under isometric conditions and rapid thermal transitions. Our results indicated that rapid thermal denaturation of two collagenous tissues, under isometric constraint, is *irreversible* during the first heating cycle, and thereafter there is a *reversible* "thermoelastic contraction" of the rubbery, denatured collagen.

As mentioned earlier, many studies have indicated that the effect of thermal damage on collagen can either be reversible or irreversible depending on the severity of thermal energy, rate of its delivery and duration of heating [50, 150, 158-160, 279]. It is believed that while moderate heating may induce a local unfolding within the protein that can be reversed upon cooling, more severe heating results in a time-dependent irreversible transformation of the triple helical structure into a more random structure [50, 279]. It is suggested that a particular subdomain along the molecule (i.e. between residues 877-941) may also be more susceptible to the breaking of consecutive hydrogen bonds [150].

Recently, Chen et al. [30, 160] have conducted a series both isotonic and free shrinkage investigations under isothermal conditions, to study the heat-induced changes in bovine chordae tendineae. Accordingly, the loads used in the isotonic shrinkage ranged from 0-650 kPa. The loads used in the current study corresponded to 470, and 490 kPa for CT and PC respectively. Chen's studies indicated that subsequent to both isotonic and free shrinkage tests, cooling of the thermally damaged tissue resulted in their partial reversibility (i.e. renaturation) in a time-dependent manner. This was suggested to be due to absorption of water via the formation of additional hydrogen bonds or water bridges within the more random molecular structure [169, 254]. However, the isotonic studies further highlighted the importance of imposed mechanical load during heating, influencing both the extent of shrinkage and subsequent recovery of the tissues, i.e.: the higher the load, the slower the shrinkage process and also smaller the recovery during partial recovery [30]. It was suggested that the applied mechanical loads ($0 < P < 650$ kPa) increased the order of the collagen,

thereby decreasing the configurational entropy rather than changing heat-labile bonds thus the activation energy. The influence of configurational entropy on the thermal stability of collagenous tissues is further studied in Chapter 4.

Many other studies have revealed that thermally denatured collagen (both fibrous and in solution) experiences a partial renaturation upon its return to a basal temperature [38, 138, 169, 254, 278, 280]. Following a heat-induced denaturation, the inextensible collagen protein may be transformed into a rubber elastic protein. It is believed that in addition to re-establishment new hydrogen bonds, the renaturation of the collagen (at least in vitro), requires the correct alignment of the peptide chains, so that they can intertwine to form a triple helix with their ends in register [278, 281]. Hence, it appears that if the thermal denaturation leads to a "disorganization" rather than a "decomposition" (as in HIT testing at high isotherms), the denatured protein should theoretically be able to revert back to its natural form [282]. In principle though, it is possible for peptide chains to form triple helical structures without coming into complete register. As a result, a large molecular aggregate may be produced that is only stable at lower temperature (4-24°C) [281]. Generally, the reduced tendency of the various collagen derivatives to reform into native molecules may have thermodynamic origins [281]. In other words, the native structure is re-formed preferentially, only if it is energetically favorable [281]. In light of these discussions, it is tempting to suggest that for a protein to undergo a reversible event, at least two conditions must be provided: firstly the reversibility must thermodynamically be favorable and secondly a particular mechanism (pathway) must be present for the reversibility to ensue. For instance, following thermal damage to a collagenous tissue, the individual collagen chain must be close enough so that various linkages can be reestablished, resulting in correct fibres realignment. Regardless of specific mechanism of renaturation, there has been no prior attempt to characterize renaturation of collagenous tissues under isometric conditions and dynamic temperature changes.

Generally, denaturation of proteins can occur under a variety of physical conditions, including high temperature, extreme pH, and very high pressures [287]. As mentioned before, depending on the severity of these conditions, the denaturation can either be reversible or irreversible. What defines reversibility is still controversial and may vary from

one study to another; for instance, if the thermal denaturation of a particular enzyme led to its inactivation, the authors referred to this phenomena as an irreversible event [288]. In thermodynamic terms, the reversibility of a chemical reaction presumes that a system exists in an equilibrium state, and as such equilibrium transition models can be used to perform the various analysis to determine the transition temperature, T_m, or the transition enthalpy, ΔH [289]. At the same time, the reversibility of a chemical reaction can also be defined in terms the amount reactants (A) and products (B), as well as the rate constants for forward and back reactions according to:

$$A \underset{k_{-1}}{\overset{k_1}{\rightleftharpoons}} B$$

where, the k_1 and k_{-1} are the rate constants for forward and reverse reaction respectively [289]. Subsequently, in this study the term reversibility was defined in terms of changes in asymptotic loads and the comparison of three time constants (τ_i) at various thermal and cooling cycles.

Current results report on the thermomechanical behaviour of the two collagenous tissues under isometric and isothermal condition after they have been exposed to repeated hot-cold cycles. A schematic representation of this observation is shown in Figure 3.9 and 3.10. Both figures are representative plots of normalized load vs. time data during the heating cycles (Figure 3.9) and the cooling cycle (Figure 3.10). As shown clearly in Figure 3.9, the nature of load changes in heat cycle 1 is quite different than those occurring in either heat cycle 2 or 3. For instance, the fact that the "toe" region of the thermal transition occurred at higher loads in heat cycles 2 and 3 relative to the heat cycle 1, may indicate the structural changes occurring during the first heating cycle drastically altered the mechanism of contraction. It is speculated that following the first heating cycle where collagenous tissues are *possibly* thermally denatured (possibly, since the tissues are held under isometric constraints), the tissue samples exhibit rubber elastic properties, undergoing thermoelastic contraction with each subsequent heating cycle.

Strictly speaking, for a material to exhibit "true" rubber-like elasticity, three primary requirements must be met [200, 283]: (a) the material must consist of polymeric chains,

(b) the polymer chains must be kinetically free and sufficiently flexible so that they behave like a random coil molecule, and (c) these random coils must be joined together via (sparse) stable crosslinkages establishing a stable interaction [200, 276, 283, 284]. The flexibility and mobility of a native collagen protein is quite limited due to the presence of extensive crosslinkages (both inter- and intramolecular) as well as the steric hindrance influence of particular amino acid groups (i.e. pyrrolidine ring of hydroxyproline) [215, 285]. Nevertheless, many investigators have discovered that upon heating, the "crystalline" collagen is transformed into an "amorphous" molecule, and as such many of the heat labile bonds (including secondary bonds and in some cases covalent bonds) are disrupted. The protein then, becomes more "resilient" and extensible similar to an elastic protein [19, 30, 141, 172, 275, 286]. Providing the energy in the form of heat, dramatically increases the kinetic energy of the polypeptide chain, hence, increasing the thermal gyration, eventually leading to the disruption of the hydrogen bonding within the collagen triple helix [153, 172]. It is therefore believed that upon thermal denaturation of collagen, and the disruption of various bonds and crosslinks, the molecule is more kinetically free and sufficiently flexible to assume various conformations, and to behave as a rubber in response to cooling and heating.

The load experiments further validated this notion of thermal denaturation in heat cycle 1. In fact, as shown in Figure 3.1 and also Figures 3.2-3.4, the initial/relaxed loads never return to the original initial values set prior to the first heating cycle (PC: 50 g, and CT: 30 g) irrespective of the crosslinking treatments and tissue types. This represents the irreversible stage of protein denaturation, which occurred irrespective of tissue treatments. Exogenous crosslinking were expected to change the dynamics of thermal denaturation. Generally, crosslinking (both endogenous and exogenous) will hinder intramolecular Brownian motions of the polypeptide chains hence making collagen more thermally (and also mechanically) stable [172]. It is suggested that the restriction on molecular motion originates not only from bridging of the two polypeptide chains but also from further restriction on the rotation of the peptide backbone [69]. Therefore, various exogenous crosslinking agents have been used to improve the mechanical properties of various collagenous-based biomaterials, prior to implantation. These crosslinks may be added to the tropocollagen molecule within its

individual helical strands (intrahelical crosslinks) or between adjacent different molecules (interhelical crosslinks) with a crosslinking agent [218].

A previous comparative study into the differences between bovine PC treated with glutaraldehyde and EDC revealed that both treatments equally increased resistance to solubilisation by collagenase, and trypsin [85]. Furthermore, mechanical testing revealed that EDC-fixed tissues were more extensible and more elastic than glutaraldehyde-treated materials. Similarly as shown in Chapter 2, while the thermal stabilities (as shown by the T_d) of the glutaraldehyde- and EDC-treated PC samples were statistically indistinguishable, those in CT were significantly different. This may well be related to the architectural differences in the two tissues originating from different collagen densities as well as fibre orientations, leading to a different pattern of crosslinking.

In this study, the asymptotic loads in each heating and cooling cycles were interpreted as measures of tissues' contraction under isometric constraints. In other words, the higher the extent of thermal damage, the more uncoiled the configuration of collagenous tissues would be, resulting in higher contraction, as reflected by a higher load. From our current data, it is speculated that crosslinking effectively limits the fibre mobility and as such alters its vibrational and uncoiling dynamics relative to the fresh PC and CT. This is also indicated upon the gross examination of the tissues after the fixation, which revealed that both tissues shrunk to a certain extent (especially in the glutaraldehyde-treated tissues). This shrinkage may be related to the contraction of the collagen network and its tendency to achieve a coiled high entropy state, due to intermolecular and intramolecular crosslinks within collagen fibres [290]. This shrinkage may also be related to the reduction of the free volume due to the ejection of the water molecules from the fixed tissue [290]. A reduction in the free volume may influence the configurational entropy of the thermally labile domain of the polypeptide chains governing the rate of denaturation and thereby increase the temperature of the denaturation [172, 178]. According to the polymer-in-a-box theory introduced by Miles et al. [178], the change in configurational entropy of the collagen molecule on denaturation is reduced by its confinement by surrounding molecules in the fiber. In fact, it was shown that in collagen fibres that have been dehydrated to different levels, the interaxial spacing is directly related to the volume fraction of water [178]. Figures 3.3 and 3.4 indicated

that EDC-fixed tissues contracted more (as indicated by higher loads) than did glutaraldehyde-fixed tissues during the heating cycle 2 and 3. This may be consistent with the observation that glutaraldehyde reduced the moisture content more dramatically than the EDC-fixed counterparts [290].

The different architectures of the PC and CT may also contribute to the tissues' contraction behaviour and their attainment of the maximum asymptotic load during the heating cycles 2 and 3. In fact, other investigators (using skin samples), have shown that collagen density and orientation play a significant role in the amount of isotonic shrinkage, and that tissues with a higher density of collagen contracted more than did loosely packed counterparts [262, 263]. In Chapter 2, it was also revealed that during the rapid denaturation of the PC and CT, the latter sample with more densely packed collagen and more isotropic geometry produced almost four times more force.

More importantly, to compare the extent of the contraction between the two tissue types, the relaxed load changes were calculated and the results are shown in Figure 3.5-3.8. Figure 3.5 represents the data for fresh CT and PC. In both tissue types the differences between pre-denaturation load and those achieved during the first and second cooling cycles (as shown by white and light grey columns), clearly indicate that loads in the subsequent heating cycles do not return to its original value, and that there are significant and large differences between asymptotic loads. It is speculated that such trend may be an indication of heating damage sustained by the collagenous tissues during the first heating cycle, where they are possibly irreversibly thermally denaturated. On the other hand, the small differences in asymptotic loads, between the cooling cycles 1 and 2 (Figure 3.8), may be an indication that due to denaturation in the first heating cycle, the collagenous tissues are now transformed into rubber elastic elastomers and hence behave as one also. Hence, it can be concluded that reversible thermal contraction is indeed an evidence of rubber elasticity following the tissue denaturation during the first heating cycle.

Another important feature of the data is related to the effect of crosslinking in reducing the relaxed load changes in the thermal cycles relative to the fresh tissues (Figure 3.6, and 3.7). As eluded earlier, this may be related to the ability of the crosslinking agents to limit the

vibration of the collagen fibres during the thermal cycles and hence reducing the level of thermal damage and also thermal contraction. Finally, it is speculated that differences in tissue architectures may explain why the relaxed load change in CT is significantly (p-value < 0.0001) higher than in PC (Figure 3.5). It is interesting to note that crosslinking of the tissue seem to mask such tissue effect (Figure 3.6 and 3.8).

A triple exponential model was used to fit the load decay data in the two collagenous tissues (PC and CT) and to characterize their repeatability dynamics following three thermal cycles. The same model was also used in Chapter 2 to characterize the rapid thermal denaturation of the PC and CT under isometric constraint. The application of the triple exponential model has allowed us previously to divide the rapid thermal denaturation of collagen under isometric constraints into three phases. In these experiments, the same 3-exponential model was successfully used to fit the contraction and relaxation data during the thermal and cooling cycles. Each phase was defined by a characteristic time constants (τ_i) and a corresponding coefficient (C_i). Although it was speculated that each phase might correspond to a series of uncoiling events in the triple helical structure of the collagen, its exact validation requires additional detailed molecular experiments. The contribution of each time constant to the entire denaturation process was determined by its coefficients. Our data suggested that the first time constant (τ_1) was not only the shortest time period during the entire length of tissue unwinding, but also it contributed to more than 50% of the denaturation process as shown by its C_1 value (Table 3.1, 3.2, 3.3, and 3.4). The consequence of this finding is that the most important micro-structural changes during both the thermal and cooling transitions in both collagenous tissues occur during this short period. Although, there are other time constants (τ_2 and τ_3) their smaller coefficients suggest that these time constants do not contribute as significantly to the denaturation process. Consequently, in this study the values for τ_1 in both PC and CT, irrespective of their crosslinking treatments, were used to repeatability among the three heat cycles and equally between two cooling cycles.

Figure 3.11 compares the thermal reversibility of fresh PC and CT based on the values of the first time constant (τ_1) during the three heating cycles. They are interesting data in that the results are dependent on tissue architecture. If the τ_1 values in each thermal cycles are used

as the metric of reversibility of thermal denaturation, then thermal denaturation is fully reversible in PC and only a partial reversibility in CT. It is speculated that such differences in dynamics of the thermal denaturation may be explained in terms of the different structures and crosslinking patterns that exist in PC and CT. In fact, Rasmussen et al. [262, 263], using dermis as their experimental model, have indicated that both the collagen density and orientation played a role in the amount of thermal shrinkage, and that the dermis with higher density of collagen contracted more than loosely packed dermis. Both the raw asymptotic load (Figure 3.2) as well as the τ_1 results (Figure 3.11) for the fresh chordae indicated that relative to PC, the CT counterpart maybe more thermally stable and have different reversibility dynamics. Although the exact mechanism(s) is yet to be determined, it is believed that more aligned conformation of the CT versus the anisotropic structure of the PC might account for such differences in the thermal stability and the dynamics of denaturation. It is quite important to note, however, that slower dynamics of denaturation (i.e. higher τ_1 value) should not be interpreted as an indication of superior thermal stability. In fact, establishing a link between the dynamics of denaturation (as examined by DHIT tests) and the thermal stability (as examined by HIT tests) requires a more in-depth analysis of the molecular interactions in various crosslinking within the given collagenous tissues. Nevertheless, the comparison of the τ_1 in the first heating cycle versus the second and third heating cycles in Figure 3.11 indicated that at least with CT, the thermal transition occurs at significantly slower rate (i.e. longer τ_1) in heat cycle 1 relative to the subsequent heating cycles 2 and 3. At the same time and upon the examination of the τ_1 values for the cooling cycles, is clear that tissue relaxation occurs in a repeatable manner during the cooling cycles 1 and 2 with no significant differences between either of the tissues (Figure 3.12, and Tables 3.3 and 3.4).

Finally exogenous crosslinking of the tissues altered the dynamics of the reversibility (Figure 3.13, 3.14 and Table 3.1 and 3.2). A few observations are noteworthy: Firstly the denaturation dynamics are significantly delayed by introducing the two crosslinking agents as shown in Figure 3.13 and 3.14. The relatively longer τ_1 (specifically during the first heating cycle, shown by white columns) suggest a dramatic delaying of the dynamics of rapid thermal denaturation probably due to limitation of chain's mobility by introducing the exogenous

crosslinks. Secondly, and as far as the reversibility was concerned, it appears that the influence of crosslinking agents are literally abolished after the first heating cycles and that fresh and crosslinked tissues (i.e. both PC and CT) have similar dynamics behaviour during heating cycles 2 and 3 (Figure 3.13 and 3.14). More analyses must be conducted to study the fate of these exogenous crosslinkages following the first denaturation events. Thus, exogenous crosslinking influences the dynamics of thermal transitions in thermal cycle 1 (presumably the thermal denaturation transition) more so than the subsequent thermoelastic contractions. This observation may suggest that while additional crosslinks stabilize the helix against denaturation, they have little effect on the behaviour of the denatured "rubber".

3.5 Conclusion

The results indicated that the rapid thermal denaturation of two collagenous tissues under isometric conditions during the first heat cycle 1 is irreversible. Thereafter there is reversible thermoelastic contraction and relaxation of the rubbery, denatured collagen in response to heating and cooling respectively. This likely means that collagen structure behaved as a rubber elastic after its thermal denaturation. This may occur due to rupturing of enough hydrogen bond linkages that leave the molecule sufficiently kinetically free and flexible to behave as a true rubber. The influence of exogenous crosslinking was only observed during the first heating cycle; after the initial denaturation events, the effects of crosslinkages were abolished. Finally, the architectural differences between the two tissues may have partly accounted for the different dynamics of reversibility.

4 The Influence of Electrostatic and Entropic Factors on the Dynamics of Thermal Denaturation of Mitral Chordæ Tendineæ Under Rapid and Slow Temperature Changes

4.1 Introduction

Extensive studies have been conducted over the years to understand the mechanisms of thermal denaturation and the various factors (i.e. mechanical loads and electrostatic forces) influencing this important molecular event. Understanding these mechanisms may have far reaching implications in clinical domains, potentially minimizing the unpredictability of various clinical procedures.

It is known that various forces maintain the native conformation of the collagen molecule. The effects of salt solutions [50, 139, 143, 254, 291-297] and mechanical loads [30, 34, 145, 167, 168, 178, 298] on the stability of collagen triple helix have been described. Electrostatic interactions are believed to be one of the main contributing factors to collagen's total energy of stabilisation [299]. This idea originates from the observation that approximately 40% of the Gly-X-Y triplets of collagen contain at least one charged residue in the X or Y position [300-302]. Considering such a structural feature, it is not surprising that the electrostatic interactions contribute to the formation of both inter- and intra-chain ion pairs within the triple helix. As a result, various factors (i.e. added salts, alcohols, sugar, pH) that undermine these forces could influence the thermal denaturation characteristics of collagen from different sources [143, 303, 304]. Using optical rotatory technique, Von Hippel al. [295] established a direct correlation between the different salt concentrations and the temperatures at which collagen to gelatin (partially denatured collagen) transition (i.e. melting temperature, T_m) occurs. It has been suggested that such differences in collagen thermal stability at various salt concentrations may imply that different mechanisms are responsible for the stabilisation of the collagen molecule [305]. For instance, neutral salts may influence the rate of collagen renaturation by competitively reorganizing the water involved in stabilizing the collagen helix [295].

Equally important is the significance of mechanical loads in changing the dynamics of the thermal denaturation, recognized as early as 1949 by Weir et al. [171]. Their study showed that while the denaturation of collagen, as indicated by its shrinkage, was delayed in the presence of tensile load (or tanning agents), it was accelerated by an increase in temperature

(or hydration level). Much more recently, Humphrey et al. [30, 34, 145, 168] have conducted a series of detailed thermomechanical studies to precisely characterise the effect of complex mechanical loads under supra-physiological temperatures on various model soft tissues. In an earlier study, using the chordae tendineae as their tissue model, it was suggested that while the thermal shrinkage process was delayed under larger uniaxial isotonic loads, it was accelerated at higher temperature [30, 160]. These findings further suggested a time-temperature-load equivalency whereby similar levels of denaturation, as reflected by tissue shrinkage, can be attained via many combinations of heating time, temperature level, and mechanical loading [34, 145]. In their latest studies, and to specifically address the issue of complex loading in soft tissues in vivo, the effect of multiaxial stresses on a bovine epicardium was examined. Consistent with the earlier uniaxial studies, it was found that the epicardial shrinkage decreased with larger biaxial loads, and increased at higher temperatures. However, they failed to obtain a similar time-temperature-load equivalency since the multiaxial thermomechanics proved to be too complex to predict this event [34, 145].

In the previous two chapters, I have described and characterised the dynamics of rapid thermal denaturation and dynamics of its reversibility. On the basis of the current state of knowledge, and to probe further into the dynamics of the thermal denaturation of chordae tendineae, the following two hypotheses have prompted the current study: (i) changing collagen's external milieu, by introducing a neutral salt (i.e. NaCl) at various concentrations will destabilise the native conformations of the protein and hence affect its dynamics of denaturation and diminish its thermal stability. (ii) The presence of small mechanical loads will impede the α-chains mobility (i.e. lower its configurational entropy), increasing the protein's thermal stability and delaying its thermal transformation under dynamic temperature change.

Hence, the hydrothermal isometric tension (HIT) test was used to evaluate the quasi-static thermal stability of the chordae tendineae under various treatments, while the dynamic hydrothermal isometric tension (DHIT) test was used to assess the rapid kinetics of thermal denaturation all under isometric constraints.

4.2 Materials and Methods

4.2.1 Tissue Preparations

Bovine hearts (from mature cattle) were obtained immediately after slaughter from a local abattoir (O.H. Armstrong, Kingston, NS) and were transported to the laboratory on ice. The chordae tendineae were obtained from the fresh bovine hearts. For this experiment all mitral chordae tendineae samples were marginal and were obtained from the left ventricular chamber of the heart. The sample length ranged from 15 to 30 mm, and the mean unloaded diameter (n = 12) was 0.89 ± 0.04 (mm).

All the chordae were then rinsed three times for 5 minutes in Hanks' solution (pH 7.4, 310 mOs), and then kept in Hanks' at 4°C until subsequent treatment with two exogenous crosslinking agents.

4.2.2 Crosslinking Procedure

Tissue samples were assigned to one of the three treatment groups: (1) fresh, (2) glutaraldehyde and (3) 1-ethyl-3-(3-dimethylaminopropyl) carbodiimide hydrochloride (EDC). The exact details of crosslinking procedure were described in chapter 2.

4.2.3 Electrostatic Experiment: Sample Preparation

Sodium chloride (NaCl) of analytical grade was obtained from Sigma-Aldrich (St.Louis, MO). NaCl was selected since it is considered to be an inert salt [306]. The neutral salt solutions of various concentrations (0.1, 0.5, and 1.0 M) were prepared in double distilled water (dd H_2O). For some salt concentrations, the pH of the solution had to be adjusted to 7.4 by adding of either 0.1 M NaOH or 0.1 M HCl. All designated "salt" chordae tendineae were equilibrated in their respective salt concentrations for a period of 24 hr prior to the thermomechanical studies. No evidence of chordae solubilisation was observed upon gross examination of the tissues samples after the salt incubation.

4.2.4 Thermomechanical Tests

DHIT: Temperature-jump Thermomechanical Tests: ***System Description:*** The two-container, quick-change temperature system allowed for the simultaneous exposure of up to six samples to near-step changes in temperature (transition time < 1 s) under computer control. A full description, as well as the operational details of the DHIT, has been provided in Chapter 2. For the entropic studies, the hot and cold tanks were each filled with 4 litres of ddH_2O. However, since the electrostatic experiments were to be conducted in three different salt concentrations (i.e. 0.1, 0.5, 1.0 M), three 10 litre salt solutions of each concentration were prepared prior to the experiments. The DHIT setup was slightly modified for the electrostatic studies since the immersion heater inside the hot tank was copper-coated. In the presence of high salt concentrations, copper ions may be released and interfere with charged amino acids in the collagenous tissues. To avoid the corrosion of this coating, the hot tank was half-filled with ddH_2O, and a 400 ml beaker containing the salt solution was placed inside this tank. The stationary module, containing isometrically constrained tissues samples, could then be placed inside this salt-containing beaker during the hot cycles of the experiment. The cold tank however, did not require any modifications, since no observable corrosion occurred during the brief exposures prior to transfer to the hot tank.

The isometric constraint for the electrostatic experiments was a fixed length corresponding to an initial load of 30 g for all chordae tendineae. The entropic studies were then performed under two different isometric initial extensions (i.e. 30, and 60 g).

4.2.5 Data Analysis

A detailed description of the analytical methodology used to curve-fit the load decay data was provided in Chapter 2. Briefly, the data were first corrected and subsequently normalized with respect to the maximum asymptotic load reached during each cycle. The Levant-Marquardt nonlinear least squares method (DeltaGraph 5.0, SPSS Inc.) was applied to the normalized data from fresh and crosslinked mitral chordae tendineae with various loads and salt concentrations to identify the three characteristic time constants (τ_i) and corresponding coefficients (C_i). Equation 4.1 represents the typical three exponential

equation used to characterize the rapid structural changes induced during the thermal cycle in all tissues. This equation related the normalized force (load) ratio to three exponential functions:

$$1 - \frac{F(t)}{F_{max}} = C_1 e^{-t/\tau_1} + C_2 e^{-t/\tau_2} + C_3 e^{-t/\tau_3} \qquad \textbf{Equation 4.1}$$

where $C_1 + C_2 + C_3 = 1$.

While single- and double-exponential models were unsuccessful, a triple-exponential model provided an excellent fit to the data. The robustness and uniqueness of the three-exponential fits was established using wide variations in the seeds supplied to the nonlinear least-squares routine. A sample calculation is provided in Appendix 1. Finally the fit of the triple exponential model was verified using maximized regression coefficients (r^2).

4.2.6 Statistical Analysis

The time constants and coefficient data were initially examined using a multi-factorial analysis of variance (ANOVA) with different variables of interests, including: crosslinking treatments, salt concentrations, and initial load. Subsequently, a more detailed, one-way analysis of variance was conducted on each of the individual variables. Similarly, a Fisher's least significant difference post-hoc test was then used to extract individual differences (StatView 5.0.1. SAS). All results are expressed as the mean ± one standard error of the mean (SEM). The minimal level of statistical significance was set at p-value < 0.05.

4.2.7 Summary of Experimental Conditions for DHIT Tests

Electrostatic Studies: The DHIT analyses were conducted only on fresh mitral chordae tendineae samples incubated in 3 salt concentrations: control (no salt), 0.1, 0.5, and 1.0 M NaCl solutions. Initial loads were set at 30 g.

Entropic Experiments: The DHIT analyses were conducted on the fresh, EDC-treated and glutaraldehyde-treated mitral chordae tendineae. Experiments were conducted under two different initial loads (i.e. 30, 60 g). Incubation medium was double distilled water.

4.2.8 HIT: Slow Rate Thermomechanical Tests

The apparatus used to perform the HIT tests has been described previously [192]. As in the DHIT tests, the electrostatic studies were conducted using an initial load of 30 g, while the entropic studies were performed under two initial loads, i.e. 30, and 60 g. The samples were placed in a 4-litre Pyrex beaker, and depending on the type of the experiment, the beaker was filled with either double distilled water (entropic experiments) or various concentrations of salt solutions (electrostatic experiments). Variations in load with changing water temperature were monitored via strain-gauged cantilever load cells and associated strain gauge amplifier/conditioners. The analogue outputs of the strain gauge conditioners and the thermistor amplifier were connected to a National Instrument 12 bit A/D, D/A board (Model NB-MIO-16L) in a Macintosh Centris 650 computer. On/off heater control was achieved by connecting the analogue output of the board to a custom-built transistor relay device. Data acquisition and heater control were programmed under LabVIEW 3.0 software (National Instrument). The load/temperature/time data were collected at 1 s intervals throughout the heating period and at 30 s intervals during the isotherm. The 90 ± 0.2 °C isotherm was maintained under on-off computer control of the heater for 4 hr. It is important to mention that while in DHIT the time length for the tissue to reach the isothermal temperature from 25°C was in the order of approximately 1-2 seconds, in the HIT tests this period was extended to approximately 45 minutes (heating rate 1-2 °C/min).

4.2.9 Data Analysis

DTT Experiments: Determination of the Denaturation Temperature (T_d): The denaturation temperature (T_d) of the tissues for both entropic and electrostatic studies was defined as the temperature during slow heating at which the load vs. temperature plot began to increase abruptly [192]. The T_d is a measure of the thermal energy required to break the

intramolecular hydrogen bonds that stabilize the collagen triple helix. As was suggested by Lee et al. [192], when the triple helix is treated with exogenous crosslinking agents, the denaturation temperature can also be used as an indirect way of measuring the crosslinks; the higher the T_d value, the greater the degree of crosslinking.

Determination of Half-time of Load Relaxation ($t_{1/2}$): This analysis was only conducted for mitral chordae tendineae in the electrostatic studies. The relaxation observed over the 90°C isotherm (during the HIT tests) was expressed as $F(t)/F_{max}$: the ratio of the force, F, at time, *t*, to the maximum force at the beginning of the isotherm (F_{max}). The relaxation of a denatured, purely collagenous network undergoing peptide bond hydrolysis, follows a Maxwell-type relationship as described by Le Lous et al. [141].

$$\frac{F(t)}{F_{max}} = e^{-kt} \qquad \textbf{Equation 4.2}$$

The logarithm of $F(t)/ F_{max}$ was plotted versus time (during the 90 °C isotherm). This resulted in a straight line. The data from the last 10,000 s of the isotherm was used to obtain the slope of the line by linear regression (Excel X, Microsoft Corp.) and also used to calculate the half-life of stress relaxation, $t_{1/2}$, where $F(t_{1/2}) = 1/2\ F_{max}$. As a result, Equation 4.2 becomes:

$$\frac{1}{2} = e^{-kt_{1/2}} \qquad \textbf{Equation 4.3}$$

Taking the logarithm of both sides of Equation 4.3 gives $t_{1/2} = ln(2)/k$, where $-k$ is the slope of the last 10,000 seconds of the plot of $[F(t)/F_{max}]$ versus time.

The $t_{1/2}$ is dependent on the hydrolysis of the peptide bonds within the denatured collagen matrix and is believed to be proportional to the polymeric chain density and inversely proportional to the number of bonds ruptured per unit time [140]. As peptide bonds hydrolyze, chains slip past each other, resulting in a reduction in the load-bearing capability of the tissue. Therefore, this particular parameter could indicate whether or not various salt

concentrations have any influence on the thermal stability of peptide bonds in the collagen backbone.

4.2.10 Statistical Analysis

Values of T_d and $t_{1/2}$ for both electrostatic and load experiments were obtained by averaging the individual results for each experiments. For the electrostatic study, T_d, were analysed using two, single-factor analyses of variance with crosslinking treatments and salt concentrations as the variables of interest. The stress decay half-life, $t_{1/2}$, data were also examined using, a one-way analysis of variance with salt concentrations as the only variable of interest. A Fisher's least significant difference post-hoc test was then used to extract individual differences (StatView 5.0.1. SAS). All results are expressed as the mean ± one standard error of the mean (SEM). The minimal level of statistical significance was set at p-value < 0.05. A linear regression model (StatView 5.0.1. SAS) was used to fit and to correlate the overall stress decay versus the denaturation temperature data. A regression coefficient (r^2), and a p-value were then determined to determine the strength of the correlation between the two variables.

4.2.11 Summary of Experimental Conditions for HIT Tests

Electrostatic Experiments: The HIT analyses were conducted to determine the T_d for the fresh, EDC and glutaraldehyde treated mitral chordae tendineae incubated in three salt concentrations: control (no salt), 0.1, 0.5, and 1.0 M NaCl solutions. The $t_{1/2}$ was only determined for fresh mitral chordae tendineae incubated in various salt solutions. Initial loads were at 30 g.

Entropic Experiments: The DTT analyses were conducted on the fresh, EDC and glutaraldehyde treated mitral chordae tendineae to determine their T_d at 30 and 60 g; the stress decay half-life experiments ($t_{1/2}$) were not performed for the entropic experiment. Incubation medium was double distilled water.

4.3 Results

4.3.1 Electrostatic Studies

HIT Tests: Table 4.1 indicated there exists a downward shift in both T_d and $t_{1/2}$ when tissue samples were treated with neutral salt at various concentrations. In other words, the NaCl had a clear thermal destabilising effect on fresh chordal samples as indicated by T_d and $t_{1/2}$ relative to the control (non-salted) group. The one-way ANOVA analyses revealed that the T_d of the control chordae (69.0°C ± 1.0) was significantly higher than those in different salt concentrations (p-value < 0.0001). Interestingly, the lack of any statistical differences in denaturation temperatures among the various concentration groups suggested that chordal samples are equally destabilised irrespective of salt concentrations.

Parallel to the previous findings, the results from stress decay half-life, $t_{1/2}$, suggested that there are significant differences in thermal stabilities of fresh chordae and those incubated in the various salt concentrations (Table 4.1). The "salted" samples (irrespective of their concentrations) exhibited significantly shorter relaxation half-lives. The calculated $t_{1/2}$ for the control group (47.0 ± 10.0 hr) is at least twice as long as for any tissue incubated in salt solutions, irrespective of their concentrations. Once again, the analysis of $t_{1/2}$ within the various salt concentrations failed to generate any statistical differences, among the different half-lives. Hence, from both T_d and $t_{1/2}$ results, although the presence of NaCl has altered the thermal stability of fresh chordae tendineae, they failed to generate any significant differences in the thermal stabilities due to variations in salt concentrations.

In light of these findings and to further examine the possible correlation between the two parameters of the quasi-static tests, a scatter plot of T_d and $t_{1/2}$ is shown in Figure 4.1. As was shown before, the tissue incubated in various salt concentrations had a lower

Treatments	Denaturation Temperature, T_d (°C)	Half-Life of Stress Decay, $t_{1/2}$ (hr)
Control (no salt)	69.0 ± 1.0[a] (n = 7)	47.0 ± 10.0[a] (n = 7)
0.1 Molar	66.0 ± 0.2[b] (n = 10)	17.0 ± 2.5[b] (n = 10)
0.5 Molar	67.0 ± 0.3[b] (n = 8)	16.5 ± 4.0[b] (n = 8)
1.0 Molar	67.0 ± 0.4[b] (n = 6)	22.0 ± 7.0[b] (n = 6)

Table 4.1. Mean denaturation temperature, T_d, and stress decay half-life, $t_{1/2}$, for fresh marginal chordae tendineae in different NaCl concentrations. The mean ± SE, p-value < 0.05 was created by one-way analysis of variance with a single variable of interest of salt concentrations, for each column. This was followed by a post-hoc Fisher's test. For each measurement (T_d and $t_{1/2}$), values labelled with the same letter are not significantly different.

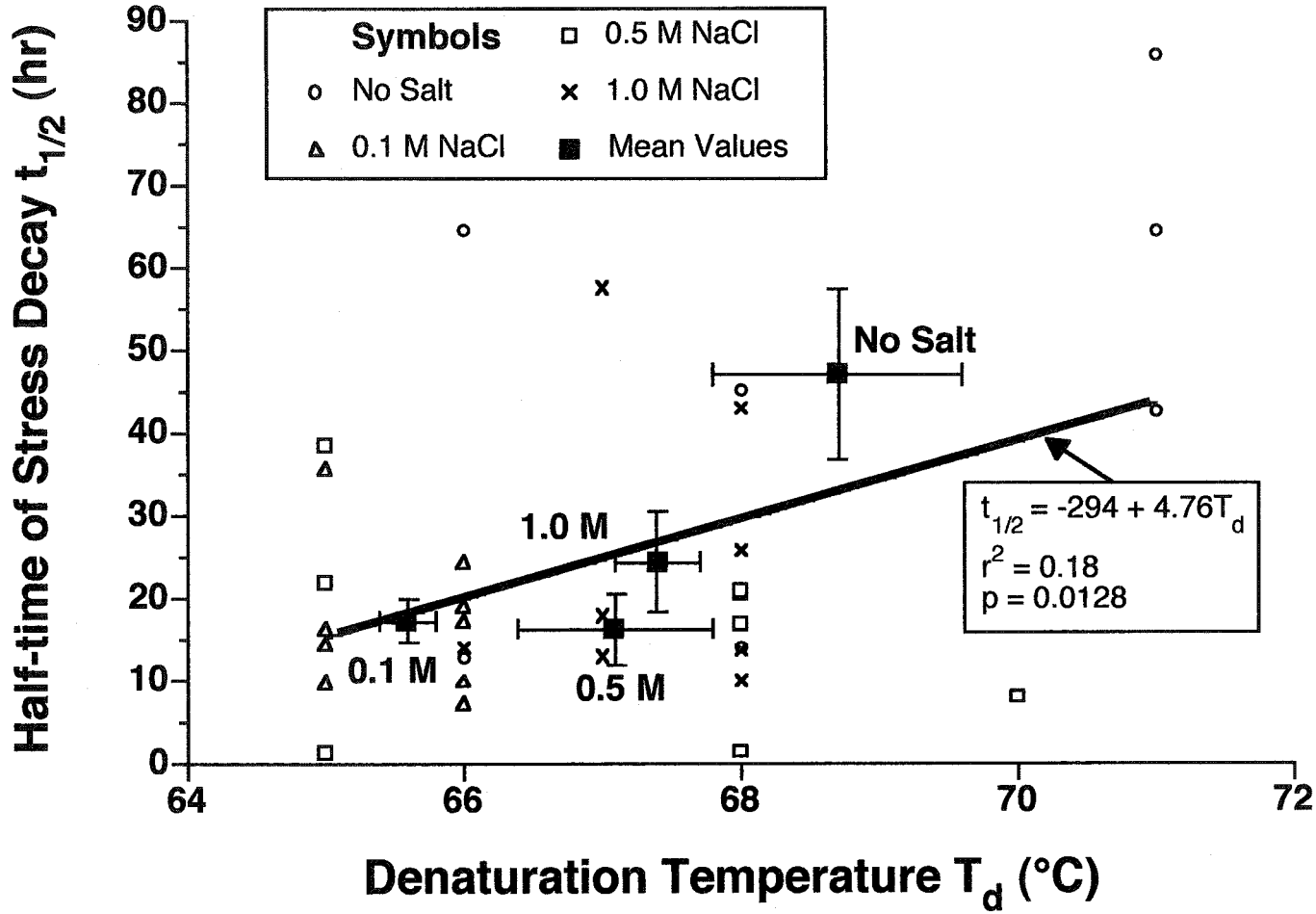

Figure 4.1 Scatter plot of stress decay half-life ($t_{1/2}$) versus denaturation temperature (T_d), as a function of different salt concentrations. The regression coefficient ($r^2 = 0.18$) suggests a weak correlation between the two variables. The mean ± SE, p-value < 0.05, created by two-way analysis of variance with two different variables ($t_{1/2}$ and T_d), followed by post-hoc Fisher's tests.

denaturation temperature and shorter stress decay half-life. As such these samples are found on the bottom-left part of this scatter plot. Conversely, the untreated chordal samples not only possess a higher denaturation temperature but also significantly longer stress decay half-life. Although, the regression coefficient ($r^2 = 0.18$) of this plot is quite small, it still suggests the presence of a weak correlation between the T_d and $t_{1/2}$. The individual single-factor analysis of variance was conducted on both T_d and $t_{1/2}$ as a function of salt concentrations to extract the statistical differences between the two groups.

The data of T_d for fresh and crosslinked chordae tendineae in various salt concentrations are shown in Table 4.2. Two one-way analysis of variance with different variables of salt concentrations and crosslinking treatments were conducted. The comparison in the control (untreated) group revealed, unsurprisingly, that treatment of tissues with two different crosslinking agents (i.e. EDC and glutaraldehyde) enhanced the thermal stability by at least 14 °C (the differences in the Table 4.2 are shown by capital letters). The same effects are also observed in most salt-treated tissues. The significance of such observations may be that crosslinking with the exogenous agents seem to protect the chordal samples from electrostatically destabilising effects of different salt concentrations. Furthermore, it is important to notice that, when comparing the denaturation temperatures within most salt concentrations (except 0.5 M), the glutaraldehyde treated samples have a higher and significantly different value than the EDC-treated samples. Hence, glutaraldehyde-treated chordal samples seemed to be more thermally resistant to the influence of salts versus the EDC-treated chordae.

On another level, the one-way analysis of variance with salt concentration as the main variable of interest revealed that there were no significant statistical differences among the control group and different salt concentrations (except 0.5 M). Once again the crosslinking seem to protect the tissues from deleterious effect of salts and also improved the thermal stability of the tissue samples relative to untreated chordae tendineae.

DHIT tests: These tests permitted the measurement of the various time constants and their corresponding coefficients, and indicated whether or not these parameters were modified by the presence of the neutral salt. These tests were only carried out on fresh (non- crosslinked)

Treatment	Control	0.1 M	0.5 M	1.0 M
Fresh	$69.0 \pm 1.0^{a,A}$	$66.0 \pm 0.2^{b,A}$	$67.0 \pm 0.3^{b,A}$	$67.0 \pm 0.4^{b,A}$
	(n = 7)	(n = 10)	(n = 8)	(n = 6)
EDC	$83.0 \pm 1.0^{a,B}$	$83.0 \pm 1.0^{a,B}$	$85.0 \pm 0.3^{b,B}$	$83.0 \pm 0.5^{a,B}$
	(n = 5)	(n = 5)	(n = 5)	(n = 5)
Glutaraldehyde	$86.0 \pm 0.3^{a,C}$	$86.0 \pm 0.2^{a,C}$	$82.0 \pm 0.2^{b,C}$	$85.0 \pm 0.3^{a,C}$
	(n = 5)	(n = 5)	(n = 5)	(n = 5)

Table 4.2. The influence of crosslinking and various NaCl concentrations on the denaturation temperature, T_d, of fresh and crosslinked (EDC and glutaraldehyde) marginal mitral chordae tendineae. The mean ± SE with p-value < 0.05 was created by single-factor analysis of variance with two different variables: crosslinking (along each column) and salt concentrations (down each row). This analysis was followed by a post-hoc Fisher's test. While the capital letters correspond to the differences crosslink treatments, the small letters represent the differences with respect to the salt concentrations. Values labelled with the same letter are not significantly different.

tissues. Table 4.3 showed that the multi-staged nature of the rapid thermal denaturation was maintained in the controls and at all different salt concentrations. Similar to the previous chapters, the first time constant (τ_1) represented the shortest time period during the entire uncoiling, followed by an intermediate (τ_2) and finally longest time constants (τ_3). The contribution of each of these time constants to the entire denaturation process was emphasized by their corresponding coefficients constants (C_i). To analyse if τ_i or C_i, varied as a function of different salt concentrations, a one-way ANOVA, with respect to salt concentration was conducted (differences were shown with the small letters) (Table 4.3). The differences with each variable, indicated that all τ_i and most C_i values, were significantly different from each other in a given salt concentration group (comparison along each row). Such statistical differences among the three τ_i and C_i parameters led to the conclusion that despite the presence of salt ions, the rapid thermal denaturation remained a three-staged phenomenon. The statistical differences of the most important time constant (i.e. τ_1) revealed that the dynamics of rapid thermal denaturation appeared to be slower in salt-treated chordal relative to the control group (Figure 4.2). Similar analysis, this time on the first coefficient (C_1) for all fresh and crosslinked tissues resulted in no statistical differences representing at least 70% of the thermal denaturation (Table 4.3). The second and third time constants as well as their corresponding coefficients are also shown in the Table 4.3, and as shown by their corresponding coefficients, they are less significant contributors to the denaturation than is τ_1.

4.3.2 Effect of Initial Extension on the Stability of Chordae Tendineae

HIT tests: Figure 4.3 demonstrates the influence of two different initial loads (i.e. 30 and 60 g), and thereby different fixed extensions, on the denaturation temperature of fresh CT and two exogenously crosslinked (glutaraldehyde and EDC) chordae tendineae. The effect of loading on fresh and crosslinked tissues were examined using two separate single-factor analysis of variance with two variables of interests: crosslinking treatments and load groups. The comparison between the two load groups (differences shown by the small letters), in control and glutaraldehyde-treated chordae indicated that when increasing the load from 30 to 60 g, the thermal stability of the tissue improved slightly yet significantly. Comparison among the three treatments also revealed that possibly both crosslinking and increased loads

Treatment	Time Constants (s)			Coefficients (%)		
	τ_1	τ_2	τ_3	C_1	C_2	C_3
Control (no salt)	1.9 ± 0.2[a] (n = 14)	74 ± 17[a] (n = 14)	802 ± 210[a] (n = 14)	70 ± 3.0[a] (n = 14)	16 ± 2[a] (n = 14)	15 ± 3[a] n = 14
0.1 M	3.2 ± 0.3[b] (n = 12)	93 ± 14[a] (n = 12)	860 ± 120[a] (n = 12)	74 ± 1.3[a] (n = 12)	17 ± 1[a] (n = 12)	9.0 ± 2[a] (n = 12)
0.5 M	4.4 ± 0.7[b] (n = 10)	144 ± 44[a] (n = 10)	1791 ± 510[b] (n = 10)	72 ± 1.4[a] (n = 10)	23 ± 2[b] (n = 10)	5.0 ± 2.0[b] (n = 10)
1.0 M	4.0 ± 0.7[b] (n = 12)	110 ± 23[a] (n = 12)	990 ± 390[a] (n = 12)	73 ± 2.4[a] (n = 12)	15 ± 2[a] (n = 12)	12 ± 4[a] (n = 12)

Table 4.3 Influence of different NaCl concentrations in altering the dynamics of multi-staged nature of rapid thermal denaturation of fresh marginal mitral chordae tendineae. The mean ± SE with p-value < 0.05 was created by single-factor analysis of variance with salt concentration as the variable of interest. This analysis was followed by a post-hoc Fisher's test. Values labelled with the same letter are not significantly different

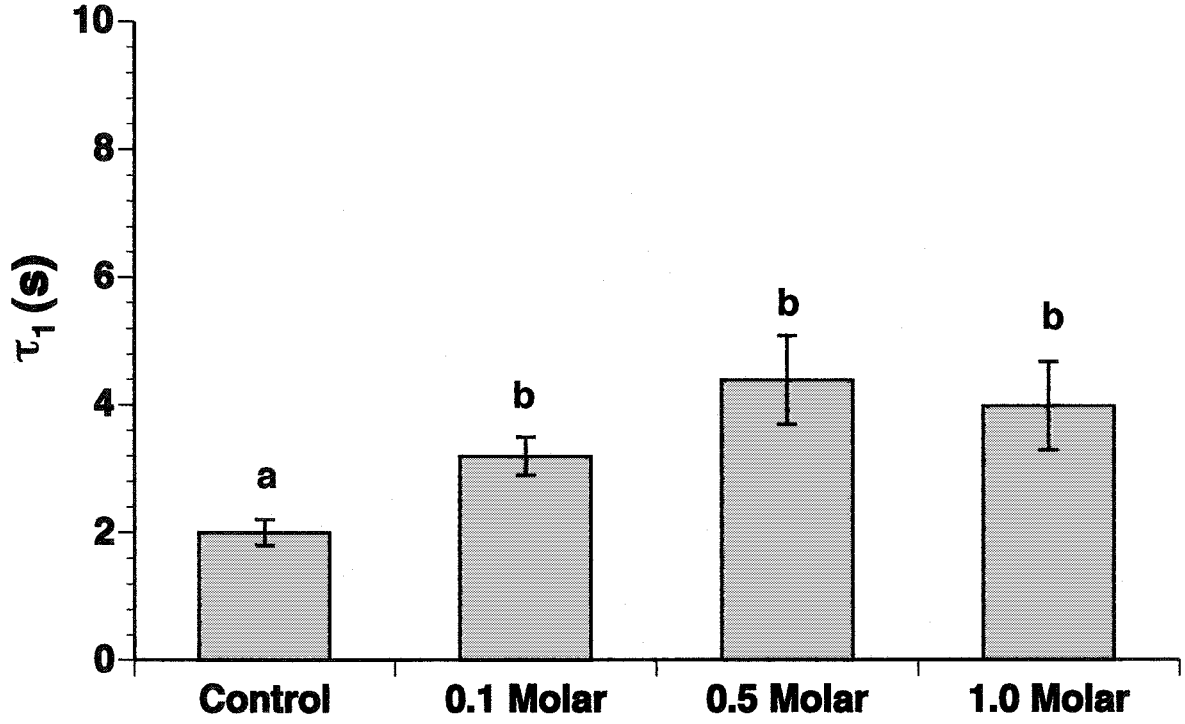

Figure 4.2 Effect of different salt concentrations on rapid thermal transition of the fresh marginal mitral chordae tendineae samples as indicated by the first time constant (τ_1). The number of samples (n) are as follow: Control = 14, 0.1 M = 12, 0.5 M = 10 and 1.0 M = 12. The mean ± SE, p-value < 0.05 created by a single analysis of variance with salt concentration as the variable of interest, followed by post-hoc Fisher's test. Values labelled with the same letter are not significantly different.

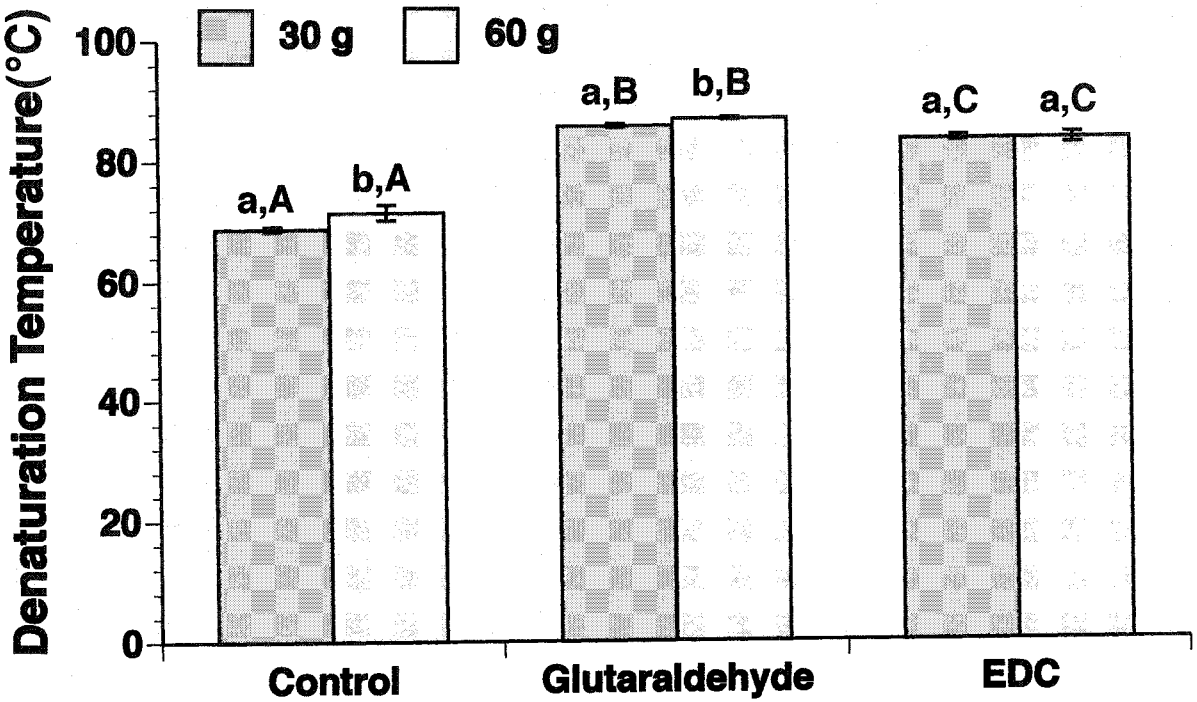

Figure 4.3 Effect of various loads on thermal denaturation (T_d) of fresh, glutaraldehyde- and EDC-treated marginal mitral chordae tendineae. The number of samples (n) for the 30 g group are as follow: control = 20, glutaraldehyde and EDC = 11. For all the 60 g tissue groups is 6. The mean ± SE, p-value < 0.05 was created by 2-separate one-way analysis of variance with individual variables of interests: loads and crosslinking treatments. These analyses were followed by a post-hoc Fisher's test. While the capital letters correspond the differences with respect to the different crosslinks, the small letters correspond to those with respect to the load groups. Values labelled with the same letter are not significantly different.

contributed to an improved thermal stability of the chordal samples.

DHIT tests: Table 4.4 shows the entire data set on the effects of initial extensions on the multi-staged nature of the thermal denaturation in fresh, and crosslinked tissues. Two separate single-factor analysis of variance were conducted to distinguish the differences between the two load groups in a given treatment (i.e. fresh τ_i and C_i in 30 vs. 60 g), and also the individual τ_i and C_i within a given load (i.e. 30 g τ_i and C_i, in fresh, glutaraldehyde and EDC-treated samples). Generally, the three consecutive time constants (τ_1, τ_2, τ_3) and their corresponding coefficients (C_1, C_2, C_3) in all individual load groups of each tissues treatments remained statistically different (analysis not shown). This indicated that the 3-staged nature of rapid denaturation was not altered by the presence of various loads. Figure 4.4 shows the specific influence of different loads on the first time constant (τ_1) in the fresh-, glutaraldehyde- and EDC-treated chordae tendineae. Examination of the τ_1 in the control group revealed that there were no statistical differences between the 30 g and 60 g groups (shown by small letters). In contrast, comparison within both crosslinking groups, suggested that imposing a higher initial extension resulted in slower dynamics of denaturation in both glutaraldehyde- and EDC-treated chordae. In fact, while the τ_1 for glutaraldehyde groups at 30 g was 2.7 ± 0.4 s, at 60 g it was increased by almost a factor of three to 6.4 ± 1.0 s. This may be an indication that the combined effect of crosslinking and increased load may contribute to a slower dynamics of helix-coil transition as indicated not only by τ_1 but also by τ_2 and τ_3 as shown on Table 4.4. Interestingly, although there were significant differences between the τ_1 values of control group relative to glutaraldehyde and EDC group at 60 g, this variable was virtually unchanged in 30 g group.

Load (g)	Time Constants (s)			Coefficients (%)		
	τ_1	τ_2	τ_3	C_1	C_2	C_3
			Fresh			
30	$2.0 \pm 0.2^{A,a}$ (n = 14)	$74 \pm 17.0^{A,a}$ (n = 14)	$802 \pm 210^{A,a}$ (n = 14)	$69.0 \pm 3.0^{A,a}$ (n = 14)	$16.5 \pm 2.3^{A,a}$ (n = 14)	$15.0 \pm 2.5^{A,a}$ (n = 14)
60	$2.6 \pm 0.3^{A,a}$ (n = 6)	$186 \pm 80.5^{A,a}$ (n = 6)	$770 \pm 43^{A,a}$ (n = 6)	$67.0 \pm 1.5^{A,a}$ (n = 6)	$16.0 \pm 3.0^{A,a}$ (n = 6)	$16.0 \pm 3.3^{A,a}$ (n = 6)
			Glutaraldehyde			
30	$2.7 \pm 0.4^{A,a}$ (n = 23)	$49.0 \pm 7.0^{A,a}$ (n = 23)	$678 \pm 103^{A,a}$ (n = 23)	$63.0 \pm 3.1^{A,a}$ (n = 23)	$27.0 \pm 3.5^{A,a}$ (n = 23)	$10.0 \pm 1.2^{B,a}$ (n = 23)
60	$6.4 \pm 1.0^{B,b}$ (n = 7)	$146.0 \pm 37.0^{A,a}$ (n = 7)	$1310 \pm 274^{B,b}$ (n = 7)	$59.0 \pm 6.2^{A,a}$ (n = 7)	$26.1 \pm 5.0^{A,a}$ (n = 7)	$15.0 \pm 1.7^{A,a}$ (n = 7)
			EDC			
30	$2.7 \pm 0.4^{A,a}$ (n = 28)	$53.0 \pm 7.0^{A,a}$ (n = 28)	$550 \pm 25.0^{A,a}$ (n = 28)	$65.0 \pm 3.0^{A,a}$ (n = 28)	$20.0 \pm 3.0^{A,a}$ (n = 28)	$15.0 \pm 1.7^{A,a}$ (n = 28)
60	$8.0 \pm 2.4^{B,b}$ (n = 5)	$472.0 \pm 120^{B,b}$ (n = 5)	$450 \pm 73.1^{A,a}$ (n = 5)	$42.0 \pm 11.0^{B,b}$ (n = 5)	$36.0 \pm 4.0^{B,b}$ (n = 5)	$32.5 \pm 8.5^{B,b}$ (n = 5)

Table 4.4 Effect of two different loads (30 and 60 g) in altering the dynamics of multi-staged nature of rapid thermal denaturation of fresh marginal mitral chordae tendineae. The mean ± SE with p-value< 0.05 was created by single-factor analysis of variance with two variables of interest: comparison between two loads in a given tissue treatments (small letters), and comparison between the similar load groups in the different crosslink treatments (capital letters). This analysis was followed by a post-hoc Fisher's test. Values labelled with the same letter are not significantly different.

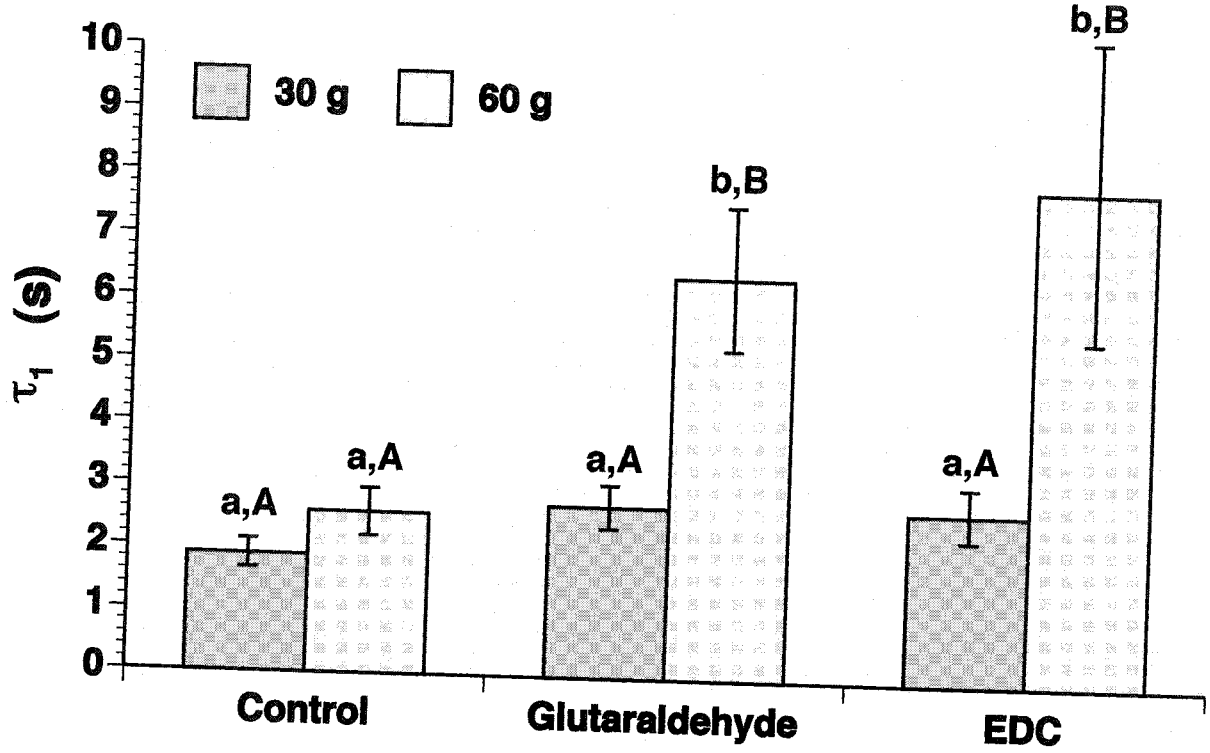

Figure 4.4 Effect of two different loads in altering the dynamics of rapid thermal denaturation as indicated by the first time constants (τ_1). Number of samples (n) for the 30 g group are as follow: control = 18, glutaraldehyde = 23, EDC = 28; Number of samples for the 60 g group are: control = 8, glutaraldehyde = 7, and EDC = 5. The mean ± SE, p-value < 0.05 was created by one-way analysis of variance with two individual variables of interests: loads and crosslinking treatments. This analysis was followed by a post-hoc Fisher's test. While the capital letters correspond to the differences in crosslinking treatments, the small letters correspond to those with respect to the load groups. Values labelled with the same letter are not significantly different.

4.4 Discussion

4.4.1 Effect of NaCl on the Thermal Stability of Chordae Tendineae

Two types of thermomechanical tests (i.e. HIT and DHIT) were performed here to examine the effect of NaCl on the thermal stability and the dynamics of thermal denaturation of marginal mitral chordae tendineae. The results of our denaturation temperature tests (DTT) clearly indicated that, in the presence of NaCl solution (irrespective of their concentrations) chordae become thermally less stable (as shown by low T_d), relative to the control group (Table 4.1). The denaturation temperature corresponds to the rupture of the majority of the intrahelical hydrogen bonds within the collagen triple helix leading to its transition from an ordered, helix form into a more random, and rubber-like configuration [89, 91, 193]. At the same time, native intermolecular crosslinks may also contribute to thermal stability by coupling the nonhelical terminal end of a collagen molecule to an adjacent triple helix [91]. Although the regression coefficient ($r^2 = 0.18$) for the Figure 4.1 suggests a weak correlation between the denaturation temperature and stress decay half-life, it may still be suggested that in the presence of salt ions, the inter- and intramolecular interactions are possibly destabilised, by various electrostatic mechanism(s), thereby influencing the thermal stability of the collagen network in chordae tendineae.

It has previously been shown that salt ions are able to affect the thermal stability of proteins in three ways: (i) by directly interfering with various electrostatic, hydrophobic, and hydrogen bonding interactions, and hence influencing the critical balance of forces stabilizing the collagen triple helix [292, 306], (ii) by indirectly influencing the structure and properties of the solvents (i.e. water) which surrounds the protein [50, 295, 307], or (iii) by the combination of the two. Von Hippel and co-workers [295] suggested that neutral salts are able to alter the melting temperature of the collagen triple helix through a direct interaction wherein salt lies within the H-bond, rather than attacking the interchain crosslinks themselves. As mentioned in Chapter 1, the ability of the triple helix to form both intra- and interchain ion pairs may be due the fact that 40% of the Gly-X-Y triplets of collagen contain at least one charged residue in the X or Y position, hence electrostatic interactions play an

essential role in stabilising the collagen triple helix and significantly contributing to the total energy of stabilisation of the triple helix [299-302]. Moreover, a detailed analysis of primary collagen structure shows a considerable number of pairs of closely situated amino-acid residues bearing opposite electric charges (Glu^-–Arg^+, Asp^-–Arg^+, Asp^-–Lys^+, Glu^-–Lys^+, etc) [300, 308]. It is highly probable that a reduction in collagen thermal stability may partially be attributed to the salt ions' ability to directly interact with various charged groups [143]. As such, they are capable of shielding these groups, hence thermally destabilising the collagen triple helix [143].

Additionally, salt ions can also indirectly affect the stability of the triple helix by influencing the structure and properties of the solvents (i.e. water). Since collagen is a highly hydrated protein, conditions affecting its water content may also influence its thermal stability [50, 295, 307]. In fact, in a crystal formed by a collagen-like peptide, adjacent triple helices have little or no direct contact; the connections are maintained by hydrogen-bonded water bridges [51, 309].

The mechanism of the thermal stabilization/destabilization of the collagen triple helix originates from the competition of the protein surface groups and various salt ions with water molecules [143]. Some salts (i.e. kosmotropes, water structure makers) tend to reduce the interface area and stabilize the proteins against thermal uncoiling [306]. They are preferentially excluded from the protein interfacial area. In other words, in their presence, proteins are preferentially hydrated, and hence thermally stable. By destabilising the structure of the bulk water, other salts (chaotropes, water structure breakers) have the opposite effect. The solute effect of such kind is generally termed a Hofmeister or Lyotropic effect. The ability of salts and various low-molecular solutes to exhibit such lyotropic effect has long been known and have also been shown in numerous studies of different interfaces [310]. While salts such as NaCl and KCl are known to have little effect on the native protein structure due to the position of the Cl^- ion in the Hofmeister series (i.e. neither kosmotropic nor chaotropic), others such as $(NH_4)_2SO_4$, and KH_2PO_4 stabilise the native structure and yet others such as KSCN and LiBr destabilize it [311]. NaCl was selected since it neither stabilizes nor destabilizes the collagen triple helix. Nevertheless, it does have a marked effect on the morphological structure of the collagen. Small-angle light scattering (SALS) studies

have indicated a decrease in intensity, which is proportional to the concentration of the NaCl solution [312]. The process was reversible since removal of the NaCl by intense washing resulted in nearly complete recovery of SALS pattern of an untreated specimen. Generally, SALS has the ability to characterize tissue features on a micron scale, and hence it is suitable for the analysis of collagen structure and architecture [313, 314]. This is in contrast to X-ray scattering that characterize structural features on a nanoscale features. Burjanadze et al. [315] reported a decrease in thermal stability upon addition of 0.1 M NaCl to a collagen solution, while sugar and polyols were found to increase the thermal stability of acid-soluble calf skin collagen. Russell et al. [303] also observed denaturation at lower temperature of solubilised calf skin collagen in alcohol-buffer media upon addition of up to 1 M KCl. They have however, suggested that the latter observation is considered to be due to modulation of the electrostatic interactions.

As was mentioned before, the stress decay half-life is dependent on the hydrolysis of the peptide bonds within the denatured collagen matrix. In fact, it is proportional to the polymeric chain density and inversely proportional to the number of bonds ruptured per unit time [141]. As peptide bonds hydrolyse, chains slip past each other resulting in a reduction in the load bearing capability of the tissue. Thermally stable crosslinks within the denatured network provide structural reinforcement and delay this process. Accordingly, it may be speculated that the shorter $t_{1/2}$ in the "salted" chordae may be due to the effect of the salt ions by either decreasing the number of thermally stable crosslinks and/or reducing the stability of backbone peptide bonds. It is however, interesting to note that in the presence of the salt, irrespective of the concentration, chordae becomes thermally weaker as shown by lower $t_{1/2}$ and T_d. In other words, both results from DTT and HIT suggest, that salt ions destabilise the collagen structure by weakening all of the interactions (e.g. hydrogen bonds, covalent crosslinks and etc.). This is in some way shown by the scatter plot in Figure 4.1, which suggest a weak correlation between $t_{1/2}$ and T_d.

Upon a closer examination of the data (Figure 4.1, and Table 4.1), it is clear that although NaCl has thermally destabilised the chordae tendineae, this was not accomplished in a concentration-dependent manner. In fact, despite using three different salt concentrations, there were little or no statistical variations in different parameters ($t_{1/2}$ and T_d) of thermal

stability. Conversely, other studies have clearly established a dependence of collagen thermal stability based on different salt concentration [143, 295]. This may suggest that different mechanisms may be responsible for the salt effect on collagen thermal stability. In a study, using an acid-soluble collagen type I from calf skin, Komsa-Penkova et al. [143] has shown that at lower range of concentration (i.e. < 0.02 M), all salts reduced the T_d. This effect was attributed to screening of electrostatic interactions leading to collagen destabilisation. At higher concentrations (i.e. 0.02-0.5 M), the different salts either slightly stabilised or further destabilised the collagen molecule in a salt-specific way that correlated with their position in the lyotropic series. This effect (Hofmeister effect) was generally associated with indirect protein-salt interaction exerted via competition for water molecules between ions and the protein surface. At still higher concentrations (0.2-0.8 M, depending on different salts), the T_d and solution opacity increased for all salts due to protein salting out effect [143]. The discrepancy on the salt concentrations effect and its relation to the thermal stability of the collagen triple helix may draw attention to the possibility that different electrostatic mechanism(s) may be involved in stabilization of soluble collagen versus the fibrillar form.

The data in Table 4.2 clearly indicate that both crosslinked tissues exhibited superior thermal stabilities relative to the fresh chordae irrespective of the salt concentrations. Furthermore, the glutaraldehyde treated samples have consistently higher T_d than the EDC group (except in 0.5 M). As suggested in Chapter 2, this might indicate that a more effective crosslinking pattern is provided by the glutaraldehyde than by the EDC. However, as Cheung and Nimni [69, 70] suggested, glutaraldehyde crosslinking creates an artificial chemical barrier on the surface of the collagen fibres that acts as an effective impediment, limiting the access of different ions and other molecules within the collagen fibres. It is therefore speculated such that glutaraldehyde's hydrophobic core may also limit the access of the salt ions into the collagen fibres and hence protect them against the deleterious effect of different salts. Hence, although exogenous crosslinking, in general, appear to make the collagenous tissues more "thermally" and "mechanically" stable [316, 317], the current findings further suggest that such agents may also protect them from the "electrostatic" interference of the salt ions. As shown in Table 4.2, although there is a clear difference between non-salted and salted T_d in the fresh chordae, such variations in T_d disappear once the tissues are exogenously crosslinked. In other words, there were no statistical differences between the control and

"salted" crosslinked tissues: hence, upon introduction of either of the crosslinking agents, the tissues are protected from the destabilising effects of the salt at any concentrations.

Another mechanism by which collagenous tissues may become thermally stabile, relates to the morphological changes that occur upon crosslinking of the tissues, in particular changes in tissue's moisture content. For instance, it was shown that crosslinking of the bovine pericardia, significantly lowered the moisture content of the tissue and led to its shrinkage [290]. The percent moisture content was calculated based on the measured wet and dry tissue weights. Accordingly, tissue shrinkage indeed attributed to the reduction of the free volume in the tissue and thus expelling of some water molecule out of the fixed tissues [290].

On the basis of the current findings then, one or any combinations of the following three hypotheses may rationalize our data. First the shrinkage of collagen fibres due to exogenous crosslinking may shorten the interfibrillar distances in the collagen triple helix, hence limiting the access of the salt ions to any charged group within the triple helix (this may also "squeeze" the water molecule out of the chains). This in turn, may prevent the direct electrostatic interference of salt ions and hence, thermally stabilise the collagen triple helix. Secondly, by exogenously crosslinking of the collagen fibrils, the available charged amino acids sites are now simply unavailable. Finally, crosslinking with glutaraldehyde creates a chemical barrier around the collagenous fibres, limiting the access of various salt ions, hence protecting the underlying collagen network. Many more studies however, need to be conducted to elucidate the exact nature of the protein-salt interactions.

The statistical analyses revealed that the τ_1 for all the salt-treated tissues, irrespective of the salt concentrations, increased significantly relative to the fresh samples (Figure 4.2). This suggests that it take almost twice as long for the "salted" tissues to undergo the same uncoiling event as in the fresh samples. It can, then, be speculated that the longer time period may imply the presence of stronger chain interactions, which in turn, requires more time to reach a given energy threshold necessary to rupture these bonds. Hence, using the current results, it may be suggested that the salt ions will thermally destabilise the collagen molecule, and at the same time delay the transition dynamics of thermal denaturation by possibly interfering with this event. As was discussed in Chapter 2, it may be speculated that

the event(s) occurring during the τ_1 period may correspond to the initial rupturing of the heat labile, non-covalent hydrogen bonds. Indeed, as shown in Table 4.3, salts generally, delayed the overall dynamics of denaturation (i.e. helix-coil transition) as indicated by on overall increase in all other time constants (e.g. τ_1, τ_2, τ_3). Although more detailed studies into the exact nature of the salt-protein interaction must be conducted to exactly elucidate this event, it is possible that non-specific binding of the salt to the triple helix may impede dynamics of the helix-coil transition. Despite such general delaying of the uncoiling process relative to control group, the presence of the salt did not alter the 3-staged dynamics of thermal denaturation, as defined by three time constants: fast (τ_1), intermediate (τ_2) and slow (τ_1), and their corresponding coefficients (C_1, C_2, and C_3).

The preceding discussion focused mainly on the effect of salts on the collagen fibrils within the chordae tendineae. However, the thermal behaviour of this tissue may also be influenced by the presence of another connective tissue component of the of normal chordae tendineae: i.e. proteoglycans (PG) [125]. Although not quantified, the presence of PGs in the human chordae was demonstrated by immunohistochemical studies [124]. The PGs are macromolecular glycoconjugates consisting of specialized polysaccharide chains called glycosaminoglycans (GAGs) attached covalently to a protein core by a specific carbohydrate sequence. Structurally, GAGs are linear polymers of negatively charged repeated disaccharides [318]. Functionally, due to their polyanionic character, GAGs can bind other molecules, especially cationic amines, peptides, and proteins. In particular, an electrostatic interaction between collagen and different types of GAGs has been demonstrated by qualitative methods in vitro [319-321] and at physiological ionic strength [322]. Using collagen from rat skin, Obrink et al. [323], have further indicated that the binding of collagen to various GAGs and PGs occur via complex electrostatic interactions and more importantly such interactions can be abolished by increasing the ionic strengths. Furthermore, an important property of proteoglycans, is their ability to bind water; it is believed that such interactions strongly influence the mechanical characteristics of connective tissues [324].

As suggested earlier, salt ions may be able to compete directly or indirectly with various charged components and water molecules to destabilise the collagen structure. Similarly, it would not be surprising if the same interaction occurred with the charged (i.e. anionic)

structure of the GAGs and/or PGs. This may further lead to thermal weakening of the chordae tendineae, and altering its thermomechanical behaviour. Although highly speculative, the presence of salts may have influenced the collagen-GAG electrostatic interactions, and resulted in a tissue with weaker thermomechanical properties. More detailed studies must be conducted to fully understand the thermomechanical behaviour of the PGs and GAGs, and how the various factors (i.e. ionic strength) may alter these behaviours.

Furthermore, a review of literature indicated that different exogenous crosslinkers have different effects on the stability of GAGs. In fact, Simionescu et al. [325] suggested that although glutaraldehyde readily crosslinks collagen, it does not have the capacity of crosslinking the GAGs. Hence, they suggested that this may partially contribute to bioprosthetic heart valve degeneration (via enzymatic mechanism) and subsequent structural failure [325]. Conversely, EDC and NHS have been used to covalently crosslink various GAGs (e.g. dermatan surlfate, heparin, heparan sulfate and condriotin sulfate) to collagen components [326]. The mechanism for such crosslinking may be related to availability of the carboxylic groups in GAGs molecules. As mentioned in Chapter 1, EDC crosslinking is performed by the activation of the carboxylic acid groups, which subsequently react with free amino groups to form an amide bond [327]. Finally, despite the apparent effectiveness of EDC in crosslinking GAGs, the current thermomechanical studies (HIT and DHIT) suggested that glutaraldehyde-treated chrodae are more stable than the EDC-treated samples. The reason for this is yet to be determined.

4.4.2 Effect of Extension on the Thermal Stability of Chordae Tendineae

Figure 4.3 indicates that by doubling the load from 30 to 60 g (or 470, and 950 kPa), and thereby increasing the isometric length of the chorda, there was an enhanced thermal stability in fresh- and glutaraldehyde-treated chordae as shown by the corresponding T_d. The significance of the mechanical load in altering the various aspects of *isotonic* thermal denaturation has long been studied [30, 34, 145, 167, 168, 178]. Weir et al. [171] have conducted a series of studies to show the effect of various loads in altering the dynamics of thermal denaturation of a collagenous tissue (i.e. kangaroo tail). It was revealed that heat-

induced shrinkage is a rate process that proceeds at temperature- and load-dependent rates. The shrinkage tests were conducted on tissue samples that were 10-cm long and 1 mm in diameter, using loads of 3.6, 14.4, and 40.2 g. The shrinkage was measured using a cathetometer. While increased mechanical loads decreased the rate of shrinkage, increased temperature enhanced the rate. Furthermore, such shrinkage was also correlated to a first-order chemical kinetics, with the specific reaction rates related to temperature via the Arrhenius relation (i.e. absolute reaction rate theory). In recent studies, Humphrey et al. [30] have independently confirmed and extended Weir's findings. Using chordae tendineae as the model tissue (10-mm long and 0.7 mm in diameter), it was suggested that the applied loads (0, 100, 300, 500, and 650 kPa) are likely to increase the order of the collagen fibres, and thus decrease the configurational entropy, rather than changing the hydrogen bonding in the triple helix, and thus the activation energy (E_a) (the detailed definition and the significance of the E_a is provided in section 1.8). This conclusion was reached in light of the fact that the E_a was nearly constant, potentially suggesting that energy barrier to denaturation was indeed independent of the load imposed during heating. This seems reasonable, since the elasticity of soft tissues is mostly due to changes in configurational entropy, due to the underlying long-chain polymeric structure and no variations in the internal energy [199, 328, 329]. Application of a higher load on fresh chordae has led to an enhanced thermal stability as indicated by a higher denaturation temperature, possibly through a mechanism which involves lowering of the configurational entropy and hence limiting the molecular mobility of the collagen fibres during the thermal gyration. Furthermore, as shown in Figure 4.3, the configurational entropy of the collagen fibres was shown to be further lowered upon crosslinking with two exogenous agents, leading to a small yet significant increase in denaturation temperature relative to the control group. It is therefore suggested, that both tissue crosslinking as well as the imposition of the higher mechanical loads, stabilise the tissue by limiting the chain mobility during the thermal gyration.

Furthermore, although there were relative improvements in the thermal stabilities for the higher load group (i.e. 60 g) in both control and glutaraldehyde-treated chordae, such trends were indeed quite small (Figure 4.3). This may be related to the effectiveness of the current loads in limiting the chain mobility and reducing the configurational entropy. In fact, a plot of averaged load-extension (Appendix 2), indicated that the applied range of loads in this

study was quite small, well below the linear (rising) portion of stress-strain curve. Nevertheless, it is rather astonishing that the thermal stability of the chordae has improved at such small load range. Hence, future experiments should consider applying a higher range of mechanical loads to further limit the α-chains mobility. Current technical limitations with the DHIT system (i.e. the limitations with the range and specificity of cantilever load cells) made it impossible to repeat these studies under higher mechanical loads

Table 4.4 shows the data of the effect two loads on altering the dynamics of the thermal denaturation. Generally, all the time constants (τ_1, τ_2, and τ_3) are indeed delayed in the presence of higher load in control, for glutaraldehyde- and EDC-treated chordae. It is probable that the same mechanism of lowering of the configurational entropy of the α-chains may also play a role in slowing the rate of the thermal denaturation under rapid thermal transition. Additionally, Table 4.4 indicated that the application of higher mechanical load did not alter the 3-staged dynamics of the rapid thermal denaturation. Finally, the load "stabilisation effect", was even more pronounced in the crosslinked tissues than the control group (Figure 4.4). As was explained before, the double effects of loads and exogenous crosslinking may contribute to this "extra" delaying phenomenon, ultimately leading to more stabilised triple helix structure. More interestingly, is the observation that even by imposing small mechanical loads, the dynamics of thermal denaturation changed. This can only stress the importance of entropical forces during the rapid thermal denaturation events.

4.5 Conclusion

The main objective of this study was to further understand the dynamics of the thermal denaturation of the chordae tendineae when influenced by such factors as the presence of neutral salt, and imposition of various loads. As a general conclusion, the thermal stability of the chordae tendineae was interfered with by such factors as electrostatic and entropic forces. In other words, the presence of salt clearly destabilised the fresh chordae samples by diminishing their denaturation temperature and their stress decay half-life. Furthermore the DHIT results revealed that the presence of the salt somehow delayed the dynamics of denaturation relative to the fresh samples. Such effects were nearly absent in the crosslinked samples. In addition to collagen, the interference with the electrostatic forces and the water content of the tissue may also influence the structural integrity of the GAGs.

In a parallel study, the load experiments were quite similar in that only slightly increasing the loads could indeed improve the thermal stability of the collagenous chordae tendineae, as indicated by small yet significant increase in denaturation temperature. Furthermore, the DHIT experiments also revealed that dynamics of thermal denaturation can indeed be delayed in the presence of a higher load, but the dynamic and multi-staged nature of the thermal denaturation remained the same. The effect of crosslinking was to further stabilise the triple helices and along with the load effects this led to an added delaying of the thermal denaturation.

5 TOWARD A TISSUE-ENGINEERED HEART: THE COMPARATIVE THERMOMECHANICAL STUDIES OF THE VARIOUS COLLAGENOUS CARDIAC TISSUES

5.1 Introduction

Cardiovascular disease remains a significant cause of morbidity and mortality in the world [330-333]. Successful treatment has been limited in many situations by the poor performance of synthetic materials used for tissue replacement. Recently, the Life Initiative, an international consortium of tissue engineers headed by Dr. Michael Sefton of the University of Toronto, has proposed the goal of developing a completely tissue-engineered heart [334, 335]. Clearly, realization of this ambitious goal will require substantial improvements in cellular and scaffold technologies. Furthermore, progress toward this goal will be made through the parallel development of effective, likely near-native, tissue engineered components of the cardiovascular system that will later be synthesized into a larger organ structure, namely a heart. Achievements made during the development of these individual tissue components will provide many therapeutic advances and enhance our understanding of fundamental issues involved in cardiovascular tissue engineering.

Collagen is the major component of the extracellular matrix in the load-bearing elements of the heart and is most important for the maintenance of their structural integrity and functions [122, 125, 126, 336-338]. The goal of the present investigation was to further study the structure/function relations that may exist in such load-bearing tissues as the aortic valve (AV) and mitral valve (MV) in the left side of the heart, the mitral chordae tendineae (MCT) and the tricuspid chordae tendineae (TCT) located in left and right ventricular chambers of the heart respectively, and the pericardial sac.

It is generally believed that both biochemical and biomechanical stimuli induce extracellular matrix remodelling in soft connective tissues [339, 340]. The remodelling processes affect the morphology and the mechanical behaviour of the stimulated tissues [341]. Mechanically-induced extracellular matrix remodelling plays a crucial role in tissue engineering of load-bearing structures, such as heart valves [342] and cartilage [343]. There is now evidence that myocardial collagen, in the heart, as well as collagen in other tissues (i.e. lung, skin, and muscle), is being synthesized and degraded (i.e. remodelling) quite rapidly [344]. It is suggested that alteration in either of these processes may be essential in altering the tissue

collagen levels in normal or diseased states [345]. Using a finite element modelling technique, Kunzelman et al. [346] concluded that mitral valves are capable of modulating their collagen synthesis in order to accommodate varying leaflet stresses so that valve function is conserved. It was stated that "based on the results of our finite element models, we can offer an explanation for the increased procollagen expression and decreased collagen concentration found in the sheep studies. The end result of these tissue alterations would be a thicker mitral valve leaflet, with an increased absolute amount of collagen" [346]. This may happen due to the substantially greater mechanical loads in the left side of the heart relative to the right side, and may explain why the left side is more frequently involved in disease states [338]. The proof for an enhanced rate of collagen turnover in mitral valves was provided biochemically by an increased rate of hydroxyproline synthesis [110, 337]. Mori et al. [337] have indicated that after in vitro incubation of four heart valves with ^{3}H proline, the amount of ^{3}H hydroxyproline synthesized was used as a measure of collagen synthesis. Of the four valves examined, the mitral valve showed the highest hydroxyproline-specific activity.

It is generally accepted that superior mechanical properties in collagen fibrils are largely the result of strong axial and lateral bonding afforded by inter- and intramolecular collagen crosslinks. Increased crosslink formation has been observed with development and maturation in various collagenous tissues where tissues become more stable [152, 153, 209, 347, 348]. It is believed that newly-laid crosslinks are converted from reactive, heat-labile, and immature aldimine crosslinks into the non-reducible, heat-stable and mature type. Over the past decade, our group has been using a thermomechanical approach [i.e. hydrothermal isometric tension (HIT)], originally developed by Allain [190] and Le Lous [140, 195], to directly assess the structural-mechanical relationships in the collagen matrix of various collagenous tissues during maturation and development [152, 153, 237]. Under slow heating conditions, HIT directly assesses changes in the mechanical behaviour of collagenous tissue that result from a course of thermally-induced structural transitions in collagen. Recently, we have also developed a new thermomechanical system [i.e. dynamic hydrothermal isometric tension (DHIT)], in which the dynamics of the thermal denaturation of collagenous tissues can be studied under rapid thermal transitions as shown in Chapter 2. Furthermore, using bovine PC and MCT as the model tissues, we have demonstrated mathematically that such

transitions occur in three-stages, and further speculated that each stage may indeed correspond to the unravelling of particular types of molecular interactions or crosslinkages. The main difference between DHIT and HIT was the rate of tissue heating. In fact, as shown in Chapter 2, the heat transfer analysis revealed that while it takes less than 1 second (i.e.~ 0.5 s) for the tissue to reach 90°C using the DHIT test; by contrast, this event occurred over a period of approximately 45 minutes using the HIT technique.

It is the aim of the current work, then, to use both HIT and DHIT techniques along with the uniaxial stress-strain test, to assess the thermomechanical properties of five cardiac tissues and examine their structure-function relations. It is believed that emerging data of this sort are of profound importance in the rational design and eventual development of a complete, tissue-engineered heart.

5.2 Materials and Methods

5.2.1 Tissue Preparations

Intact pericardia (PC) and enclosed hearts (from mature cattle) were obtained fresh from slaughter from local abattoir (O.H. Armstrong, Kingston, NS) and were transported to the laboratory on ice. In this study four tissue types from the bovine heart were selected due to their different functions as well as fibrous architectures. These included: intact pericardium[1], marginal TCT and MCT located on the right and left ventricles respectively, and anterior leaflets of the MV and aortic valve.

The left ventral surfaces of the pericardia were cleaned of any adherent fat by gently stripping off the attachments with a scalpel. Subsequently, the base-to-apex direction was marked using one suture placed at the aortic root and the other at the apex of the heart. A large rectangular section of the ventral PC (~10 cm square) was excised with sutures included and kept in Hanks' solution. The experimental rectangular samples each measuring 0.5 mm x 2.0 mm, were excised in the loading direction (base-to-apex) using a double scalpel blade cutter.

The chordae tendineae (CT) were obtained from the fresh bovine heart. For this experiment, the left and right ventricular chambers of the heart were exposed, and the marginal CT samples were dissected from both sides. The choice of the marginal CT in these experiments originates from the careful observation and measurements that there is an almost two-to-one ratio of marginal to basal insertions into the leaflet tissues [116]. This difference in anatomic structure would indicate that more of the stress carried by the leaflets in systole would be substantially transferred to the marginal chordae [116]. The sample length ranged from 15 to

[1] The pericardial HIT data presented here, were previously collected by Professor J. M. Lee as part of a separate and yet to be published study. The methodology was identical to that described herein.

30 mm, and the mean original unloaded diameters for TCT and MCT were identical with no statistical significance [0.89 ± 0.04 and 0.90 ± 0.06 (mm) respectively (n = 12)].

The mitral valves (MV) were excised and the anterior leaflets were separated from the posterior leaflets. Chordae tendineae were trimmed, and the anterior leaflet was then sectioned into a strip of 5.0 mm wide and 10 mm long, parallel to the free edge (i.e. circumferentially). The circumferential direction was selected since it is in the direction of the principle collagen fibres, presumably along the lines of principle stress [349].

The leaflets were cut from the aortic valve (AV) and pinned to a cork dissecting board with ventricular surface up. A single strip of tissue was cut from each leaflet. The strips were approximately 5.0 mm in width and a mean length of 8.0 mm, with the long axis parallel to the major circumferential collagen fibre bundles observed in the fibrosa.

Following each tissue preparation, all the samples were washed three times for 5 minutes in Hanks' solution (pH 7.4, 310 mOs), and subsequently kept in separate Hanks' solution at 4°C until the actual experiment was conducted.

5.2.2 Thermomechanical Tests

Temperature-jump Thermomechanical Tests (DHIT): ***System Description:*** The two-container, quick-change temperature system allowed for the simultaneous exposure of up to six samples to near-step changes in temperature (transition time < 1 seconds) under computer control. A full description as well as the operational details of the DHIT has been provided in Chapter 2. Briefly, the mounted samples were initially immersed in a 4 L stainless steel vessel (cold tank) of 25°C double-distilled water for 30 minutes and extended to yield an initial load of 50 g for PC and 30 g for all other tissue samples (i.e. MCT and TCT, MV and AV). After a brief incubation (~10 minutes) period in the cold tank the tissue samples were rapidly transferred (< 1 s) into the hot tank at 90°C, and the load-temperature-time data were collected using software custom written by Mr. Christopher Pereira under LabVIEW 3.0 software (National Instrument).

Data Analysis: A detailed description of the analytical methodology used to curve fit the DHIT load rise data for PC and CT has been given in detail in Chapter 2. Briefly, the data was first corrected and subsequently normalized with respect to the maximum asymptotic load reached during the isotherm. The Levant-Marquardt nonlinear least squares method (DeltaGraph 5.0, SPSS Inc.) was applied to the normalized data from MV, AV, MCT, and TCT to identify the three characteristic time constants (τ_i) and corresponding coefficients (C_i). Equation 5.1 represents the typical three exponential model used to characterize the rapid structural changes induced during the thermal cycle in all tissues. This equation related the force ratio to three exponential functions:

$$1 - \frac{F(t)}{F_{max}} = C_1 e^{-t/\tau_1} + C_2 e^{-t/\tau_2} + C_3 e^{-t/\tau_3} \qquad \textbf{Equation 5.1}$$

where $C_1 + C_2 + C_3 = 1$.

While single- and double-exponential models were unsuccessful, a triple-exponential model provided an excellent fit to the data from MCT, TCT, MV and AV during the thermal cycle. The robustness and uniqueness of the three-exponential fits was established using wide variations in the seeds supplied to the nonlinear least-squares routine. A sample calculation of the seeding is provided in Appendix 1. Finally the validity of the triple exponential model was verified using regression coefficients (r^2).

Statistical Analysis: The time constants and coefficient data were examined using a one-way analysis of variance (ANOVA) with the tissue type as the main variable. A Fisher's least significant difference post-hoc test was used for multiple comparisons, to highlight individual differences (StatView 5.0.1. SAS). All data are presented as the mean ± one standard error of the mean (SEM). The minimal level of statistical significance was set at *p*-value < 0.05.

Slow Rate Thermomechanical Tests (HIT): ***System Description and measurements of*** T_d ***and*** $t_{1/2}$***:*** The system allowed for simultaneous testing of up to six samples under computer control. The tissues samples were gripped in spring clamps and extended to the desired initial load depending on the nature of the experiment. The apparatus used to perform the HIT tests has been described in Chapter 4, and as well in a previous publication [192]. Both calculations for T_d and $t_{1/2}$ were fully described in Chapter 4.

Statistical Analysis: A linear regression model (Excel X, Microsoft Corp.) was used to fit the stress decay data and its validity was verified using the regression coefficient (r^2). The data for T_d and $t_{1/2}$ were then examined using a one-way analysis of variance (ANOVA) with tissue type as the variable. A Fisher's least significant difference post-hoc test was used to extract individual differences using the StatView 5.0.1 software (SAS Institute Inc.). All data are represented as the mean ± SEM. The minimal level of statistical significance was set at p-value < 0.05.

5.2.3 Mechanical Testing

The MCT and TCT were mechanically tested using a custom-built MTS planar biaxial servohydraulic system interfaced to a Power G3 Macintosh computer with a data acquisition hardware (National Instruments' NB-MIO-16L A/D board) and software custom-written by Prof. J.M. Lee (LabView 6.0, National Instruments) [350]. The system consisted of four micro-processor-controlled independently moving servo-hydraulic actuators. For the present study, only two of the actuators were used to conduct a simple uniaxial stress-strain analysis on chordal samples. Prior to testing, the chordal samples were rinsed thoroughly in Hanks' solution. The sample length ranged from 15 to 30 mm, and the mean original unloaded diameters for TCT and MCT were individually measured by a digital caliper (Mitutoyo Corp.), with no significant statistical differences [0.89 ± 0.04 and 0.90 ± 0.06 (mm) respectively (n = 12)]. Each test sample was mounted between screw-tightened, cantilever-style, sandpaper-lined brass grips to a nominal gauge length of approximately 10 mm. These grips were lined with #240 waterproof sandpaper to avoid slippage. Each chordal sample was tested in Hanks' physiological solution at room temperature. In order to measure each of the chordal sample's actual gauge length and width, a video image under a small load (0.5

g) was acquired using an overhead CCD camera for later determination of gauge length. To standardize gauge length, zero extension was thus taken at the point where a 0.5 g load was detected, and the extension gauge on the MTS was then set to zero. The moist sample was then extended at 2 mm/min until rupture, the load and position data continually recorded under LabVIEW 6.0 software. The load in each was measured using a cantilever load cell (Transducer Techniques GS-9.02, 1000 g) mounted on one of the actuators. The output voltage signal from the load cell and from the actuator was collected using a 12 bit analog-to-digital board (National Instruments) and a commercially available data acquisition software package (LabView 6.0), on a Macintosh computer.

5.2.4 Data Analysis

Stress-Strain Data: The custom-written LabView program saved time (s), extension (mm) and force (N) in a text format for importation into Excel X (Microsoft Corp.) for conversion of load data to stress and extension data to strain using the calculated dimensions.

Fracture Data: Extension of the tissue samples to fracture provided the following parameters: the ultimate tensile strength (UTS) (defined as the stress at fracture), the strain at fracture (defined as the maximum value of strain before rupture, i.e. extensibility), the tissue modulus (defined as the maximal slope of the linear portion of the stress-strain curve, i.e. stiffness), and the area under the curve (defined as the energy per unit volume required to rupture the tissue samples, i.e. toughness).

5.2.5 Statistical Analysis

One-way analysis of variance (ANOVA) with tissue type as the variable, followed by a Fisher's least significant difference post-hoc test was conducted to determine significant differences between individual treatment groups. Data are presented as mean ± standard error of the mean (SE). The minimal level of statistical significance was set at p-value < 0.05.

5.3 Results

5.3.1 HIT tests

The load versus temperature profile revealed dramatic differences in the thermomechanical behaviour of chordal samples versus the valvular ones. Generally, as seen previously in Figure 2.4, all tissues exhibited the following responses under slow heating conditions (1-2 °C/min): (i) initial slow fall in load (i.e. stress relaxation) followed by (ii) a sharp and sudden increase in load at the denaturation temperature T_d and (iii) rising load after denaturation reaching a maximum at, or very soon after, the 90°C isotherm was achieved. After reaching 90°C isotherm, the loads in all tissues began to undergo gradual stress decays. The only exception was the MV, where all tissues have failed shortly after reaching the isothermal temperature (i.e. 90°C).

Denaturation Temperature (T_d): The denaturation temperature was taken as the point of sudden rise in the load-temperature profile (Table 5.1). Statistical differences were assessed using a one-way ANOVA, with tissue type as the main variable. The TCT, located in the right side of the heart, denatured at a significantly higher temperature (73.8 ± 1.5°C) than did the MCT (68.7 ± 0.7°C). Interestingly, despite the different transvalvular pressures on the MV and the AV, they exhibit identical denaturation temperatures, and hence seemingly identical thermal stabilities (Table 5.1).

Half-life Stress Decay ($t_{1/2}$): Probably, one of the most revealing aspect of the current study was the complete failure of the MV leaflets shortly after reaching the isothermal temperature. As a result, the stress decay calculations could not be conducted in these samples. Conversely, the stress decay analysis of the TCT, as measured from the slope $F(t)/F_{max}$ vs. time, revealed that they hardly underwent any significant amount of load decay. There was, however, a significant difference between the MCT (47.2 ± 10.3 hr) and AV (10.3 ± 2.3 hr) stress decay half-life. Finally the stress decay value for PC indicated that they were the least stable tissues samples, since their isothermal load decay half-life was only 4.0 ± 0.1 hr.

Tissues	Denaturation Temperature, T_d (°C)	Stress Decay, Half-life $t_{1/2}$ (hr)
Mitral Chordae Tendineae	68.7 ± 0.7^{a}	47.2 ± 10.3^{a}
	(n = 7)	(n = 7)
Tricuspid Chordae Tendineae	73.8 ± 1.5^{b}	**No Measurable**
	(n = 5)	**Stress Decay**
Mitral Valve	67.6 ± 0.4^{ac}	**Failed**
	(n = 5)	
Aortic Valve	68.2 ± 0.4^{a}	10.3 ± 2.3^{b}
	(n = 5)	(n = 5)
Pericardium*	67.0 ± 1.0^{c}	4.0 ± 0.1^{c}
	(n = 48)	(n = 48)

Table 5.1 Thermomechanical data from DTT and HIT testing of chordae tendineae (tricuspid and mitral), valvular leaflets (aortic and mitral), and pericardium. Values shown are mean ± SE, p-value < 0.05 was created by a single-factor analysis of variance with the tissue type as the variable of interest. This was then followed by a post-hoc Fisher's test. Values labelled with the same letters are not significantly different. *Note that the data for the pericardium were previously collected and kindly provided by Prof. J.M. Lee.

5.3.2 DHIT profile

As indicated in the previous chapters, the DHIT system was used to impose near-step changes of temperature (< 1 s) as means to study the dynamics of denaturation in various collagenous tissues. The force-time data were then characterized with three time constants, using the Levenberg-Marquardt nonlinear least square method (Equation 5.1). The same methodology was used to compare the dynamics of thermal denaturation in different cardiac components. Almost all tissues responded similarly to near instant temperature jump (Figure 2.4): (i) upon entry from 25°C to 90°C there was an rapid increase in load characterized by τ_1 (and C_1) (ii) shortly after this rapid rise the slope of the load plot changed and this highlighted the beginning of the slower transition (indicated by τ_2, and C_2) (iii) finally the load approached an asymptotic level and continued constantly (characterized by τ_3, and C_3). All tissues, except the MV leaflets, which failed shortly after the immersion into 90°C showed the same thermal behaviour.

5.3.3 DHIT parameter

Characteristic Time Constants (τ_i) and the Coefficients (C_i): As shown in Chapter 2, τ_1 still represented the most dominant time constants in the multi-staged thermal denaturation process of the collagen fibres in various cardiac tissues (Table 5.2). Such significance is based on the values of the corresponding coefficients (C_1), indicating that τ_1 of tissue samples dominated more than half of the denaturation process (Table 5.2). Once again and similar to the HIT tests, all the mitral valve samples failed within minutes of the rapid transition into 90°C isotherm. The one-way analysis of variance, further reveals that the AV leaflets had the highest τ_1 value (19.5 ± 1.7 s)–the slowest transition time–than did any of the tested tissues. It is noteworthy that during the DHIT, two of the AV leaflets also failed (hence n = 4). To rule out the possibility that the failed tissue samples did not rupture, or simply slipped out the grips, both grips and tissues were carefully examined after the completion of the experiment and it was noted that the tissues indeed ruptured in mid-section.

Treatments	Time Constants (s)			Coefficients (%)		
	τ_1	τ_2	τ_3	C_1	C_2	C_3
Mitral Chordae Tendineae	1.9 ± 0.2[a] (n = 14)	74 ± 17[a] (n = 14)	802 ± 213[a] (n = 14)	69 ± 3[a] (n = 14)	16 ± 2[a] (n = 14)	15 ± 2[a] (n = 14)
Tricuspid Chordae Tendineae	4.6 ± 0.2[b] (n = 5)	65 ± 14[a] (n = 5)	513 ± 10[a] (n = 5)	62 ± 2[a] (n = 5)	21 ± 3[a] (n = 5)	16 ± 4[a] (n = 5)
Mitral Valve	Failed	Failed	Failed	Failed	Failed	Failed
Aortic Valve	19.5 ± 1.7[c] (n = 4)	210 ± 54[b] (n = 4)	709 ± 21[a] (n = 4)	84 ± 2[b] (n = 4)	10 ± 2[b] (n = 4)	6.0 ± 0.7[b] (n = 4)
Pericardium	0.6 ± 0.1[d] (n = 19)	3.7 ± 0.3[c] (n = 19)	615 ± 66[a] (n = 19)	48 ± 5[c] (n = 19)	40 ± 4[c] (n = 19)	12 ± 2[a] (n = 19)

Table 5.2 The multi-staged nature of rapid thermal denaturation chordae tendineae (tricuspid and mitral), valvular leaflets (aortic and mitral), and pericardium. The averaged values of time constants (τ_i) and coefficients (C_i) are calculated as the Mean ± SE, p-value < 0.05, created by single factor analysis of variance, with tissue type as the variable of interest. This was followed by a post-hoc Fisher's test. Values labelled with the same letter are not significantly different.

A comparison of the τ_1 values for the TCT and MCT indicated that these important time constants were significantly different from one another (p-value < 0.0001) (Table 5.2). Interestingly, the data suggest that the first denaturation (i.e. uncoiling) events occur almost 2.5 times slower in the TCT (4.6 ± 0.2 s) relative to the MCT (1.9 ± 0.2 s). At the same time, the absence of statistical significance in the C_1 values of the MCT and TCT indicated that the τ_1 makes an equal contribution in both tissues. Although the coefficients for the chordal samples are similar, both high and low extreme values for τ_1 were observed in AV and PC respectively. This may be explained in terms of the tissues' architectures and the different crosslinkages involved in these tissues.

Table 5.2 and Figure 5.1 showed the values for τ_2 and τ_3 for all the tissues as well as their corresponding coefficients (C_2 and C_3). These results are consistent with those obtained in previous Chapters, where τ_2 and τ_3 for all tissues were significantly longer and at the same time their coefficients decreased indicating a lessening of their contribution to the denaturation process.

5.3.4 Mechanical Testing

Only the MCT and TCT were subjected to the simple uniaxial stress-strain experiments. During the course of the experiment it was noticed that some tissue samples slipped out of the grips; this event could be misinterpreted as the rupture (i.e. the fracture) of the tissue sample. Hence, extra attention was focused on correct alignment as well as a well-tightened grip to avoid such slippage. In fact, whereas the slippage was a gradual release of the tissue from the grips, the tissue rupture due to excessive force was defined as a sharp and a rapid "snap" from the grip. Interestingly, most of the fractures occurred near the grips, and by the end of the experiment some tissue always remained within the grips. A typical graph of the uniaxial stress/strain results for both marginal MCT and TCT is shown in Figure 5.2. This graph showed that the stress on the MCT was higher than the TCT at all recorded strains. However, the calculation of the ultimate tensile strength (UTS) failed to produce any significant differences between the two chordae (Table 5.3). However, the calculation of other mechanical parameters revealed that the MCT were stiffer, less extensible and tougher than the TCT.

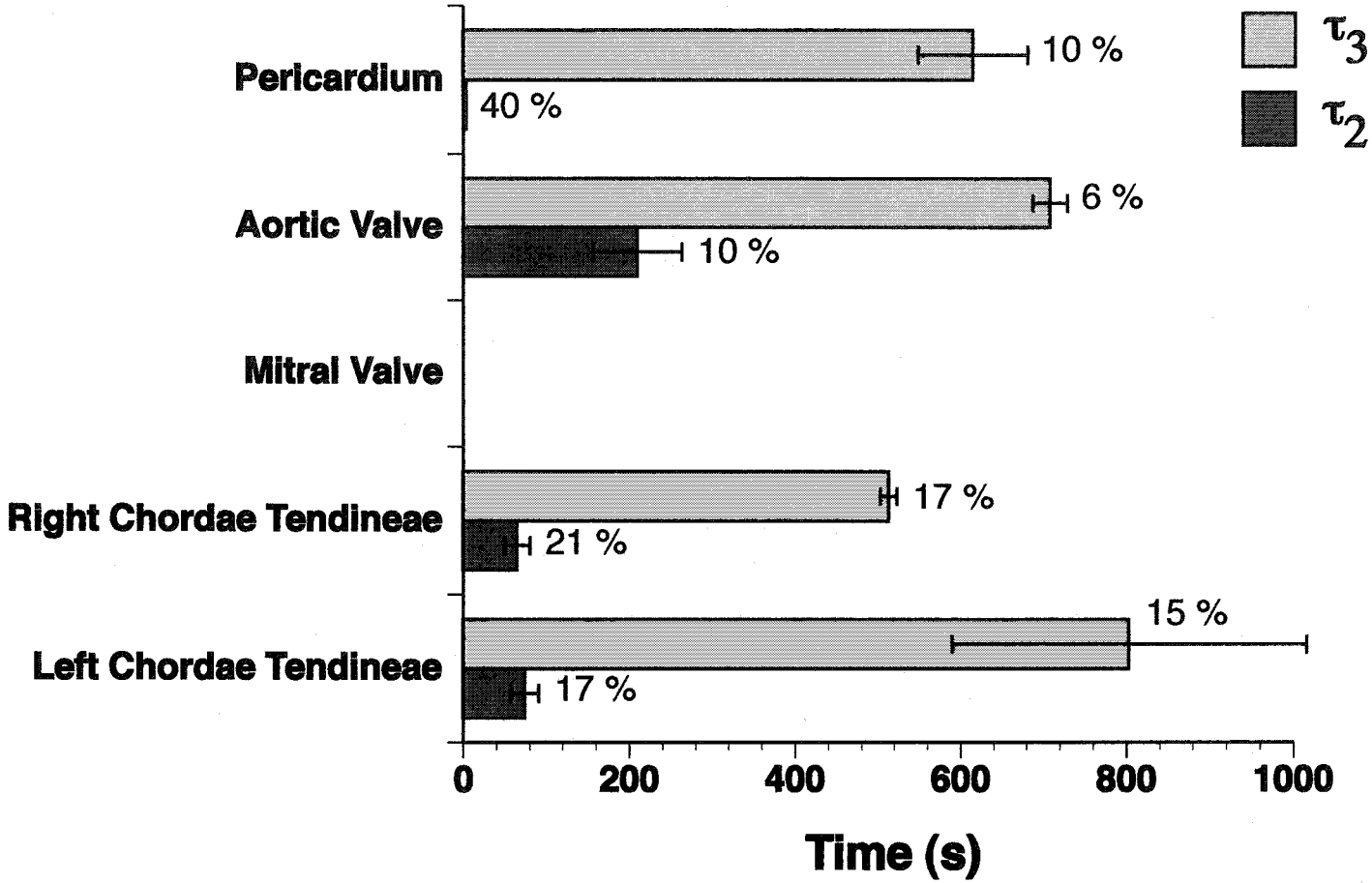

Figure 5.1 The plot of DHIT tissue/time profile for mitral and tricuspid bovine chordae tendineae, mitral valves, aortic valves and pericardium, showing the dynamics of the thermal denaturation under rapid thermal transition. The column length represents the second and the third time constants (i.e. τ_2 and τ_3) and the numbers on top of the columns represent the corresponding coefficients (i.e. C_2 and C_3). Statistical results are shown in Table 5.2

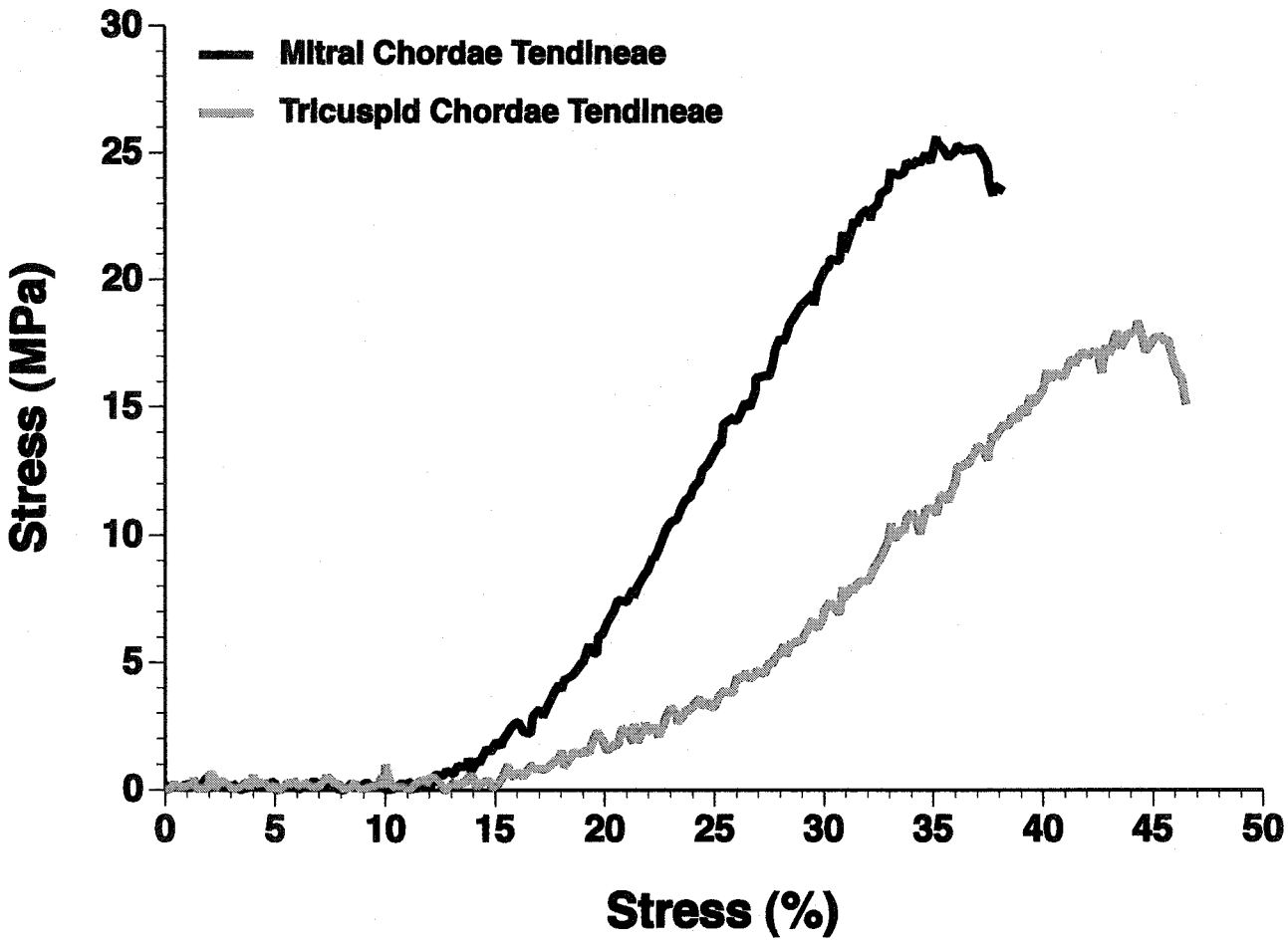

Figure 5.2 Typical stress/strain behaviour of mitral- and tricuspid marginal chordae tendineae in uniaxial tension.

Tissue	UTS (MPa)	Modulus (MPa)	Strain at Fracture (%)	Toughness (J/m^3)
Mitral Marginal Chordae Tendineae	40.0 ± 2.9^a (n = 9)	207 ± 18^a (n = 9)	29.0 ± 0.02^a (n = 9)	1490 ± 130^a (n = 9)
Tricuspid Marginal Chordae Tendineae	34.0 ± 5.2^a (n = 10)	140 ± 12^b (n = 10)	77.0 ± 0.1^b (n = 10)	900 ± 120^b (n = 10)

Table 5.3 Mechanical data from a simple uniaxial stress-strain experiment conducted on mitral- and tricuspid marginal bovine chordae tendineae. Mean ± SE, p-value < 0.05 created by analysis of variance with tissue type as the variable of interest. This was followed by a post-hoc Fisher's test. Values labelled with the same letter are not significantly different

Figures 5.3-5.5 show the data for ultimate tensile strength (UTS), modulus, and strain at fracture respectively from other investigators [135, 137] and compare them to the current data. While the bovine chordal samples were selected for the present study, those from Lim's and Berkovitz's studies were chosen from ovine and human sources respectively. It appears that while our data for the MCT were quite consistent with two other studies [135, 137], our mechanical data on the TCT were significantly different from those obtained by Lim et al. [137].

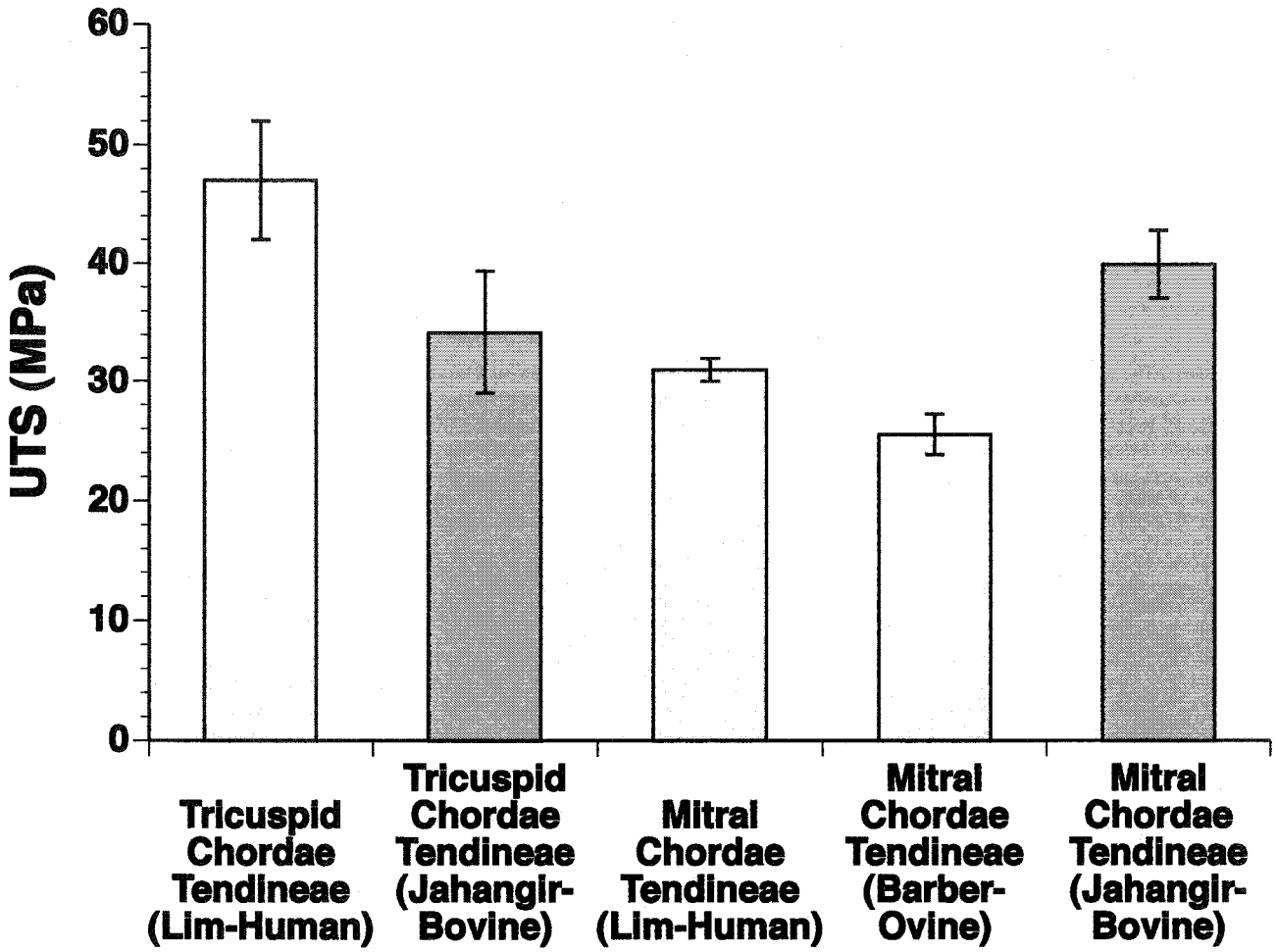

Figure 5.3 The ultimate tensile strength (UTS) values of the mitral and tricuspid chordae tendineae, obtained by two other investigators (Lim 1980 [137], and Barber 2001[135]), and comparison to the present findings.

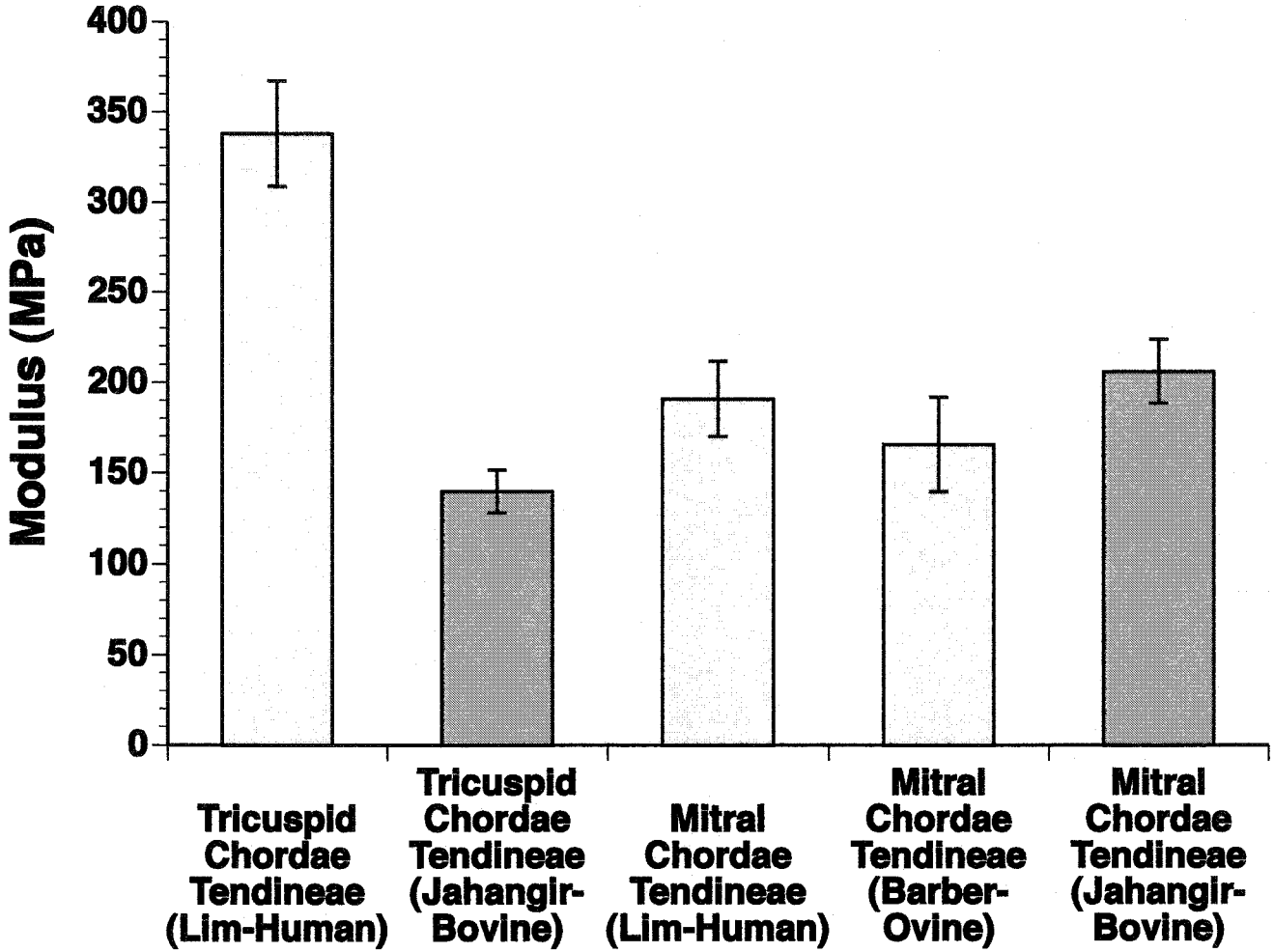

Figure 5.4 The modulus values of the mitral and tricuspid chordae tendineae, obtained by two other investigators (Lim 1980 [137], and Barber 2001[135]), and its comparison to the present findings.

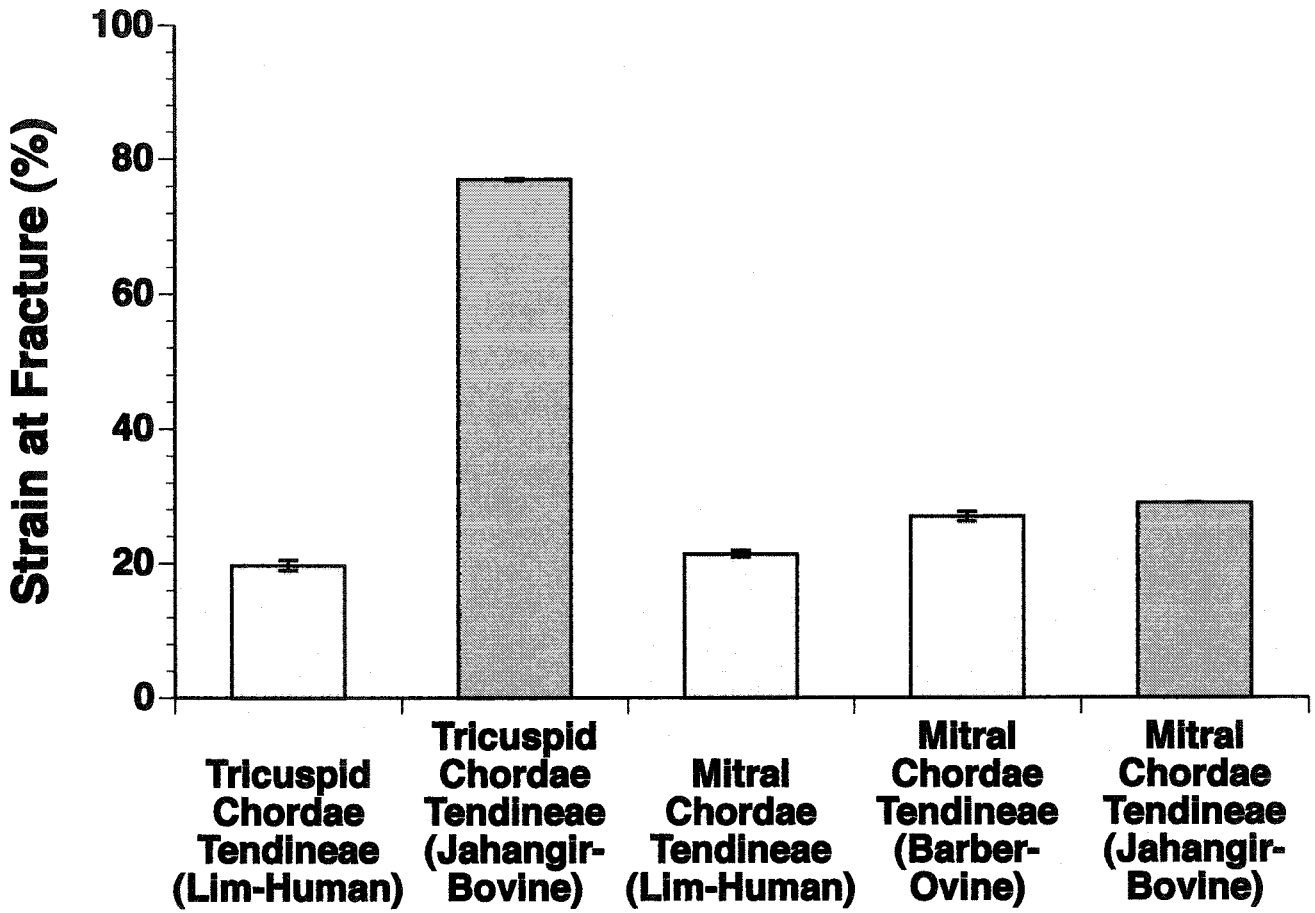

Figure 5.5 The strain at fracture values of the mitral and tricuspid chordae tendineae, obtained by two other investigators (Lim 1980 [137], and Barber 2001[135]), and comparison to the present findings.

5.4 Discussion

To our knowledge, this the first study to combine a thermomechanical and a mechanical approach to investigate the structure/function relation of various load-bearing, collagenous components of the heart. Our thermomechanical results revealed that TCT and AV have a superior thermal stability (as indicated by T_d and $t_{1/2}$) and slower dynamics of denaturation (as indicated τ_1) relative to MCT and MV. On the other hand, our mechanical data revealed that the MCT are stiffer, have lower strain at fracture and tougher than the TCT. It may therefore be concluded that tissues sustaining a higher stress may mechanically be more stable, but thermally weaker. This implies a fundamentally different approach to sustaining load.

5.4.1 Thermal Analysis

HIT Tests (Quasi-Static Heating): HIT tests have previously been used to assess the relative stabilities of the collagen triple helices in different collagenous tissues and provided indications about the nature and degree of crosslinking of collagen [140, 152, 153, 155, 237]. Dr. Lee's group in particular have used HIT to directly assess structure-function relationships during the maturation of various collagenous tissues by comparing parameters such as the (i) the denaturation temperatures (T_d) and (ii) the half time load decay ($t_{1/2}$) at sustained high temperature under isometric load [152, 153, 192].

Thermal denaturation is the uncoiling transition of collagen from the rod-like triple helix to a nearly random coil [149, 286]. From a material perspective, such a transition is accompanied by a physiochemical transformation from the normal, only slightly extensible collagen fibre, to a rubber-like form with long-range extensibility. This rubber elasticity is a result of sparse lateral crosslinks directly linking the backbones of adjacent molecules. Lloyd et al. [351] have suggested that two or more types of lateral links exist: one of which is weakened by the conditions leading to thermal denaturation, and the other of which holds until the conditions are such that collagen is solubilised. On a molecular level, the helix-coil transition and ensuing configurational changes observed during the collagen's thermal denaturation are

manifestation of rupturing of the weaker non-covalent bonds, followed by the collapse of more stable covalent crosslinkages [161, 255]. Jackson et al. [245], using bovine tendon collagen (Type I), have shown that non-covalent bonds (i.e. hydrogen and electrostatic bonds) were ruptured at lower temperature (i.e. 71°C), whereas the more stable covalent crosslinkages were cleaved at a higher temperature. Allain et al. [190] have demonstrated that maintenance of tension at temperatures up to 90°C correlated with increased levels of the thermally stable ketoamine crosslinks, while tension degradation at substantially lower temperature (75°C) correlated with the presence of thermally labile aldimine crosslinks. It can therefore be concluded that the backbone of collagen polymeric chains contains bonds with different energies, and the HIT methods can be used to obtain a preliminary indications about the nature and degree of crosslinking in various collagenous tissues in various stages of their lives [141, 152, 153, 352].

Interestingly, the thermal stability data as shown in Table 5.1, may suggest that based on T_d and the $t_{1/2}$ of the chordal samples, the absence of any stress decay in the TCT samples and a significantly higher T_d, may indicate that these tissues were more thermally stable than their counterparts in the left ventricular chamber (i.e. MCT). Generally, the denaturation temperature tends to increase with the stability of the triple helix, which in turn may be related primarily to the specific nature of the interchain hydrogen bonding [286] and secondly to increased fibril diameter and crosslink density [62, 191]. Using the developing lamb pericardium, histological analysis indeed revealed qualitative changes in fibre organization and size throughout development and maturation [152]. Equally important was the observation that during maturation, various collagenous tissues become more thermally stable due to the transformation of the reducible, heat-labile, and immature crosslinks into non-reducible, heat-stable and mature bonds [353]. It may be speculated that a higher level of mature and heat-stable crosslinks in TCT samples, may indeed be the reason for their superior thermal stabilities relative to MCT.

Similarly, the changes in the stress decay half-life ($t_{1/2}$) confirmed the T_d results for the chordal samples (Table 5.1). In the HIT testing, the $t_{1/2}$ (Table 5.1) is dependent on the hydrolysis of the primary peptide bonds within the backbone of the denatured collagen matrix. This parameter is proportional to the polymeric chain density and inversely

proportional to the number of bonds ruptured per unit time [140]. As peptide bonds hydrolyze, chains slip past each other resulting in a reduction in the load bearing capability of the tissue. Thermally stable crosslinks within the denatured network provide structural reinforcement and delay slippage, thus increasing $t_{1/2}$. In light of the current findings, the absence of isothermal stress relaxation in TCT, may suggest that this tissue is a more thermally stable chordae than the MCT, by virtue of more heat-stable and mature covalent crosslinks. Further comparative studies (i.e. treatment with sodium borohydride) must be performed to determine the nature and specifically the maturity of crosslinks in both chordal samples.

The origin of such different thermal stabilities between TCT and MCT, might lie in structure-function relation that may exist in these tissues. Generally, the chordae tendineae located in left and right ventricles are designed to withstand the large repetitive forces encountered within the heart. Upon contraction of the papillary muscle, the chordae are designed to laterally flex, imposing a substantial stress on tissues. Furthermore, ultrastructural quantification of the collagen fibrils in the CT of the sheep and rabbit has suggested a relationship between structure and mechanical loading for the collagen in the CT. Berkovitz et al. [136] examined the distribution of the collagen fibril diameter in the CT from the left and right side of the heart in sheep and have indicated that fibril diameters in the left side were far greater than in the right side. It is believed that this is due to the greater tension generated in the left side of the heart. These results were also validated by Lim et al. [127] who used human chordal samples from the left and the right side of the heart. Furthermore, to emphasize that higher mechanical load will result in a different tissue morphology, Berkovitz et al. [136] further indicated that the collagen fibrils at the base of the chordae have significantly greater diameter than those at the apex, in his view due to a greater force being generated at the base (sic). Their study demonstrated a direct link between structure and mechanical loading for collagen in the CT. Such differences in structure of the chordae in the two valves can, once again, be viewed as an adaptation by the mitral valve to withstand larger forces. It has been speculated that the greater mechanical loads in the left side rather than the right side of the heart may explain the existence of more pathological conditions (i.e. myxomatous degeneration of human heart valve) that affect the left side of the heart [338, 354].

The most significant aspect of this study was the failure of the MV leaflets shortly after reaching the isothermal temperature. After all, the mitral valve apparatus must resist high systolic transvalvular physiological pressures of 100-200 mmHg for several billion cycles during a normal lifetime, thus requiring high "mechanical durability" [355]. These pressure values are substantially higher than those sustained by the AV leaflets during diastole. The mitral valve leaflets, in particular, also possess more complex anatomical structure than the other valves [338]; For instance, the MV is the only valve with two leaflets, unlike the other three, each with three cusps. Hence, due to a higher mechanical loads imposed on the MV, it is interesting and perhaps not surprising that collagen synthesis may occur at a higher rate relative to the other valves under normal conditions to accommodate their functional demands [337, 338]. If this is indeed the case, one may speculate that the newly synthesized collagens fibres in the MV may be primarily stabilized by immature and heat-labile crosslinks. The HIT results support this notion. Despite the similarity of the T_d between MV and AV, indicating the total number of crosslinks, the failure of the MV leaflets at isothermal period may indicate a near absence of mature and heat-stable crosslinks in the these tissues–but not in AV leaflets.

As mentioned previously, although more precise biochemical analyses should be conducted to recognize the exact inter- or intramolecular nature of the crosslinkages in the various tissues in the left and right side of the heart, the current HIT results may simply provide some hints as to the possible nature of these bonds: our HIT results unequivocally indicated that tissues sustaining a relatively high mechanical loads, are usually less thermally stable than those under lower mechanical loads. Although it is highly speculative, in light of current findings, we suggest the possibility of a higher rate of remodelling in tissues under higher mechanical loads (i.e. MV and MCT). The newly laid collagens are therefore stabilized not by the mature and heat-stable crosslinks but primarily by newly formed immature and heat-labile crosslinkages. In contrast, tissues sustaining a lower pressure (AV and TCT) undergo a lower rate of remodelling and are therefore stabilized by higher number of mature and non-reducible crosslinkages.

DHIT Tests (Temperature Jump): The DHIT tests were conducted to impose near-step thermal changes (< 1 s) on the various cardiac tissues. Similar to the HIT experiment, the MVs failed (i.e. ruptured) within seconds of tissue transfer from 25°C into the 90°C tank. It may again be speculated that this is due to the near absence of hydrolytically stable mature crosslinks. The same trends seen in the HIT experiments with the chordal samples are seen here: that is to say, the MCT had significantly shorter τ_1 values than did the TCT. This implies that at the same temperature level, the first uncoiling event occurs in MCT occurs 2.5 times faster than that in TCT. These results confirm our HIT results, where it was speculated that newly synthesized collagen fibres in the MCT are stabilised by more thermally labile crosslinks, and hence require less energy to rupture and uncoil. Furthermore, the C_1 values for each tissue revealed that although they are significantly different, τ_1 still contributes to more than 60% of the denaturation process in all tissues. As far as the AVs are concerned the substantially high τ_1 value was rather surprising. In fact, during the DHIT experiments, two of the AV tissue samples also failed in a similar fashion as the MV samples. More analytical testing must be conducted to confirm these results.

In conclusion, the thermal analyses revealed that irrespective of the heating rate, MCT and MV located in the left ventricular chamber of the heart were thermally weaker than TCT and AV supporting the lower transvalvular pressure.

5.4.2 Uniaxial Mechanical Tests

These experiments were conducted to further examine the mechanical differences between the MCT and TCT. Our selection criteria for the marginal versus the basal chordae was based on a mechanical study by Kunzelman et al. [116] who indicated that marginal CT in the left side of the heart exhibited a superior stiffness relative to the basal CT in the same side of the heart. They have suggested that this may be related to the fact that there is a two-to-one insertion ratio of marginal to basal CT insertion into the leaflet tissue (sic.) [116].

Figure 5.2 shows typical stress-strain curves for the left and the right marginal CT from young but mature cattle. The nonlinear stress-strain response of the both CTs is quite typical of most other ligamentous collagenous tissues [356, 357]. Although it may appear that MCT

can sustain a higher stress than the TCT, the calculation of the ultimate tensile strength (UTS) revealed that two tissues were statistically indistinguishable (Table 5.3). In fact, Table 5.3 provides an even more complete picture of the mechanical properties of the MCT and TCT. These data indicate that (other than the UTS), MCT possess a superior mechanical property than TCT, according to the calculated parameters (i.e. stiffness, toughness and strain at fracture). This may then suggest that the structure of the MCT is more adapted to function in a more mechanically demanding environment than the TCT.

To our knowledge only one other study [137] has compared the mechanical properties of mitral and tricuspid CT, but it was conducted with human tissues. Nevertheless, the mechanical properties of the normal and the diseased mitral CT have been explored in more detail [116, 135, 358]. Figure 5.3, 5.4 and 5.5 showed comparative results of the ultimate tensile strength (UTS), modulus, and strain at fracture respectively. The differences between our study and others might be explained by the fact that while the source of chordae in this study was from mature animals, the other two studies have used human chordae of from middle–aged subjects (Lim et al: 61 and Barber et al: 47 years) [135, 137]. Furthermore, while the strain rate used in Barber was similar to that used in this study (i.e. 2 mm/s), Lim has used a significantly slower rate (0.5 mm/s). Similar studies have also concluded that chordae samples become less extensible with increasing strain rates and their viscous properties become more pronounced at lower rates of strains [355]. However, our data for the TCT suggest, unlike what was observed by Lim [137], they are substantially more extensible than are MCT (Figure 5.5).

Taken together, these data seem to indicate that thermal and mechanical stabilities may be rendered via two separate mechanisms in various collagenous tissues. Whereas the thermal stability may rely primarily on the maturity of inter- and intramolecular crosslinkages, the mechanical strength may be more the function of the actual area covered by the collagen fibrils as well as their size and diameter. Interestingly, when Lim and Boughner [127] analysed the data for comparable size of MCT and TCT, they discovered that while collagen fibril density via transmission electron microscopy (TEM) was higher in latter tissue than the former one, the average collagen fibril diameter of the TCT was only about 81% that of average collagen fibril diameter in the MCT. Furthermore when the cross-sectional areas of

the chordae of each valve that was occupied by these collagen fibrils were compared, it was found that the actual area occupied by collagen fibrils in the MCT was larger than that in the TCT of comparable size [127]. Similar to our speculation, they have also hypothesized that this difference in microstructure may be attributed to the fact that MCT, being in higher pressure chamber, are subjected to greater mechanical forces, and hence have a higher rate of collagen turnover. That the MCT are more effectively covered by collagen fibrils might enable them to tolerate greater stresses than similar size TCT.

5.5 Conclusion

The central core of this study was to establish and confirm, for the first time using thermomechanical and mechanical approaches, a distinction between the thermal and the mechanical stabilities of various collagenous tissues. Indeed, in this study we revealed the varying features of the collagen structure/function relations in the heart. We have speculated that tissues under mechanical loads (i.e. MV and MCT) are able to perform their functions using predominantly immature crosslinks, which may in turn indicate a higher rate of remodelling. Emerging data of this sort is of profound importance in the rational design and eventual development of a complete, tissue-engineered heart, as well as understanding the various pathological conditions affecting the heart.

6 General Discussion and Conclusions

6.1 General Discussion

Thermal denaturation of collagen and its implications for various clinical and biomedical engineering applications, has prompted several investigators to characterize and understand this complex molecular phenomena. Although our knowledge of collagen thermal denaturation has grown exponentially over the past century, the exact molecular mechanisms remain unclear.

In particular, the investigations into the dynamic nature of denaturation dates back to almost half a century ago when Weir et al. [171] performed a series of uniaxial isotonic tests on kangaroo tail tendon. These tissue samples were subjected to a range of temperature (30-95°C), by immersion in water, and the tissue's responses were examined with respect to the effect of different temperature levels, isotonic loading during heating, pH, NaCl and tissue crosslinking with formaldehyde. It was concluded that while shrinkage was accelerated by increased hydration, the presence of crosslinking (i.e. limiting the chain mobility) decelerated the process [171]. Many years later, Humphrey et al. [30, 34, 145, 168] conducted a series of detailed thermomechanical studies to precisely characterise the effect of complex mechanical loads under supra-physiological temperatures on various soft tissue models. In an earlier study, using the chordae tendineae as their tissue model, it was suggested that the thermal shrinkage process was delayed under larger uniaxial isotonic loads, and was accelerated at higher temperature [30, 160]. These findings further suggested a time-temperature-load equivalency whereby similar levels of denaturation, as reflected by tissue shrinkage, can be attained via many combinations of heating time, temperature level, and mechanical loading [34, 145].

In light of these findings, the main objective of the current doctoral thesis was to develop and apply a novel experimental approach to further understand the molecular details of collagen thermal denaturation. As a result, instead of rapid *isotonic* shrinkage tests used by our colleagues, for the first time we have combined the rapid temperature-jump heating protocol with a hydrothermal *isometric* tension (HIT) method to characterize the rapid thermal denaturation of the two different collagenous tissues under various conditions. Already, both

temperature-jump [18, 19, 29, 30, 34, 145, 160, 179, 180] and HIT [142, 152, 153, 155, 190, 192] methods have been separately used to investigate various aspects of the thermal denaturation of different collagenous tissues. Hence, the primary purpose of the current study was to utilize the dynamic hydrothermal isometric tension (DHIT) system to characterize the rapid thermal denaturation of two architecturally distinct collagenous tissues (bovine pericardium and mitral chordae tendineae). Furthermore, the effects of two exogenous crosslinking agents (glutaraldehyde and EDC), as well as other important factors (i.e. loads and salt concentrations) that may influence the denaturation were studied. Finally, the DHIT protocol was used to investigate the structure/function relations that exist in various load-bearing components of the heart (i.e. mitral and tricuspid chordae tendineae as well as the mitral and tricuspid valves and pericardium).

Throughout these studies the normalized force-time data from various experiments were well-fitted using the Levenberg-Marquardt nonlinear-squares method and three exponential functions each with unique time constants (τ_i) and their corresponding coefficients (C_i). These analyses took τ_1 to represent the fastest time constants followed by an intermediary τ_2 and finally the longest τ_3. Furthermore, the contribution of each of these three time constants has become more evident by their corresponding coefficients (C_i). For instance, although the τ_1 is the shortest time constant, it makes the largest contribution (on average more than 65%) to the entire denaturation event. This is followed by τ_2 and τ_3. We have speculated that each of these time constants may correspond to the duration of a specific molecular uncoiling event that may occur during the rapid thermal uncoiling. The kinetic model of unfolding proposed by Miles et al. [162] have indicated that the process of thermal denaturation begins primarily within the so-called "thermally labile regions" where partial uncoupling of the individual α-chains occur. According to this model, a collagen molecule differs in thermal stability along its chain length [162]. Hence, the τ_1 small value may represent the period during which the weak and heat labile hydrogen bonds progressively rupture upon raising the thermal energy. Similarly, the time constants with higher values (τ_2 and τ_3) may correspond to those interchain linkages that may be more heat-stable and require higher energy and a longer time period to lyse, contributing to its unravelling. Despite the importance of all the times constants, a greater emphasize was placed on the τ_1 value, due its contribution to the entire denaturation process as indicated by a significantly

large C_1 value. It is believed that the progression of these initial events may eventually result in the structural destabilisation of the helix, resulting in a complete "unzipping" of the individual α-chains and thus ending with the complete denaturation of the collagen molecule. Interestingly, exogenous crosslinking of both PC and CT with either glutaraldehyde or EDC, led to a slow down of the denaturation dynamics as shown by an increase in the overall τ_i values. It is recommended that a detailed time- and temperature-dependent analysis of thermal denaturation may allow the recognition of the exact nature of the crosslinks that are involved during this process. Such knowledge may further enhance the predictability of shrinkage/contraction of a particular collagenous tissue, and such knowledge may lead to an improvement in minimally invasive procedures where thermal energy is employed.

Next, using the DHIT approach, the two model tissues were subjected to consecutive hot and cold cycles and the dynamics of rapid heating and cooling were carefully examined. These studies revealed that following the first heating cycle, neither PC nor CT regained their original conformation. The presence of reversibility was assessed based on two parameters: (i) the comparison of the initial load in the first heating cycle and the asymptotic loads reached in first and second cooling cycles and (ii) the τ_i values characterizing each of these cycles. Based on these results, it was revealed that rapid thermal denaturation (occurring during the first heating cycle of the two collagenous tissues under isometric conditions) was in fact irreversible. This resulted in transformation of the native the collagenous tissue into a rubbery material, after which both tissues went reversible thermoelastic contraction and relaxation during the thermal and cooling cycles respectively. It was speculated that the rubber elasticity in both collagenous tissues is due to the disruption of enough hydrogen bonding during thermal denaturation to allow the collagen fibres to become kinetically free and sufficiently flexible to behave like a random coil polymer. Interestingly, the stabilising effect of exogenous crosslinking disappeared following the first heating cycle, no longer providing a significant structural support to either of the collagenous model tissues. It is believed that a thorough understanding of the possible underlying mechanisms of collagen thermoelastic reversibility may help to improve the unpredictability of different clinical procedures requiring thermal therapies.

In the next phase of the rapid thermal denaturation analyses, the effects of increased load, as well as various salt concentrations, on the dynamics of thermal denaturation were studied. Most collagenous tissues in an in vivo milieu are under complex and multi-axial load patterns. Furthermore, it has been suggested that increasing tensile mechanical loads should thermally stabilise the collagen fibrils, presumably by increasing the order of the collagen fibres and hence, decreasing the configurational entropy of the α-chains. The applied range of mechanical loads used to limit the α-chains mobility of the collagen fibrils in the chordae, was rather small and well below the linear portion of the stress-strain curve. Despite such limitations, the DHIT analyses revealed that the three-staged nature of the dynamic denaturation was maintained and more importantly, the overall dynamics of denaturation were delayed even in the presence of low mechanical constraints. The latter results were indeed noteworthy since they suggest even small load constraints may play significant roles in thermal stabilisation of the collagen molecule. Furthermore, the thermal stability of the collagenous chordae was additionally enhanced upon exogenous crosslinking with EDC or glutaraldehyde. This emphasizes the importance of entropic factors that limits the extent of α-chain mobility, resulting in an increased thermal stability of collagenous tissues.

The DHIT technique was also used to study the influence of various salt concentrations on the dynamics of thermal denaturation. Salt ions are thought to influence the thermal stability of collagen, either by interfering with electrostatic interactions amongst various charged residues in the collagen fibrils, or by indirectly influencing the structure of the water molecules that surround the triple helix [50, 295, 306, 307]. This is the first time that a collagenous tissue was exposed to various salt concentrations under a temperature-jump heating protocol and isometric conditions, to determine the dynamics of the thermal denaturation. The usual dynamic parameters (τ_i and C_i) were used to assess such alterations. Based on these metrics, although the helix-coil transition remained a three-staged phenomenon in the presence of salt at all concentrations, the dynamics of denaturation was delayed relative to the control group. Such temporal changes however, cannot be interpreted as an indication of increased thermal stability since the results from the DTT and HIT data (tests that were conducted under slow-heating protocol) clearly indicated that, irrespective of the salt concentrations, the thermal stability of the chordae decreased relative to the control group. As a result, irrespective of type of experiment, the interpretation of the DHIT results

must be conducted rather carefully since these data reveal more about the *"dynamics of thermal transitions"* rather than the *"thermal stability"* of a given collagenous tissue.

The most striking findings of the current dissertation were the combined thermomechanical and mechanical analyses of various load-bearing cardiac components, revealing varying features of collagen structure/function relation in the heart. Tissues were selected based on the levels of mechanical stress, they likely sustain; these included: mitral (left) chordae tendineae, tricuspid (right) chordae tendineae, mitral valve tissue, aortic valve tissue and pericardium. The most remarkable finding was that the mitral leaflets failed before reaching the 90°C isotherm both in HIT and DHIT. This strongly suggests a near-absence of mature, hydrolytically stable crosslinking. Furthermore, the results from both HIT and DHIT revealed that, irrespective of thermal transition rates, tricuspid chordae were more thermally stable tissues and their transition dynamics were delayed relative to the mitral chordae. These observations seem counter-intuitive given that left ventricular structures sustain significantly greater tension than do right ventricular structures. Although more in-depth analyses of the specific nature of the crosslinks in these tissues are required, our results may reflect a higher collagen turnover, and hence fewer mature crosslinks, in the left side than the right side of the heart. The pericardial tissues were both thermally weaker (as shown by T_d and $t_{1/2}$), and had much faster transition dynamics (as shown by a small τ_1 value). Such relative thermal instability of pericardium may be contributed to the fibre orientations that are believed to be loosely arranged and approximately 60° apart [258]. In other words, the tissue's unique architectural features might also influence the specific pattern of crosslinking, which in turn determines the dynamics of thermal transition as well as their thermal stabilities.

Furthermore, our combined thermomechanical and mechanical protocols revealed that the mechanical data differed significantly from the thermal data. In fact, whereas the mitral chordae was shown to be thermally weaker relative to the tricuspid chordae, they were mechanically tougher, stiffer and less extensible. While the thermal stability may rely for the most part on the maturity of inter- and intramolecular crosslinks, the mechanical strength may be more the function of the actual area covered by the collagen fibrils as well as their size and diameter and total mature and immature crosslinks. Such combined analyses may provide a better opportunity to analyse the structure/function relation of a given collagenous

tissue. Emerging data of this sort have far-reaching implications for design in tissue-engineered replacements since they suggest: (i) varying solutions to the problem of bearing repeated mechanical loads and (ii) varying susceptibilities to pathological conditions.

In conclusion, the uniqueness of this series of investigation lies in the new and innovative approach that we have chosen to study the dynamics of thermal denaturation. The DHIT provided a new window through which much-needed basic knowledge can be obtained and applied to improve various clinical procedures and the design of tissue-engineered products. More importantly, it has significantly increased our knowledge of rapid thermal denaturation.

6.2 Conclusions

6.2.1 The Characterization of Dynamic Mechanism(s) of Collagen Transformation:

(i) Rapid thermal transitions in fresh or crosslinked pericardium (PC) and chordae tendineae (CT) were three-staged phenomena.

(ii) The differences in tissue architecture between PC and CT led to a delay in the dynamics of thermal transition in the latter tissue relative to the former. This is of considerable interest, suggesting that heat-induced transition is partially determined by fibre orientation and the arrangement of the collagen fibre in each tissue.

(iii) Crosslinking of PC and CT by glutaraldehyde or carbodiimide (EDC) reduced the dynamics of rapid thermal transition in both tissues suggesting that limiting the chain mobility (i.e. reducing the configurational entropy) can effectively influence the dynamics of rapid thermal denaturation.

6.2.2 Reversibility Mechanism(s) of Collagen Transformation

(i) Exposure of bovine PC and CT to repeated and rapid hot-cold cycle transitions and the ensuing analysis revealed that the rapid thermal denaturation that occurred during the first heating cycle was indeed an irreversible event, irrespective of crosslinking treatments. While the initial events occurring during the first thermal cycle are irreversible, the reversible thermoelastic contraction and relaxation of both denatured collagenous tissues, upon heating and cooling respectively, was noteworthy.

6.2.3 The Influence of Increased Mechanical Loads on the Dynamics of Collagen Transformation

(i) Small increases in the mechanical loads (i.e. lowering the α-chain's configurational entropy) delayed the dynamics of the thermal transition in the CT, in both fresh and crosslinked tissue.

6.2.4 The Influence of External Milieu on the Dynamics of Collagen Transformation:

(i) The presence of NaCl solution delayed the dynamics of rapid thermal transition, irrespective of salt concentration. Crosslinking of the CT with either glutaraldehyde or EDC protected the chordae from the effect of salt ions.

(ii) The thermal stability analyses revealed that presence of salt ions thermally destabilized the chordae as shown by a lower denaturation temperature and shorter stress decay half-life.

6.2.5 The Thermomechanical Stability of the Various Load-Bearing Components of the Heart

(i) The rapid and slow thermal transition tests (DHIT and HIT) have strongly suggested a near absence of mature, hydrolytically stable crosslinks in mitral valve leaflets, as they all ruptured before reaching the 90°C isotherm. The aortic valve tissues largely survived these tests, suggesting that they are more thermally stable than the mitral valves.

(ii) The thermal analyses (DHIT and HIT) of tricuspid and mitral chordae revealed that the former are more thermally stable than the latter.

(iii) The mechanical data differed from thermal data. In other words, compared to the tricuspid chordae, the mitral chordae were significantly tougher, stiffer, and less extensible.

7 Recommendations

7.1 Thermal Driving Force Studies

The DHIT experiments were conducted under a single isothermal condition. In other words, the dynamics of rapid thermal denaturation of two collagenous tissues (irrespective of their crosslinking treatments), were conducted at a single isothermal temperature (90 ± 1°C) and hence under different *thermal driving forces.* Recently, Chen et al. [160] demonstrated that changing of the isothermal temperature (e.g. 65°C < T < 90°C) altered the dynamics of the denaturation of chordae tendineae at various temperatures, as measured in their analysis by a single characteristic time constant (τ_J). As mentioned earlier, the 90°C isotherm in our DHIT studies was selected since it was a significantly higher temperature (at least 17°C higher) than the denaturation temperatures (T_d) of all fresh tissue samples (Table 5.1), and approximately 4-5°C higher than that of all the crosslinked tissues (Table 2.1). It would therefore, be of interest to study the effect of varying the *thermal driving forces,* and how these changes would influence the dynamics of denaturation during the DHIT tests. Accordingly, it is suggested that, the two following series of studies be conducted: (i) An analysis of the dynamics of thermal denaturation for a given tissue, at different *thermal driving forces* (e.g. fresh chordae tendineae at 75, 80 85, 90, 95°C). (ii) A comparison the dynamics of thermal denaturation based on the specific and constant driving forces across tissues/treatments. For instance, if the fresh CT is exposed to a 75°C isotherm, that corresponds to a driving force of 6 °C (selected isotherm - T_d; hence, 69°C - 75°C); thus, to maintain this driving force of 6°C, a glutaraldehyde treated chordae tendineae (with T_d of 86°C) would be exposed to an isotherm of 91°C. The objective of the later studies would be to understand if providing the same driving force to a fresh and a crosslinked tissues would result in the similar dynamics and whether, for instance, the slower denaturation in glutaraldehyde-treated tissues was solely the result of a lower driving force *for that tissue.*

7.2 Consideration of the Multi-axial Nature of the Collagenous Model Tissues

The results obtained from the DHIT studies reflected the changes in these collagen fibres that bear load in a uniaxial direction, and does not take into account those fibres that may be oriented in the lateral direction. To better understand the rapid denaturation behaviour of

the various collagenous tissues, a multi-axial experimental device needs to be designed to study the thermal contraction of the tissues. Meanwhile, the tissues used where collagen fibres are mainly uniaxially arranged may be the best option to study such behaviours.

7.3 Application of the Higher Loads During the Entropic Studies

To better understand the influence of entropy on the dynamics of rapid thermal denaturation, the upper limits of mechanical loads should be applied to the chordae tendineae in the DHIT experiments. Given the current limitations of the DHIT systems, the present load cells must be replaced with ones that have a broader load range.

7.4 Recognition of Different Crosslinks using a Series of Time-Dependent Studies

To identify and characterize the specific nature of the crosslinks (or linkages) that may be ruptured during each stage of the rapid thermal denaturation, a series of time-dependent analyses must be conducted at various time points. For instance, tissues are immersed in a particular isotherm (e.g. 90°C) will be incubated for various time periods [i.e. short ($t < 3$ s) intermediate ($10 < t < 50$ s) and long ($100 < t < 300$ s)]. Immediately, after each incubation period, the tissues are fixed and will subsequently be analysed (enzymatically or scanning electron microscopy) for their crosslinking patterns post denaturation.

7.5 Treatment of Different Load Bearing Collagenous Cardiac Tissue with Sodium Borohydride

Both slow and rapid thermomechanical results indicated that cardiac tissues sustaining higher mechanical loads in function are maintained structurally by a series of immature and heat-labile crosslinkages. To confirm this hypothesis, a series of studies must be conducted to assess the maturity of these crosslinks. This can be accomplished by reducing the suspected immature and heat-labile crosslinkages with sodium borohydride, leading to their thermal stabilisation. Following this reduction step, both the control and the reduced tissues may

undergo both thermomechanical studies (i.e. DHIT and HIT) to assess the change in their dynamics of denaturation as well as their thermal stability.

7.6 Treatment of Collagenous Tissues with Different Salt Molecules

To further elaborate on the results of the electrostatic studies, it is recommended that different salt solutions (based on their particular lyotropic positions) be used to incubate the chordae tendineae at various concentrations. It is equally important to study the specific nature of the salt-protein interactions, and whether or not salt imposes its effect by directly by interfering with charged amino acids or indirectly by competing with water molecules. Particularly, salt-protein interaction can be blocked by the use of specific antibodies against the charged amino groups. The subsequent DHIT and HIT analysis may then determine the exact nature of the protein-salt interactions.

8 References

1. **Chvapil, M., R.I. Kronenthal, and W. Van Winkle Jr**, *Medical Surgical applications of collagen*, in *International review of connective tissue research*, D. Hall and Jackson. DS., Editors. 1970, Academic Press: New York. p. 1-61.

2. **Holl-Allen, R.T.**, *Porcine dermal collagen implants in man.* J R Coll Surg Edinb, 1984. **29**(3): p. 151-3.

3. **Holl-Allen, R.T.**, *Porcine dermal collagen repair of inguinal hernias.* J R Coll Surg Edinb, 1984. **29**(3): p. 154-7.

4. **Colin, W. and R.B. Donoff**, *Nerve regeneration through collagen tubes.* J Dent Res, 1984. **63**(7): p. 987-93.

5. **Burke, K.E., G. Naughton, E. Waldo, and N. Cassai**, *Bovine collagen implant: histologic chronology in pig dermis.* J Dermatol Surg Oncol, 1983. **9**(11): p. 889-95.

6. **DeLustro, F., S.T. Smith, J. Sundsmo, G. Salem, S. Kincaid, and L. Ellingsworth**, *Reaction to injectable collagen: results in animal models and clinical use.* Plast Reconstr Surg, 1987. **79**(4): p. 581-94.

7. **Yannas, I.V. and J.F. Burke**, *Design of an artificial skin. I. Basic design principles.* J Biomed Mater Res, 1980. **14**(1): p. 65-81.

8. **Chvapil, M.**, *Considerations on manufacturing principles of a synthetic burn dressing: a review.* J Biomed Mater Res, 1982. **16**(3): p. 245-63.

9. **Pruitt, B.A., Jr. and N.S. Levine**, *Characteristics and uses of biologic dressings and skin substitutes.* Arch Surg, 1984. **119**(3): p. 312-22.

10. **Bradley, W.G. and G.L. Wilkes**, *Some mechanical property considerations of reconstituted collagen for drug release supports.* Biomater Med Devices Artif Organs, 1977. **5**(2): p. 159-75.

11. **O'Brien, T.P., M.R. Sawusch, J.D. Dick, T.R. Hamburg, and J.D. Gottsch**, *Use of collagen corneal shields versus soft contact lenses to enhance penetration of topical tobramycin.* J Cataract Refract Surg, 1988. **14**(5): p. 505-7.

12. **Geggel, H.S., J. Friend, and R.A. Thoft**, *Collagen gel for ocular surface.* Invest Ophthalmol Vis Sci, 1985. **26**(6): p. 901-5.

13. **Tanner, J.C., Jr., M.A. Marcucci, W.H. Bradley, and J.W. Morgan**, *Partial nephrectomy and use of collagen grafts for renal wound closure.* J Urol, 1968. **99**(6): p. 710-2.

14. **Talman, E.A. and D.R. Boughner**, *Glutaraldehyde fixation alters the internal shear properties of porcine aortic heart valve tissue.* Ann Thorac Surg, 1995. **60**(2 Suppl): p. S369-73.

15. **Ottani, V., M. Raspanti, and A. Ruggeri**, *Collagen structure and functional implications.* Micron, 2001. **32**(3): p. 251-60.

16. **Vyavahare, N., M. Ogle, F.J. Schoen, R. Zand, D.C. Gloeckner, M. Sacks, and R.J. Levy**, *Mechanisms of bioprosthetic heart valve failure: fatigue causes collagen denaturation and glycosaminoglycan loss.* J Biomed Mater Res, 1999. **46**(1): p. 44-50.

17. **Thubrikar, M.J., J.D. Deck, J. Aouad, and S.P. Nolan**, *Role of mechanical stress in calcification of aortic bioprosthetic valves.* J Thorac Cardiovasc Surg, 1983. **86**(1): p. 115-25.

18. **Aksan, A. and J.J. McGrath**, *Thermomechanical analysis of soft-tissue thermotherapy.* J Biomech Eng, 2003. **125**(5): p. 700-8.

19. **Wright, N.T. and J.D. Humphrey**, *Denaturation of collagen via heating: An Irreversible Rate Process.* Annu Rev Biomed Eng, 2002. **4**: p. 109-28.

20. **Cilesiz, I., S. Thomsen, and A.J. Welch**, *Controlled temperature tissue fusion: argon laser welding of rat intestine in vivo. Part one.* Lasers Surg Med, 1997. **21**(3): p. 269-77.

21. **Kampmeier, J., B. Radt, R. Birngruber, and R. Brinkmann**, *Thermal and biomechanical parameters of porcine cornea.* Cornea, 2000. **19**(3): p. 355-63.

22. **Kuo, T., M.T. Speyer, W.R. Ries, and L. Reinisch**, *Collagen thermal damage and collagen synthesis after cutaneous laser resurfacing.* Lasers Surg Med, 1998. **23**(2): p. 66-71.

23. **Fitzpatrick, R.E., M.P. Goldman, N.M. Satur, and W.D. Tope**, *Pulsed carbon dioxide laser resurfacing of photo-aged facial skin.* Arch Dermatol, 1996. **132**(4): p. 395-402.

24. **Anderson, K., E.C. McCarty, and R.F. Warren**, *Thermal capsulorrhaphy: where are we today.* Sports Med Arthro Rev, 1999. **7**: p. 117-127.

25. **Arnoczky, S.P. and A. Aksan**, *Thermal modification of connective tissues: basic science considerations and clinical implications.* J Am Acad Orthop Surg, 2000. **8**(5): p. 305-13.

26. **Medvecky, M.J., B.C. Ong, A.S. Rokito, and O.H. Sherman**, *Thermal capsular shrinkage: Basic science and clinical applications.* Arthroscopy, 2001. **17**(6): p. 624-35.

27. **Tibone, J.E., P.J. McMahon, T.A. Shrader, M.D. Sandusky, and T.Q. Lee**, *Glenohumeral joint translation after arthroscopic, nonablative, thermal capsuloplasty with a laser.* Am J Sports Med, 1998. **26**(4): p. 495-8.

28. **Savoie, F.H., L.D. Field, R.N. Jenkins, W.J. Mallon, and R.A. Phelps, 2nd**, *The pain control infusion pump for postoperative pain control in shoulder surgery.* Arthroscopy, 2000. **16**(4): p. 339-42.

29. **Chen, S.S. and J.D. Humphrey**, *Heat-induced changes in the mechanics of a collagenous tissue: pseudoelastic behavior at 37 degrees C.* J Biomech, 1998. **31**(3): p. 211-6.

30. **Chen, S.S., N.T. Wright, and J.D. Humphrey**, *Heat-induced changes in the mechanics of a collagenous tissue: isothermal, isotonic shrinkage.* J Biomech Eng, 1998. **120**(3): p. 382-8.

31. **Schaefer, S.L., M.J. Ciarelli, S.P. Arnoczky, and H.E. Ross**, *Tissue shrinkage with the holmium:yttrium aluminum garnet laser. A postoperative assessment of tissue length, stiffness, and structure.* Am J Sports Med, 1997. **25**(6): p. 841-8.

32. **Chen, S.S., N.T. Wright, and J.D. Humphrey**, *Phenomenological evolution equations for heat-induced shrinkage of a collagenous tissue.* IEEE Trans Biomed Eng, 1998. **45**(10): p. 1234-40.

33. **Jun, J.H., J.L. Harris, J.D. Humphrey, and S. Rastegar**, *Effect of thermal damage and biaxial loading on the optical properties of a collagenous tissue.* J Biomech Eng, 2003. **125**(4): p. 540-8.

34. **Harris, J.L., P.B. Wells, and J.D. Humphrey**, *Altered mechanical behavior of epicardium due to isothermal heating under biaxial isotonic loads.* J Biomech Eng, 2003. **125**(3): p. 381-8.

35. **Tao, L., J.D. Humphrey, and K. Rajagopal**, *A mixture theory for heat-induced alterations in hydration and mechanical properties in soft tissues.* Int J Eng Sci, 2001. **39**: p. 1535-1556.

36. **Bailey, A.J., R.G. Paul, and L. Knott**, *Mechanisms of maturation and ageing of collagen.* Mech Ageing Dev, 1998. **106**(1-2): p. 1-56.

37. **Voet, D. and J. Voet**, *Biochemistry*. Vol. 2. 1995, New York, Chichester, Brisbane, Toronto, Singapore: John Wliley and Sons, Inc.

38. **Kuhn, K.**, *The structure of collagen*. Essays Biochem, 1969. **5**: p. 59-87.

39. **Bigi, A., M. Borghi, G. Cojazzi, M. Fichera, and S. Panzavolta**, *Structural and Mechanical properties of crosslinked drawn gelatin films*. Journal of Thermal Analysis and Calorimetry, 2000. **61**: p. 451-459.

40. **Bailey, A.J.**, *Molecular mechanisms of ageing in connective tissues*. Mech Ageing Dev, 2001. **122**(7): p. 735-55.

41. **Prockop, D.J. and K.I. Kivirikko**, *Collagens: molecular biology, diseases, and potentials for therapy*. Annu Rev Biochem, 1995. **64**: p. 403-34.

42. **Holmgren, S.K., K.M. Taylor, L.E. Bretscher, and R.T. Raines**, *Code for collagen's stability deciphered*. Nature, 1998. **392**(6677): p. 666-7.

43. **Ramachandran, G.N.**, *Structure of collagen at the moelcualr level*, in *Treatise on Collagen*, G.N. Ramachandran, Editor. 1967, Academic Press: London. p. 103-183.

44. **Rich, A. and F. Crick**, *The molecular structure of collagen*. J Mol Bio, 1961. **3**: p. 483-506.

45. **Engel, J., H.T. Chen, D.J. Prockop, and H. Klump**, *The triple helix in equilibrium with coil conversion of collagen-like polytripeptides in aqueous and nonaqueous solvents. Comparison of the thermodynamic parameters and the binding of water to (L-Pro-L-Pro-Gly)n and (L-Pro-L-Hyp-Gly)n*. Biopolymers, 1977. **16**(3): p. 601-22.

46. **Berg, R.A. and D.J. Prockop**, *The thermal transition of a non-hydroxylated form of collagen. Evidence for a role for hydroxyproline in stabilizing the triple-helix of collagen*. Biochem Biophys Res Commun, 1973. **52**(1): p. 115-20.

47. **Inouye, K., S. Sakakibara, and D.J. Prockop**, *Effects of the stereo-configuration of the hydroxyl group in 4-hydroxyproline on the triple-helical structures formed by homogenous peptides resembling collagen*. Biochim Biophys Acta, 1976. **420**(1): p. 133-41.

48. **Inouye, K., Y. Kobayashi, Y. Kyogoku, Y. Kishida, S. Sakakibara, and D.J. Prockop**, *Synthesis and physical properties of (hydroxyproline-proline-glycine)10: hydroxyproline in the X-position decreases the melting temperature of the collagen triple helix*. Arch Biochem Biophys, 1982. **219**(1): p. 198-203.

49. **Burjanadze, T.V.**, *Hydroxyproline content and location in relation to collagen thermal stability*. Biopolymers, 1979. **18**(4): p. 931-8.

50. **Privalov, P.L.**, *Stability of proteins. Proteins which do not present a single cooperative system*. Adv Protein Chem, 1982. **35**: p. 1-104.

51. **Bella, J., B. Brodsky, and H.M. Berman**, *Hydration structure of a collagen peptide*. Structure, 1995. **3**(9): p. 893-906.

52. **Nimni, M.E.**, *Collagen*. Vol. 1-4. 1988, Boca Raton, Florida: CRC Press.

53. **Privalov, P.L., E.I. Tiktopulo, and V.M. Tischenko**, *Stability and mobility of the collagen structure*. J Mol Biol, 1979. **127**(2): p. 203-16.

54. **Privalov, P.L.**, *Stability of proteins: small globular proteins*. Adv Protein Chem, 1979. **33**: p. 167-241.

55. **Suzuki, E., R.D.B. Fraser, and T.P. MacRae**, *Role of hydroxyproline in the stabilization of the collagen molecule via water moelcules*. Int J. Biol. Macromolec., 1980. **2**(54-56).

56. **Fraser, R.D., T.P. MacRae, and E. Suzuki**, *Chain conformation in the collagen molecule*. J Mol Biol, 1979. **129**(3): p. 463-81.

57. **Shinyashiki, N., N. Asaka, S. Mashimo, S. Yagihara, and N. Sasaki**, *Microwave dielectric study on hydration of moist collagen*. Biopolymers, 1990. **29**(8-9): p. 1185-91.

58. **Eberhardt, E.S., N. Panasik Jr., and R.T. Raines**, *Inductive effects on the energetics of prolyl peptide bond isomerization: implications for collagen folding and stability*. J Am Chem Soc, 1996. **118**: p. 12261-12266.

59. **Panasik Jr., N., E.S. Eberhardt, A.S. Edison, D.R. Powell, and R.T. Raines**, *Inductive effects on the structure of proline residues*. Int J Pept Protein Res, 1994. **44**: p. 262-269.

60. **Holmgren, S.K., L.E. Bretscher, K.M. Taylor, and R.T. Raines**, *A hyperstable collagen mimic*. Chem Biol, 1999. **6**(2): p. 63-70.

61. **Nimni, M.E.**, *The molecular organization of collagen and its role in determining the biophysical properties of the connective tissues*. Biorheology, 1980. **17**(1-2): p. 51-82.

62. **Parry, D.A.**, *The molecular and fibrillar structure of collagen and its relationship to the mechanical properties of connective tissue*. Biophys Chem, 1988. **29**(1-2): p. 195-209.

63. **Viidik, A., C.C. Danielson, and H. Oxlund**, *On fundamental and phenomenological models, structure and mechanical properties of collagen, elastin and glycosaminoglycan complexes.* Biorheology, 1982. **19**(3): p. 437-51.

64. **Jorge-Herrero, E., P. Fernandez, J. Turnay, N. Olmo, P. Calero, R. Garcia, I. Freile, and J.L. Castillo-Olivares**, *Influence of different chemical cross-linking treatments on the properties of bovine pericardium and collagen.* Biomaterials, 1999. **20**(6): p. 539-45.

65. **Lee, J., Haberer, SA., Pereira, CA., Naimark, WA., Courtman, DW., Wilson, GJ.**, *High strain rate testing and structural analysis of pericardial bioprosthetic materials*, in *Biomaterials Mechanical Properties ASTM STO 1173*, H. Kambic, Yokobori, AT.,, Editor. 1994, Am. Soc. for Testing and Materials: Philadelphia. p. 19-42.

66. **Woo, S.L., R.E. Debski, J.D. Withrow, and M.A. Janaushek**, *Biomechanics of knee ligaments.* Am J Sports Med, 1999. **27**(4): p. 533-43.

67. **Kawahara, J., T. Ohmori, T. Ohkubo, S. Hattori, and M. Kawamura**, *The structure of glutaraldehyde in aqueous solution determined by ultraviolet absorption and light scattering.* Anal Biochem, 1992. **201**(1): p. 94-8.

68. **Korn, A.H., S.H. Feairheller, and E.M. Filachione**, *Glutaraldehyde: nature of the reagent.* J Mol Biol, 1972. **65**(3): p. 525-9.

69. **Cheung, D.T. and M.E. Nimni**, *Mechanism of crosslinking of proteins by glutaraldehyde II. Reaction with monomeric and polymeric collagen.* Conn Tiss Res, 1982. **10**(2): p. 201-16.

70. **Cheung, D.T. and M.E. Nimni**, *Mechanism of crosslinking of proteins by glutaraldehyde I: reaction with model compounds.* Conn Tiss Res, 1982. **10**(2): p. 187-99.

71. **Trowbridge, E.A. and C.E. Crofts**, *The standardisation of gauge length: its influence on the relative extensibility of natural and chemically modified pericardium.* J Biomech, 1986. **19**(12): p. 1023-33.

72. **Lee, J.M., S.A. Haberer, and D.R. Boughner**, *The bovine pericardial xenograft: I. Effect of fixation in aldehydes without constraint on the tensile viscoelastic properties of bovine pericardium.* J Biomed Mater Res, 1989. **23**(5): p. 457-75.

73. **Vesely, I., D. Boughner, and T. Song**, *Tissue buckling as a mechanism of bioprosthetic valve failure.* Ann Thorac Surg, 1988. **46**(3): p. 302-8.

74. **Vesely, I. and R. Noseworthy**, *Micromechanics of the fibrosa and the ventricularis in aortic valve leaflets.* J Biomech, 1992. **25**(1): p. 101-13.

75. **Vesely, I., A.H. Menkis, B. Rutt, and G. Campbell**, *Aortic valve/root interactions in porcine hearts: implications for bioprosthetic valve sizing.* J Card Surg, 1991. **6**(4): p. 482-9.

76. **Duncan, A.C., D. Boughner, and I. Vesely**, *Viscoelasticity of dynamically fixed bioprosthetic valves. II. Effect of glutaraldehyde concentration.* J Thorac Cardiovasc Surg, 1997. **113**(2): p. 302-10.

77. **Duncan, A.C., D. Boughner, and I. Vesely**, *Dynamic glutaraldehyde fixation of a porcine aortic valve xenograft. I. Effect of fixation conditions on the final tissue viscoelastic properties.* Biomaterials, 1996. **17**(19): p. 1849-56.

78. **Broom, N.D. and D. Marra**, *Effect of glutaraldehyde fixation and valve constraint conditions on porcine aortic valve leaflet coaptation.* Thorax, 1982. **37**(8): p. 620-6.

79. **Olde Damink, L.H., P.J. Dijkstra, M.J. van Luyn, P.B. van Wachem, P. Nieuwenhuis, and J. Feijen**, *In vitro degradation of dermal sheep collagen cross-linked using a water-soluble carbodiimide.* Biomaterials, 1996. **17**(7): p. 679-84.

80. **Olde Damink, L.H., P.J. Dijkstra, M.J. van Luyn, P.B. van Wachem, P. Nieuwenhuis, and J. Feijen**, *Cross-linking of dermal sheep collagen using a water-soluble carbodiimide.* Biomaterials, 1996. **17**(8): p. 765-73.

81. **Petite, H., J.L. Duval, V. Frei, N. Abdul-Malak, M.F. Sigot-Luizard, and D. Herbage**, *Cytocompatibility of calf pericardium treated by glutaraldehyde and by the acyl azide methods in an organotypic culture model.* Biomaterials, 1995. **16**(13): p. 1003-8.

82. **Petite, H., V. Frei, A. Huc, and D. Herbage**, *Use of diphenylphosphorylazide for cross-linking collagen-based biomaterials.* J Biomed Mater Res, 1994. **28**(2): p. 159-65.

83. **Anselme, K., H. Petite, and D. Herbage**, *Inhibition of calcification in vivo by acyl azide cross-linking of a collagen-glycosaminoglycan sponge.* Matrix, 1992. **12**(4): p. 264-73.

84. **Petite, H., I. Rault, A. Huc, P. Menasche, and D. Herbage**, *Use of the acyl azide method for cross-linking collagen-rich tissues such as pericardium.* J Biomed Mater Res, 1990. **24**(2): p. 179-87.

85. **Naimark, W.A., C.A. Pereira, K. Tsang, and J.M. Lee**, *HMDC crosslinking of bovine pericardial tissue: a role of the solvent environment in the design of bioprosthetic materials.* J Mat Sci: Materials in Medicine, 1995. **6**: p. 235-41.

86. **Hanthamrongwit, M., W.H. Reid, and M.H. Grant**, *Chondroitin-6-sulphate incorporated into collagen gels for the growth of human keratinocytes: the effect of cross-linking agents and diamines*. Biomaterials, 1996. **17**(8): p. 775-80.

87. **Sung, H.W., H.L. Hsu, C.C. Shih, and D.S. Lin**, *Cross-linking characteristics of biological tissues fixed with monofunctional or multifunctional epoxy compounds*. Biomaterials, 1996. **17**(14): p. 1405-10.

88. **Shen, S.H., H.W. Sung, R. Tu, C. Hata, D. Lin, Y. Noishiki, and R.C. Quijano**, *Characterization of a polyepoxy compound fixed porcine heart valve bioprosthesis*. J Appl Biomater, 1994. **5**(2): p. 159-62.

89. **Pereira, C.A., J.M. Lee, and S.A. Haberer**, *Effect of alternative crosslinking methods on the low strain rate viscoelastic properties of bovine pericardial bioprosthetic material*. J Biomed Mater Res, 1990. **24**(3): p. 345-61.

90. **Courtman, D.W., C.A. Pereira, V. Kashef, D. McComb, J.M. Lee, and G.J. Wilson**, *Development of a pericardial acellular matrix biomaterial: biochemical and mechanical effects of cell extraction*. J Biomed Mater Res, 1994. **28**(6): p. 655-66.

91. **Lee, J.M., C.A. Pereira, and L.W. Kan**, *Effect of molecular structure of poly(glycidyl ether) reagents on crosslinking and mechanical properties of bovine pericardial xenograft materials*. J Biomed Mater Res, 1994. **28**(9): p. 981-92.

92. **Wong, S.**, *Chemistry of protein conjugation and cross-linking*. 1991, Boca Raton: CRC Press. 1-133.

93. **Lee, J., Edwards, HHL., Pereira, CA., Samii, SI.**, *Crosslinking of tissue-derived biomaterials in 1-ethyl-3-(3-dimethylaminopropyl)-carbodiimide*. J Mat Sci: Materials in Medicine, 1996. **7**: p. 531-541.

94. **Gratzer, P.F. and J.M. Lee**, *Control of pH alters the type of cross-linking produced by 1-ethyl-3-(3- dimethylaminopropyl)-carbodiimide (EDC) treatment of acellular matrix vascular grafts*. J Biomed Mater Res, 2001. **58**(2): p. 172-9.

95. **Gilles, M.A., A.Q. Hudson, and C.L. Borders, Jr.**, *Stability of water-soluble carbodiimides in aqueous solution*. Anal Biochem, 1990. **184**(2): p. 244-8.

96. **Lee, J.M. and S.E. Langdon**, *Thickness measurement of soft tissue biomaterials: a comparison of five methods*. J Biomech, 1996. **29**(6): p. 829-32.

97. **Grabarek, Z. and J. Gergely**, *Zero-length crosslinking procedure with the use of active esters*. Anal Biochem, 1990. **185**(1): p. 131-5.

98. **Mann, D., W. Lew, E. Ban-Hayashi, R. Shabetai, L. Waldman, and M.M. LeWinter**, *In vivo mechanical behavior of canine pericardium.* Am J Physiol, 1986. **251**(2 Pt 2): p. H349-56.

99. **Bailey, A.J.**, *Perspective article: the fate of collagen implants in tissue defects.* Wound Repair Regen, 2000. **8**(1): p. 5-12.

100. **Naimark, W.A., J.M. Lee, H. Limeback, and D.T. Cheung**, *Correlation of structure and viscoelastic properties in the pericardia of four mammalian species.* Am J Physiol, 1992. **263**(4 Pt 2): p. H1095-106.

101. **Khanna, R.**, *Synergy between fatigue damage and enzymatic degradation of bioprosthetic heart valve materials*, in *Mechanical engineering*. 2000, Dalhousie University: Halifax. p. 127.

102. **Davis, E.C.**, *Stability of elastin in the developing mouse aorta: a quantitative radioautographic study.* Histochemistry, 1993. **100**(1): p. 17-26.

103. **Mecham, R.P., T.J. Broekelmann, C.J. Fliszar, S.D. Shapiro, H.G. Welgus, and R.M. Senior**, *Elastin degradation by matrix metalloproteinases. Cleavage site specificity and mechanisms of elastolysis.* J Biol Chem, 1997. **272**(29): p. 18071-6.

104. **Simionescu, D., R.V. Iozzo, and N.A. Kefalides**, *Bovine pericardial proteoglycan: biochemical, immunochemical and ultrastructural studies.* Matrix, 1989. **9**(4): p. 301-10.

105. **Simionescu, D., R. Alper, and N.A. Kefalides**, *Partial characterization of a low molecular weight proteoglycan isolated from bovine parietal pericardium.* Biochem Biophys Res Commun, 1988. **151**(1): p. 480-6.

106. **Ishihara, T., V.J. Ferrans, M. Jones, S.W. Boyce, O. Kawanami, and W.C. Roberts**, *Histologic and ultrastructural features of normal human parietal pericardium.* Am J Cardiol, 1980. **46**(5): p. 744-53.

107. **Ishihara, T., V.J. Ferrans, M. Jones, S.W. Boyce, and W.C. Roberts**, *Structure of bovine parietal pericardium and of unimplanted Ionescu- Shiley pericardial valvular bioprostheses.* J Thorac Cardiovasc Surg, 1981. **81**(5): p. 747-57.

108. **Allen, D.J., L.J. DiDio, A. Zacharias, I. Fentie, A.J. McGrath, L.B. Puig, P.N. Pomerantzeff, and E.J. Zerbini**, *Microscopic study of normal parietal pericardium and unimplanted Puig- Zerbini pericardial valvular heterografts.* J Thorac Cardiovasc Surg, 1984. **87**(6): p. 845-55.

109. **Spodick, D.H.**, *Macrophysiology, microphysiology, and anatomy of the pericardium: a synopsis.* Am Heart J, 1992. **124**(4): p. 1046-51.

110. **Schoen, F.J. and R.J. Levy**, *Founder's Award, 25th Annual Meeting of the Society for Biomaterials, perspectives. Providence, RI, April 28-May 2, 1999. Tissue heart valves: current challenges and future research perspectives.* J Biomed Mater Res, 1999. **47**(4): p. 439-65.

111. **Sacks, M.S., C.J. Chuong, and R. More**, *Collagen fiber architecture of bovine pericardium.* ASAIO J, 1994. **40**(3): p. M632-7.

112. **Lee, J.B.D.**, *Bioprosthetic heart valves - Tissue Mechanics and Implications for design*, in *Blood compatible Material and devices.* 1991, Technomic Pub.

113. **Broom, N.D.**, *Simultaneous morphological and stress-strain studies of the fibrous components in wet heart valve leaflet tissue.* Connect Tissue Res, 1978. **6**(1): p. 37-50.

114. **Harkness, R.**, *Biological function of collagen.* Biol. Rev, 1961. **36**: p. 399-463.

115. **Zioupos, P., J.C. Barbenel, and J. Fisher**, *Anisotropic elasticity and strength of glutaraldehyde fixed bovine pericardium for use in pericardial bioprosthetic valves.* J Biomed Mater Res, 1994. **28**(1): p. 49-57.

116. **Kunzelman, K.S. and R.P. Cochran**, *Mechanical properties of basal and marginal mitral valve chordae tendineae.* ASAIO Trans, 1990. **36**(3): p. M405-8.

117. **Barber, J.E., F.K. Kasper, N.B. Ratliff, D.M. Cosgrove, B.P. Griffin, and I. Vesely**, *Mechanical properties of myxomatous mitral valves.* J Thorac Cardiovasc Surg, 2001. **122**(5): p. 955-62.

118. **Fenoglio, J., Jr. and P. Tuan duc**, *Ruptured chordae tendineae. An electron microscopic study.* Hum Pathol, 1972. **3**(3): p. 415-20.

119. **Caulfield, J.B., D.L. Page, J.A. Kastor, and C.A. Sanders**, *Connective tissue abnormalities in spontaneous rupture of chordae tendineae.* Arch Pathol, 1971. **91**(6): p. 537-41.

120. **Millington-Sanders, C., A. Meir, L. Lawrence, and C. Stolinski**, *Structure of chordae tendineae in the left ventricle of the human heart.* J Anat, 1998. **192**(Pt 4): p. 573-81.

121. **Sato, I.**, *Coil-like structure of the inner core of chordae tendineae.* Clin Anat, 2002. **15**(3): p. 196-8.

122. **Lee, Y.S., C.H. Chang, H.C. Chen, and G.F. Liang**, *Scanning and transmission electron microscopic studies on isolated ruptures of chordae tendineae.* Jpn Heart J, 1983. **24**(3): p. 355-67.

123. **Lim, K.O. and D.R. Boughner**, *Scanning electron microscopical study of human mitral valve chordae tendineae.* Arch Pathol Lab Med, 1977. **101**(5): p. 236-8.

124. **Akhtar, S., K.M. Meek, and V. James**, *Ultrastructure abnormalities in proteoglycans, collagen fibrils, and elastic fibers in normal and myxomatous mitral valve chordae tendineae.* Cardiovasc Pathol, 1999. **8**(4): p. 191-201.

125. **Scott-Jupp, W., N.L. Barnett, P.J. Gallagher, J.L. Monro, and J.K. Ross**, *Ultrastructural changes in spontaneous rupture of mitral chordae tendineae.* J Pathol, 1981. **133**(3): p. 185-201.

126. **Akhtar, S., K.M. Meek, and V. James**, *Immunolocalization of elastin, collagen type I and type III, fibronectin, and vitronectin in extracellular matrix components of normal and myxomatous mitral heart valve chordae tendineae.* Cardiovasc Pathol, 1999. **8**(4): p. 203-11.

127. **Lim, K.O. and D.R. Boughner**, *Morphology and relationship to extensibility curves of human mitral valve chordae tendineae.* Circ Res, 1976. **39**(4): p. 580-5.

128. **Sokoloff, L., S.K. Elster, and N. Righthand**, *Sclerosis of the chordae tendineae of mitral valve.* Circulation, 1950. **1**: p. 782.

129. **Rusted, I.E., C.H. Scheifley, and J.E. Edwards**, *Studies of the mitral valve. I. Anatomic features of the normal mitral valve and associated structures.* Circulation, 1952. **6**(6): p. 825-31.

130. **Brock, R.C.**, *The surgical and pathological anatomy of the mitral valve.* Br Heart J, 1952. **14**(4): p. 489-513.

131. **Chiechi, M.A., W.M. Lees, and R. Thompson**, *Functional anatomy of the normal mitral valve.* J Thorac Surg, 1956. **32**(3): p. 378-98.

132. **Frater, R.W. and F.H. Ellis, Jr.**, *The anatomy of the canine mitral valve, with notes on function and comparisons with other mammalian mitral valves.* J Thorac Cardiovasc Surg, 1961. **1**: p. 171-8.

133. **Lam, J.H., N. Ranganathan, E.D. Wigle, and M.D. Silver**, *Morphology of the human mitral valve. I. Chordae tendineae: a new classification.* Circulation, 1970. **41**(3): p. 449-58.

134. **Morse, D.E., W.C. Hamlett, and C.W. Noble, Jr.**, *Morphogenesis of chordae tendineae. I: Scanning electron microscopy.* Anat Rec, 1984. **210**(4): p. 629-38.

135. **Barber, J.E., N.B. Ratliff, D.M. Cosgrove, 3rd, B.P. Griffin, and I. Vesely,** *Myxomatous mitral valve chordae. I: Mechanical properties.* J Heart Valve Dis, 2001. **10**(3): p. 320-4.

136. **Berkovitz, B.K. and S. Robinson,** *Ultrastructural quantification of collagen fibrils in chordae tendineae of the sheep and rabbit.* J Anat, 1991. **178**: p. 127-32.

137. **Lim, K.O.,** *Mechanical properties and ultrastructure of normal human tricuspid valve chordae tendineae.* Jpn J Physiol, 1980. **30**(3): p. 455-64.

138. **Verzar, F., H. Spichtin, and W. Gasche,** *Renaturation of collagen fibers after different methods of denaturation.* Gerontologia, 1965. **11**(3): p. 226-34.

139. **Bianchi, E., G. Conio, A. Ciferri, D. Puett, and L. Rajagh,** *The role of pH, temperature, salt type, and salt concentration on the stability of the crystalline, helical, and randomly coiled forms of collagen.* J Biol Chem, 1967. **242**(7): p. 1361-9.

140. **Le Lous, M., F. Flandin, D. Herbage, and J.C. Allain,** *Influence of collagen denaturation on the chemorheological properties of skin, assessed by differential scanning calorimetry and hydrothermal isometric tension measurement.* Biochim Biophys Acta, 1982. **717**(2): p. 295-300.

141. **Le Lous, M., J.C. Allain, L. Cohen-Solal, and P. Maroteaux,** *The rate of collagen maturation in rat and human skin.* Conn Tiss Res, 1982. **9**(4): p. 253-62.

142. **Le Lous, M., J.C. Allain, L. Cohen-Solal, and P. Maroteaux,** *Hydrothermal isometric tension curves from different connective tissues. Role of collagen genetic types and noncollagenous components.* Conn Tiss Res, 1983. **11**(2-3): p. 199-206.

143. **Komsa-Penkova, R., R. Koynova, G. Kostov, and B.G. Tenchov,** *Thermal stability of calf skin collagen type I in salt solutions.* Biochim Biophys Acta, 1996. **1297**(2): p. 171-81.

144. **Tiktopulo, E.I. and A.V. Kajava,** *Denaturation of type I collagen fibrils is an endothermic process accompanied by a noticeable change in the partial heat capacity.* Biochemistry, 1998. **37**(22): p. 8147-52.

145. **Harris, J.L. and J.D. Humphrey,** *Kinetics of thermal damage to a collagenous membrane under biaxial isotonic loading.* IEEE Trans Biomed Eng, 2004. **51**(2): p. 371-9.

146. **Nimni, M. and R. Harkness,** *Molecular structures and functions of collagen,* in *Collagen,* M. Nimni, Editor. 1988, Boca Raton: Florida. p. 1-79.

147. **Verzar, F.**, *Aging of the collagen fibre*, in *International review of connective tissue research*, D. Hall, Editor. 1964, Academic Press: New York. p. 243-300.

148. **Thomsen, S.**, *Pathologic analysis of photothermal and photomechanical effects of laser-tissue interactions*. Photochem Photobiol, 1991. **53**(6): p. 825-35.

149. **Flory, P. and R. Garrett**, *Phase transition in collagen and gelatin systems*. J Am Chem Soc, 1958. **80**: p. 4836-4835.

150. **Miles, C.A., T.V. Burjanadze, and A.J. Bailey**, *The kinetics of the thermal denaturation of collagen in unrestrained rat tail tendon determined by differential scanning calorimetry*. J Mol Biol, 1995. **245**(4): p. 437-46.

151. **Miles, C.A.**, *Kinetics of collagen denaturation in mammalian lens capsules studied by differential scanning calorimetry*. Int J Biol Macromol, 1993. **15**(5): p. 265-71.

152. **Naimark, W.A., S.D. Waldman, R.J. Anderson, B. Suzuki, C.A. Pereira, and J.M. Lee**, *Thermomechanical analysis of collagen crosslinking in the developing lamb pericardium*. Biorheology, 1998. **35**(1): p. 1-16.

153. **Wells, S.M., S.L. Adamson, B.L. Langille, and J.M. Lee**, *Thermomechanical analysis of collagen crosslinking in the developing ovine thoracic aorta*. Biorheology, 1998. **35**(6): p. 399-414.

154. **Nagy, I.Z., V.N. Toth, and F. Verzar**, *High-resolution electron microscopy of thermal collagen denaturation in tail tendons of young, adult and old rats*. Conn Tiss Res, 1974. **2**(4): p. 265-72.

155. **Allain, J.C., M. Le Lous, S. Cohen, S. Bazin, and P. Maroteaux**, *Isometric tensions developed during the hydrothermal swelling of rat skin*. Connect Tissue Res, 1980. **7**(3): p. 127-33.

156. **Ross, E.V., J.R. McKinlay, and R.R. Anderson**, *Why does carbon dioxide resurfacing work? A review*. Arch Dermatol, 1999. **135**(4): p. 444-54.

157. **Miles, C.A. and M. Ghelashvili**, *Polymer-in-a-box mechanism for the thermal stabilization of collagen molecules in fibres*. Biophy J, 2000. **76**: p. 3243-3252.

158. **Wall, M.S., X.H. Deng, P.A. Torzilli, S.B. Doty, S.J. O'Brien, and R.F. Warren**, *Thermal modification of collagen*. J Shoulder Elbow Surg, 1999. **8**(4): p. 339-44.

159. **Leikina, E., M.V. Mertts, N. Kuznetsova, and S. Leikin**, *Type I collagen is thermally unstable at body temperature*. Proc Natl Acad Sci U S A, 2002. **99**(3): p. 1314-8.

160. **Chen, S.S., N.T. Wright, and J.D. Humphrey**, *Heat-induced changes in the mechanics of a collagenous tissue: isothermal free shrinkage.* J Biomech Eng, 1997. **119**(4): p. 372-8.

161. **Bailey, A.J. and D. Lister**, *Thermally labile cross-links in native collagen.* Nature, 1968. **220**(164): p. 280-1.

162. **Miles, C.A. and A.J. Bailey**, *Thermally labile domains in the collagen molecule.* Micron, 2001. **32**(3): p. 325-32.

163. **Miles, C.A.**, *Kinetics of collagen denaturation in mammalian lens capsules studied by differential scanning calorimetry.* Int J Biol Macromol, 1993. **15**(5): p. 265-71.

164. **Hickman, D., T.J. Sims, C.A. Miles, A.J. Bailey, M. de Mari, and M. Koopmans**, *Isinglass/collagen: denaturation and functionality.* J Biotechnol, 2000. **79**(3): p. 245-57.

165. **Miles, C.A. and A.J. Bailey**, *Response to Engel and Bachinger's critique of collagen denaturation as a rate process.* Matrix Biol, 2001. **20**(4): p. 263-5, 267-9.

166. **Danielsen, C.C.**, *Thermal stability of reconstituted collagen fibrils. Shrinkage characteristics upon in vitro maturation.* Mech Ageing Dev, 1981. **15**(3): p. 269-78.

167. **Viidik, A.**, *Aging of collagen in complex tissues. A micromethodological study of the thermal reaction.* Experientia, 1972. **28**(6): p. 641-2.

168. **Kang, T., J. Resar, and J.D. Humphrey**, *Heat-induced changes in the mechanical behavior of passive coronary arteries.* J Biomech Eng, 1995. **117**(1): p. 86-93.

169. **Hormann, H. and H. Schlebusch**, *Reversible and irreversible denaturation of collagen fibers.* Biochemistry, 1971. **10**(6): p. 932-7.

170. **Flory, P.**, *Principles of polymer chemistry.* 1953, Ithaca, NY: Cornell University Press. 541-594.

171. **Weir, C.**, *Rate of Shrinkage of Tendon Collagen Heat, Entropy, and Free Energy of Activation of the Shrinkage of Untreated Tendon. Effect of Acid, Salt, Pickle, and Tannage on the Activation of Tendon Collagen.* Journal of Am Leather Chemists Assoc, 1949. **44**: p. 108-140.

172. **Gustavson, K.**, *The contraction of collagen, particularly hydrothermal shrinkage and crosslinking reactions*, in *The chemistry and reactivity of collagen*. 1956, New York Academic Press: New York.

173. **Pankhurst, K.**, *Incipient shrinkage of collagen and gelatin*. Nature, 1947. **159**(4042): p. 538.

174. **Bailey, A.J.**, *Collagen: Anture's framework in the medical, food, and leather industries*. J Soc Leath Tech Chem, 1992. **76**: p. 111.

175. **Thomsen, S., J.A. Pearce, and W.F. Cheong**, *Changes in birefringence as markers of thermal damage in tissues*. IEEE Trans Biomed Eng, 1989. **36**(12): p. 1174-9.

176. **Boedtker, H. and P. Doty**, *The native and denatured state of soluble collagen*. J Am Chem Soc, 1956. **78**: p. 7.

177. **Burge, R.E. and R.D. Hynes**, *The thermal denaturation of collagen in solution and its structural implications*. Journal of Molecular Biology, 1959. **1**: p. 155-164.

178. **Miles, C.A. and M. Ghelashvili**, *Polymer-in-a-box mechanism for the thermal stabilization of collagen molecules in fibers*. Biophys J, 1999. **76**(6): p. 3243-52.

179. **Humphrey, J.D.**, *Remodeling of a collagenous tissue at fixed lengths*. J Biomech Eng, 1999. **121**(6): p. 591-7.

180. **Sankaran, V. and J.T. Walsh, Jr.**, *Birefringence measurement of rapid structural changes during collagen denaturation*. Photochem Photobiol, 1998. **68**(6): p. 846-51.

181. **Stiller, W.**, *Arrhenius equation and non-equilibrium kinetics*. 1989, Leipzig: Teubner-Texte zur Physik.

182. **Dewey, W.C.**, *Arrhenius relationships from the molecule and cell to the clinic*. Int J Hyperthermia, 1994. **10**(4): p. 457-83.

183. **Moussa, N.A., E.N. Tell, and E.G. Cravalho**, *Time progression of hemolysis of erythrocyte populations exposed to supra-physiological temperatures*. ASME J. Biomech. Eng., 1979. **101**: p. 213-217.

184. **Freire, E.I.**, *Differential Scanning Calorimetry*, in *Protein stability and folding : theory and practice*, B.A. Shirley, Editor. 1995, Humana Press: Totowa, N.J. p. x, 377.

185. **Mentink, C.J., M. Hendriks, A.A. Levels, and B.H. Wolffenbuttel**, *Glucose-mediated cross-linking of collagen in rat tendon and skin.* Clin Chim Acta, 2002. **321**(1-2): p. 69-76.

186. **Bachinger, H.P., N.P. Morris, and J.M. Davis**, *Thermal stability and folding of the collagen triple helix and the effects of mutations in osteogenesis imperfecta on the triple helix of type I collagen.* Am J Med Genet, 1993. **45**(2): p. 152-62.

187. **Loke, W.K. and E. Khor**, *Validation of the shrinkage temperature of animal tissue for bioprosthetic heart valve application by differential scanning calorimetry.* Biomaterials, 1995. **16**(3): p. 251-8.

188. **Zeeman, R., P. Dijkstra, P. van Wachem, M. van Luyn, M. Hendriks, P. Cahalan, and J. Feijen**, *Successive epoxy and carbodiimide cross-linking of dermal sheep collagen.* Biomaterials, 1999. **20**: p. 921-931.

189. **Andreassen, T.T., K. Seyer-Hansen, and A.J. Bailey**, *Thermal stability, mechanical properties and reducible cross-links of rat tail tendon in experimental diabetes.* Biochim Biophys Acta, 1981. **677**(2): p. 313-7.

190. **Allain, J.C., M. Le Lous, S. Bazin, A.J. Bailey, and A. Delaunay**, *Isometric tension developed during heating of collagenous tissues. Relationships with collagen cross-linking.* Biochim Biophys Acta, 1978. **533**(1): p. 147-55.

191. **Veis, A.**, in *Treatise on collagen*, G.N. Ramachandran, Editor. 1967, Academic Press: London. p. 367-439.

192. **Lee, J.M., C.A. Pereira, D. Abdulla, W.A. Naimark, and I. Crawford**, *A multi-sample denaturation temperature tester for collagenous biomaterials.* Med Eng Phys, 1995. **17**(2): p. 115-21.

193. **Flory, P. and O. Spurr**, *Melting equilibrium for collagen fibres under stress: elasticity in the amorphous state.* J of Am Chem Soc, 1961. **83**: p. 1308-1316.

194. **Horgan, D.J., N.L. King, L.B. Kurth, and R. Kuypers**, *Collagen crosslinks and their relationship to the thermal properties of calf tendons.* Arch Biochem Biophys, 1990. **281**(1): p. 21-6.

195. **Le Lous, M., L. Cohen-Solal, J.C. Allain, J. Bonaventure, and P. Maroteaux**, *Age related evolution of stable collagen reticulation in human skin.* Connect Tissue Res, 1985. **13**(2): p. 145-55.

196. **Hukins, D.W.L.**, *Biomechanical properties of collagen*, in *Collagen in health and disease*, J.B. Weiss and M.I.V. Jayson, Editors. 1982, Churchill Livingstone: Edinburgh ; New York. p. 49-72.

197. **Gosline, J.M.**, *The elastic properties of rubber-like proteins and highly extensible tissues*. Symp Soc Exp Biol, 1980. **34**: p. 332-57.

198. **Gosline, J.M. and J. Rosenbloom**, *Elastin*, in *Extracellular Matrix Biochemistry*, K.A. Piez and A. Reddi, Editors. 1984, Elsevier: New York, Amsterdam, Oxford. p. 191-226.

199. **Lawton, R.**, *The thermoelastic behavior of isolated aortic strips of the dog*. Circulation Research, 1954. **11**: p. 344-353.

200. **Treloar, L.**, *The physics of rubber elasticity*. third ed. 1975, Oxford: Clarendon Press.

201. **Urry, D.W.**, *Elastin and Elastases*, L. Robert and W. Hornebeck, Editors. 1989, CRC Press: Boca Raton.

202. **Lennox, F.G.**, *Shrinkage of collagen*. Biochem Biophys Acta, 1949. **3**: p. 170-187.

203. **Flory, P.J.**, *Role of crystallization in polymers and proteins*. Science, 1956. **124**: p. 53-60.

204. **Krag, S., C.C. Danielsen, and T.T. Andreassen**, *Thermal and mechanical stability of lens capsule*. Curr. Eye Res., 1997. **17**: p. 470-477.

205. **Sporl, E., U. Genth, K. Schmalfuss, and T. Seiler**, *Thermomechanical behavior of the cornea*. Ger J Ophthalmol, 1996. **5**(6): p. 322-7.

206. **Rasmussen, D.M., K.G. Wakim, and R.K. Winkelmann**, *Isotonic and Isometric Thermal Contraction of Human Dermis. 3. Scleroderma and Cicatrizing Lesions*. J Invest Dermatol, 1964. **43**: p. 349-55.

207. **Chvapil, M. and J. L.**, *The shrinkage temperature of collagen fibres isolated from the tail tendon of rats of various ages and from different placers of the same tendon*. Gerontologia, 1963. **1**: p. 18-29.

208. **Svoboda K.K.H., G.H., Trinkaus-Randall V**, *Collagen expression and orientation in ocular tissue*. Prog. Polym. Sci., 1998. **23**: p. 329-374.

209. **Flandin, F., C. Buffevant, and D. Herbage**, *A differential scanning calorimetry analysis of the age-related changes in the thermal stability of rat skin collagen*. Biochim Biophys Acta, 1984. **791**(2): p. 205-11.

210. **Miles, C.A. and A.J. Bailey**, *Response to Engel and Bachinger's critique of collagen denaturation as a rate process*. Matrix Biol, 2001. **20**(4): p. 263-5.

211. **Engel, J. and H.P. Bachinger**, *Cooperative equilibrium transitions coupled with a slow annealing step explain the sharpness and hysteresis of collagen folding.* Matrix Biol, 2000. **19**(3): p. 235-44.

212. **Bachinger, H.P. and J. Engel**, *Thermodynamic vs. kinetic stability of collagen triple helice.* Matrix Biol, 2001. **20**(4): p. 267-9.

213. **Ward, I.**, *Mechanical properties of solid polymers.* 1985, New York: John-Wiley & Sons Ltd. 27-55.

214. **Brinkmann, R., N. Koop, G. Geerling, J. Kampmeier, S. Borcherding, K. Kamm, and R. Birngruber**, *Diode laser thermokeratoplasty: application strategy and dosimetry.* J Cataract Refract Surg, 1998. **24**(9): p. 1195-207.

215. **Miller, E.J.**, *Collagen Types: structure, distribution, and functions*, in *Collagen*, M. Nimni, Editor. 1988, Boca Raton: Florida. p. 139-156.

216. **Brodsky, B. and N.K. Shah**, *Protein motifs. 8. The triple-helix motif in proteins.* Faseb J, 1995. **9**(15): p. 1537-46.

217. **van der Rest, M. and R. Garrone**, *Collagen family of proteins.* Faseb J, 1991. **5**(13): p. 2814-23.

218. **Khor, E.**, *Methods for the treatment of collagenous tissues for bioprostheses.* Biomaterials, 1997. **18**(2): p. 95-105.

219. **Bear, R.S.**, *The structure of collagen fibrils*, in *Advances in protein chemsitry*, M.L. Anson, K. Baliey, and J. Edsall, Editors. 1952, Academic Press: New York. p. 69-160.

220. **Brown, P.C., B.R. Consden, and L.E. Glynn**, *Observations on the shrink temperature of collagen and its variations with age and disease.* Ann. Rheum. Dis., 1958. **17**: p. 196-208.

221. **Wiederhorn, N. and G. Reardon**, *Studies concerned with the structure of colagen. II Stress-strain behaviour of thermally contracted collagen.* J. Polym. Sci., 1952. **9**(4): p. 325-315.

222. **Verzar, F.**, *Differenzierung verschiedener crosslinks des kollagens.* Z. Physiol. Chem., 1963. **335**: p. 38-52.

223. **Cheung, D.T., N. Perelman, E.C. Ko, and M.E. Nimni**, *Mechanism of crosslinking of proteins by glutaraldehyde III. Reaction with collagen in tissues.* Connect Tissue Res, 1985. **13**(2): p. 109-15.

224. **Carslaw, H.S. and J.C. Jaeger**, *Conduction of heat in solids*. 2nd ed. 1959, Oxford: Clarendon Press. viii, 510.

225. **Choi, B. and A.J. Welch**, *Analysis of thermal relaxation during laser irradiation of tissue*. Lasers Surg Med, 2001. **29**(4): p. 351-9.

226. **Lillie, M.A. and J.M. Gosline**, *The effects of hydration on the dynamic mechanical properties of elastin*. Biopolymers, 1990. **29**(8-9): p. 1147-60.

227. **Sasaki, N. and A. Enyo**, *Viscoelastic properties of bone as a function of water content*. J Biomech, 1995. **28**(7): p. 809-15.

228. **Lee, J.M., D.R. Boughner, and D.W. Courtman**, *The glutaraldehyde-stabilized porcine aortic valve xenograft. II. Effect of fixation with or without pressure on the tensile viscoelastic properties of the leaflet material*. J Biomed Mater Res, 1984. **18**(1): p. 79-98.

229. **Duncan, A.C. and D. Boughner**, *Effect of dynamic glutaraldehyde fixation on the viscoelastic properties of bovine pericardial tissue*. Biomaterials, 1998. **19**(7-9): p. 777-83.

230. **Cohen, R.E., C.J. Hooley, and N.G. McCrum**, *Viscoelastic creep of collagenous tissue*. J Biomech, 1976. **9**(4): p. 175-84.

231. **Rupley, J.A. and G. Careri**, *Protein hydration and function*. Adv Protein Chem, 1991. **41**: p. 37-172.

232. **Elden, H.R.**, *Physical properties of collagen fibers*. Int Rev Connect Tissue Res, 1968. **4**: p. 283-348.

233. **Frank, C., D. Amiel, S.L. Woo, and W. Akeson**, *Normal ligament properties and ligament healing*. Clin Orthop, 1985(196): p. 15-25.

234. **Ferry, J.D.**, *Nature of viscoelastic behaviour*, in *Viscoelastic properties of polymers*. 1980, John Wiley & Sons: New York, Chichester, Brisbane, Toronto, Singapore. p. 1-33.

235. **Rabkin, S., D.G. Berghause, and H.F. Bauer**, *Mechanical properties of the isolated canine pericardium*. J Appl Physiol, 1974. **36**(1): p. 69-73.

236. **Lee, J.M. and D.R. Boughner**, *Tissue mechanics of canine pericardium in different test environments. Evidence for time-dependent accommodation, absence of plasticity, and new roles for collagen and elastin*. Circ Res, 1981. **49**(2): p. 533-44.

237. **Lee, J.M. and D.R. Boughner**, *Mechanical properties of human pericardium. Differences in viscoelastic response when compared with canine pericardium.* Circ Res, 1985. **57**(3): p. 475-81.

238. **Sanjeevi, R., N. Somanathan, and D. Ramaswamy**, *A viscoelastic model for collagen fibres.* J Biomech, 1982. **15**: p. 181-183.

239. **Viidik, A.**, *A rheological model for uncalcified parallel-fibred collagenous tissue.* J Biomech, 1968. **1**: p. 3-11.

240. **Silver, F.H., A. Ebrahimi, and P.B. Snowhill**, *Viscoelastic properties of self-assembled type I collagen fibers: molecular basis of elastic and viscous behaviors.* Connect Tissue Res, 2002. **43**(4): p. 569-80.

241. **Haut, R.C. and R.W. Little**, *A constitutive equation for collagen fibers.* J Biomech, 1972. **5**(5): p. 423-30.

242. **Haut, T.L. and R.C. Haut**, *The state of tissue hydration determines the strain-rate-sensitive stiffness of human patellar tendon.* J Biomech, 1997. **30**(1): p. 79-81.

243. **Rochdi, A., L. Foucat, and J.P. Renou**, *Effect of thermal denaturation on water-collagen interactions: NMR relaxation and differential scanning calorimetry analysis.* Biopolymers, 1999. **50**(7): p. 690-6.

244. **Ramachandran, G.N., M. Bansal, and R.S. Bhatnagar**, *A hypothesis on the role of hydroxyproline in stabilizing collagen structure.* Biochim Biophys Acta, 1973. **322**(1): p. 166-71.

245. **Jackson, D., S. Ayad, and G. Mechanic**, *Effect of heat on some collagen cross-links.* Biochem Biophys Acta, 1974. **336**: p. 100-107.

246. **Vangsness, C.T., Jr., W. Mitchell, 3rd, M. Nimni, M. Erlich, V. Saadat, and H. Schmotzer**, *Collagen shortening. An experimental approach with heat.* Clin Orthop, 1997(337): p. 267-71.

247. **Chahine, C.**, *Changes in hydrothermal stability of leather and parchment with deterioration: a DSC study.* Thermochimica Acta, 2000. **365**: p. 101-110.

248. **Robins, S.P.**, *Analysis of the crosslinking components in collagen and elastin.* Methods Biochem Anal, 1982. **28**: p. 329-79.

249. **Chimich, D., N. Shrive, C. Frank, L. Marchuk, and R. Bray**, *Water content alters viscoelastic behaviour of the normal adolescent rabbit medial collateral ligament.* J Biomech, 1992. **25**(8): p. 831-7.

250. **Galante, J.O.**, *Tensile properties of the human lumbar annulus fibrosus.* Acta Orthop Scand, 1967: p. Suppl 100:1-91.

251. **Armstrong, C.G. and V.C. Mow**, *Variations in the intrinsic mechanical properties of human articular cartilage with age, degeneration, and water content.* J Bone Joint Surg Am, 1982. **64**(1): p. 88-94.

252. **Elden, H.R.**, *Hydration of Connective Tissue and Tendon Elasticity.* Biochim Biophys Acta, 1964. **79**: p. 592-9.

253. **Thornton, G.M., N.G. Shrive, and C.B. Frank**, *Altering ligament water content affects ligament pre-stress and creep behaviour.* J Orthop Res, 2001. **19**(5): p. 845-51.

254. **Luescher, M., M. Ruegg, and P. Schindler**, *Effect of hydration upon the thermal stability of tropocollagen and its dependence on the presence of neutral salts.* Biopolymers, 1974. **13**(12): p. 2489-2503.

255. **Bailey, A.J.**, *Intermediate labile intermolecular crosslinks in collagen fibres.* Biochim Biophys Acta, 1968. **160**(3): p. 447-53.

256. **Bailey, A.J., C.M. Peach, and L.J. Fowler**, *Chemistry of the collagen cross-links. Isolation and characterization of two intermediate intermolecular cross-links in collagen.* Biochem J, 1970. **117**(5): p. 819-31.

257. **Lumry, R. and H. Eyring**, *Conformation changes of proteins.* J Phys Chem, 1954. **58**: p. 110-20.

258. **Elias, H. and L.J. Boyd**, *Notes on the anatomy, embryology, and histology of the pericardium. II.* N Y Med Coll News Notes, 1960. **2**: p. 50-75.

259. **Fentie, I.H., D.J. Allen, M.H. Schenck, and L.J. Didio**, *Comparative electron microscopic study of bovine, porcine and human parietal pericardium, as materials for cardiac valve bioprostheses.* J Submicrosc Cytol, 1986. **18**(1): p. 53-65.

260. **Fenoglio, J.J., Jr., P. Tuan Duc, A.L. Wit, A.L. Bassett, and B.M. Wagner**, *Canine mitral complex. Ultrastructure and electromechanical properties.* Circ Res, 1972. **31**(3): p. 417-30.

261. **Lee, Y.S., C.H. Chang, H.C. Chen, and G.F. Liang**, *Scanning and transmission electron microscopic studies on isolated ruptures of chordae tendineae.* Jpn Heart J, 1983. **24**(3): p. 355-67.

262. **Rasmussen, D.M., K.G. Wakim, and R.K. Winkelmann**, *Isotonic and Isometric Thermal Contraction of Human Dermis. ii. Age-Related Changes.* J Invest Dermatol, 1964. **43**: p. 341-8.

263. **Rasmussen, D.M., K.G. Wakim, and R.K. Winkelmann**, *Isotonic and Isometric Thermal Contraction of Human Dermis. i. Technic and Controlled Study.* J Invest Dermatol, 1964. **43**: p. 333-9.

264. **Na, G.C., L.J. Phillips, and E.I. Freire**, *In vitro collagen fibril assembly: thermodynamic studies.* Biochemistry, 1989. **28**(18): p. 7153-61.

265. **Woodroof, E.A.**, *Use of glutaraldehyde and formaldehyde to process tissue heart valves.* J Bioeng, 1978. **2**(1-2): p. 1-9.

266. **Kopp, J. and M. Bonnet**, *Stress-strain and isometric tension measurements in collagen*, in *Advances in Meat Research, collagen as food*, A.M. Pearson, T.R. Dutson, and A.J. Bailey, Editors. 1987, AVI: New York. p. 163-185.

267. **Jorge-Herrero, E., P. Fernandez, M. Gutierrez, and J.L. Castillo-Olivares**, *Study of the calcification of bovine pericardium: analysis of the implication of lipids and proteoglycans.* Biomaterials, 1991. **12**(7): p. 683-9.

268. **Brinkmann, R., B. Radt, C. Flamm, J. Kampmeier, N. Koop, and R. Birngruber**, *Influence of temperature and time on thermally induced forces in corneal collagen and the effect on laser thermokeratoplasty.* J Cataract Refract Surg, 2000. **26**(5): p. 744-54.

269. **Verzar, F. and I.Z. Nagy**, *Electronmicroscopic analysis of thermal collagen denaturation in rat tail tendons.* Gerontologia, 1970. **16**(2): p. 77-82.

270. **Andrews, J.R. and J.R. Dugas**, *Diagnosis and treatment of shoulder injuries in the throwing athlete: the role of thermal-assisted capsular shrinkage.* Instr Course Lect, 2001. **50**: p. 17-21.

271. **Manta, J.P., S. Organ, R.P. Nirschl, and F.A. Pettrone**, *Arthroscopic transglenoid suture capsulolabral repair. Five-year followup.* Am J Sports Med, 1997. **25**(5): p. 614-8.

272. **Haly, A.R. and J.W. Snaith**, *Calorimetry of rat tail tendon collagen before and after denaturation: the heat of fusion of its absorbed water.* Biopolymers, 1971. **10**(9): p. 1681-99.

273. **Tatham, A.S. and P.R. Shewry**, *Elastomeric proteins: biological roles, structures and mechanisms.* Trends Biochem Sci, 2000. **25**(11): p. 567-71.

274. **Tatham, A.S. and P.R. Shewry**, *Comparative structures and properties of elastic proteins*. Philos Trans R Soc Lond B Biol Sci, 2002. **357**(1418): p. 229-34.

275. **Gosline, J., M. Lillie, E. Carrington, P. Guerette, C. Ortlepp, and K. Savage**, *Elastic proteins: biological roles and mechanical properties*. Philos Trans R Soc Lond B Biol Sci, 2002. **357**(1418): p. 121-32.

276. **Flory, P.J.**, *Princinple of Polymer Chemistry*. 1953, Ithaca, New York: Cornell University Press.

277. **Verzar, F.**, *Das altern des kollagens*. Helv. Phsiol. Acta, 1956. **14**: p. 207-221.

278. **Kuehn, K., J. Engel, B. Zimmermann, and W. Grassmann**, *Renaturation of Soluble Collagen. 3. Reorganization of Native Collagen Molecules from Completely Separated Units*. Arch Biochem Biophys, 1964. **105**: p. 387-403.

279. **Brandts, J.F.**, *Conformational transitions of proteins in water and in aqueous mixtures*, in *Structure and stability of biological macromolecule*. 1969, Marcel Dekker: New York.

280. **Kuehn, K. and B.K. Zimmermann**, *Renaturation of Soluble Collagen. Iv. Regeneration of Native Collagen Molecules from Alpha-Subunits*. Arch Biochem Biophys, 1965. **109**: p. 534-41.

281. **Rauterberg, J. and K. Kuhn**, *The renaturation behaviour of modified collagen molecules*. Hoppe Seylers Z Physiol Chem, 1968. **349**(5): p. 611-22.

282. **Wu, H.**, *Studies on denaturation of proteins XIII. A theory of denaturation*. Advances in Protein Chemistry, 1995. **46**: p. 6-28.

283. **Mark, J.**, *Some aspects of rubberlike elasticity useful in teaching basic concepts in physical chemistry*. Journal of Chemical Education, 2002. **79**(12): p. 1437.

284. **Gosline, J.**, *The elastic properties of rubber like proteins and highly extensible tissues*. Symp Soc Exp Biol, 1980. **34**: p. 331-357.

285. **Nimni, M., D. Cheung, B. States, M. Kodama, and K. Sheikh**, *Bioprosthesis derived from cross-linked and chemically modified collagenous tissues.*, in *Collagen*, M.E. Nimni, Editor. 1988, Boca Raton: Florida. p. 1-38.

286. **von Hippel, P.**, *Structure and stabilization of the collagen molecule in solution*, in *Treatise on collagen*, G.N. Ramachandran, Editor. 1967, Academic Press.: London, New York,. p. 253.

287. **Tanford, C.**, *Protein denaturation*. Adv Protein Chem, 1968. **23**: p. 121-282.

288. **Klibanov, A.M.**, *Approaches to enzyme stabilization.* Biochem Soc Trans, 1983. **11**(1): p. 19-20.

289. **Price, N.C. and R.A. Dwek**, *Principles and problems in physical chemistry for biochemists.* 1974, Oxford: Clarendon Press.

290. **Sung, H.W., Y. Chang, C.T. Chiu, C.N. Chen, and H.C. Liang**, *Crosslinking characteristics and mechanical properties of a bovine pericardium fixed with a naturally occurring crosslinking agent.* J Biomed Mater Res, 1999. **47**(2): p. 116-26.

291. **Finch, A. and D.A. Ledward**, *Differential scanning calorimetric study of collagen fibres swollen in aqueous neutral salt solutions.* Biochim Biophys Acta, 1973. **295**(1): p. 296-300.

292. **Russell, A.E. and D.R. Cooper**, *Structural and functional factors in the hydrogen bonding of polar organic solvents to acid-soluble collagen. Effect on renaturation kinetics and thermal stability.* Biochemistry, 1969. **8**(10): p. 3980-90.

293. **Brown, E.M., H.M. Farrell, Jr., and R.J. Wildermuth**, *Influence of neutral salts on the hydrothermal stability of acid- soluble collagen.* J Protein Chem, 2000. **19**(2): p. 85-92.

294. **Zanaboni, G., A. Rossi, A.M. Onana, and R. Tenni**, *Stability and networks of hydrogen bonds of the collagen triple helical structure: influence of pH and chaotropic nature of three anions.* Matrix Biol, 2000. **19**(6): p. 511-20.

295. **Von Hippel, P.H. and K.Y. Wong**, *The effect of ions on the kinetics of formation and the stability of the collagenfold.* Biochemistry, 1962. **1**: p. 664-74.

296. **Fung, B.M. and S.C. Wei**, *The effect of alkali and alkaline earth salts on the structure of hydrated collagen fibers as studied by deuterim NMR.* Biopolymers, 1973. **12**(5): p. 1052-62.

297. **Ciferri, A., L.V. Rajagh, and D. Puett**, *Interaction between proteins and salt solutions. 3. Effect of salt type and concentration on the shrinkage temperature.* Biopolymers, 1965. **3**(4): p. 461-80.

298. **Wright, N.T., S.S. Chen, and J.D. Humphrey**, *Time-temperature equivalence of heat-induced changes in cells and proteins.* J Biomech Eng, 1998. **120**(1): p. 22-6.

299. **Miller, M., Scheraga, HA.,**, *Calculation of the structures of collagen models. Role of interchain interactions in determining the triple-helical coiled-coil conformation. I. Poly (Glycyl-Prolyl-Prolyl).* J of Poly Sci, 1976. **54**: p. 171-200.

300. **Traub, W. and P.P. Fietzek**, *Contribution of the alpha2 chain to the molecular stability of collagen.* FEBS Lett, 1976. **68**(2): p. 245-9.

301. **Nemethy, G. and H.A. Scheraga**, *Free energy of hydration of collagen models and the enthalpy of the transition between the triple-helical coiled-coil and single-stranded conformations.* Biopolymers, 1989. **28**(9): p. 1573-84.

302. **Venugopal, M.G., J.A. Ramshaw, E. Braswell, D. Zhu, and B. Brodsky**, *Electrostatic interactions in collagen-like triple-helical peptides.* Biochemistry, 1994. **33**(25): p. 7948-56.

303. **Russell, A.E.**, *Effect of alcohols and neutral salt on the thermal stability of soluble and precipitated acid-soluble collagen.* Biochem J, 1973. **131**(2): p. 335-42.

304. **Gekko, K. and S. Koga**, *Increased thermal stability of collagen in the presence of sugars and polyols.* J Biochem (Tokyo), 1983. **94**(1): p. 199-205.

305. **Komsa-Penkova, R., R. Koynova, G. Kostov, and B. Tenchov**, *Discrete reduction of type I collagen thermal stability upon oxidation.* Biophys Chem, 2000. **83**(3): p. 185-95.

306. **Von Hippel, P.H. and T. Schleich**, *The efects of neutral salts on the structure and conformational stability of macromolecules in solution*, in *Structure and stability of biological macromolecules*, S.N. Timasheff and G.D. Fasman, Editors. 1969, Dekker: New York,. p. 417-574.

307. **Von Hippel, P.H. and K.Y. Wong**, *The collagen-gelatin phase transition. 1. Further studies of the effects of solvent environment and polypeptide chain composition.* Biochemistry, 1963. **2**: p. 1387-1398.

308. **Fietzek, P.P. and K. Kuhn**, *The primary structure of collagen.* Int Rev Connect Tissue Res, 1976. **7**: p. 1-60.

309. **Bella, J., M. Eaton, B. Brodsky, and H.M. Berman**, *Crystal and molecular structure of a collagen-like peptide at 1.9 A resolution.* Science, 1994. **266**(5182): p. 75-81.

310. **Collins, K.D. and M.W. Washabaugh**, *The Hofmeister effect and the behaviour of water at interfaces.* Q Rev Biophys, 1985. **18**(4): p. 323-422.

311. **Stryer, L.**, *Biochemistry.* 3rd ed. 1988, New York, N.Y.: W.H. Freeman. xxxii, 1089.

312. **Chang, E.P. and J.C. Chien**, *The effect of ions on the superstructures of reconstituted collagen.* Biopolymers, 1973. **12**(5): p. 1063-9.

313. **Sacks, M.S. and C.J. Chuong**, *Characterization of collagen fiber architecture in the canine diaphragmatic central tendon.* J Biomech Eng, 1992. **114**(2): p. 183-90.

314. **Sacks, M.S. and D.B. Smith**, *Effects of accelerated testing on porcine bioprosthetic heart valve fiber architecture.* Biomaterials, 1998. **19**(11-12): p. 1027-36.

315. **Burjanadze, T.V. and E.L. Kisiriya**, *Dependence of thermal stability on the number of hydrogen bonds in water-bridged collagen structure.* Biopolymers, 1982. **21**(9): p. 1695-701.

316. **Speer, D.P., M. Chvapil, C.D. Eskelson, and J. Ulreich**, *Biological effects of residual glutaraldehyde in glutaraldehyde-tanned collagen biomaterials.* J Biomed Mater Res, 1980. **14**(6): p. 753-64.

317. **Heidemann, E.**, *The chemistry of tanning*, in *Collagen*, M.E. Nimni, Editor. 1988, Boca Raton: Florida. p. 40-60.

318. **Heingard, D. and M. Paulsson**, *Structure and Metabolism of Proteoglycans*, in *Extracellular Matrix Biochemistry*, K.A. Piez and A. Reddi, Editors. 1984, Elsevier: New York. p. 278-328.

319. **Mathews, M.B.**, *The interaction of collagen and acid mucopolysaccharides. A model for connective tissue.* Biochem J, 1965. **96**(3): p. 710-6.

320. **Steven, F.S., J. Knott, D.S. Jackson, and V. Podrazky**, *Collagen-protein-polysaccharide interactions in human intervertebral disc.* Biochim Biophys Acta, 1969. **188**(2): p. 307-13.

321. **Podrazky, V., F.S. Steven, D.S. Jackson, J.B. Weiss, and S.J. Leibovich**, *Interaction of tropocollagen with protein-polysaccharide complexes. An analysis of the ionic groups responsible for interaction.* Biochim Biophys Acta, 1971. **229**(3): p. 690-7.

322. **Obrink, B. and A. Wasteson**, *Nature of the interaction of chondroitin 4-sulphate and chondroitin sulphate-proteoglycan with collagen.* Biochem J, 1971. **121**(2): p. 227-33.

323. **Obrink, B.**, *A study of the interactions between monomeric tropocollagen and glycosaminoglycans.* Eur J Biochem, 1973. **33**(2): p. 387-400.

324. **Anderson, J.**, *Biochemical basis of connective tissue disease*, in *Pathological basis of the connective tissue diseases*, D. Gardner, Editor. 1992, Edward Arnold: London, Melbourne. p. 173-226.

325. **Simionescu, D.T., J.J. Lovekamp, and N.R. Vyavahare**, *Glycosaminoglycan-degrading enzymes in porcine aortic heart valves: implications for bioprosthetic heart valve degeneration.* J Heart Valve Dis, 2003. **12**(2): p. 217-25.

326. **Pieper, J.S., T. Hafmans, J.H. Veerkamp, and T.H. van Kuppevelt**, *Development of tailor-made collagen-glycosaminoglycan matrices: EDC/NHS crosslinking, and ultrastructural aspects.* Biomaterials, 2000. **21**(6): p. 581-93.

327. **Pieper, J.S., A. Oosterhof, P.J. Dijkstra, J.H. Veerkamp, and T.H. van Kuppevelt**, *Preparation and characterization of porous crosslinked collagenous matrices containing bioavailable chondroitin sulphate.* Biomaterials, 1999. **20**(9): p. 847-58.

328. **Dorrington, K.L. and N.G. McCrum**, *Elastin as a rubber.* Biopolymers, 1977. **16**(6): p. 1201-22.

329. **Hoeve, C. and P. Flory**, *The elastic properties of elastin.* Journal of Applied Physics, 1958. **80**: p. 6523-6526.

330. **Association, A.H.**, *Heart and stroke statistical update.* 2001.

331. **Mann, B.K. and J.L. West**, *Tissue engineering in the cardiovascular system: progress toward a tissue engineered heart.* Anat Rec, 2001. **263**(4): p. 367-71.

332. **Langer, R. and J.P. Vacanti**, *Tissue engineering.* Science, 1993. **260**(5110): p. 920-6.

333. **Sodian, R., S.P. Hoerstrup, J.S. Sperling, S.H. Daebritz, D.P. Martin, F.J. Schoen, J.P. Vacanti, and J.E. Mayer, Jr.**, *Tissue engineering of heart valves: in vitro experiences.* Ann Thorac Surg, 2000. **70**(1): p. 140-4.

334. **Akins, R. and M. Sefton**, *Tissue engineering the human heart.* New Surg., 2001. **1**: p. 26-32.

335. **Sefton, M.V.**, *Functional considerations in tissue-engineering whole organs.* Ann N Y Acad Sci, 2002. **961**: p. 198-200.

336. **Kunzelman, K.S., R.P. Cochran, S.S. Murphree, W.S. Ring, E.D. Verrier, and R.C. Eberhart**, *Differential collagen distribution in the mitral valve and its influence on biomechanical behaviour.* J Heart Valve Dis, 1993. **2**(2): p. 236-44.

337. **Mori, Y., R.I. Bashey, and A. Angrist**, *The in vitro biosynthesis of collagen in bovine heart valves*. Biochem. Med., 1967. **1**: p. 295.

338. **Bashey, R.**, *Collagen in heart valves*, in *Collagen*, M. Nimni, Editor. 1988, CRC: Boca Raton, FL. p. 257-274.

339. **Streuli, C.**, *Extracellular matrix remodelling and cellular differentiation*. Curr Opin Cell Biol, 1999. **11**(5): p. 634-40.

340. **Mann, B.K., R.H. Schmedlen, and J.L. West**, *Tethered-TGF-beta increases extracellular matrix production of vascular smooth muscle cells*. Biomaterials, 2001. **22**(5): p. 439-44.

341. **Hayashi, K.**, *Biomechanical studies of the remodeling of knee joint tendons and ligaments*. J Biomech, 1996. **29**(6): p. 707-16.

342. **Hoerstrup, S.P., R. Sodian, S. Daebritz, J. Wang, E.A. Bacha, D.P. Martin, A.M. Moran, K.J. Guleserian, J.S. Sperling, S. Kaushal, J.P. Vacanti, F.J. Schoen, and J.E. Mayer, Jr.**, *Functional living trileaflet heart valves grown in vitro*. Circulation, 2000. **102**(19 Suppl 3): p. III44-9.

343. **Buschmann, M.D., Y.A. Gluzband, A.J. Grodzinsky, and E.B. Hunziker**, *Mechanical compression modulates matrix biosynthesis in chondrocyte/agarose culture*. J Cell Sci, 1995. **108 (Pt 4)**: p. 1497-508.

344. **Laurent, G.J.**, *Rates of collagen synthesis in lung, skin and muscle obtained in vivo by a simplified method using [3H]proline*. Biochem J, 1982. **206**(3): p. 535-44.

345. **Turner, J.E., M.H. Oliver, D. Guerreiro, and G.J. Laurent**, *Collagen metabolism during right ventricular hypertrophy following induced lung injury*. Am J Physiol, 1986. **251**(5 Pt 2): p. H915-9.

346. **Kunzelman, K.S., D.W. Quick, and R.P. Cochran**, *Altered collagen concentration in mitral valve leaflets: biochemical and finite element analysis*. Ann Thorac Surg, 1998. **66**(6 Suppl): p. S198-205.

347. **Bailey, A.J. and S.P. Robins**, *Embryonic skin collagen. Replacement of the type of aldimine crosslinks during the early growth period*. FEBS Lett, 1972. **21**(3): p. 330-334.

348. **Robins, S.P. and A.J. Bailey**, *Relative stabilities of the intermediate reducible crosslinks present in collagen fibres*. FEBS Lett, 1973. **33**(2): p. 167-74.

349. **Barber, J.E., N. Ratliff, and I. Vesely**, *Mechanics of explanted bioprosthetic heart valves*. Biomed Sci Instrum, 1999. **35**: p. 29-32.

350. **Langdon, S.E., R. Chernecky, C.A. Pereira, D. Abdulla, and J.M. Lee**, *Biaxial mechanical/structural effects of equibiaxial strain during crosslinking of bovine pericardial xenograft materials.* Biomaterials, 1999. **20**(2): p. 137-53.

351. **Lloyd, D.J. and M. Garrod**, *A contribution to the theory of the structure of protein fibres with special reference to the so-called thermal shrinkage of the collagen fibre.* Trans. Faraday. Soc., 1948. **44**: p. 441-451.

352. **Cohen-Solal, L., M. Le Lous, J.C. Allain, and F. Meunier**, *Absence of maturation of collagen crosslinks in fish skin?* FEBS Lett, 1981. **123**(2): p. 282-4.

353. **Bailey, A.J., S.P. Robins, and G. Balian**, *Biological significance of the intermolecular crosslinks of collagen.* Nature, 1974. **251**(5471): p. 105-9.

354. **Lim, K.O., D.R. Boughner, and D.G. Perkins**, *Ultrastructure and mechanical properties of chordae tendineae from a myxomatous tricuspid valve.* Jpn Heart J, 1983. **24**(4): p. 539-48.

355. **Lim, K.O. and D.R. Boughner**, *Mechanical properties of human mitral valve chordae tendineae: variation with size and strain rate.* Can J Physiol Pharmacol, 1975. **53**(3): p. 330-9.

356. **Dorrington, K.L.**, *The theory of viscoelasticity in biomaterials.* The Mechanical Properties of Biological Materials, ed. J.F.V. Vincent and J.D. Currey. 1980: Cambridge University Press. 289-314.

357. **Fratzl, P., K. Misof, I. Zizak, G. Rapp, H. Amenitsch, and S. Bernstorff**, *Fibrillar structure and mechanical properties of collagen.* J Struct Biol, 1998. **122**(1-2): p. 119-22.

358. **Clark, R.E.**, *Stress-strain characteristics of fresh and frozen human aortic and mitral leaflets and chordae tendineae. Implications for clinical use.* J Thorac Cardiovasc Surg, 1973. **66**(2): p. 202-8.

359. **Harrington, W.F. and P.H. Von Hippel**, *Formation and stabilization of the collagen-fold.* Arch Biochem Biophys, 1961. **92**: p. 100-13.

Appendix 1: Seeding and Multiexponential Analysis

A1.1 Selection of Appropriate Multi-Exponential Models

One of the most fundamental aspects of this Ph.D. project was to ensure that all the nonlinear normalized load-time data, belonging to all tissues and treatments, would be well-fitted with an appropriate Levenberg-Marquardt algorithm, a nonlinear least-squares method. Various exponential (i.e. single-, double-, triple-and quadruple-) models were applied to the data from the DHIT tests. It was eventually determined that a triple exponential model provided the best fit to the data from pericardium, mitral and tricuspid chordae tendineae as well as mitral and tricuspid valves. The curve-fitting procedure was conducted using the DeltaGraph Version 5 (SPSS Inc), performing a maximum of 30 iterations. Upon completion of this procedure a regression coefficient (r^2) was calculated. The decision on whether or not to accept or discard a particular exponential model was based on the r^2 parameter and assessment of the residuals. Figures A1.1-A1.4 exhibits some typical curve fitting graphs using various exponential models, along with the corresponding regression coefficients.

Alternatively, to further ensure the appropriateness of the fits provided by the exponential models used to characterize our load decay data, different plots of normalized load versus the logarithm of time were plotted. The results were curves with three distinct slopes (Figures A1.5- A1.8). However, only those data fitted with the 3-exponential model provided the best fit to the data (Figure A1.7). In fact, while the 1-, 2- and 4-exponentials provided an inadequate fit, the 4-exponaential yielded coefficients with negative values, possibly due to over-specification of the parameters (i.e. 8 parameters being used). Finally, the three transitional slopes, further validated the earlier suggestion that rapid thermal denaturation of collagen maybe viewed as a three-step phenomenon and confirmed the appropriateness of the triple exponential function to fit the data.

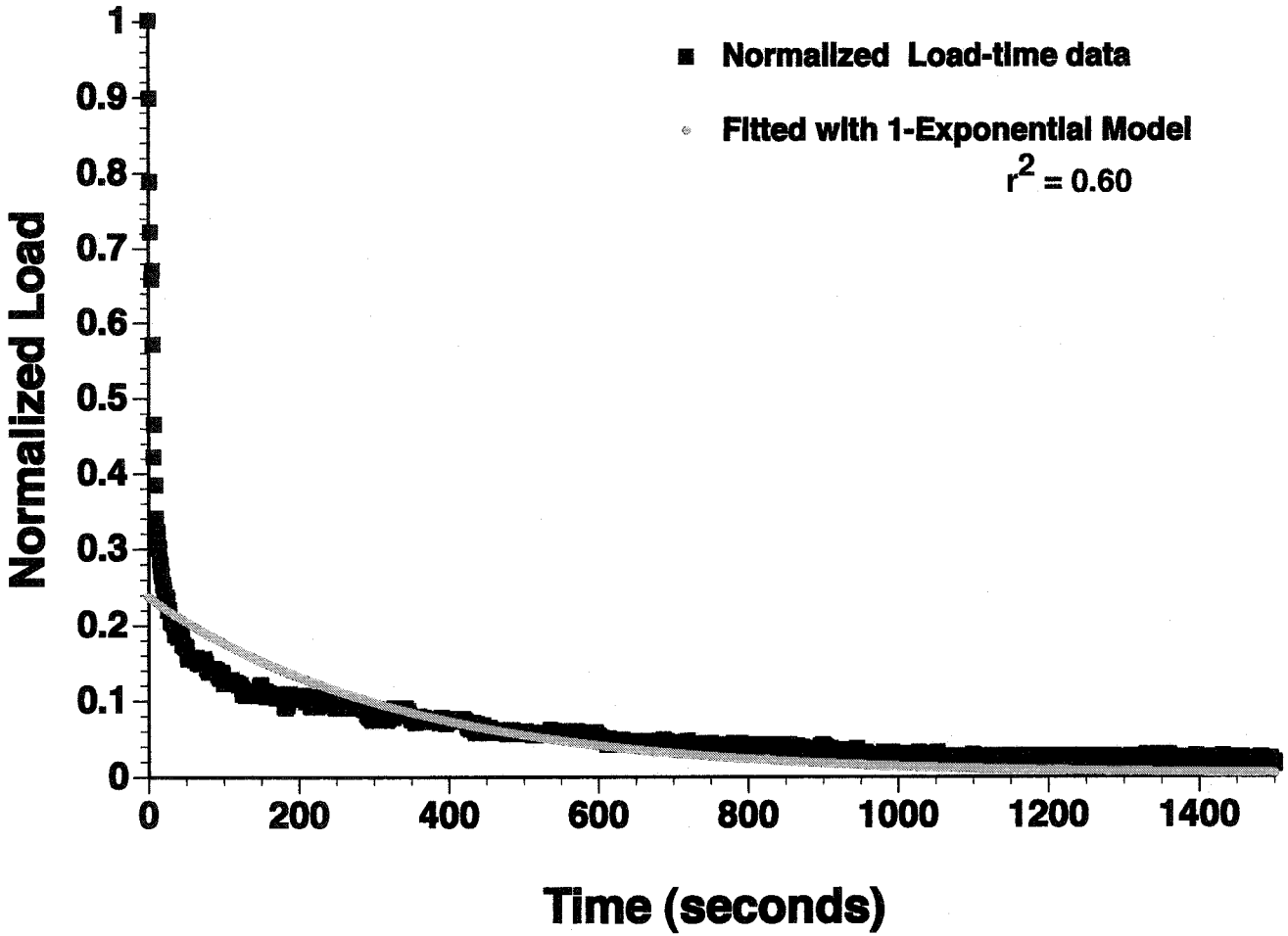

Figure A.1.1 Normalized load-time data fitted with 1-exponential model

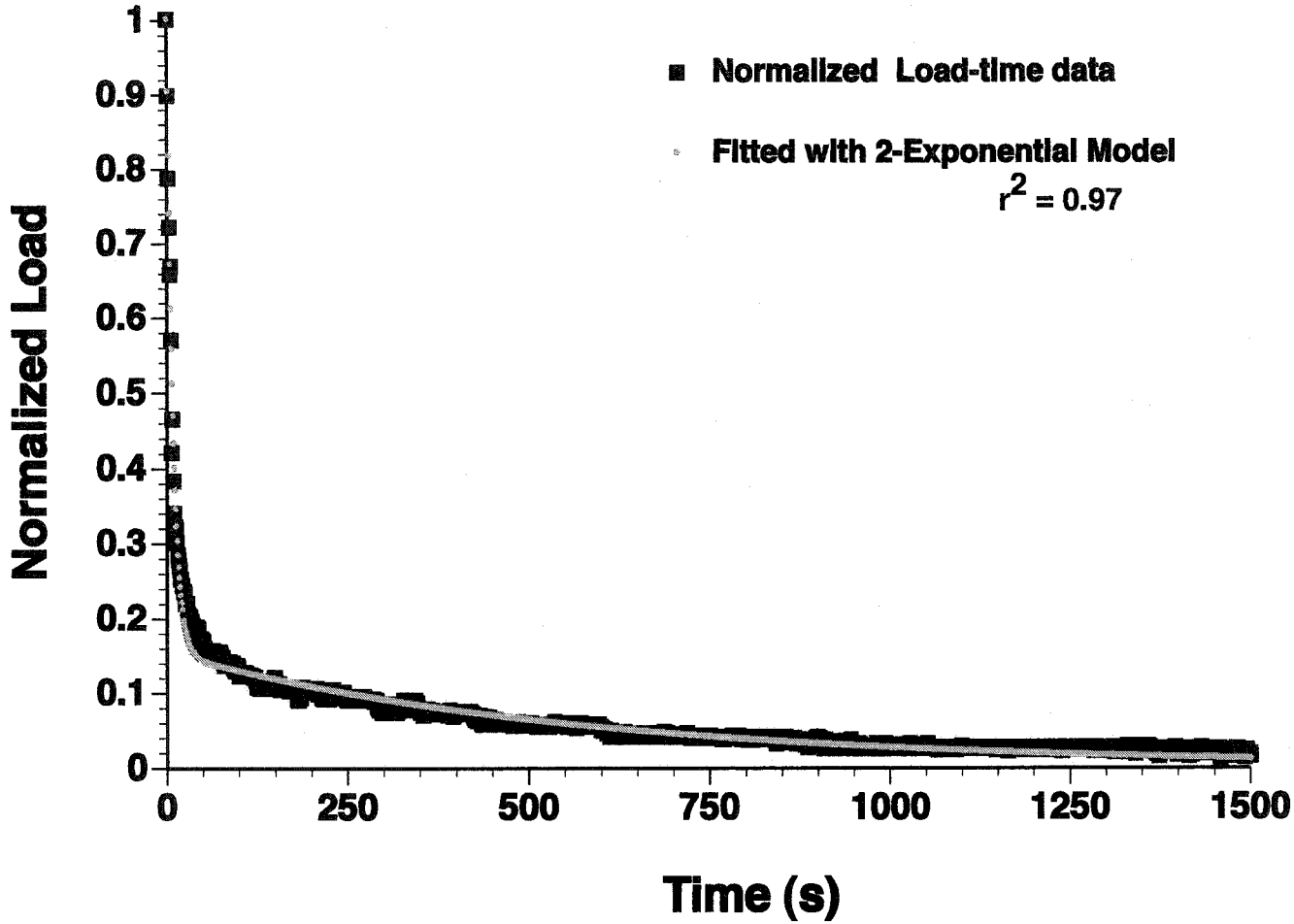

Figure A.1.2 Normalized load-time data fitted with 2-exponential model

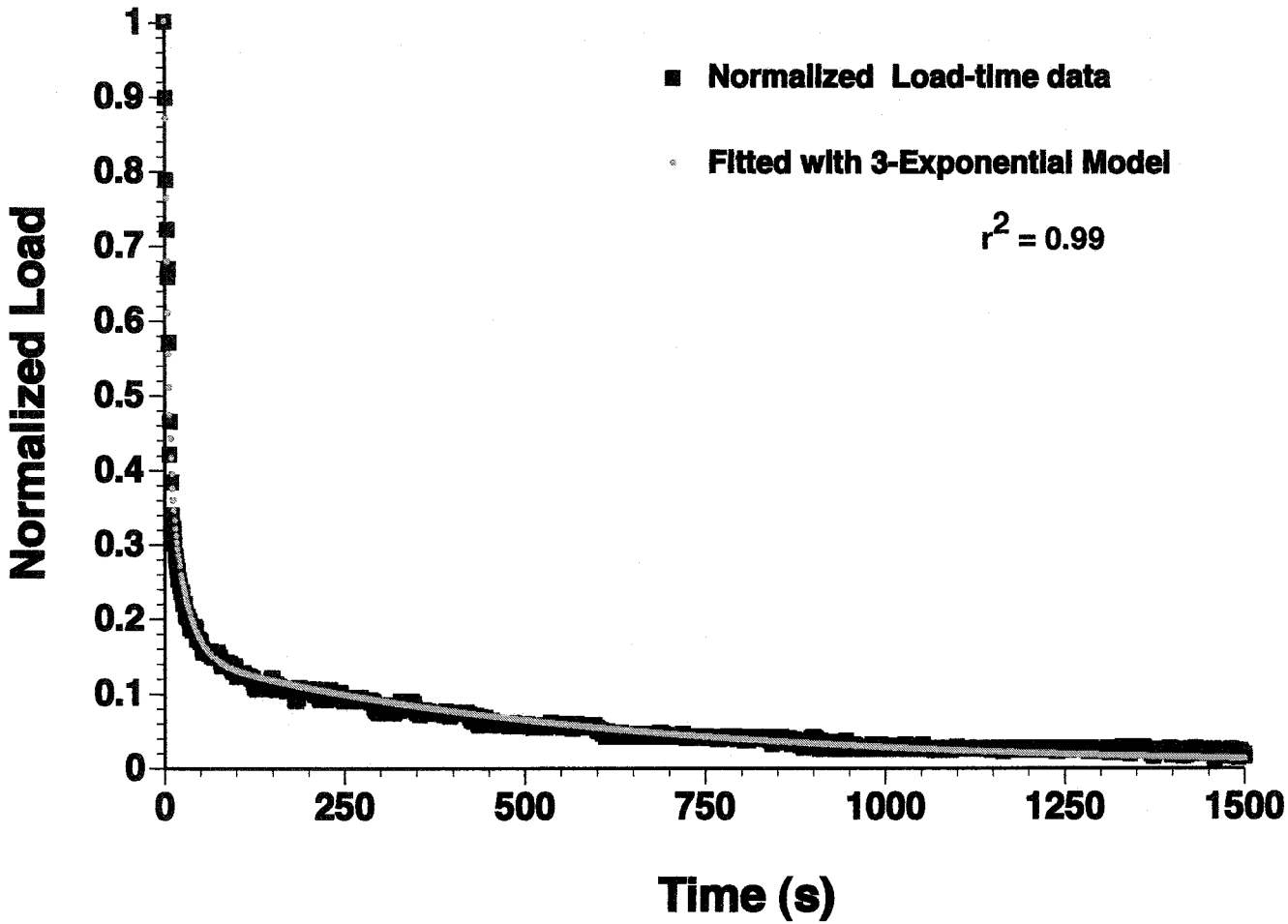

Figure A.1.3 Normalized load-time data fitted with 3-exponential model

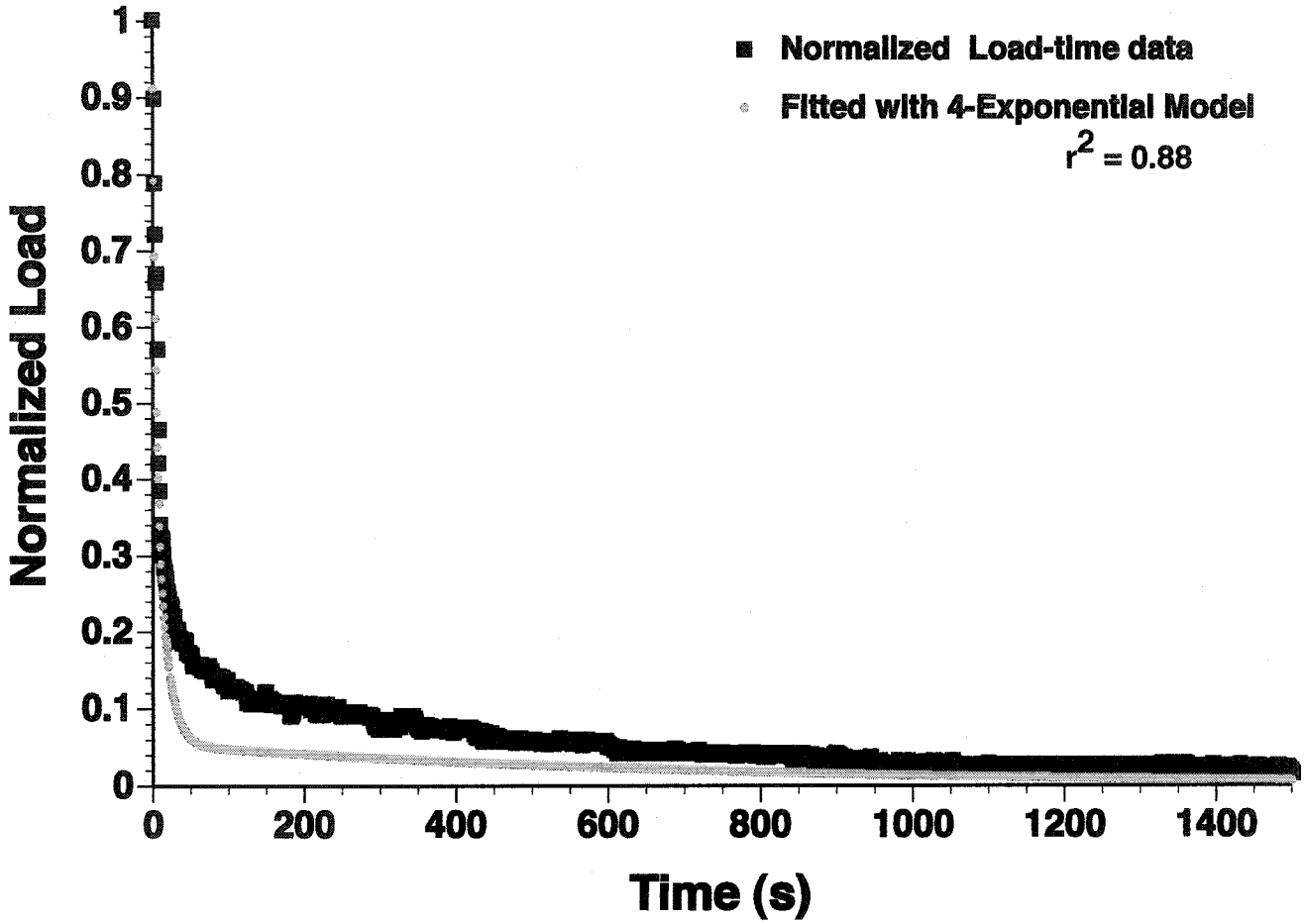

Figure A.1.4 Normalized load-time data fitted with 4-exponential model

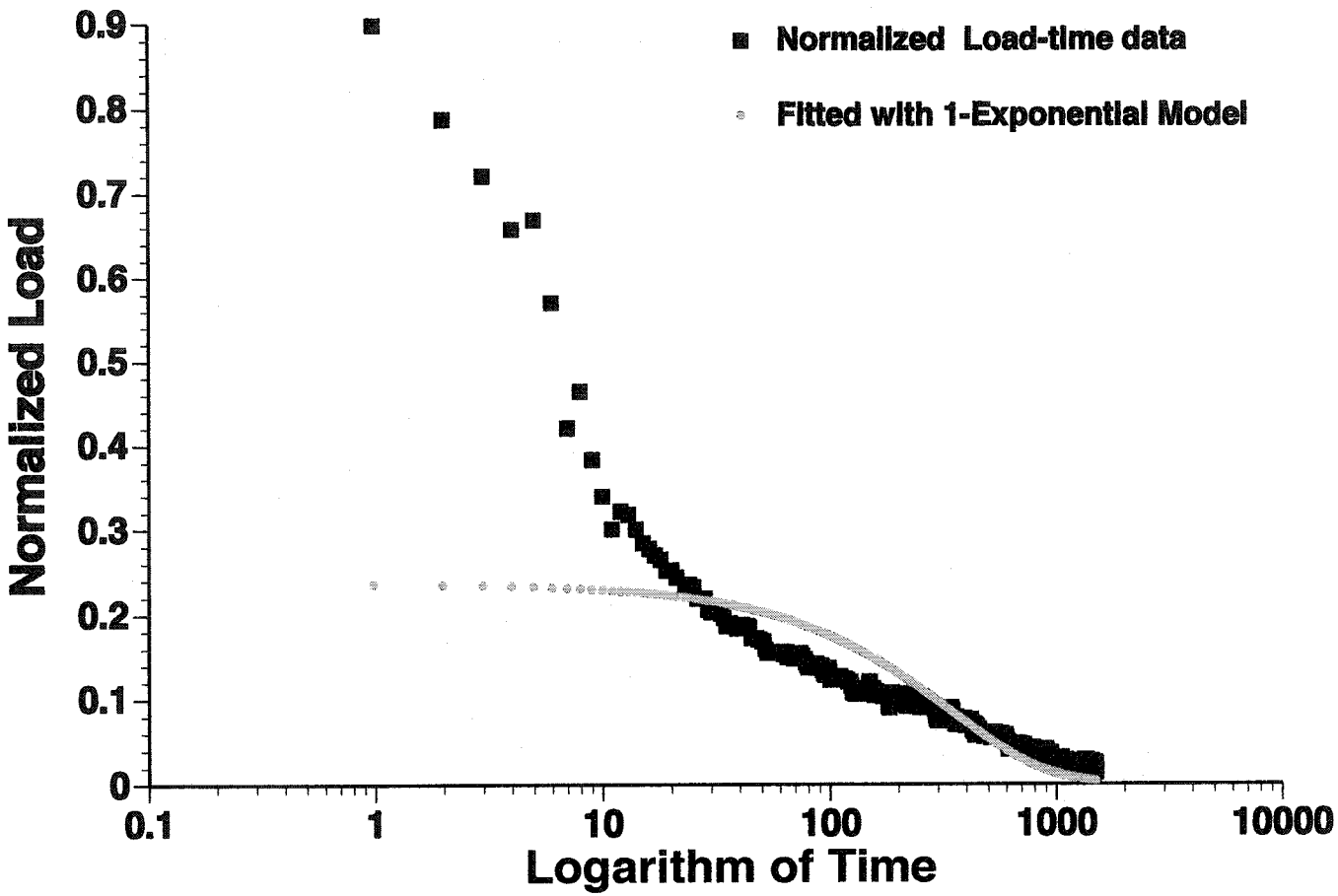

Figure A.1.5 Plot of Normalized load versus logarithm of time, and the inappropriateness of the 1-exponential model to fit the data.

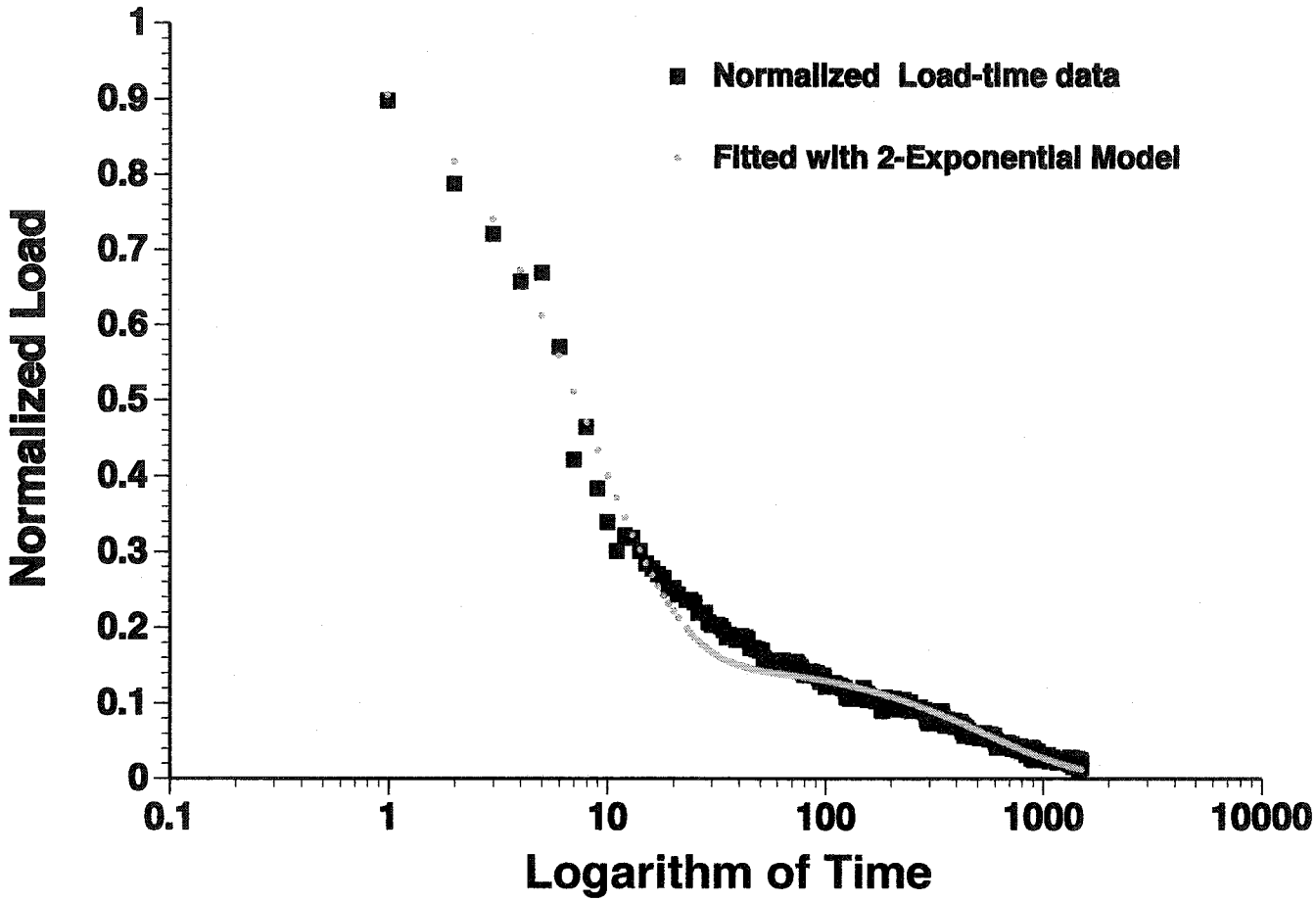

Figure A.1.6 Plot of Normalized load versus logarithm of time, and relatively well-fitted 2-exponential model used to fit the data.

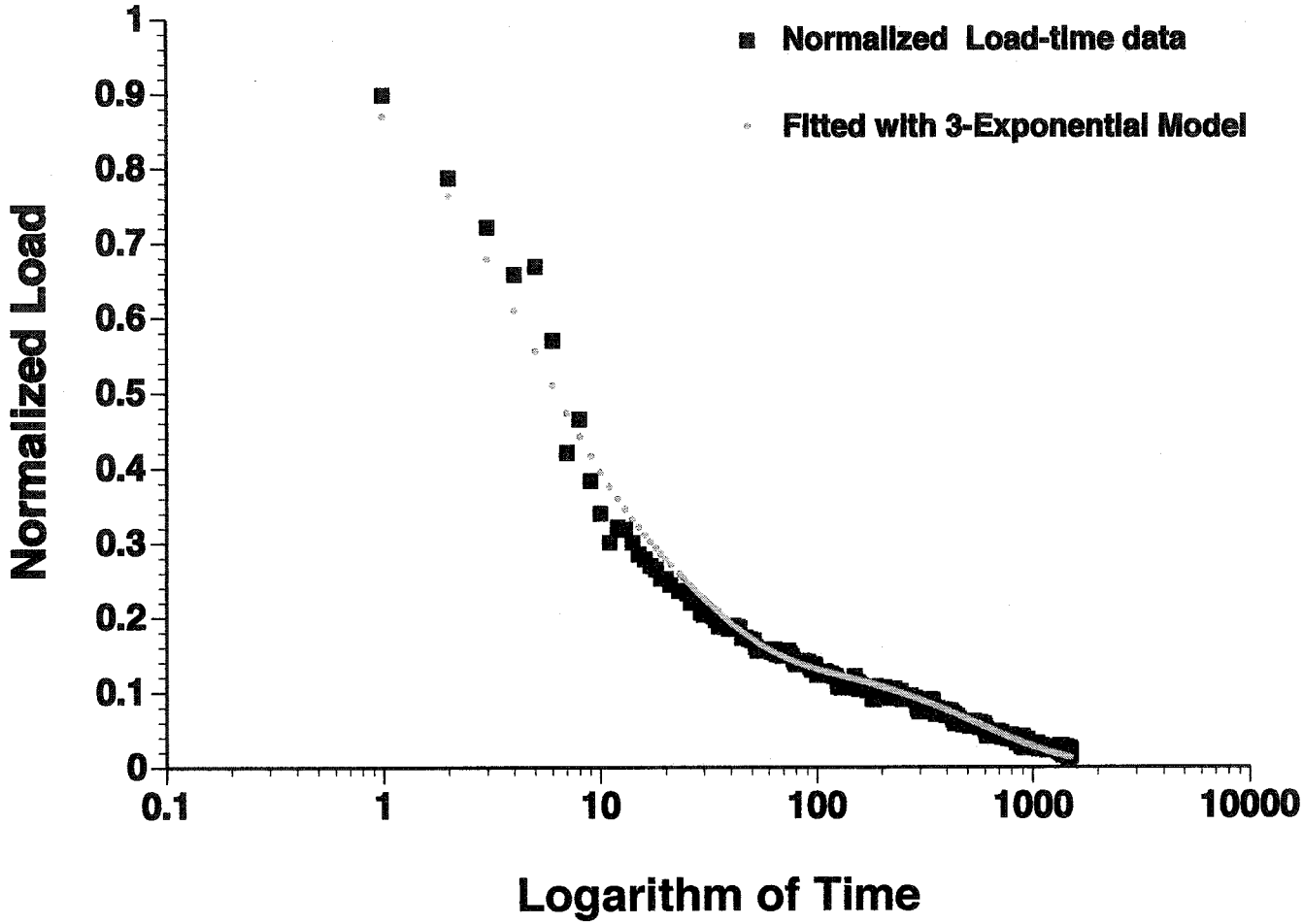

Figure A.1.7 Plot of Normalized load versus logarithm of time. The 3-exponential model provided the fit to the data.

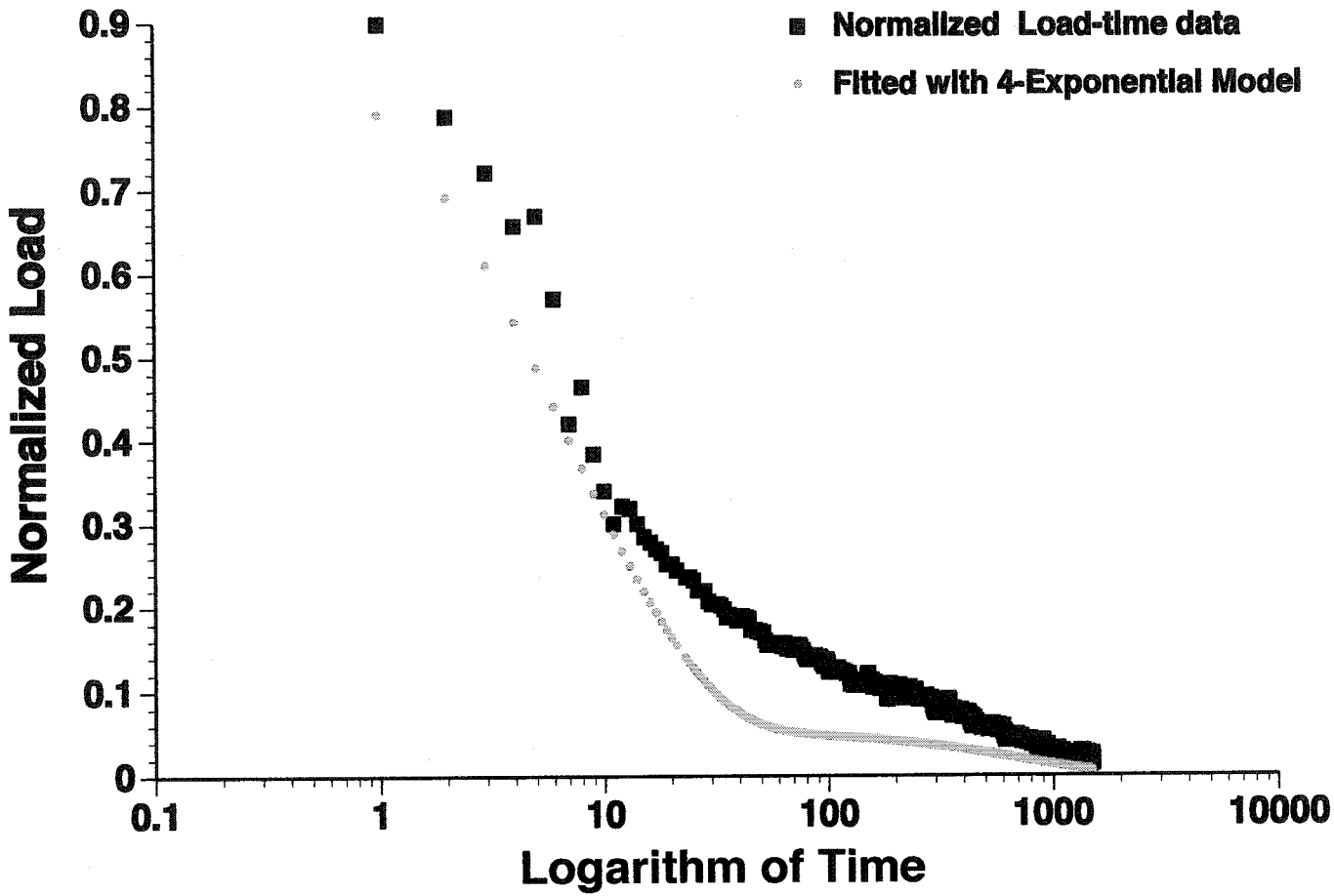

Figure A.1.8 Plot of Normalized load versus logarithm of time, and the inappropriateness of the 4-exponential model to fit the data.

A1.2 Optimization of Curve Fitting: Data Seeding

Once the triple-exponential model was chosen to fit the data, its robustness and the uniqueness of the fit was established using wide variations in the seeds supplied to the nonlinear least-squares routine. The seeding analyses were conducted firstly by providing a series of near-random values to each parameter (C_1, τ_1, C_2, τ_2, C_3, and τ_3) of the triple exponential function, with the Levant-Marquardt algorithm fitting the data. As shown in Table A1.1, the final triple exponential parameters, as calculated by the Levant-Marquardt algorithm, were shown to be relatively constant despite wide variation in the initial input values. The result of this analysis revealed that τ_1 was the most stable time constant, followed by τ_2 and finally τ_3. The stability of each τ_i parameter depended on its relative C_i value: i.e. the larger C_i, the narrower the range of τ_i values outputted from various seeds.

It is, however, acknowledged that there maybe more than one (non-unique) set of parameters that may be used to fit our data within the constraints given to the non-linear least squares routine. However, to maintain a certain level of uniformity and consistency in our approach, and after repeated and exhaustive trials with various combinations of the seed values, all the data presented in this thesis were fitted with the first solution set of parameters yielded from a single set of seeds (C_1 = 5.0E-1, τ_1^{-1} = 3.0E-2, C_2 = 3.5E-1, τ_2^{-1} = 8.8E-4, C_3 = 1.5E-1, τ_3^{-1} = 5.0E-3). In almost all cases, this particular set of numbers generated a near-perfect fit with an acceptable regression coefficient (r^2).

	Input Parameters						Calculated Parameters					
Trial	C_1	τ_1	C_2	τ_2	C_3	τ_3	C_1	τ_1	C_2	τ_2	C_3	τ_3
1	8.0 E-1	3.0 E-2	1.0 E-2	1.0 E-3	1.0 E-1	1.0 E-4	8.3 E-1	3.1 E-1	1.1 E-1	1.5 E-2	6.0 E-2	9.4 E-4
2	8.0 E-1	6.0 E-2	1.0 E-2	2.0 E-3	1.0 E-1	2.0 E-4	9.0 E-1	3.3 E-1	9.2 E-2	4.7 E-2	8.3 E-3	2.9 E-3
3	4.0 E-1	1.0 E-2	3.0 E-2	1.0 E-3	3.0 E-1	1.0 E-4	8.5 E-1	3.0 E-1	1.1 E-1	1.1 E-2	4.0 E-2	6.6 E-4
4	6.0 E-1	3.0 E-2	2.0 E-2	5.0 E-3	2.0 E-1	8.0 E-3	8.2 E-1	2.9 E-1	1.2 E-1	2.4 E-2	6.0 E-2	1.1 E-3
5	5.0 E-1	8.0 E-2	4.0 E-2	5.0 E-3	1.0 E-1	8.0 E-3	8.5 E-1	2.9 E-1	1.0 E-1	1.2 E-1	5.0 E-2	1.3 E-3

Table A1.1 A Sample seeding analysis using 3-exponential Levant-Marquardt algorithm

Appendix 2: Extension-Load Analysis

A2.1 Extension (mm)-Load (mm) Analysis:

To assess the effectiveness of the selected range of loads imposed on marginal chordae tendineae during the entropic studies, the load-extension data from the uniaxial mechanical tests were calculated and plotted. These results suggested that our selected load ranges (30 and 60 g), were small relative to the loads in the linear rising portion of the curve or the ultimate tensile strength. It is speculated that the selected loads may have simply resulted in a small amount of collagen fibre alignment ("toe" region). Hence, subsequent mechanical studies should consider using higher loads (e.g. 800 g), which would result in stiffening of the structure and more loading of the triple helix itself (i.e. "linear" region).

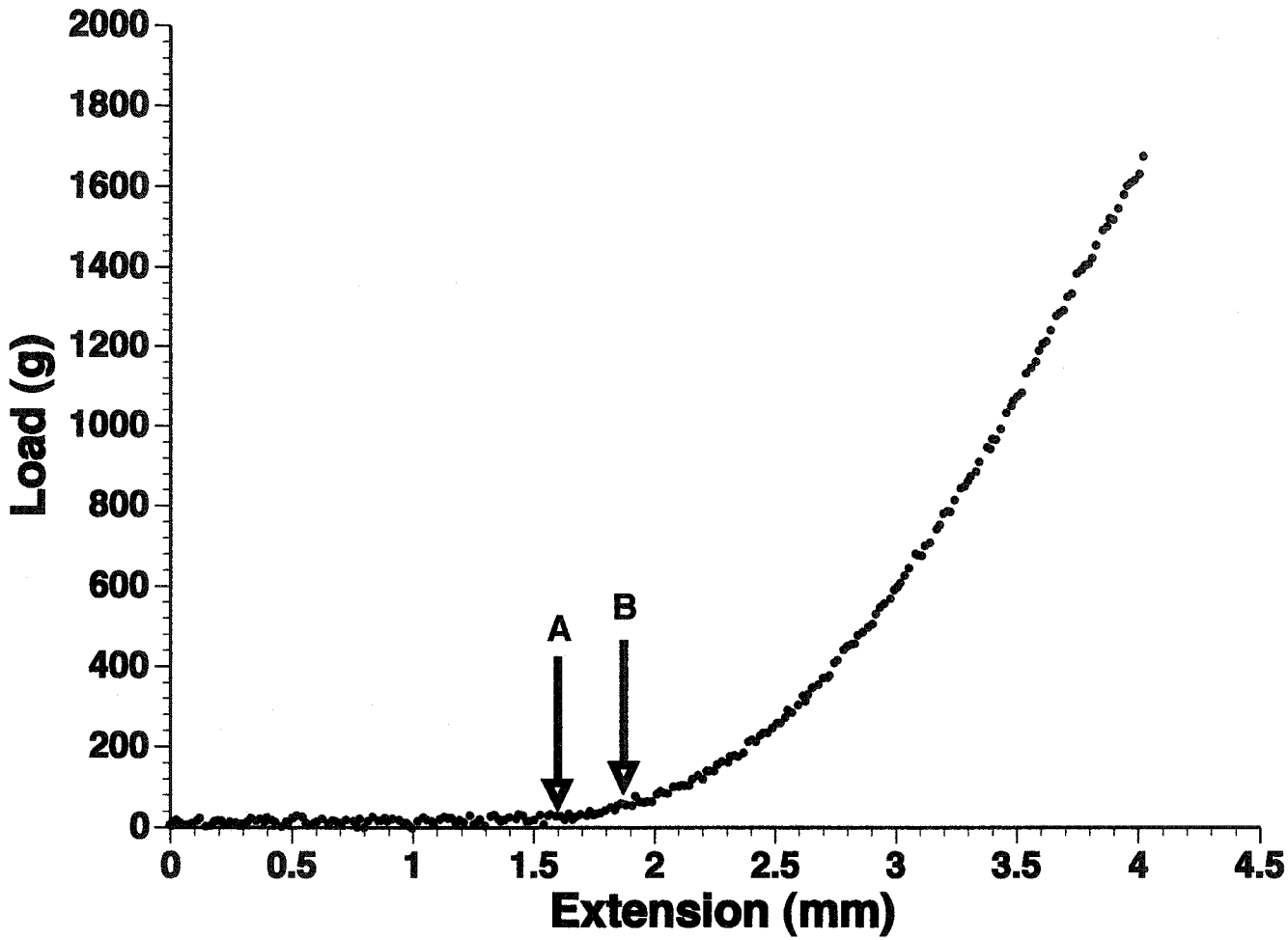

Figure A.2.1 Typical Load-extension plot of chordae tendineae. The arrows A and B show the extensions of the corresponding load 30 and 60 g, respectively.

Appendix 3: Solutions

A3.1 Hanks' Physiological Saline

Name	Minimum Assay	Lot #	Manufacturer
KCl	99.5%	117521-53408	BDH Inc.
NaCl	99.0%	42343312	Merck Scientific
$CaCl_2.2H_2O$	99.0%	70K00281	Sigma Chemical Co.
$MgSO_4.7H_2O$	99.0%	14060-551321	BDH Inc.
$NaHCO_3$	99.7%	115779-40798	BDH Inc.
Na_2HPO_4	99.0%	118621-62897	BDH Inc.
KH_2PO_4	99.0%	118814-63768	BDH Inc.
Thimersol	98.0%	86H0772	Sigma Chemical Co.
$C_6H_{12}O_6$	99.0%	117800-57340	BDH Inc.

A3.2 Crosslinking Chemicals

Name	Lot #	Manufacturer
Glutaraldehyde	12K5006	Sigma Chemical Co.
1-Ethyl-3-(3-Dimethylaminopropyly) Carbodiimide (EDC)	11K1330	Sigma Chemical Co.
H-Hydroxysuccinimide (NHS)	70K2511	Sigma Chemical Co.